PROGRESSIVE FAILURE ANALYSIS OF DOUBLE-NOTCHED COMPOSITE LAMINATES

PHAM DINH CHI

NATIONAL UNIVERSITY OF SINGAPORE

2010

PROGRESSIVE FAILURE ANALYSIS OF DOUBLE-NOTCHED COMPOSITE LAMINATES

PHAM DINH CHI

(B.ENG)

A THESIS SUBMITTED

FOR THE DEGREE OF DOCTOR OF PHILOSOPHY

DEPARTMENT OF MECHANICAL ENGINEERING

NATIONAL UNIVERSITY OF SINGAPORE

2010

Acknowledgement

It is the author's pleasure to thank his supervisor, colleagues and laboratory assistants for their assistance, advice, encouragement and guidance, without which this thesis would not have been possible.

The author owes his deepest gratitude to his supervisor Prof. Tay Tong-Earn and A/Prof. Vincent Tan Beng Chye who have provided great assistance and encouragement from the very early stages of this research and enable the author to develop an understanding of damage analysis of composite materials.

The author is indebted to many of his colleagues. The author would like to thank Dr. Sun Xiushan, Dr. Muhammad Ridha and Dr. Andi Haris for their invaluable help. Many thanks to laboratory assistants Mr. Low Chee Wah, Mr. Malik and Mr. Chiam Tow Jong for assisting him in his experiments.

Table of Contents

SUMMARY

Failure analysis in composite laminates is traditionally modeled by the material property degradation method for the in-plane damage prediction which assumes that a damage material can be replaced by an equivalent material with degraded properties. The delamination in composites, on the other hand, is often accounted for by the fracture mechanics approach which relies on the assumption of an initial crack. Therefore, a general method to account for both the in-plane damage and delamination in composites has not been fully developed. In this thesis, the progressive failure analysis of double-notched composite laminates is illustrated by the implementation of the material property degradation method, continuum damage mechanics and cohesive element method. These combined approaches help predict both the in-plane damage and delamination in composites. Furthermore, various failure criteria are employed in this thesis to significantly present a comparative study between different failure models on notched composites since most of the comparative studies in the literature have been performed only on unnotched composites.

Various failure models are used to model the damage propagation in notched cross-ply and quasi-isotropic composite laminates subjected to tension. The simulation results of laminates using both carbon/epoxy and glass/epoxy composites agree well with the experimental observations. These results

signify the necessity of introducing a fracture process in the fiber failure modeling to better predict the failure in notched composites.

In addition, the mesh-dependency and the parametric studies of cohesive elements and MPDM scheme are all presented on the notched quasi-isotropic laminate. The results of the mesh-dependency show that the FE models need to be built with three-dimensional elements and blunt notch to provide mesh-independent results. Besides, the parametric study of cohesive elements shows that the failure prediction is not so sensitive to the values of the cohesive strengths and strain energy release rates chosen while the parametric study of MPDM scheme reveals a need to assign relatively small stiffness values in MPDM to produce reasonable results.

Finally, the notch-size and ply-level scaling effects of the notched quasi-isotropic laminate are investigated. It is found that a strength reduction with increasing size of the specimens has been obtained in experiment and this trend has been captured computationally. The ply-level scaled laminate shows clearer fiber failures and delamination than the notch-size scaled laminate. These notch-size and ply-level scaling effects are reasonably mirrored by all failure models.

PUBLICATIONS

- T.E. Tay, B. Chen, X.S. Sun, **D.C. Pham**, *A comparative study of progressive failure models for composites*. The joint 9th World Congress on Computational Mechanics and 4th Asian Pacific Congress on Computational Mechanics, Sydney Australia, 2010.

- T.E. Tay, G. Liu, X.S. Sun, M. Ridha, V.B.C. Tan., **D.C. Pham**, H.T. Pham, Coauthor of Book chapter: *Progressive Failure Analysis of Composites*. Strength and life of composites, Stanford University, 2009.

- T.E. Tay, **D.C. Pham**, V.B.C. Tan, *Application of EFM and Cohesive Elements to Progressive Failure of Notched Composites.* The 13th Compability and durability workshop, Singapore, 2008.

- T.E. Tay, G. Liu, V.B.C. Tan, X.S. Sun, and **D.C. Pham**, *Progressive Failure Analysis of Composites.* Journal of Composite Materials, 2008. **42**(18): p. 1921-1966.

LIST OF FIGURES

LIST OF TABLES

LIST OF SYMBOLS

K	Element stiffness matrix
u	Nodal displacement vector of an element
f	Nodal force vector of an element
C	Material stiffness matrix
B	Strain-displacement matrix
X_C	Longitudinal compressive strength of composites
X_T	Longitudinal tensile strength of composites
Y_C	Transverse compressive strength of composites
Y_T	Transverse tensile strength of composites
Z_C	Out-of-plane compressive strength of composites
Z_T	Out-of-plane tensile strength of composites
Subscript 1,2,3	Directions of material coordinate system where 1 refers to the fiber direction
S_{12}, S_{13}, S_{23}	Shear strength of composites
ε_{ij}^{T}	Critical tensile strain of composites
ε_{ij}^{C}	Critical compressive strain of composites
ε_{ij}	Strain components
σ_{ij}	Stress components
σ_{mi}	Stress components in the matrix phase
C_m	Back-calculated compressive strength of composites in MMF
T_m	Back-calculated tensile strength of composites in MMF

E_1, E_2, E_3	Young's moduli of composites
E_1^D, E_2^D, E_3^D	Degraded Young's moduli of composites
G_{12}, G_{23}, G_{13}	Shear moduli of composites
$G_{12}^D, G_{23}^D, G_{13}^D$	Degraded shear moduli of composites
$\upsilon_{12}, \upsilon_{13}, \upsilon_{23}$	Poisson's ratios of composites
D_i^T	Degradation factors in tension mode
D_i^C	Degradation factors in compression mode
E_D	Strain energy in CDM
d_f	Damage variable for fiber failure modeling in CDM
d_f'	Damage variable for fiber failure modeling in MCDM and MChristensen
d_1	Damage variable for matrix failure modeling in CDM
d_2	Damage variable for matrix failure modeling in CDM
Y_{F1}, Y_{F2}	Critical tensile and compressive damage force in fiber direction
Y_S	Brittle damage threshold for fiber-matrix interface
E_t	Transverse tensile failure strain
E_S	Shear tensile failure strain
b	Coupling coefficient
Y_{01}	Tensile force initiating damage in transverse direction
Y_{02}	Shear force initiating damage in transverse direction

Chapter 1

Introduction and literature review

1.1 Introduction

Recently, there has been a great increase in the use of advanced composites as primary structural materials, especially in the aircraft and wind turbine industries. More substantial parts of composites are being used for the building of wind turbines and new generation airliners such as Airbus 380 or Boeing 787, featuring light-weight and high-efficiency constructions. Composites have wide applications in aircraft and wind turbine industries because of their low weight, high strength and stiffness, high fatigue life and good corrosion resistance.

However, most of composites in general contain notches as defects or as circular and semi-circular cutouts for easy access or fastening applications. Unfortunately, the presence of notches in composites significantly influences the performance of composite structures, especially for sharp notches. Therefore, a study of notch effects on composite structures is important and needs to be investigated. Some researchers have analyzed the failure of some particular notched structures and proposed methodologies to predict the failure of these structures [1-4]. Nevertheless, the failure of notched composites has not been fully understood in general due to the complex failure mechanisms

involving the matrix cracking, fiber failure, fiber kinking, fiber/matrix debonding, delamination, etc.

In order to account for the complex failure mechanisms in notched composites, a progressive failure analysis is performed to enable the prediction of crack initiation and propagation in composite structures. A progressive failure analysis comprises a damage initiation predicted by a failure theory and a material damage model to simulate a loss in the load-carrying capability of the part and advances the progression of damage. The results of failure analysis are dependent on the choice of the failure criterion and associated damage modeling technique. It is therefore important to employ reliable failure theories and damage modeling techniques for the progressive failure analysis to correctly mirror the complex mechanisms in notched composites. In the following sections, a literature review of failure theories, in-plane damage and delamination modeling techniques is presented.

1.2 Review of Some Failure Theories for Composite Materials

Since composite materials have been widely used in structural designs, it is important to determine the ultimate stresses or loads at which the composite structures will fail. Therefore, several failure theories have been proposed in the literature [5-8] to predict the failure state of composite structures. Some of the popular failure theories are discussed in this section.

1.2.1 Maximum stress and maximum strain failure theories

One of the earliest macroscopic failure theories is the maximum stress theory [9] and maximum strain theory [10]. They have been proposed by extending isotropic failure theories to account for the anisotropic heterogeneous of composites. According to maximum stress and maximum strain failure theories, failure occurs when at least one of the stress or strain components exceeds its corresponding strength and its critical strain, respectively. The failure conditions are then expressed in the form of six sub-criteria for both maximum stress (Equations 1-1 to 1-6) and maximum strain theories (Equations 1-7 to 1-12). In each of the expression, X_T, X_C are the longitudinal tensile and compressive strengths of composite whereas Y_T, Y_C, Z_T, Z_C are the transverse tensile and compressive strengths of composite and S_{12}, S_{23}, S_{13} are the shear strengths of composite. The maximum stress and maximum strain theories are still used in the failure analysis of composite structures because they are easy to understand and implement in the analysis. However, one shortcoming of these criteria is that they do not take into account any stress and strain interaction under multi-axial state of stress.

$$-X_C \leq \sigma_{11} \leq X_T \tag{1-1}$$

$$-Y_C \leq \sigma_{22} \leq Y_T \tag{1-2}$$

$$-Z_C \leq \sigma_{33} \leq Z_T \tag{1-3}$$

$$-S_{12} \leq \sigma_{12} \leq S_{12} \tag{1-4}$$

$$-S_{13} \leq \sigma_{13} \leq S_{13} \tag{1-5}$$

$$-S_{23} \leq \sigma_{23} \leq S_{23} \tag{1-6}$$

$$-\varepsilon_{11}^{C} \leq \varepsilon_{11} \leq \varepsilon_{11}^{T} \tag{1-7}$$

$$-\varepsilon_{22}^{C} \leq \varepsilon_{22} \leq \varepsilon_{22}^{T} \tag{1-8}$$

$$-\varepsilon_{33}^{C} \leq \varepsilon_{33} \leq \varepsilon_{33}^{T} \tag{1-9}$$

$$-\varepsilon_{12}^{C} \leq \varepsilon_{12} \leq \varepsilon_{12}^{T} \tag{1-10}$$

$$-\varepsilon_{13}^{C} \leq \varepsilon_{13} \leq \varepsilon_{13}^{T} \tag{1-11}$$

$$-\varepsilon_{23}^{C} \leq \varepsilon_{23} \leq \varepsilon_{23}^{T} \tag{1-12}$$

1.2.2 Tsai-Hill failure theory

To overcome the shortcomings of maximum stress and maximum strain theories, Tsai and Azzi adapted Hill's theory, which was originally proposed for anisotropic ductile materials, to anisotropic and brittle composites and developed a so-called Tsai-Hill theory [11]. The Tsai-Hill failure theory is expressed in term of one single criterion that allows for interaction among the stress components (Equation 1-13). Strength parameters *F, G, H, L, M, N* in Tsai-Hill criterion can be determined through a series of experiments of one-dimensional loading. A major disadvantage of this failure theory is that it does not distinguish between tensile and compressive strengths which are usually different for composite materials.

$$(G+H)\sigma_{11}^{2} + (F+H)\sigma_{22}^{2} + (F+H)\sigma_{33}^{2} - 2H\sigma_{11}\sigma_{22} - 2G\sigma_{11}\sigma_{33}$$
$$-2F\sigma_{22}\sigma_{33} + 2L\sigma_{12}^{2} + 2M\sigma_{23}^{2} + 2N\sigma_{13}^{2} = 1 \tag{1-13}$$

1.2.3 Tsai-Wu failure theory

To address the disadvantage of Tsai-Hill failure theory, Tsai and Wu introduced a failure theory capable of accounting for the difference between

tensile and compressive strengths [12]. Similar to the Tsai-Hill failure theory, Tsai-Wu theory which allows for the stress interaction is expressed in Equation 1-14 in term of one single criterion by stress tensors $\sigma_i, \sigma_j (i, j = 1,2, \dots 6)$ and coefficients $F_i, F_{ij} (i, j = 1,2, \dots 6)$ instead of having multiple sub-criteria. However, different from the Tsai-Hill failure theory which describes the stress interaction terms as functions of the other terms, the Tsai-Wu failure theory treats the interaction terms as independent material properties. In general, the Tsai-Wu theory is preferably used in the failure analysis of composite materials since it is simple and able to predict the composite strength under general stage of stress.

$$F_i \sigma_i + F_{ij} \sigma_i \sigma_j = 1 \tag{1-14}$$

The above equation can be written in expanded form:

$$f_1\sigma_1 + f_2(\sigma_2 + \sigma_3) + f_{11}\sigma_1^2 + f_{22}(\sigma_2^2 + \sigma_3^2) + f_{44}\sigma_{12}^2 + f_{66}(\sigma_{13}^2 + \sigma_{23}^2) + 2f_{12}(\sigma_1\sigma_2 + \sigma_1\sigma_3) + 2f_{23}\sigma_2\sigma_3 = 1 \tag{1-15}$$

where the coefficients f_i, f_{ij} in Equation 1-15 can be obtained from the longitudinal tensile and compressive strengths of composite X_T, X_C and transverse tensile and compressive strengths of composite Y_T, Y_C and out-of-plane tensile and compressive strengths of composites Z_T, Z_C:

$$f_1 = \frac{1}{X_T} - \frac{1}{X_C} \tag{1-16}$$

$$f_{11} = \frac{1}{X_T X_C} \tag{1-17}$$

$$f_2 = \frac{1}{Y_T} - \frac{1}{Y_C} \tag{1-18}$$

$$f_{22} = \frac{1}{Y_T Y_C} \tag{1-19}$$

$$f_3 = \frac{1}{Z_T} - \frac{1}{Z_C} \tag{1-20}$$

$$f_{33} = \frac{1}{Z_T Z_C} \tag{1-21}$$

$$f_{44} = \frac{1}{S_{12}^2} \tag{1-22}$$

$$f_{55} = \frac{1}{S_{23}^2} \tag{1-23}$$

$$f_{66} = \frac{1}{S_{13}^2} \tag{1-24}$$

$$f_{12} = -\frac{1}{2}(f_{11} f_{22})^{1/2} \tag{1-25}$$

$$f_{23} = f_{22} - \frac{f_{44}}{2} \tag{1-26}$$

A major disadvantage of the Tsai-Wu criterion is that it has not distinguished fiber-dominated failure from matrix-dominated failure (except for the special cases of unidirectional laminates). Therefore, a simple set of criteria is added with the Tsai-Wu criterion to determine the failure modes. If $\sigma_{11} \geq X_T$, fiber tensile failure is assumed, but if $\sigma_{11} < X_C$, fiber compressive failure is assumed. Otherwise, only matrix failure is assumed.

1.2.4 Hashin failure theory

To take account of the distinct failure modes of matrix and fiber, Hashin [13] proposed a criterion with matrix-dominated and fiber-dominated modes. He analyzed the damage in composite in each mode under different tensile and compressive loading states. The failure prediction by Hashin theory is expressed by sub-criteria including the tensile fiber mode, compressive fiber mode, tensile matrix mode and compressive matrix mode. Although the Hashin criterion has a clear distinction between fiber and matrix failure modes, it is in general very conservative to predict the failure in composite. Moreover, the Hashin theory consider each failure modes as independent sub-criteria, thus does not account for the interaction between tension and compression when multi-axial loads are applied. Each of the failure modes of Hashin failure theory is given as follows:

Tensile fiber mode ($\sigma_{11} > 0$):

$$\left(\frac{\sigma_{11}}{\sigma_A^+}\right)^2 + \frac{1}{\tau_A^2}(\sigma_{12}^2 + \sigma_{13}^2) = 1 \tag{1-27}$$

Compressive fiber mode ($\sigma_{11} < 0$):

$$-\left(\frac{\sigma_{11}}{\sigma_A^-}\right) \quad = 1 \tag{1-28}$$

Tensile matrix mode ($\sigma_{22} + \sigma_{33} > 0$):

$$\frac{1}{(\sigma_A^+)^2}(\sigma_{22}^2+\sigma_{33}^2)+\frac{1}{(\tau_T^+)^2}\left(\sigma_{23}^2-\sigma_{22}\sigma_{33}\right)+\frac{1}{(\tau_A^+)^2}(\sigma_{12}^2+\sigma_{13}^2)=1 \qquad (1\text{-}29)$$

Compressive matrix mode ($\sigma_{22}+\sigma_{33}<0$):

$$\frac{1}{(\sigma_T^-)}\left[\left(\frac{\sigma_T^-}{2\tau_T}\right)^2-1\right](\sigma_{22}+\sigma_{33})+\frac{1}{4\tau_T^2}(\sigma_{22}+\sigma_{33})^2$$

$$+\frac{1}{\tau_T^2}\left(\sigma_{23}^2-\sigma_{22}\sigma_{33}\right)+\frac{1}{(\tau_A)^2}(\sigma_{12}^2+\sigma_{13}^2)=1 \qquad (1\text{-}30)$$

where σ_A^+, σ_A^- and τ_A are the tensile, compressive failure stresses in the fiber direction and axial shear failure stress. σ_T^+, σ_T^- and τ_T are the tensile, compressive failure stresses transverse to the fiber direction and transverse shear failure stress.

1.2.5 Christensen failure theory

Christensen [14] proposed a failure theory for highly anisotropic materials with separated matrix-controlled and fiber-controlled modes. The failure analysis by Christensen theory is characterized by two failure criteria, one criterion for matrix failure prediction considering stress interaction (Equation 1-31) and a maximum stress for fiber failure prediction (Equation 1-32). Except for the additional implementation of fiber-controlled mode, the Christensen theory expressed the matrix-controlled mode look like Tsai-Wu theory. The only difference is that Christensen criterion does not consider the longitudinal stress σ_{11} in the matrix-controlled mode.

$$\left(\frac{1}{Y_t}-\frac{1}{Y_c}\right)(\sigma_{22}+\sigma_{33})+\frac{1}{Y_tY_c}(\sigma_{22}+\sigma_{33})^2+\frac{1}{S^2}\left(\sigma_{23}^2-\sigma_{22}\sigma_{33}\right)+\frac{1}{S^2}\left(\sigma_{12}^2+\sigma_{13}^2\right)\leq 1 \tag{1-31}$$

$$-X_c \leq \sigma_{11} \leq X_t \tag{1-32}$$

1.2.6 Micromechanics of failure (MMF)

Micromechanical-based failure criteria were recently developed by Ha *et al* [15] to account for specific modes of failure at the micro-scale. Essentially, it is the application of quadratic-type failure criterion at the local points of micromechanics FE block models, in which the fibers and matrix are modeled explicitly. Thermal stresses and strains are considered in MMF. It is noted that the MMF clearly defines fiber-dominated and matrix-dominated failures by quadratic-type criterion. However, in this work, the candidate has chosen to apply maximum stress criterion for fiber-dominated failures for simplicity and only the matrix-dominated failure is expressed by quadratic-type criterion.

The micromechanical models considered in MMF have square and hexagonal packing arrays (Figure 1-1). Although more realistic random arrays may be modeled, the two idealized cases are used here for convenience and simplicity. The hexagonal array has a total of 19 reference points and the square array has a total of 17 reference points in the matrix phase. When a load is applied on a FE model, a set of macro-stresses are obtained for each element in the FE

model. These macro-stresses are then transformed to micro-stresses at the reference points of micromechanical blocks by amplification factors. The amplification factors are obtained from these points by applying a unit load in each x, y and z direction.

Matrix-dominated mode in MMF can be expressed by:

$$\sigma_{VM}^2 + (C_m - T_m) I_1 - C_m T_m < 0 \tag{1-33}$$

Fiber-dominated mode:

$$-X_C \leq \sigma_{11} \leq X_T \tag{1-34}$$

where C_m, T_m are transverse compressive and tensile strengths of the composite which are back-calculated from material properties of the constituent matrix and fiber.

I_1 and σ_{VM} in Equation (1-33) are derived from the micro-stresses σ_{mi} of reference points in the matrix phase:

$$I_1 = \sigma_{m11} + \sigma_{m22} + \sigma_{m33} \tag{1-35}$$

$$I_2 = \sigma_{m11}\sigma_{m22} + \sigma_{m22}\sigma_{m33} + \sigma_{m33}\sigma_{m11} - \left(\sigma_{m12}^2 + \sigma_{m23}^2 + \sigma_{m13}^2\right) \tag{1-36}$$

$$\sigma_{VM} = \sqrt{I_1^2 - 3I_2} \tag{1-37}$$

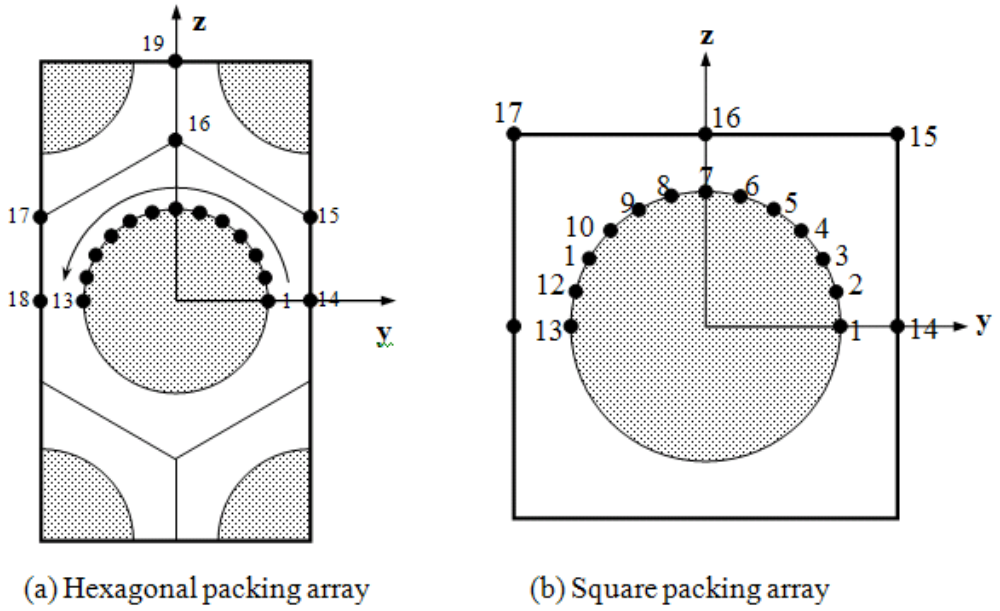

(a) Hexagonal packing array (b) Square packing array

Figure 1-1 Selected points on micromechanics blocks.

Each amplification point has one ellipsoidal failure envelope which is determined by Equations 1-33. A total of 36 ellipsoidal envelopes is obtained corresponding to 36 references points in the matrix phase of square and hexagonal packing models. Tay *et. al.* [16] illustrated the intersecting envelopes in the σ_1-σ_2 plane from 36 reference points within the micromechanical block models for TM7/epoxy material (Figure 1-2). The final failure envelope for the composite is defined within the inner boundaries of all the intersecting regions, and the maximum stress criterion for fiber-dominated failure.

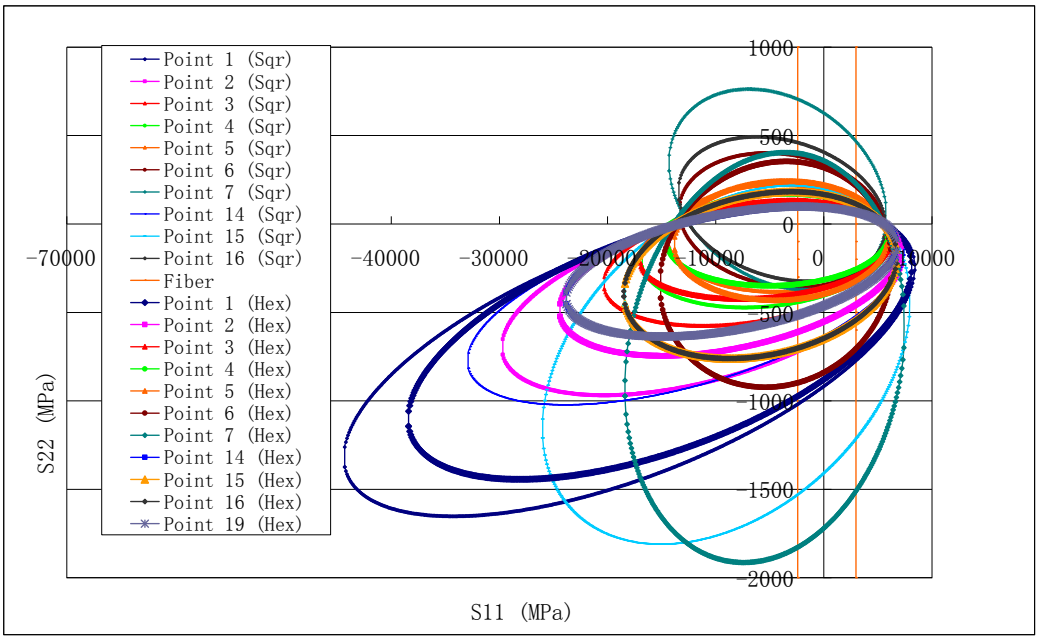

Figure 1-2 Intersection of elliptical envelopes from points within micromechanics block models for a TM7/epoxy material [16].

The final failure envelope for TM7/epoxy material is represented by the shaded areas in Figure 1-3. The maximum stress criterion which is simply applied for fiber-dominated failure is represented by the two vertical boundaries on the right and left of the failure envelope in Figures 1-3, denoting maximum longitudinal tensile and compressive strengths. The failure envelope is bounded at the top and bottom by matrix-dominated failure. T_m and C_m are therefore determined by the intersection of the top and bottom boundary of the failure envelope with the vertical axis.

The failure envelope and determination of T_m and C_m for other composite materials can be obtained similarly. The failure envelope for MMF model is used to identify the damage in composite. Elements are considered to be failed by MMF when their stress components are outside the failure envelope for MMF model. Otherwise, no failure is predicted.

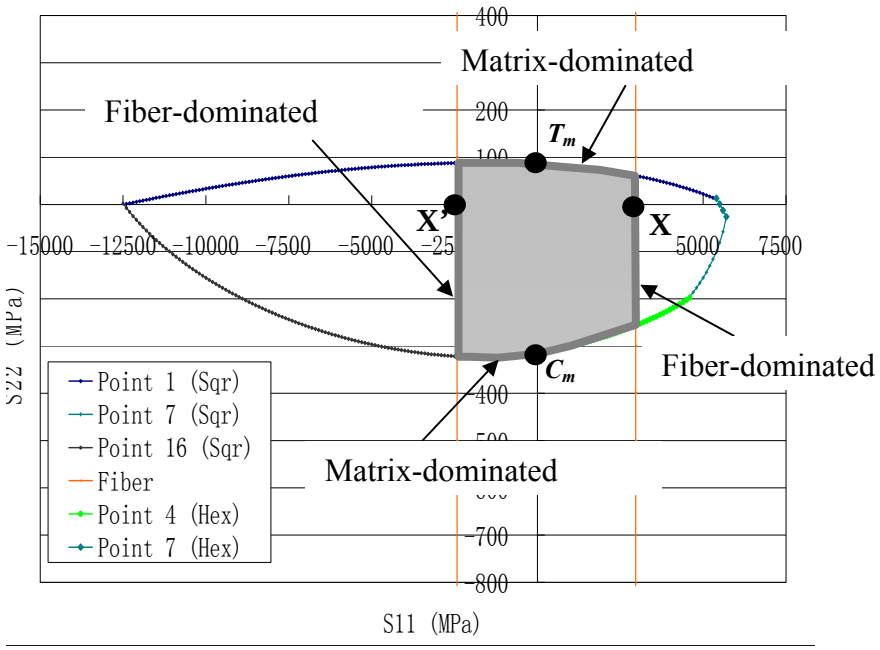

Figure 1-3 Failure envelope for MMF model (TM7/epoxy) [16].

1.3 Review of in-plane damage modeling techniques

There are some in-plane damage modeling techniques proposed for composite laminates in literature, among which the material property degradation method (MPDM) and the continuum damage mechanics (CDM) are widely used. The MPDM is the most popular method to account for the in-plane progressive damage in composites once the damage is identified by a failure criterion such as the Tsai-Wu criterion or Christensen criterion. On the other hand, the continuum damage mechanics (CDM) can identify the damage by its criterion and advances the progression of damage in composites based on the strain energy and a set of damage variables. In this section, a review of MPDM and CDM is discussed.

1.3.1 Material property degradation method (MPDM)

The material property degradation method (MPDM) is one of the most popular approaches to model in-plane progressive failure in composites. The idea of the MPDM is that a damaged material can be described by that virgin material with degraded properties. Once damage is identified in composite materials by a failure criterion, the MPDM is applied to reflect the loss on load-bearing capabilities of these materials by degrading their properties. Models of MPDM in the literature range from very conservative MPDM, such as the ply-discount method, to simple MPDM applied to finite element model and to much more sophisticated MPDM based on continuum damage mechanics or fracture mechanics. A brief review of these MPDM models is given below.

1.3.1.1 Ply-discount method

A very conservative version of MPDM is the ply-discount method. In this method, a stress analysis is first applied to composite laminate to identify the first ply that is damaged. The material properties of this ply are therefore degraded to describe its loss in load-bearing capability. A new stress analysis using the updated properties of damaged ply is then carried out to identify the next failed ply and the properties of this failed ply will be also degraded. This procedure is repeated until final failure is predicted. The ply-discount method has been used widely earlier in the literature based on the assumption that the damaged ply cannot sustain any more load and that all of the material properties of the failed ply are completely degraded [17-19]. The advantage of

the ply-level method is that it is simple to understand and implement. However, the damaged ply in reality is still capable of carrying additional load despite the presence of initial damage. Therefore, the ply-discount method is so conservative and may lead to underestimation of the strength and stiffness of composite laminates.

To make the ply-discount method more consistent, different ply-discount strategies have been proposed in literature [20-27], assuming that only chosen material properties of the failed plies are reduced or zeroed, depending on the failure mechanisms responsible for the ply failure. Among these strategies, some introduced different degradation factors to account for different matrix and fiber modes. As a consequence, these predictions of the laminate strengths and stiffnesses may be improved than the original ply-discount method but they are still under-predicted the experiment. Overall, the idea to apply MPDM for the whole ply is conservative and fails to recognize that the damaged ply still has residual stiffnesses which are not necessarily degraded to zero.

1.3.1.2 MPDM applied to finite element

To overcome the drawback of the ply-discount method, many of the application of the MPDM presented in literature are applied directly to finite element. In this case, a stress analysis is performed in finite element model to identify the failed elements in each ply. To reflect the damage, the material properties of these failed elements are degraded. A stress analysis with

updated properties of failed elements is then carried out to identify the next failed elements. This procedure is repeated until all damages are accounted for. It is noted that only the elastic moduli of failed elements are degraded instead of the whole ply.

Tan [28] and Tan and Nuismer [29] and applied simple MPDM to finite elements by implementing two-dimensional (2D) progressive damage models for notched laminates containing central holes subjected to in-plane tensile or compressive loading. In these studies, three degradation factors D_i (i = 1, 2, 6) were used to account for the damage of the lamina. The Poisson's ratio was not degraded and only the moduli and shear modulus were modified to reflect the failure of element:

$$E_{11} = D_1 E_{11}^0 \tag{1-38}$$

$$E_{22} = D_2 E_{22}^0 \tag{1-39}$$

$$G_{12} = D_6 G_{12}^0 \tag{1-40}$$

where E_{11}^0, E_{22}^0 and G_{12}^0 are the material properties of the undamaged lamina and E_{11}, E_{22} and G_{12} are the material properties of the damaged lamina. The predicted damage progression patterns agreed with experimental results but the predicted ultimate strength values were very sensitive to the selected values of the degradation factors. Additionally, it was assumed that the stiffness reduction due to tensile and compression is the same. This may be

incorrect in composite materials since the failed elements due to compression are still able to sustain additional load.

To account for different failure modes by MPDM, Camanho *et al* [30] assigned different degradation factors to three-dimensional (3D) finite element models to predict damage progression and strength of mechanically fastened joints in carbon fiber-reinforced plastics failing in bearing, net-tension and shear-out modes. Four failure modes are assumed by using Hashin's failure theory. The effect of damage on the elastic properties is shown below:

Matrix tensile or shear cracking: $E_{22}^{d} = D_2^{T} E_{22}$; $G_{12}^{d} = D_4^{T} G_{12}$; $G_{23}^{d} = D_4^{T} G_{23}$

Fiber tensile fracture: $E_{11}^{d} = D_1^{T} E_{11}$

Matrix compressive or shear cracking: $E_{22}^{d} = D_2^{C} E_{22}$; $G_{12}^{d} = D_4^{C} G_{12}$; $G_{23}^{d} = D_4^{C} G_{23}$

Fiber compressive fracture: $E_{11}^{d} = D_1^{C} E_{11}$

where superscripts *T*, *C* and *d* are used to denote tension, compression and degraded material properties, respectively. By assuming constant degradation factors D_i such as D_1^{T}=0.07, $D_2^{T} = D_4^{T}$=0.2, D_1^{C}=0.14, $D_2^{C} = D_4^{C}$=0.4, a good agreement between experimental results and numerical predictions is obtained.

Instead of choosing a relatively small and constant degradation factors, Reddy *et al* [31] proposed a gradual stiffness reduction scheme to study the failure of composite laminates under tensile or bending load. When an element failure is

indicated by a failure criterion, the stiffness properties of that element are reduced gradually only to a level at which the failure criterion is no longer satisfied. This gradual stiffness reduction scheme results in the partial unloading of elements and allows repeated failures for the same element (accumulation of damage in the element). In order to simulate this gradual degradation and repeated failures of an element, an assumption is made that the degraded elastic properties of equivalent damaged elements are constant multiples of the elastic properties before current failure step. The constant is called the stiffness reduction coefficient (SRC) and its value may be adjusted between 0 and 1.

In addition, by applying MPDM and relaxation of springs to crude micromechanical subcells, Kwon and Craugh [1] not only predict the matrix cracking or splitting but also the triangular delamination in the cross-ply laminate as observed in Kortschot and Beaumont's experiment [32]. However, the use of these springs to connect FE nodes may require tremendous computational time when a fine mesh is used.

Furthermore, in order to model both general damage and delamination in composites, sophisticated models of MPDM with continuum mechanics (CDM) approaches were introduced. Barbero and Lonetti [33] employed an CDM-based approach to illustrate an inelastic damage model for fiber reinforced laminates, whereby a second order damage tensor is proposed and whose eigenvalues represent the density of distributed microcracks. A fourth-order damaged or reduced stiffness tensor is defined with the damage

variables. The damage parameters by this approach were calibrated from experiment to determine the damage evolution laws. Hence, reducing the number of parameters in the model would be advantageous to application. Feith and Shercliff [34] also used the CDM-based approach to investigate the effect of continuous versus constant degradation of material stiffnesses as failure progresses in bonded L-peel joints under bending. They found that for constant degradation, the results are not mesh dependent but load increment size dependent.

Ahn *et al*. [35-38] studied notched composites under compression with a macro-micromechanics model. Chamis [39] described CODSTRAN, a composites mechanics and FE program for progressive damage, where an iterative material degradation scheme is applied at the local scale to update the macroscopic constituent properties. In an effort to reduce computational effort, Riccio and Marciano [40] smeared the properties of eight plies into one finite element in order to reduce the number of degrees of freedom when investigating bolted joints of 32-ply laminates, resulting in a model with four elements in the thickness direction.

It can be seen that the MPDM performed with finite element method has provided better predictions for the strength and stiffness of composite laminates. This approach is widely used in failure analysis because it is simple to understand and implement and does not cost much computational efforts. However, there are still drawbacks of MPDM that need to be addressed. One of the most important drawbacks of MPDM is that after the material properties

or stiffness of the failed elements are degraded quite close to zero, the inversion of these element's stiffness can lead to divergence, especially when a very fine mesh is used. To overcome this drawback, the degradation factors are assigned with a relative small constant (not very small) or continuously changed according to the loading conditions.

1.3.2 Continuum damage mechanics (CDM)

Earlier research on application of CDM to composite materials are provided by Talreja [41], Allen *et al*. [42, 43], Lee *et al*. [44], Allix *et al*. [45, 46] and Ladeveze *et al* [47, 48]. Ladeveze [47, 48] used a strain energy E_D to describe the initiation and evolution of damage in composites in meso-scale by considering damage at one single-layer and the interface between layers. Ladeveze developed a continuum model using scalar internal variables to account for the damage progression and a material function to take into account the nonlinear behavior. These internal variables are derived from thermal forces.

The strain energy in CDM is expressed by:

$$
\begin{aligned}
E_D &= \frac{1}{2}\underline{\underline{\sigma}} : \underline{\underline{\underline{\underline{C_D}}}} : \underline{\underline{\sigma}} \\
&= \frac{1}{2(1-d_F)}\left[\frac{\langle\sigma_{11}\rangle_+^2}{E_1^0} + \frac{\varphi(\langle-\sigma_{11}\rangle_+)}{E_1^0} - \left(\frac{\nu_{12}^0}{E_1^0}+\frac{\nu_{21}^0}{E_2^0}\right)\sigma_{11}\sigma_{22} - \left(\frac{\nu_{13}^0}{E_1^0}+\frac{\nu_{31}^0}{E_3^0}\right)\sigma_{11}\sigma_{33} - \left(\frac{\nu_{32}^0}{E_3^0}+\frac{\nu_{23}^0}{E_2^0}\right)\sigma_{33}\sigma_{22}\right] \\
&+ \frac{\langle-\sigma_{22}\rangle_+^2}{E_2^0} + \frac{\langle-\sigma_{33}\rangle_+^2}{E_3^0} + \frac{1}{2}\left[\frac{1}{(1-d_1)}\left(\frac{\langle\sigma_{22}\rangle_+^2}{E_2^0}+\frac{\langle\sigma_{33}\rangle_+^2}{E_3^0}\right) + \frac{1}{(1-d_2)}\left(\frac{\sigma_{12}^2}{G_{12}^0}+\frac{\sigma_{23}^2}{G_{23}^0}+\frac{\sigma_{31}^2}{G_{31}^0}\right)\right]
\end{aligned}
\tag{1-41}
$$

where:

- Subscripts 1, 2, 3 refer to the fiber direction, transverse direction and out-of-plane normal direction, respectively. Superscript 0 refers to the original value of the indicated quantity.
- d_F represents the fiber-direction degradation, d_1 represents the transverse direction degradation and d_2 represents shear degradation. All scalar variables d_F, d_1 and d_2 remain constant within the thickness.
- φ is a material function that takes into account the nonlinear behavior.
- $\langle a \rangle_+ = a$ if $a > 0$ and $\langle a \rangle_+ = 0$ if $a <= 0$.

The forces associated with the mechanical dissipation are:

$$Y_F = \frac{\partial}{\partial d_F} E_D \Big|_{\sigma, d_F}$$
$$= \frac{1}{2(1-d_F)^2}\left(\frac{\sigma_{11}^2}{E_1^0} - \left(\frac{\nu_{12}^0}{E_1^0} + \frac{\nu_{21}^0}{E_2^0}\right)\sigma_{11}\sigma_{22} - \left(\frac{\nu_{13}^0}{E_1^0} + \frac{\nu_{31}^0}{E_3^0}\right)\sigma_{11}\sigma_{33} - \left(\frac{\nu_{32}^0}{E_3^0} + \frac{\nu_{23}^0}{E_2^0}\right)\sigma_{33}\sigma_{22}\right)$$

$$Y_{d_1} = \frac{\partial}{\partial d_1} E_D \Big|_{\sigma, d_1} = \frac{1}{2(1-d_1)^2}\left(\frac{\sigma_{22}^2}{E_2^0} + \frac{\sigma_{33}^2}{E_3^0}\right),$$
$$Y_{d_2} = \frac{\partial}{\partial d_2} E_D \Big|_{\sigma, d_2} = \frac{1}{2(1-d_2)^2}\left(\frac{\sigma_{12}^2}{G_{12}^0} + \frac{\sigma_{23}^2}{G_{23}^0} + \frac{\sigma_{13}^2}{G_{13}^0}\right),$$

(1-42)

An equivalent damage force is introduced as:

$$\underline{Y}(t) = \sup_{\tau \le t}\left(Y_{d_2}(\tau) + bY_{d_1}(\tau)\right) \tag{1-43}$$

The damage evolution law is then defined based on Y_F, Y_{d1}, Y_{d2} and Y. The associated damage driving forces Y_F, Y_{d1} and Y_{d2} are similar to the energy-release rate in fracture mechanics. They are in the unit of energy per unit volume.

Denoting that the values of variables d_1, d_2 and d_F are zero for no damage and unit for complete damage. Fiber-direction damage evolution is observed as a brittle fracture process, and the damage evolution law of d_F is therefore straightforward:

$$\begin{cases} d_F = 1 \text{ if } (Y_F > Y_{F1} \text{ when compression or } Y_F > Y_{F2} \text{ when tension}) \\ d_F = 0 \text{ otherwise} \end{cases} \tag{1-44}$$

where Y_{F1}, Y_{F2} are material constants that need to be determined by experiment.

Transverse damage evolution and shear damage evolution are both associated with matrix micro-cracking and fiber-matrix debonding mechanisms. The damage variables d_1 and d_2 are determined by:

$$d_1 = \frac{\left\langle \sqrt{\underline{Y}} - Y_{01} \right\rangle_+}{Y_{c1}} \text{ if } Y_{d1} < Y_S \tag{1-45}$$
$$d_1 = 1 \text{ otherwise}$$

$$d_2 = \frac{\left\langle \sqrt{\underline{Y}} - Y_{02} \right\rangle_+}{Y_{c2}} \quad \text{if } Y_{d1} < Y_S \qquad (1\text{-}46)$$
$$d_2 = 1 \text{ otherwise}$$

where $b, Y_{01}, Y_{02}, Y_{c1}, Y_{c2}, Y_S$ are material constants that need to be determined. Determination of these parameters is presented in Chapter 2.

1.4 Review of delamination modeling techniques

Since the MPDM and CDM cannot be used for delamination modeling at the interfaces whose thickness are very small, the fracture mechanic approach and the cohesive element method are often applied.

1.4.1 Fracture Mechanics approach

The delamination in composites is often accounted for as cracks in fracture mechanics which can be treated individually. Once the damage initiation is predicted by a fracture criterion, the crack propagation modelling methodology is then applied. One example of the application of fracture mechanics was given by Bakuskas *.et. al.* [49] who used a node-splitting technique to generate new crack surface after the initial damage is predicted by maximum stress criterion. Good agreement between experiment and simulation was obtained, but this model has its disadvantage to model a heterogeneous region at potential damage regions which are not always easy

to determine. Other examples were presented by Tay *.et. al.* [50] and Shen *.et. al.* [51] who adopted a node-release technique to advance crack propagation in fully three-dimensional (3D) models.

Conventional fracture mechanics has been mostly used to analyze delamination growth in laminated composites despite their limitations such as their inability to capture delamination kinking and interaction with microcracks. One of the most restrictive limitations of fracture mechanics is that a pre-existing crack or delamination must be assumed in order to advance the propagation of crack. Therefore, conventional fracture mechanics is not used to predict initiation. In order to solve this limitation, some researchers employ strength-based failure criteria to predict the damage initiation while employs fracture mechanic to predict the damage propagation. Brewer and Lagace [52] used a quadratic stress criterion to predict the delamination onset. Similarly, Hou *et al* [53] proposed a reduced form of the Tsai-Wu criterion to account for delamination onset instead of using the fracture mechanics. For propagation prediction, cohesive elements with fracture mechanics are often the choices [1, 39, 54]. While these methods practically help overcome limitations of fracture mechanics, they do not necessarily remove the need to introduce a small pre-crack length or characteristic length in order to proceed with propagation.

1.4.2 Cohesive Element Method

In order to better predict the damage onset and propagation without the assumption of an existing crack, the cohesive element method is introduced. The idea of cohesive element method was proposed by Dugdale [55] and Barenblatt [56] which can be related to Griffith's theory of fracture when the cohesive zone size is negligible compared with other characteristic dimensions. Different types of cohesive element methods were proposed by Camanho *et al* [57] including point cohesive elements, line cohesive elements and plane cohesive elements. Since then, these cohesive element methods have been widely applied to model the delamination in composites and attracted great interests of various studies in literature.

In one of the cohesive element methods, the point cohesive element method simply uses duplicate coincident nodes at the interfaces where damage is expected to occur and connects them by spring elements. This method has been successful in predicting delamination growth in many studies [58-62].

The line cohesive element method, on the other hand, is more complicated and is used to predict delamination growth in 2D plane strain conditions. It is based on the assumption that the thickness of the interface between adjacent plies is negligibly small compared to the other dimensions of composite laminate so that a finite element discretization of the interfaces can be obtained. The damage variables in this cohesive element method are tractions and relative displacements between the structural components of the interface. The line cohesive element method is successfully used to analyze the

delamination in double-cantilever beams and mixed-mode fracture specimens [63-67].

The concept of line cohesive element method is extended to three-dimensional cases by plane cohesive elements which model the interfaces between plies by upper and lowers surface of cohesive elements. These two surfaces of the plane cohesive elements will act as a single layer before the damage initiation is predicted. Once the damage is initiated, the connection between these surfaces is severed. The plane cohesive elements have been presented in several studies and achieved good agreement between experiment and numerical prediction [60, 68-71].

The cohesive element methods have shown advantages for predicting the delamination in composite laminate. They overcome the drawback of fracture mechanics that need an existing crack to advance the damage propagation. However, the cohesive element methods still require knowing the potential damage sites in advance to insert cohesive elements along such those paths. Otherwise, cohesive element should place at every potential region where damage is expected to occur.

1.5 Objectives and Significance of the study

In view of the above review of failure theories, it can be seen that numerous failure theories have been proposed in the literature for the failure analysis of composite materials. The earlier theories such as the maximum stress, the

maximum strain, Hashin, the Tsai-Hill and the Tsai-Wu failure theories are still widely used despite their shortcomings, because they are simple, easy to understand and implement in analysis. The maximum stress and maximum strain criteria are non-interactive theories which have been shown to produce poor predictions in general [72]. In contrast, interactive theories such as the Tsai-Wu criterion generally perform better [73]. However, the Tsai-Wu criterion in its original form does not have separated matrix and fiber failure modes. Therefore, recent failure theories such as the Christensen or MMF criteria are used to provide prediction for separated modes. While the former has its limitation at the macro-scale level, the latter requires inputs from micromechanical model. It is therefore necessary to perform a comparative study of these failure criteria to provide a general view of their predictive capabilities in composite structures.

In addition to failure theories, various modeling techniques have been proposed in literature to model the in-plane progressive failure and delamination in composites. For in-plane damage modeling, the material property degradation method (MPDM) and continuum damage mechanics (CDM) are mostly applied. The general MPDM has limitations to apply for elements with small thickness since it is easy to encounter divergence problems when the stiffnesses of these elements are degraded very close to zero. The CDM, on the other hand, requires lots of input parameters to account for the progressive damage in composites. For delamination modeling, the cohesive element method and the fracture mechanics approach are often chosen. The fracture mechanics approach relies on the assumption of an initial

flaw or crack, and thus cannot be used to predict the delamination onset in composite structures. The cohesive element method is able to overcome the drawback of the fracture mechanics approach as it does not need to define any pre-existing flaw or crack. However, the cohesive element method requires a *priori* knowledge for the potential initiation site so that cohesive elements can be placed along such a path. Otherwise, cohesive elements should be placed at every potential region. Since each modeling technique has its disadvantages for either in-plane damage or delamination prediction, a combination of them may help fully predict both the in-plane damage and delamination in composites.

The objective of this study is to employ the material degradation method (MPDM) and continuum damage mechanics (CDM) to predict the in-plane failure of double-notched composite laminates while the cohesive element method is used to model delamination onset and propagation at the interfaces. The MPDM uses relatively small (10^{-6}) and constant degradation factors and is coupled with various failure criteria such as the Tsai-Wu, Christensen and MMF. Since most of the comparative studies in the literature have been performed on unnotched composites [5-8], it is the author's strategy to present a comparative study of various failure models on notched composites to assess the predictive capability of each failure model as well as to study the size scale effects of notched composites.

The combination of the MPDM, CDM with the cohesive element method may contribute to a better understanding of progressive failure analysis in notched

composites when both the in-plane damage and delamination are accounted for. The results of the present study may significantly reveal that which failure model is capable of correctly predicting the strengths of notched composite laminates. In addition, the results of the size scale effects of notched composites may also provide significant trends in the strength prediction of notched composite laminates when the notch-size and the whole laminate are scaled.

1.6 Scope of the study

This thesis presents a computational study of progressive failure in double-notched $[90/0]_s$ and $[45/90/-45/0]_s$ composite laminates based on the implementation of the material degradation method (MPDM) and continuum damage mechanics (CDM). For each cross-ply and quasi-isotropic laminate, two different composite materials used in this thesis are carbon/epoxy and glass/epoxy. The MPDM is coupled with failure criteria including the Tsai-Wu criterion, Christensen criterion and a recently-proposed Micromechanics of Failure (MMF) criterion to predict the initiation and propagation of the in-plane damage. Besides models of MPDM with different failure criteria, the CDM model is also employed to account for both the initiation and evolution of the in-plane failure. For both models of MPDM and CDM, the cohesive element method is used to model the onset and propagation of delamination at the interfaces.

In this thesis, tensile tests have been first performed on the notched $[90/0]_s$ and $[45/90/-45/0]_s$ carbon/epoxy laminates. These experimental results will be compared to the simulation results by various failure models. Besides, the comparisons of analyses of notched $[90/0]_s$ and $[45/90/-45/0]_s$ glass/epoxy laminates are done with the experimental data obtained from Hallett and Wisnom [74]. In addition to the analyses of composite laminates, the mesh dependency study and parametric studies of cohesive elements and MPDM scheme are presented on the quasi-isotropic carbon/epoxy laminate. Finally, the notch-size and ply-level scaling effects are experimentally and computationally investigated on the quasi-isotropic carbon/epoxy laminate. The MPDM and all failure criteria are coded into the user-defined material subroutine UMAT and the analysis is carried out with the implicit solver of commercial FE software ABAQUS 6.9.

Chapter 2

MPDM, CDM, Failure theories and Cohesive element method

In this chapter, the principle and implementation of the material degradation method (MPDM) are first demonstrated, followed by the implementation of failure theories in the FE code. In addition, the introduction and implementation of modified versions of CDM and Christensen criteria are presented. Also, details of cohesive elements used in this thesis are provided in this chapter.

2.1 Material property degradation method (MPDM)

2.1.1 Principles of MPDM

The MPDM is based on the idea that a damage material can be replaced by an equivalent material with degraded material properties or stiffnesses. In other words, the MPDM describes a material stiffness degradation scheme that the stiffness matrix of the element is degraded to reflect the damage of elements. The state of damage depends on either partial failure (matrix failure) or complete failure (fiber failure) predicted. If fiber-dominated failure is

predicted, the MPDM will fully degrade all the elastic moduli E_1, E_2, E_3 and shear moduli G_{12}, G_{13}, G_{23} of composite materials to very small values (10^{-6} of the original values). When matrix-dominated failure is predicted, the MPDM will keep the longitudinal modulus E_1 (fiber direction) but degrade all the other properties of the material, meaning that the damaged matrix can only sustain the longitudinal load and cannot transfer any load in transverse and shear directions.

2.1.2 Implementation of MPDM

The force-stiffness for a finite element is given by [75]:

$$K.u = f \tag{2-1}$$

where K is the elemental stiffness matrix, u is the vector of nodal displacements and f is the vector of nodal forces. The stiffness matrix K can be determined through strain operator B and the material stiffness matrix C:

$$K = \int_{\Omega} B^T C B d\Omega \tag{2-2}$$

For a case of fiber-reinforced composite which is generally orthotropic in nature in the material principle directions, the material stiffness matrix C is:

$$C = \begin{bmatrix} C_{11} & C_{12} & C_{13} & 0 & 0 & 0 \\ C_{21} & C_{22} & C_{23} & 0 & 0 & 0 \\ C_{31} & C_{32} & C_{33} & 0 & 0 & 0 \\ 0 & 0 & 0 & C_{44} & 0 & 0 \\ 0 & 0 & 0 & 0 & C_{55} & 0 \\ 0 & 0 & 0 & 0 & 0 & C_{66} \end{bmatrix} \quad (2\text{-}3)$$

where the stiffness coefficients $C_{ij}(i,j = 1,2,\dots 6)$ may be expressed in terms of nine engineering constants E_1, E_2, E_3, G_{12}, G_{13}, $G_{23}, \nu_{12}, \nu_{23}$ and ν_{13} as follows:

$$C_{11} = \frac{1-\nu_{23}\nu_{32}}{E_2 E_3 \Delta} \quad (2\text{-}4)$$

$$C_{12} = C_{21} = \frac{\nu_{21}+\nu_{23}\nu_{31}}{E_2 E_3 \Delta} = \frac{\nu_{12}+\nu_{32}\nu_{13}}{E_1 E_2 \Delta} \quad (2\text{-}5)$$

$$C_{13} = C_{31} = \frac{\nu_{31}+\nu_{23}\nu_{32}}{E_2 E_3 \Delta} = \frac{\nu_{13}+\nu_{23}\nu_{12}}{E_1 E_2 \Delta} \quad (2\text{-}6)$$

$$C_{22} = \frac{1-\nu_{13}\nu_{31}}{E_1 E_3 \Delta} \quad (2\text{-}7)$$

$$C_{23} = C_{32} = \frac{\nu_{32}+\nu_{12}\nu_{31}}{E_1 E_3 \Delta} = \frac{\nu_{23}+\nu_{21}\nu_{13}}{E_1 E_2 \Delta} \quad (2\text{-}8)$$

$$C_{33} = \frac{1-\nu_{12}\nu_{21}}{E_1 E_2 \Delta} \quad (2\text{-}9)$$

$$C_{44} = G_{12} \tag{2-10}$$

$$C_{55} = G_{13} \tag{2-11}$$

$$C_{66} = G_{12} \tag{2-12}$$

$$\Delta = \frac{1-\nu_{12}\nu_{21}-\nu_{13}\nu_{31}-\nu_{23}\nu_{32}-2\nu_{21}\nu_{32}\nu_{13}}{E_1E_2E_3} \tag{2-13}$$

Once either the matrix or fiber failure is indicated by a failure theory, the material properties such as E_1, E_2, E_3, G_{12}, G_{13} and G_{23} will be degraded by degradation factors $D_i^T (i = 1,2, \dots 6)$ referring to tension mode and $D_i^C (i = 1,2, \dots 6)$ referring to compression mode. The degraded material properties $E_1^D, E_2^D, E_3^D, G_{12}^D, G_{23}^D, G_{13}^D$ of the failed elements referring to each mode are defined as follows:

For tensile matrix-dominated failure:

$$E_2^D = D_2^T E_2 \tag{2-14}$$

$$E_3^D = D_3^T E_3 \tag{2-15}$$

$$G_{12}^D = D_4^T G_{12} \tag{2-16}$$

$$G_{23}^D = D_5^T G_{23} \tag{2-17}$$

$$G_{13}^{D} = D_{6}^{T} G_{13} \tag{2-18}$$

For compressive matrix-dominated failure:

$$E_{2}^{D} = D_{2}^{C} E_{2} \tag{2-19}$$

$$E_{3}^{D} = D_{3}^{C} E_{3} \tag{2-20}$$

$$G_{12}^{D} = D_{4}^{C} G_{12} \tag{2-21}$$

$$G_{23}^{D} = D_{5}^{C} G_{23} \tag{2-22}$$

$$G_{13}^{D} = D_{6}^{C} G_{13} \tag{2-23}$$

For tensile fiber-dominated failure:

$$E_{1}^{D} = D_{1}^{T} E_{1} \tag{2-24}$$

$$E_{2}^{D} = D_{2}^{T} E_{2} \tag{2-25}$$

$$E_{3}^{D} = D_{3}^{T} E_{3} \tag{2-26}$$

$$G_{12}^{D} = D_{4}^{T} G_{12} \tag{2-27}$$

$$G_{23}^{D} = D_5^T G_{23} \tag{2-28}$$

$$G_{13}^{D} = D_6^T G_{13} \tag{2-29}$$

For compressive fiber-dominated failure:

$$E_1^{D} = D_1^C E_1 \tag{2-30}$$

$$E_2^{D} = D_2^C E_2 \tag{2-31}$$

$$E_3^{D} = D_3^C E_3 \tag{2-32}$$

$$G_{12}^{D} = D_4^C G_{12} \tag{2-33}$$

$$G_{23}^{D} = D_5^C G_{23} \tag{2-34}$$

$$G_{13}^{D} = D_6^C G_{13} \tag{2-35}$$

It should be noted that the same constant value of 10^{-6} is assigned for all the degradation factors under tension mode in this thesis, i.e. D_i^T=10^{-6} for $i = 1,2,\dots 6$. Since all the composite laminates studied this thesis are subjected to tension, the degradation factors for MPDM in compressive mode are not so important, especially for the D_1^C referring to compressive fiber failure which is not considered in tension mode. The degradation factors D_i^C are implemented

only for the compressive matrix failure and are assumed that D_i^C=10^{-6} for $i = 2, \dots 6$. The selection of the degradation factor value for MPDM scheme and its influence will be discussed in chapter 5.

In MPDM, the elements are considered to be completely failed when all the stiffnesses of those failed elements are completely degraded (considered as fiber failure). A matrix failure or partial failure can become a fiber failure or complete failure in the next calculation with updated stiffnesses. The degradation scheme of MPDM which accounts for different matrix and fiber failure modes is then applied for all of the elements in the model and this procedure is repeated until all the failed elements are predicted. The stiffness matrix will be derived from Equation 2-2 and the nodal force is obtained from Equation 2-1.

2.2 Implementation of Failure theories in FE code Abaqus

In order for the MPDM to be implemented in a damage progression program, it has to be guided by a failure theory such as the Tsai-Wu, Christensen or MMF criterion. A review of these criteria has been discussed in Chapter 1. Since the Tsai-Wu and Christensen criteria can use the composite material properties to determine failures in matrix-dominated and fiber-dominated modes, the implementation of these criteria into FE code is therefore straight forward. The failure envelopes for the Tsai-Wu and Christensen models are described in this section. Besides, the MMF requires the determination of T_m

and C_m before it is implemented in the FE code. Hence, both of the determination of T_m, C_m and failure envelope for the MMF model are presented.

2.2.1 Tsai-Wu and Christensen criteria

The failure envelopes of these failure criteria for carbon/epoxy material are shown in Figure 2-1 and those for glass/epoxy material are shown in Figure 2-2. The material properties of carbon/epoxy and glass/epoxy composites are given in Table 2-1 and 2-2. The parameters used in the Tsai-Wu and Christensen criteria are the longitudinal tensile and compressive strengths of composite X_T, X_C, transverse tensile and compressive strengths of composite Y_T, Y_C, out-of-plane tensile and compressive strengths of composites Z_T, Z_C and in-plane shear strengths. Using these parameters in the matrix-dominated and fiber-dominated modes, the failure envelopes of Tsai-Wu and Christensen criteria are obtained. These failure envelopes are used to identify the failed elements in composites. The elements are considered to be failed by Tsai-Wu or Christensen criterion when their predicted stresses are found outside the failure envelope of Tsai-Wu or Christensen criterion, respectively. Otherwise, no failure is predicted.

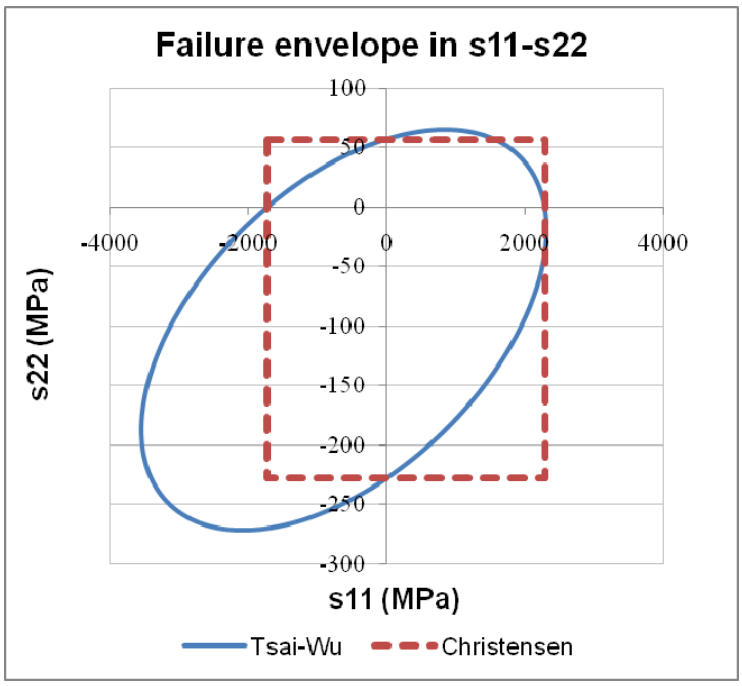

Figure 2-1 Failure envelopes for Tsai-Wu and Christensen criteria (carbon/epoxy material).

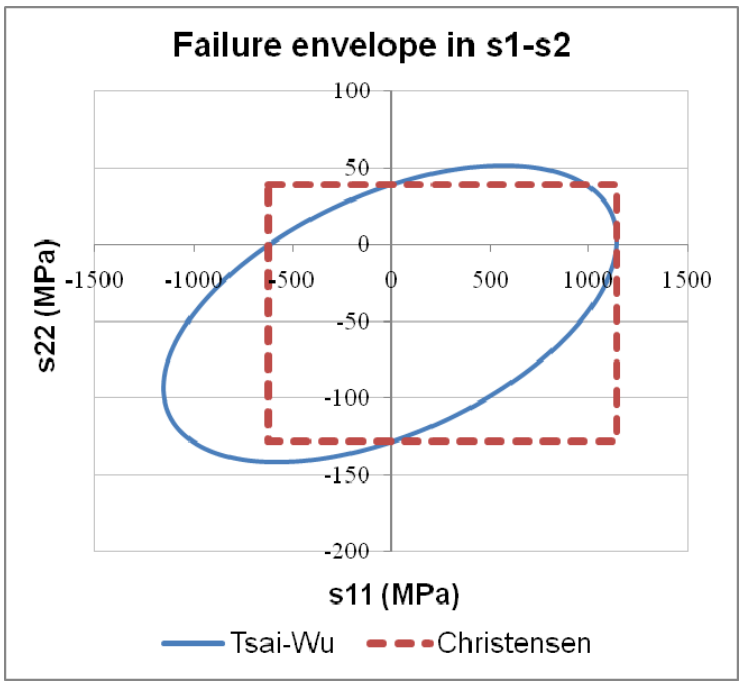

Figure 2-2 Failure envelopes for Tsai-Wu and Christensen models (glass/epoxy material).

Table 2-1 Material properties of carbon/epoxy composite [76].

Modulus in fiber direction E_1 (GPa)	147
Transverse moduli E_2= E_3 (GPa)	10.3
Shear moduli G_{12}=G_{13} (GPa)	7
Shear modulus G_{23} (GPa)	3.7
Poisson's ratios v_{12}= v_{13}	0.3
Poisson's ratio v_{23}	0.5
Longitudinal tensile strength X_T (MPa)	2280
Longitudinal compressive strength X_C (MPa)	1725
Transverse tensile strength Y_T (MPa)	57
Transverse compressive strength Y_C (MPa)	228
Out-of-plane tensile strength Z_T (MPa)	57
Out-of-plane compression strength Z_C (MPa)	228
Shear strength S_{12}=S_{13} (MPa)	75
Coefficient of thermal expansion in fiber direction α_1(/^{o}C)	-0.396×10^{-6}
Coefficients of thermal expansion in transverse directions α_2= α_3 (/^{o}C)	21.6×10^{-6}

Table 2-2 Material properties of glass/epoxy composite [76].

Modulus in fiber direction E_1 (GPa)	41
Transverse moduli E_2= E_3 (GPa)	10.4,10.4
Shear moduli G_{12}=G_{13} (GPa)	4.3
Shear modulus G_{23} (GPa)	3.5, 4.3
Poisson's ratios v_{12}= v_{13}	0.28, 0.5
Poisson's ratio v_{23}	0.28
Longitudinal tensile strength X_T (MPa)	1140
Longitudinal compressive strength X_C (MPa)	620
Transverse tensile strength Y_T (MPa)	39
Transverse compressive strength Y_C (MPa)	228
Out-of-plane tensile strength Z_T (MPa)	39
Out-of-plane compression strength Z_C (MPa)	128
Shear strength S_{12}=S_{13} (MPa)	89
Coefficient of thermal expansion in fiber direction α_1(/^{o}C)	7
Coefficients of thermal expansion in transverse directions α_2= α_3 (/^{o}C)	26

2.2.2 Micromechanics of failure (MMF)

The matrix-dominated and fiber-dominated modes of MMF were described in Chapter 1. The determinations of T_m, C_m and failure envelope for MMF model were also described in Chapter 1. For the two composite materials used in thesis which are reported in Tables 2-1 and 2-2, the value of T_m, C_m and failure envelopes can be obtained similarly.

The final failure envelope for carbon/epoxy material is shown in Figure 2-3. Two vertical boundaries on the right and left of the failure envelope are determined from the longitudinal tensile X_T and compressive strengths X_T of carbon/epoxy material. The top and bottom boundaries of the envelope are the inner boundaries of all the intersecting envelopes. As a consequence, the values T_m = 58 MPa, C_m = 228 MPa are obtained by the upper and lower intersection points of the final envelope with the vertical axis.

Similarly, the final failure envelope obtained for glass/epoxy material is shown in Figure 2-4. Two vertical boundaries on the right and left of the failure envelope are determined from the longitudinal tensile X_T and compressive strengths X_T of glass/epoxy material. The top and bottom boundaries of the envelope are the inner boundaries of all the intersecting envelopes. The values of T_m = 39 MPa, C_m = 130 MPa are obtained for glass/epoxy material.

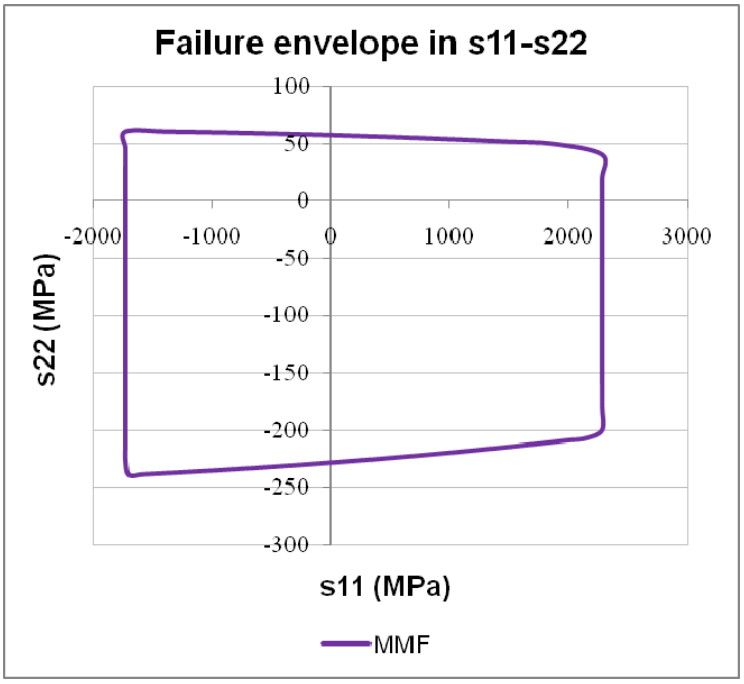

Figure 2-3 Failure envelope for MMF model (carbon/epoxy material).

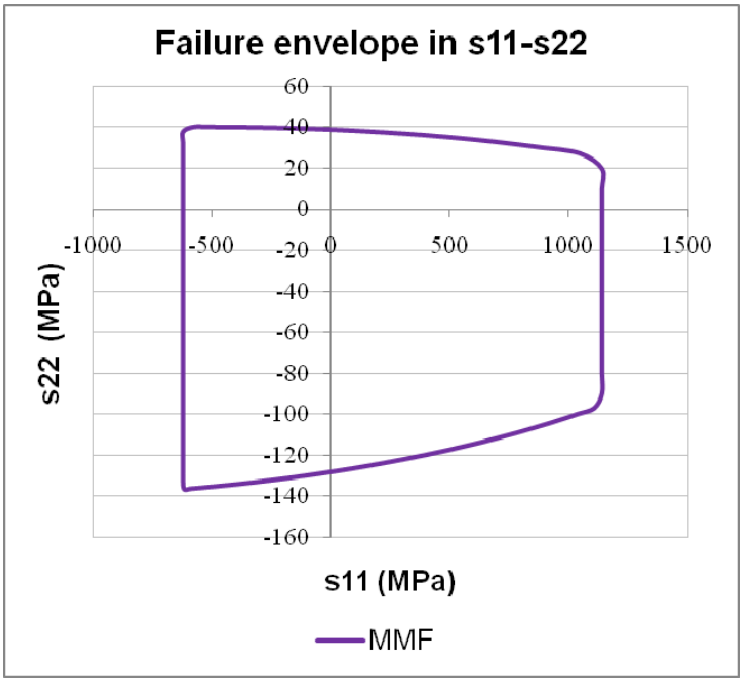

Figure 2-4 Failure envelope for MMF model (glass/epoxy material).

2.3 Continuum Damage Mechanics (CDM)

2.3.1 Determination of Y_{F1} and Y_{F2} for fiber-dominated mode

Since damage evolution in fiber direction is observed as a brittle fracture process, the damage variable d_F accounting for this damage evolution will be determined when the damage driving force Y_F exceeds the value of Y_{F1} for compression and Y_{F2} for tension (Equation 1-44). Considering the mode of pure tension along the fiber direction for a unidirectional composite, Y_F from Equation 1-42 becomes:

$$Y_F = \frac{1}{2(1-d_F)^2}\frac{{\sigma_{11}}^2}{E_1^0} \tag{2-36}$$

The values of Y_{F1} and Y_{F2} can be determined from the experimental tensile and compressive strengths X_T and X_C by:

$$Y_{F1} = \frac{{X_C}^2}{2E_1^0} \tag{2-37}$$

$$Y_{F2} = \frac{{X_T}^2}{2E_1^0} \tag{2-38}$$

For carbon/epoxy material, $Y_{F1} = 10.12\,\text{MPa}$ and $Y_{F2} = 17.68\,\text{MPa}$.

For glass/epoxy material, $Y_{F1} = 4.69\,\text{MPa}$ and $Y_{F2} = 15.85\,\text{MPa}$

2.3.2 Determination of Y_S

Y_S describes the brittle behavior of the fiber-matrix interface in transverse tension. Considering the pure in-plane transverse tension mode:

$$Y_F = 0$$

$$Y_{d2} = 0$$

$$Y_{d1} = \frac{1}{2(1-d_1)^2}\frac{\sigma_{22}^2}{E_2^0} = \frac{1}{2}E_2^0\varepsilon_{22}^{\ 2} \tag{2-39}$$

where E_2^0 is the original transverse moduli of the material.

When ε_{22} reaches the experimental failure strain E_t, the material fails either by matrix cracking or fiber/matrix debonding. Therefore Y_s can be determined by:

$$Y_S = \frac{1}{2}E_2^0 E_t^{\ 2} \tag{2-40}$$

It can be seen that Y_s is identified as the brittle damage threshold for fiber-matrix interface.

For carbon/epoxy material, $Y_S = 0.16\,\text{MPa}$.

For glass/epoxy material, $Y_S = 0.07\,\text{MPa}$.

2.3.3 Determination of $Y_{01}, Y_{02}, Y_{c1}, Y_{c2}$

- From Equation 2-39, the force in the pure in-plane transverse tension mode is:

$$Y_{d1} = \frac{1}{2} E_2^0 {\varepsilon_{22}}^2$$

The equivalent damage force is:

$$\underline{Y}(t) = \sup_{\tau \le t}(bY_{d1}(\tau)) = \frac{b}{2} E_2^0 {\varepsilon_{22}}^2 \tag{2-41}$$

The damage variable associated in this transverse tension mode is:

$$d_1 = \frac{\sqrt{\underline{Y}} - Y_{01}}{Y_{c1}} = \frac{\sqrt{\frac{b}{2} E_2^0}}{Y_{c1}} \varepsilon_{22} - \frac{Y_{01}}{Y_{c1}} \tag{2-42}$$

Y_{01} and Y_{c1} can be written in the following forms:

$$Y_{01} = \sqrt{\frac{b}{2} E_2^0 \varepsilon_{c1}} \tag{2-43}$$

$$Y_{c1} = k_1 Y_{01} \tag{2-44}$$

Then Equation (2-42) becomes:

$$d_1 = \frac{\varepsilon_{22} - \varepsilon_{c1}}{k\varepsilon_{c1}} \tag{2-45}$$

Similarly, for the pure in-plane shear loading mode, we have:

$$Y_{d2} = \frac{1}{2(1-d_2)^2}\frac{\sigma_{12}^2}{G_{12}^0} = \frac{1}{2}G_{12}^0\varepsilon_{12}^{\ 2} \tag{2-46}$$

The equivalent damage force is:

$$\underline{Y}(t) = \sup_{\tau \le t}(Y_{d_2}(\tau)) = \frac{1}{2}G_{12}^0\varepsilon_{12}^{\ 2} \tag{2-47}$$

The damage variable associated in the in-plane shear mode is:

$$d_2 = \frac{\sqrt{\underline{Y}} - Y_{02}}{Y_{c2}} = \frac{\sqrt{\frac{1}{2}G_{12}^0}}{Y_{c2}}r_2\varepsilon_{12} - \frac{Y_{02}}{Y_{c2}} \tag{2-48}$$

Y_{02} and Y_{c12} can be written in the following forms:

$$Y_{02} = \sqrt{\frac{1}{2}G_{12}^0}\varepsilon_{c2} \tag{2-49}$$

$$Y_{c2} = k_2 Y_{02} \tag{2-50}$$

Then Equation (2-48) becomes:

$$d_2 = \frac{\varepsilon_{12} - \varepsilon_{c2}}{k\varepsilon_{c2}} \tag{2-51}$$

- The stress in transverse direction is expressed by:

$$\sigma_2 = E_2^0(1-d_1)\varepsilon_{22} = E_2^0\left(1 - \frac{\varepsilon_{22} - \varepsilon_{c1}}{k_1\varepsilon_{c1}}\right)\varepsilon_{22} \tag{2-52}$$

When ε_{22} reaches the failure strain E_t, σ_2 will reach the transverse tensile strength Y_T of composites. The Equation (2-46) becomes:

$$E_2^0\left(1 - \frac{E_t - \varepsilon_{c1}}{k_1\varepsilon_{c1}}\right)E_t = Y_T$$

$$k_1 = \frac{(E_t - \varepsilon_{c1})E_t E_2^0}{\varepsilon_{c1}(E_t E_2^0 - Y_T)} \tag{2-53}$$

- Similarly, the in-plane shear stress is expressed by:

$$\sigma_2 = \sigma_{12} = G_{12}^0(1-d_2)\varepsilon_{12} = \sigma_{12} = G_{12}^0\left(1 - \frac{\varepsilon_{12} - \varepsilon_{c2}}{k\varepsilon_{c2}}\right)\varepsilon_{12} \tag{2-54}$$

When ε_{12} reaches the failure strain E_s, σ_{12} will reach the in-plane shear strength S_{12} of composites. The Equation (2-54) becomes:

$$G_{12}^{0}\left(1-\frac{E_s-\varepsilon_{c2}}{k\varepsilon_{c2}}\right)E_s=S_{12}$$

$$k_2=\frac{\left(E_s-\varepsilon_{c2}\right)E_sG_{12}^{0}}{\varepsilon_{c2}\left(E_sG_{12}^{0}-S_{12}\right)} \tag{2-55}$$

2.3.4 Determination of b

The parameter *b* is a coupling coefficient between transverse tension damage force and shear damage force. When the material is about to fail, both tension stiffness loss and shear stiffness loss should be at the critical value. Therefore when the matrix is failed by shear, its tensile stiffness should also be fully degraded.

$b * \max(Y_{d1}) = \max(Y_{d2})$

$$\max(Y_{d1})=\frac{1}{2}E_{22}^{0}E_t^{\,2}$$

$$\max(Y_{d2})=\frac{1}{2}G_{12}^{0}E_S^{\,2}$$

Hence, b can be determined:

$$b=\frac{G_{12}^{0}E_S^{\,2}}{E_2^{0}E_t^{\,2}} \tag{2-56}$$

Overall, with the value of transverse tensile strain E_t and in-plane shear strain E_s, the values of k_1, k_2, b can be obtained in Equations 2-54, 2-55 and 2-56. The values of $Y_{01}, Y_{02}, Y_{c1}, Y_{c2}$ are then determined by Equations 2-43, 2-44, 2-49 and 2-50. The values of all parameters calculated for carbon/epoxy and glass/epoxy materials are summarized in Table 2-3.

Table 2-3 Values of parameters used in CDM models for carbon/epoxy and glass/epoxy materials.

	Carbon/epoxy material	**Glass/epoxy material**
Critical tensile damage force in fiber direction Y_{F1} (MPa)	10.12	4.69
Critical compressive damage force in fiber direction Y_{F2} (MPa)	17.69	15.85
Brittle damage threshold for fiber-matrix interface Y_S (MPa)	0.16	0.07
Transverse tensile failure strain E_t	0.0055	0.0038
Shear failure strain E_s	0.01	0.02
Coupling coefficient b	2.25	11.45
k_1	6.17	5.83
k_2	17.94	17.94
Transverse tension damage starting force Y_{01} (MPa)	0.19	0.13
Y_{c1} (MPa)	1.17	0.75

Shear damage starting force Y_{02} (MPa)	0.13	0.19
Y_{c2} (MPa)	2.33	3.4

2.4 Modification of continuum damage mechanics (CDM) and Christensen models

2.4.1 Modification of CDM model

Generally, different criteria have different modeling strategies for matrix-dominated and fiber-dominated modes. The Tsai-Wu, Christensen and MMF do not predict the gradual failure of local matrix but only predict the matrix either intact or completely failed. In contrast, the CDM can predict the initial matrix damage and describes a gradual stiffness degradation of the material stiffness which results in a nonlinear stress-strain response. However, all of these failure criteria do not consider the progressive failure of local fiber and just model the fiber failure by completely degrading all the stiffnesses of the failed elements. As can be seen in fracture mechanics, whenever a fracture develops, a certain amount of energy or fracture energy is dissipated to form new surfaces. That means the stiffnesses of the failed elements are gradually degraded so that the total energy dissipation will be equal to the fracture energy. This fracture energy is described by the area under the softening curve. It can be observed that conventional failure models such as Tsai-Wu, Christensen, CDM and MMF models do not take into consideration the fracture process after the fiber failure. Therefore, modified version of the

CDM (called MCDM) is introduced by modeling the fracture process from the initiation of fiber failure until the ultimate failure [77].

Similar to the CDM model, the MCDM model described the matrix-dominated damage by thermal forces and damage variables d_1, d_2.

Thermo forces:

$$Y_F = \frac{\partial}{\partial d_F} E_D \Big|_{\sigma, d_F}$$
$$= \frac{1}{2(1-d_F)^2}\left(\frac{\sigma_{11}^2}{E_{11}^0} - \left(\frac{\nu_{12}^0}{E_{11}^0} + \frac{\nu_{21}^0}{E_{22}^0}\right)\sigma_{11}\sigma_{22} - \left(\frac{\nu_{13}^0}{E_{11}^0} + \frac{\nu_{31}^0}{E_{33}^0}\right)\sigma_{11}\sigma_{33} - \left(\frac{\nu_{32}^0}{E_{33}^0} + \frac{\nu_{23}^0}{E_{22}^0}\right)\sigma_{33}\sigma_{22}\right)$$

$$Y_{d_1} = \frac{\partial}{\partial d_1} E_D \Big|_{\sigma, d_1} = \frac{1}{2(1-d_1)^2}\left(\frac{\sigma_{22}^2}{E_{22}^0} + \frac{\sigma_{33}^2}{E_{33}^0}\right),$$

$$Y_{d_2} = \frac{\partial}{\partial d_2} E_D \Big|_{\sigma, d_2} = \frac{1}{2(1-d_2)^2}\left(\frac{\sigma_{12}^2}{G_{12}^0} + \frac{\sigma_{23}^2}{G_{23}^0} + \frac{\sigma_{13}^2}{G_{13}^0}\right),$$

An equivalent damage force is introduced as:

$$\underline{Y}(t) = \sup_{\tau \le t}(Y_{d_2}(\tau) + bY_{d_1}(\tau))$$

Matrix-failure in transverse direction:

$$\begin{cases} d_1 = \dfrac{\left\langle \sqrt{\underline{Y}} - Y_{01} \right\rangle_+}{Y_{c1}} & \text{if } Y_{d1} < Y_S \\ d_1 = 1 \text{ otherwise} \end{cases}$$

Matrix-failure in shear direction:

$$\begin{cases} d_2 = \dfrac{\left\langle \sqrt{\underline{Y}} - Y_{02} \right\rangle_+}{Y_{c2}} & \text{if } Y_{d1} < Y_S \\ d_2 = 1 \text{ otherwise} \end{cases}$$

where parameters $b, Y_{01}, Y_{02}, Y_{c1}, Y_{c2}, Y_S$ in the MCDM model are determined similarly as in the CDM model.

However, the fiber failure modeling in the MCDM model is different from the CDM model. For elements that are failed by fiber-dominated mode, the CDM model will completely degrade all the stiffnesses of those elements whereas the MCDM model gradually degrades their stiffnesses. The damage variable accounting for this gradual degradation d_f' in the MCDM model evolves from zero for no damage to unit for complete damage while the damage variable d_f in the CDM model has only two values which is zero for no damage and unit for complete damage. The failure modeling strategies of the CDM and MCDM models are shown in Figure 2.5.

In the MCDM model, defining ε_0 as the damage strain when fiber damage initiates and ε_f as the critical strain when fiber is completely failed and assume a linear softening stress-strain response after the initiation of fiber damage (Figure 2-5.b), the damage variable d_f' accounting for the degradation scheme of fiber is expressed by Equation (2-61). d_f' will be zero when ε_{11} equals to ε_0 and approach unit when ε_{11} equals to ε_f.

$$d_f' = 1 - \frac{\varepsilon_0}{\varepsilon_{11}} * \frac{\varepsilon_f - \varepsilon_{11}}{\varepsilon_f - \varepsilon_0} \tag{2-61}$$

where ε_0 and ε_f can be derived from the composite strength X_t, elastic modulus E_1, fracture energy G_{IC} and a characteristic element length (l_e) by:

$$\varepsilon_0 = \frac{X_t}{E_1} \tag{2-62}$$

$$\varepsilon_f = \frac{2G_{Ic}}{X_t l_e} \tag{2-63}$$

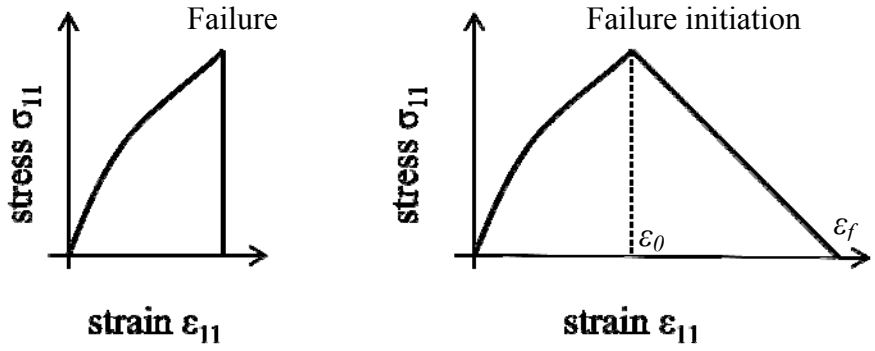

a. CDM model b. MCDM model

Figure 2-5 Failure modelling strategies in CDM and MCDM models.

2.4.2 Modification of Christensen model

Based on the same idea as the modified CDM model, the author has implemented a modified Christensen model by describing a fracture process for the fiber failure in Christensen criterion [14]. The modified version of

Christensen model, called MChristensen, is still based on the same matrix-dominated and fiber-dominated modes as Christensen criterion:

Matrix-dominated mode:

$$\left(\frac{1}{Y_t}-\frac{1}{Y_c}\right)(\sigma_{22}+\sigma_{33})+\frac{1}{Y_tY_c}(\sigma_{22}+\sigma_{33})^2+\frac{1}{S^2}\left(\sigma_{23}^2-\sigma_{22}\sigma_{33}\right)+\frac{1}{S^2}\left(\sigma_{12}^2+\sigma_{13}^2\right)\le 1$$

Fiber-dominated mode:

$$-X_c \le \sigma_{11} \le X_t$$

However, once fiber failure is predicted, the MChristensen model will gradually degrade the stiffness of the failed elements while the Christensen model quickly and completely degrades the stiffness of the failed elements. The difference between failure modeling strategies of the Christensen and MChristensen models are shown in Figure 2.6.

Denoting ε_0 as the damage strain when fiber damage initiates and ε_f as the critical strain when fiber is completely failed and assuming a linear softening stress-strain response after the initiation of fiber damage, the damage variable d_f in the MChristensen model evolve from 0 for no damage to 1 for complete damage:

$$d_f' = 1-\frac{\varepsilon_0}{\varepsilon_{11}} * \frac{\varepsilon_f-\varepsilon_{11}}{\varepsilon_f-\varepsilon_0}$$

The stiffness of the failed elements in fiber direction will be degraded accordingly:

$$E_{11}^{\ 0} = (1 - d_f)E_{11}$$

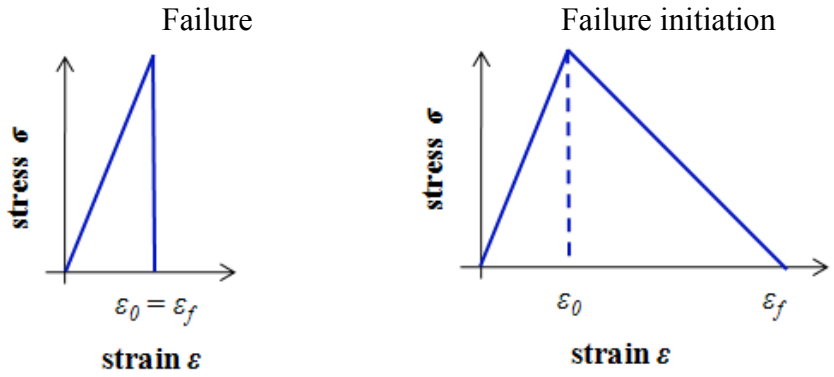

a. Christensen model b. MChristensen model

Figure 2-6 Fiber failure modelling strategies in Christensen and MChristensen models.

2.5 Cohesive element method

The principles of the cohesive element method are based on the traction-separation law. The traction-separation law was earlier proposed by Tvergaard and Hutchinson [78]. They computed crack growth resistance for an elastic-plastic solid where the traction-separation law was ideally specified on the crack plane to characterize the fracture process. The primary parameters were the work of separation per unit area Γ_0, the interface strength $\hat{\sigma}$ and shape parameters $\delta_1, \delta_2, \delta_C$. The traction separation relation used to model the

fracture process is shown in Figure 2-7. According to Tvergaard and Hutchinson, the work of separation per unit area was:

$$\Gamma_0 = \int_0^{\delta_c} \sigma . d\delta = \frac{1}{2}\hat{\sigma}\left(\delta_c + \delta_2 - \delta_1\right) \tag{2-64}$$

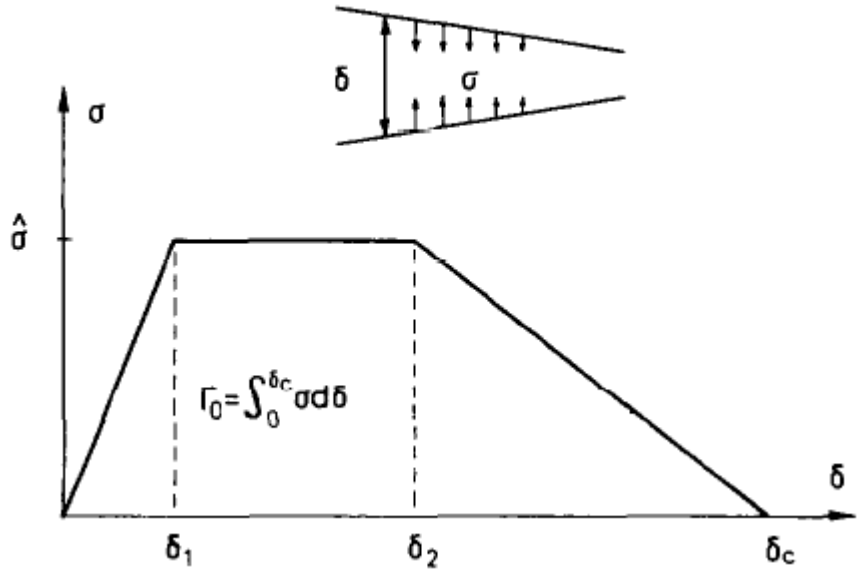

Figure 2-7 Traction-separation relation for fracture process.

In this thesis, cohesive elements are implemented as interface layers between plies. The cohesive element behavior is based on the assumption that the elements are characterized by progressive degradation of the material stiffness, which is driven by a damage process. Before the initiation of damage, elastic behavior is assumed and described by the relation of nominal stresses and nominal strains across the interface. These nominal stresses $t_n, t_{s,} t_t$ are the force components divided by the original area at each integration point, while the nominal strains $\varepsilon_n, \varepsilon_{s,} \varepsilon_t$ are the separations $\delta_{n,} \delta_{s,} \delta_t$ divided by the original

thickness T_0 of the cohesive element at each integration point. The relationship between nominal stresses and nominal strains is therefore expressed by:

$$\begin{bmatrix} t_n \\ t_s \\ t_t \end{bmatrix} = \begin{bmatrix} K_{nn} & & \\ & K_{ss} & \\ & & K_{tt} \end{bmatrix} \begin{bmatrix} \varepsilon_n \\ \varepsilon_s \\ \varepsilon_t \end{bmatrix} \tag{2-65}$$

$$\varepsilon_n = \frac{\delta_n}{T_0} \qquad \varepsilon_s = \frac{\delta_s}{T_0} \qquad \varepsilon_t = \frac{\delta_t}{T_0} \tag{2-66}$$

where determination of cohesive stiffnesses K_{nn}, K_{ss}, K_{tt} will be described later in this section. For prediction of the initiation of delamination, a stress-based quadratic criterion proposed by Hou *.et. al* [53] is selected. According to this delamination criterion, the initiation of interface damage is controlled by the normal interface stress t_n, and two shear interface stresses t_s, t_t and the cohesive strengths N, S, and T by the equation:

$$\left(\frac{t_n}{N}\right)^2 + \left(\frac{t_s}{S}\right)^2 + \left(\frac{t_t}{T}\right)^2 = 1 \tag{2-67}$$

For the propagation of delamination, a fracture mechanics-based criterion is used:

$$\left(\frac{G_n}{G_n^c}\right) + \left(\frac{G_s}{G_s^c}\right) + \left(\frac{G_t}{G_t^c}\right) = 1 \tag{2-68}$$

where G_n, G_s, and G_t are the work done by the tractions and their relative displacements in the normal and shear directions respectively. Quantities with superscript C denote the critical strain energy release rates corresponding to each fracture mode.

When delamination initiation is predicted by Hou *et al* by using Equation 2-67, the delamination evolution law of Equation 2-68 is used to determine the rate at which the material stiffness is degraded. A scalar damage variable D representing the state of damage in the material is defined; it is assigned a value of 0 for material in undamaged state, and acquires a value of 1 for completely damaged material. The post-initiation traction-separation model is therefore:

$$t_n = (1 - D)\bar{t_n} \tag{2-69}$$

$$t_s = (1 - D)\bar{t_s} \tag{2-70}$$

$$t_t = (1 - D)\bar{t_t} \tag{2-71}$$

where $\bar{t_n}, \bar{t_s}, \bar{t_t}$ are the stress components prior to damage predicted by the elastic traction-separation behavior for the current strains. In the Abaqus theory manual [79], the damage variable D is related to the effective displacement by various material softening laws.

The effective displacement is defined as

$$\delta_m = \sqrt{\delta_n^2 + \delta_s^2 + \delta_t^2} \tag{2-72}$$

where δ_n, δ_s and δ_t are the normal, and two shear displacements, respectively. Defining δ_m^0 and δ_m^f are the effective displacements at the initiation of damage and complete failure, respectively, the damage variable *D* is explicitly related to the effective displacements by:

$$D = 1 - \left\{ \frac{\delta_m^0}{\delta_m^{\max}} \right\} \left\{ 1 - \frac{1 - \exp\left(-\alpha \dfrac{\delta_m^{\max} - \delta_m^0}{\delta_m^f - \delta_m^0} \right)}{1 - \exp(-\alpha)} \right\} \tag{2-73}$$

The exponent $\alpha = 1$ is chosen in this thesis for simplicity.

Initial stiffnesses and interface strengths are necessary input parameters for the cohesive elements. The values of the initial stiffnesses (Equation 2-65) are calculated from the assumed thickness and modulus of the cohesive elements. Although the thickness of the cohesive layer is generally assigned a small enough value, if the assumed value is too small, computational time and convergence may become a problem. Once the thickness is specified, the three stiffness components for the cohesive elements can be estimated by the ratio of the modulus of cohesive layer and interface thickness:

$$K_{nn} = K_{ss} = K_{tt} = \frac{E}{T_0} \tag{2-74}$$

In Equation 2-74, the interface modulus E of the cohesive element is assumed to be that of typical epoxy resin and is given a value of 4 GPa, while the thickness of the cohesive element is given a value of 0.005mm. This thickness is referred to recent work of Hallett and Wisnom [4], Hansen and Lund [82] and it is found to give acceptably accurate results within reasonable computation time. If the thickness is chosen very small and close to zero, the computational time will be much longer and convergence is not guaranteed. In contrast, when the thickness is made bigger and close to the ply thickness, the results become less accurate. The author has chosen a thickness of 0.005mm which is approximately one twentieth of the ply thickness. A variation of cohesive thickness was reported by Blackman and Hadivina [83] who numerically investigated a DCB composite beam under bending when cohesive thickness ranges from 0.0001 to 0.5 mm. The results showed that there was no difference on the predicted ultimate loads when cohesive thickness varied from 0.0001 mm to 0.05 mm. Other results showed that the predicted did not converge when cohesive thickness varied from 0.05 mm to 0.5 mm.

For delamination onset, the values for cohesive strength parameters N, S, and T in the Hou criterion (Equation 2-67) are estimated from a study by Brewer and Lagace [52], which found that the transverse normal strength and shear strengths of a unidirectional composite are good approximations for the interlaminar normal strength N and interlaminar shear strengths S and T respectively. It is therefore assumed that the values N = 39 MPa and $S = T$ = 89 MPa for delamination modeling of glass/epoxy laminates. Besides, the

values $N = 60$ MPa and $S = T = 68$ MPa referred to Camanho and Davilla [80] are assumed for carbon/epoxy AS4/3501-6 composite material.

For delamination propagation, values of the critical strain energy release rates (SERRs) from Petrossian and Wisnom [81] are used for glass/epoxy material. They have obtained fracture toughness values $G_n = G_{IC} = 0.25$ N/mm and $G_s = G_t = G_{IIC} = 1.08$ N/mm from double cantilever beam and end-notched flexure tests for E-glass/epoxy specimens. On the other hand, referred to Camanho and Davila [80] for carbon/epoxy composite material, the SERRs $G_{IC} = 0.075$ N/mm and $G_{IIC} = G_{IIC} = 0.547$ N/mm are assumed for delamination propagation.

Chapter 3

Experimental and computational investigation of Double-notched carbon/epoxy laminates

Composite materials show significant sensitivity to notches when loaded in tension, especially when the effect of notches changes with different composite layups. A careful study of double-notched tension specimens with different layups is therefore important and needs to be investigated. In this chapter, presented are the experimental and computational results of notched $[90/0]_s$ and $[45/90/-45/0]_s$ carbon/epoxy laminates. The cross-ply laminate ($[90/0]_s$) is chosen since it is widely used in research and industry while the quasi-isotropic laminate ($[45/90/-45/0]_s$) is more general and comprises of four different ply orientations. The tensile tests have been first performed on cross-ply and quasi-isotropic laminates following the ASTM D5379 to observe the damage patterns and obtain the experimental failure loads. The simulations of various failure models are then carried out on cross-ply and quasi-isotropic carbon/epoxy laminates and validated against the experimental results.

3.1 Experimental and computational investigation of double-notched $[90/0]_s$ carbon/epoxy laminate

3.1.1 Experiment of notched $[90/0]_s$ carbon/epoxy laminate

* Sample preparation:

- Making the $[90/0]_s$ composite laminate by laying up unidirectional prepregs in desired orientations. (Figure 3-1a). The prepregs have a thickness of 0.125 mm and are made from carbon fiber-reinforced epoxy composite whose material properties were reported in Table 2-1.
- Curing the composite laminate in Autoclave (Figure 3-1b).
- Cutting notched specimens from the laminate by Waterjet technique.
- The notched specimens are cut following the ASTM D5379 [84]. The specimens have a width of 20 mm, a gauge length of 100 mm excluding a gripping length of 50 mm from each top and bottom of specimens. Two notches of 60^0 were made on either side of specimens. ASTM D5379 recommends a notch root radius of 1.3 mm in order to minimize the stress concentration at the notch roots, and thus promote a more uniform stress distribution along the notch-root axis. Therefore, the notches of specimens were made blunt and approximated to have a straight edge of 1mm at the tips (Figure 3-2).

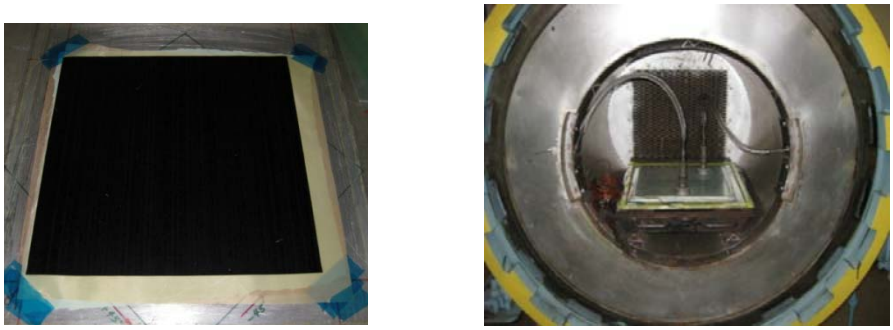

a. Composite Laminate b. Laminate cured in Autoclave

Figure 3-1 The composite laminate made from prepregs (a) and cured in Autoclave (b)

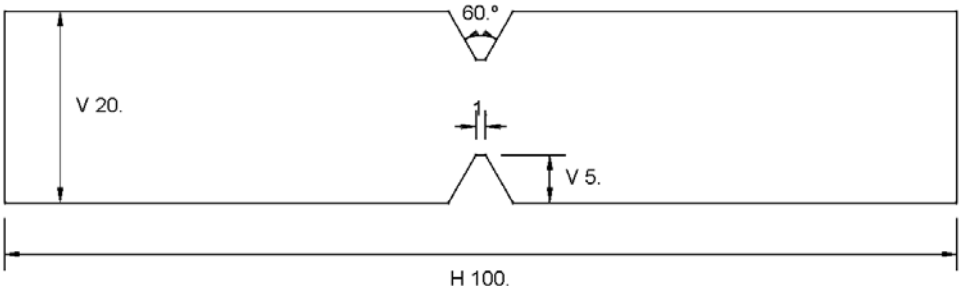

Figure 3-2 Dimensions of specimens of the $[90/0]_s$ carbon/epoxy laminate.

* Strain gauge set-up:

Strain gauges (GFLA-3-50) were attached to notched $[90/0]_s$ specimens to measure the longitudinal strain of specimens during the tensile testing. Only the strain gauge located away from the notch (corresponding to a gauge length of 90 mm) was used to obtain the longitudinal strain (Figure 3-3). Assuming that the strain at the top of the specimen (corresponding to a gauge length of 100mm) is similar to this strain, the displacement at the top of the specimen corresponding to the gauge length of 100 mm can be obtained and then plotted versus the applied load of the experiment.

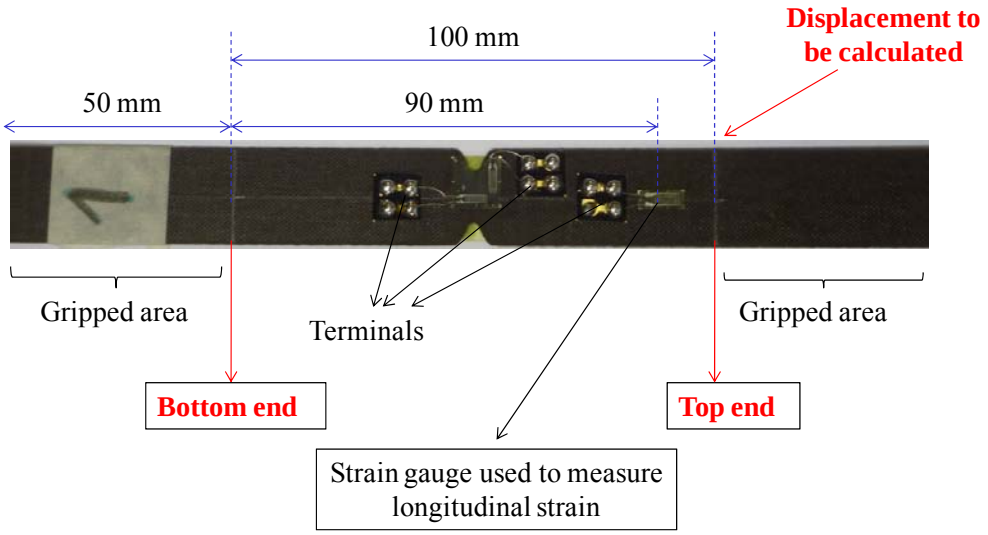

Figure 3-3 Strain gauge setup for $[90/0]_s$ notched specimens.

* Experimental set-up and procedure:

Five notched $[90/0]_s$ specimens were tested in tension by Shimadzu machine AG-25TB at a constant rate of displacement of 1 mm/min (Figure 3-4). This rate was referred to the displacement rate used for the tensile testing of $[90/0]_s$ glass/epoxy specimens with the same geometry by Hallett and Wisnom [74]. The use of a displacement rate smaller than 1 mm/min may provide more data for the load-strain or load-displacement curves than a large rate and help observe the damage development in specimens more carefully. However, since the damage patterns of carbon/epoxy specimens cannot be seen clearly without using X-ray radiography, the use of very small rate is not really needed. Only the final damage patterns will be analyzed and compared to simulation results. The experiment procedure is as follows:

- Clamping the specimens on Shimadzu machine AG-25TB (Figure 3-5).
- Connecting the wires from the terminals to the strain reader.
- Turning on the Shimadzu machine AG-25TB.
- Calibrating initial displacement and load.
- Specifying a displacement rate of 1mm for the upper load cell while the lower cell is fixed.
- Starting the machine to pull the notched specimen.
- Observing the failure behaviors and recording strain data.
- After the specimens are broken, removing the specimens from the machine.
- Turning off the machine.

- Converting the strain near the top of the specimen to the displacement over the entire gauge length of 100 mm and assess the displacement errors.
- Plotting the load vs. displacement curves of all the notched specimens.

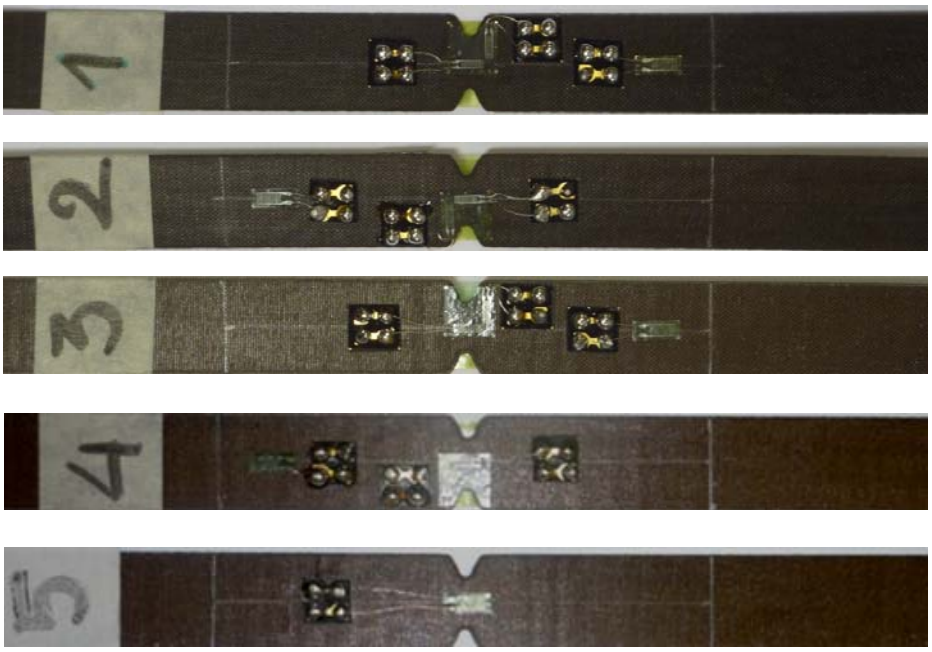

Figure 3-4 $[90/0]_s$ carbon/epoxy specimens for testing.

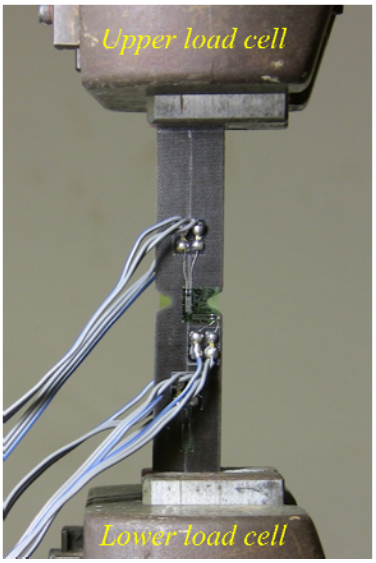

Figure 3-5 Experiment setup for $[90/0]_s$ notched specimens.

* Experimental result:

Failures of notched $[90/0]_s$ specimens after testing and their load-displacement curves are presented in Figure 3-6 and Figure 3-7, respectively. The critical displacement and failure loads of specimens are summarized in Table 3-1. Damage can be seen to initiate at each of the notch root and propagate across the width of the specimens. The final failure occurs when damage extensively develop all the way through the width of the specimens, breaking the specimens into two halves. This final failure can be observed by fiber breakages in the middle of the specimens. Besides, there is no clear delamination observed in these specimens.

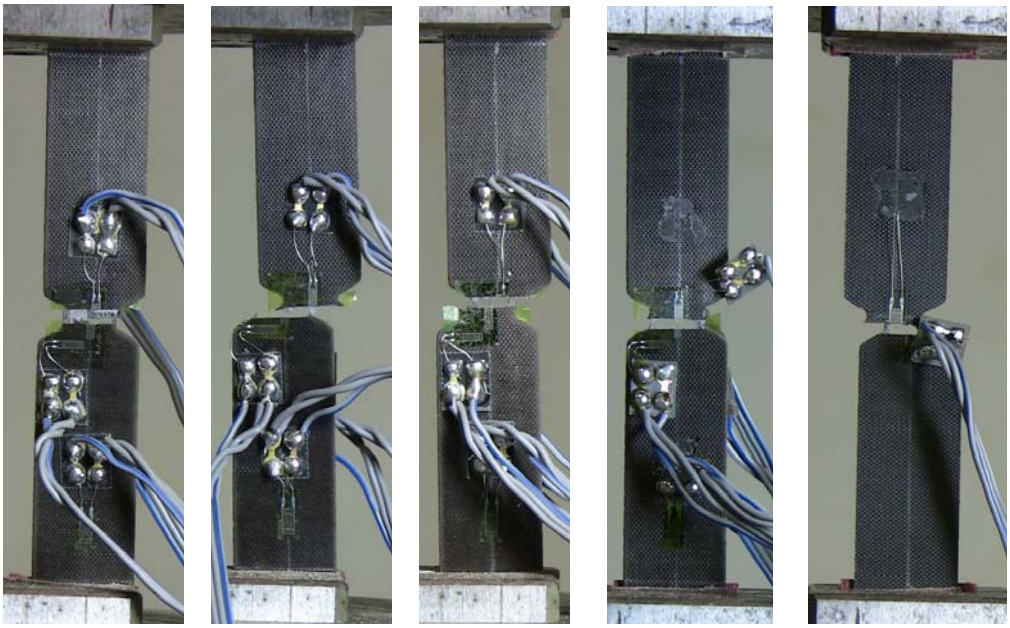

Figure 3-6 Failure of notched $[90/0]_s$ specimens after testing.

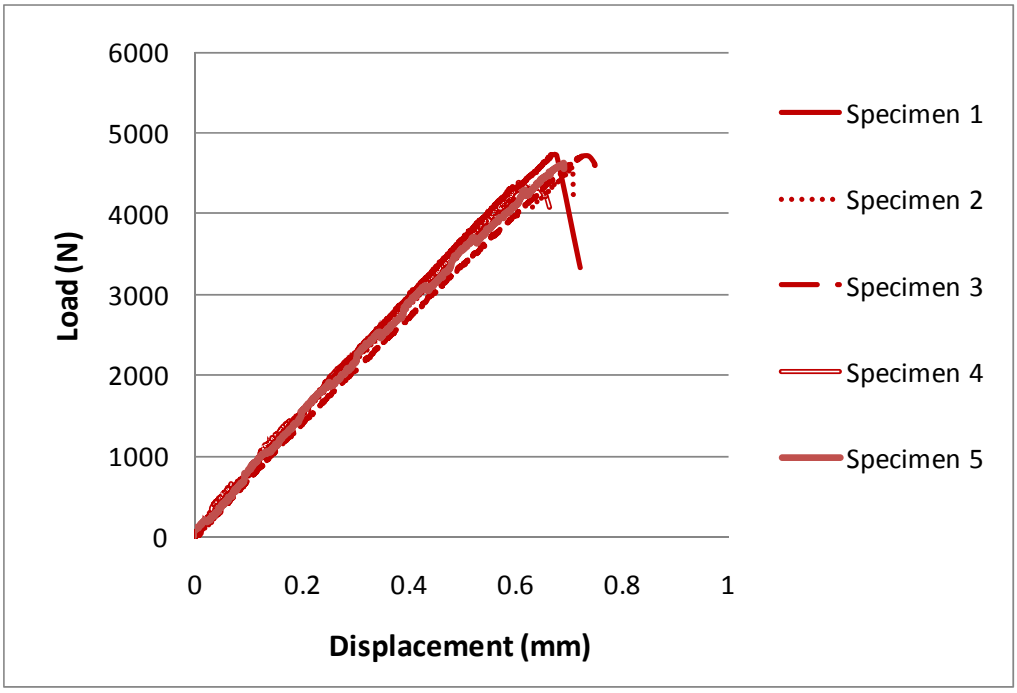

Figure 3-7 Load-displacement curves of notched $[90/0]_s$ specimens.

Table 3-1 Critical displacements (u_{crit}) and failure load (F_{crit}) of $[90/0]_s$ specimens

Specimen	u_{crit} **(mm)**	Δu_{crit} **(mm)**	F_{crit} **(N)**	ΔF_{crit} **(N)**
1	0.722138	0.014051	4823.6	119.28
2	0.71045	0.002364	4686.4	17.92
3	0.750425	0.042339	4804	99.68
4	0.6648	0.043287	4482	222.32
5	0.69262	0.015466	4725.6	21.28
Average	**0.708** ± 0.023		**4704.3** ± 96	

3.1.2 Progressive failure analysis of notched $[90/0]_s$ carbon/epoxy laminate

Because of the symmetry of the specimen, only one quarter of the specimen is modeled for the cross-ply layup. The boundary conditions and mesh of the finite element (FE) models are shown in Figure 3-8. The FE models of the notched specimens are built with 8-node three-dimensional continuum shell elements (SC8R) and 8-node hexahedral cohesive elements COH3D8 with one element in the thickness per ply. The analysis is carried out by the implicit solver of commercial software Abaqus 6.9. The ply thickness is 0.125mm and the cohesive element thickness is assumed 0.005 mm. Six failure models are used to predict the progressive failure of notched $[90/0]_s$ carbon/epoxy laminate including models of Tsai-Wu, Christensen, micromechanics of failure (MMF), continuum damage mechanics (CDM), modified version of continuum damage mechanics (MCDM) and modified version of Christensen model (MChristensen). In these models, the MPDM with degradation factor $D_i = 10^{-6}$ is used. In addition, cohesive elements are used to model the delamination at the interfaces. As discussed in chapter 2, all the parameters of cohesive elements for carbon/epoxy material are referred to Camanho and Davila [80] in which cohesive strengths $N = 60$ MPa, $S = T = 68$ MPa and strain energy release rates (SERRs) $G_{IC} = 0.075$ N/mm and $G_{IIC} = G_{IIC} = 0.547$ N/mm are assumed for delamination modeling.

A comparative study of various failure models for the $[90/0]_s$ composite laminate is performed. The predicted applied load *vs.* displacement curves are

shown in Figure 3-9 and compared to the experimental data. The damage patterns predicted by all failure models are shown in Figures 3-10 to 3-20. All the predicted damage patterns for the initiation and propagation of fiber failure agree well with the experimental observation while the matrix damage between simulation and experiment cannot be compared because the carbon/epoxy material is very dark. Additionally, it can be seen that all the failure models predict the experimental failure loads well, among which the models of CDM, MCDM and MChristensen slightly over predict the experimental failure loads while the others predict very close to the experiment. However, modeling of the failure in the 90^0 ply may be too conservative. Since quite numerous transverse cracks are predicted in the 90^0 ply before the final failure which is determined by the fiber failure in the 0^0 ply, the 90^0 ply almost lost its stiffnesses at early stage, thus resulting in a decrease in the global stiffness of composite. This decrease in global stiffness may explain for the discontinuity of the curves in Figure 3-9 and cause the critical displacements predicted by all models larger than the critical displacement in experiment.

The progressive failure patterns predicted by the Christensen model are demonstrated in Figures 3-10 to 3-15. Figure 3-10 shows that matrix cracks and splits both initiate from the notch tip at 10% maximum load and then grow upward along the vertical direction (Figure 3-11). As the applied tensile load is increased by 15% maximum load, the matrix cracks in 90^0 ply start to grow in the transverse direction (Figure 3-12) and the 90^0 ply quickly becomes saturated with numerous transverse cracks at 20% maximum load (Figure 3-

13). In Figure 3-13, the 90^0 ply has effectively exhausted its load-carrying capability, the longitudinal splits in the 0^0 ply have greatly increased in length, and fiber failure has been initiated from the notch roots accompanied by additional splitting in the 0^0 ply. Thereafter, very quick propagation of fiber failure takes place in the 0^0 ply and delamination at the [90/0] interface occurs (Figure 3-15). The final load drop is precipitated by significant fiber failure in the 0^0 ply. The predicted ultimate load by Christensen model is very close to the experiment.

The progressive failure patterns using Tsai-Wu's theory follow those of Christensen theory closely. Matrix-dominated failure dominates the 90^0 ply and longitudinal splits in the 0^0 ply initiate and propagate from the notch roots by the Tsai-Wu model very similarly to the Christensen model. Therefore, only the damage pattern after the major load drop is shown. Figure 3-16 shows the final damage pattern of the Tsai-Wu model. The final failure is caused by lots of fiber failure in the middle of the 0^0 ply and extensive matrix cracks in the 90^0 ply. It has been found that the Tsai-Wu model predicts more splitting in the 0^0 ply and delamination at the 90/0 interface than the Christensen model. The ultimate load by the Tsai-Wu model under-predicts the experiment by 6.8%.

The result for MMF is shown in Figure 3-17. Only the damage patterns just after the major load drop are shown because the initiation and propagation of matrix-dominated failure in the 90^0 ply and initiation of longitudinal splits in the 0^0 ply are very similar to the Tsai-Wu and Christensen cases. However,

much more damage in the 90^0 and 0^0 plies is predicted by the MMF model than the Tsai-Wu and Christensen models while little delamination are found. The ultimate load by MMF model under-predicts the experiment by 3.7%.

The final failure patterns predicted by the CDM, MCDM and MChristensen models are shown in Figures 3-18 to 3-20 and follow those of Christensen, Tsai-Wu and MMF models. Unlike the MMF model, more delamination is predicted by CDM, MCDM and MChristensen models. The ultimate loads predicted by CDM, MCDM and MChristensen models over-predict the experiment by about 2% and 5% and 6%, respectively. All the simulation results predicted by these failure models correlate well with the experiment.

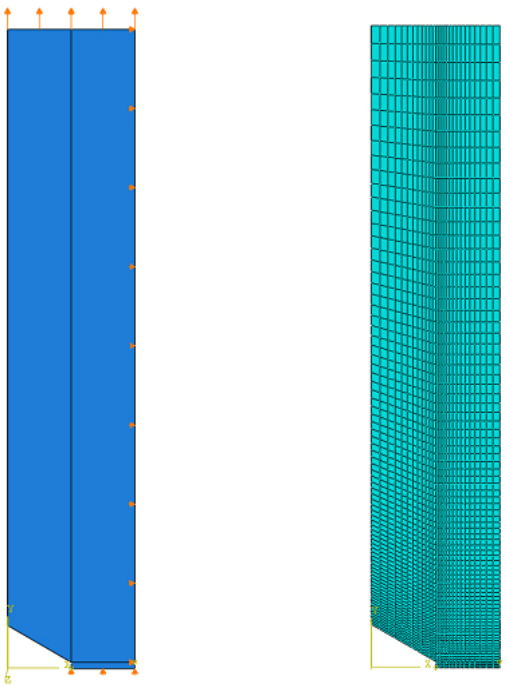

Figure 3-8 Boundary conditions and mesh of the finite element model for $[90/0]_s$ carbon/epoxy specimens.

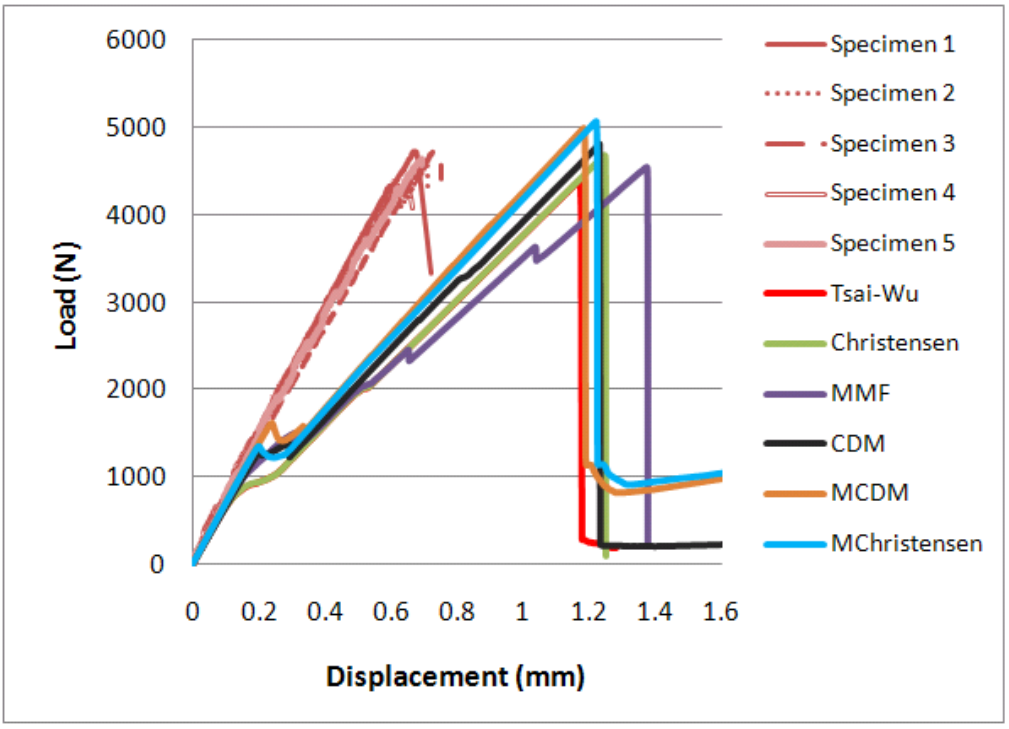

Figure 3-9 Predicted load-displacement curves and comparison with the experiment for the $[90/0]_s$ carbon/epoxy laminate.

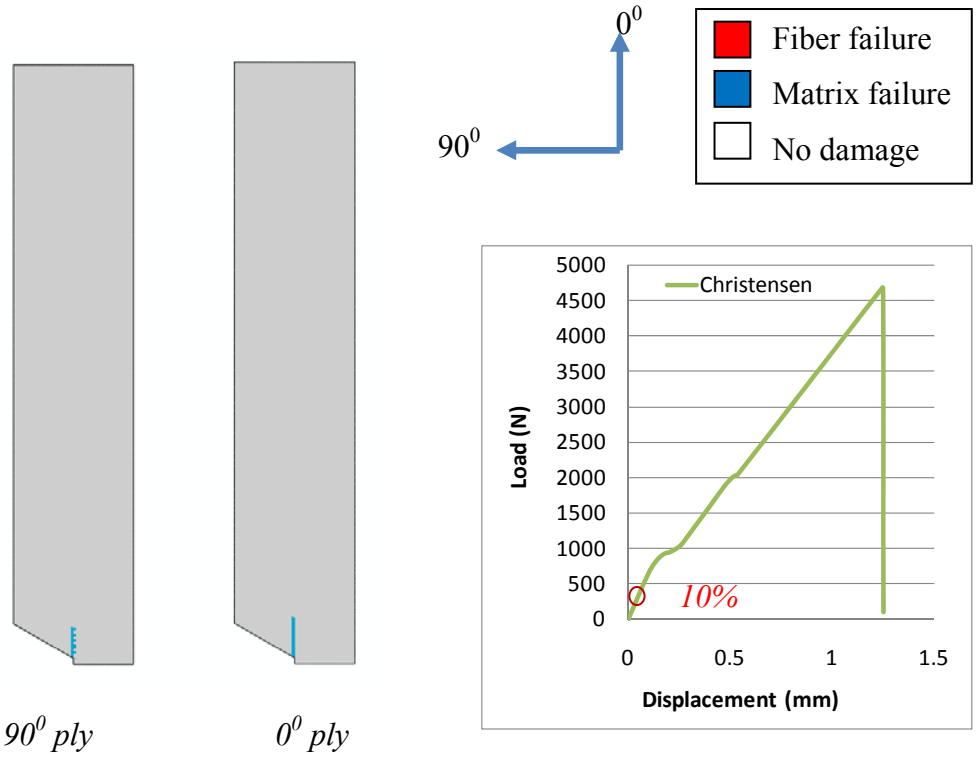

Figure 3-10 Christensen: Initiation of transverse matrix cracking in the 90^0 ply and longitudinal splitting in the 0^0 ply (10% maximum load).

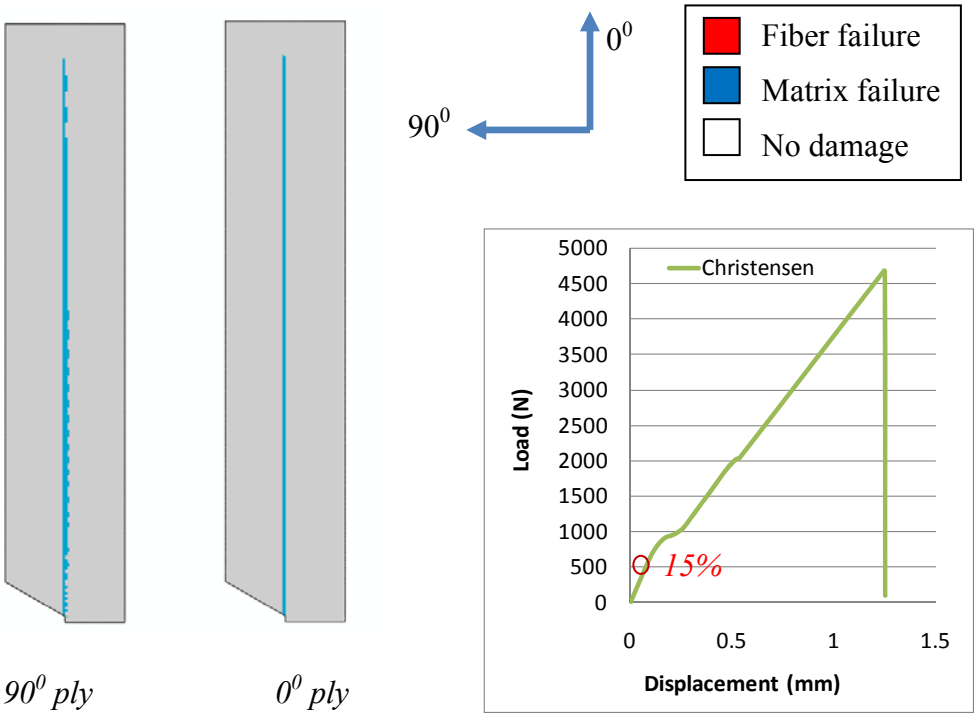

Figure 3-11 Christensen: Extension of matrix cracking in the 90^0 ply and longitudinal splitting in the 0^0 ply (15% maximum load)

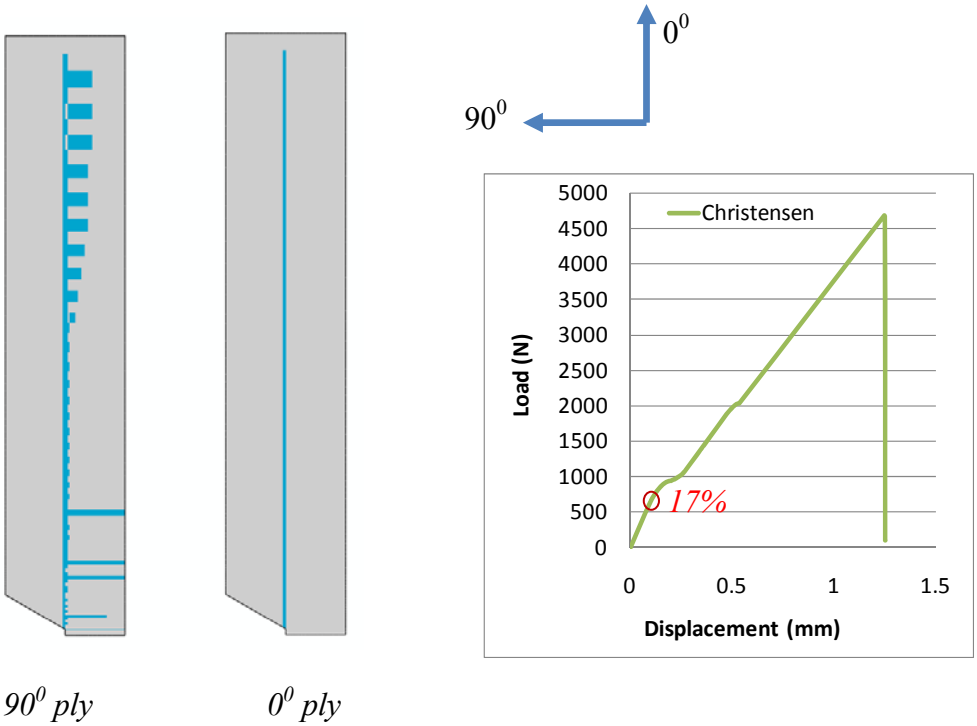

Figure 3-12 Christensen: Further extension of transverse matrix cracking in the 90^0 ply and longitudinal splitting in the 0^0 ply (17% maximum load).

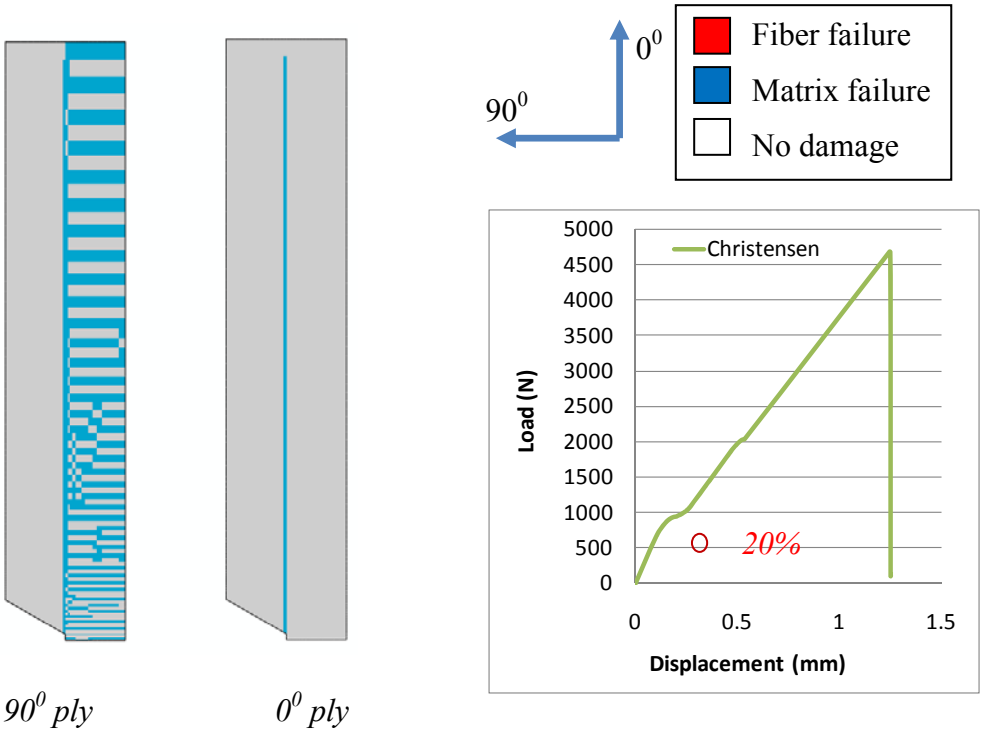

Figure 3-13 Christensen: Extensive distributed matrix cracking in 90^0 ply (20% maximum load).

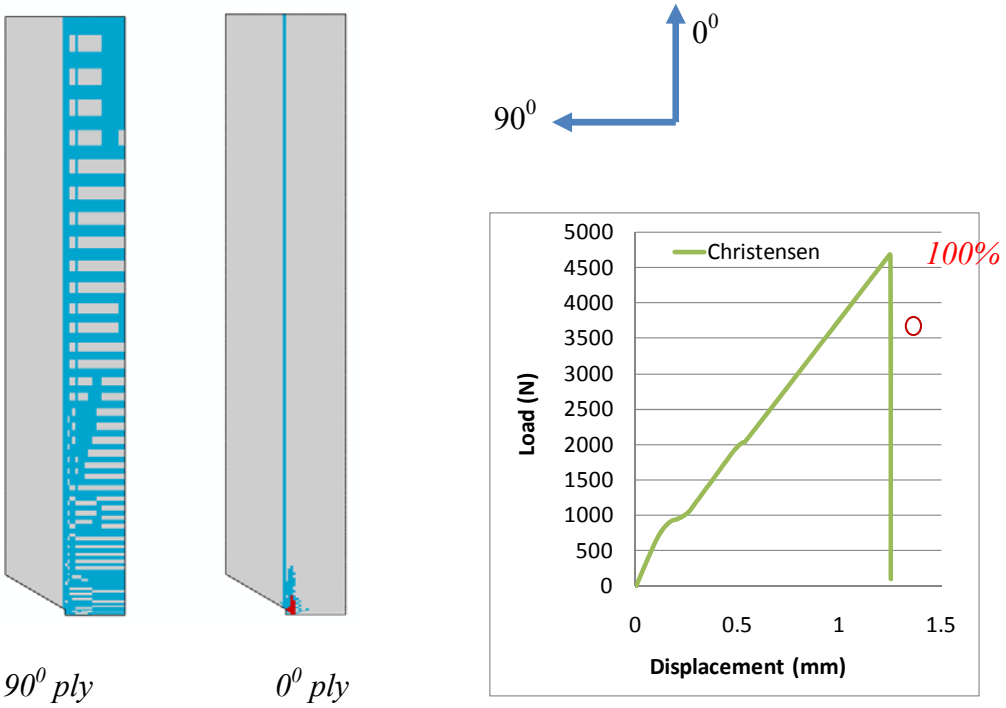

Figure 3-14 Christensen: Saturated matrix cracking in the 90^0 ply, additional longitudinal splitting and fiber failure initiation in the 0^0 ply (100% maximum load).

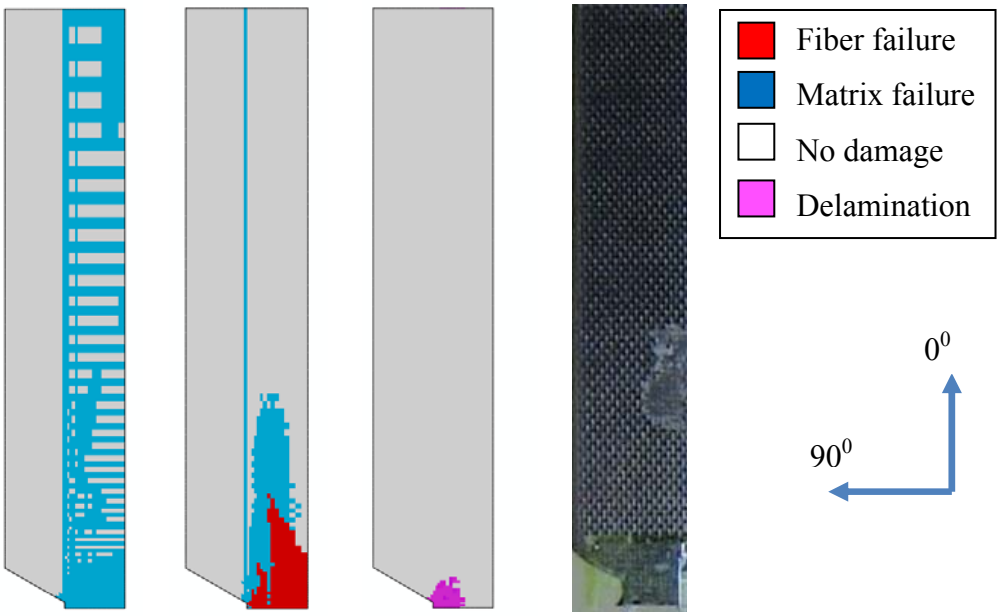

Figure 3-15 Christensen: extensive matrix failure in the 90^0 ply, splitting and fiber failure in the 0^0 ply, and delamination at the [90/0] interface (ultimate failure).

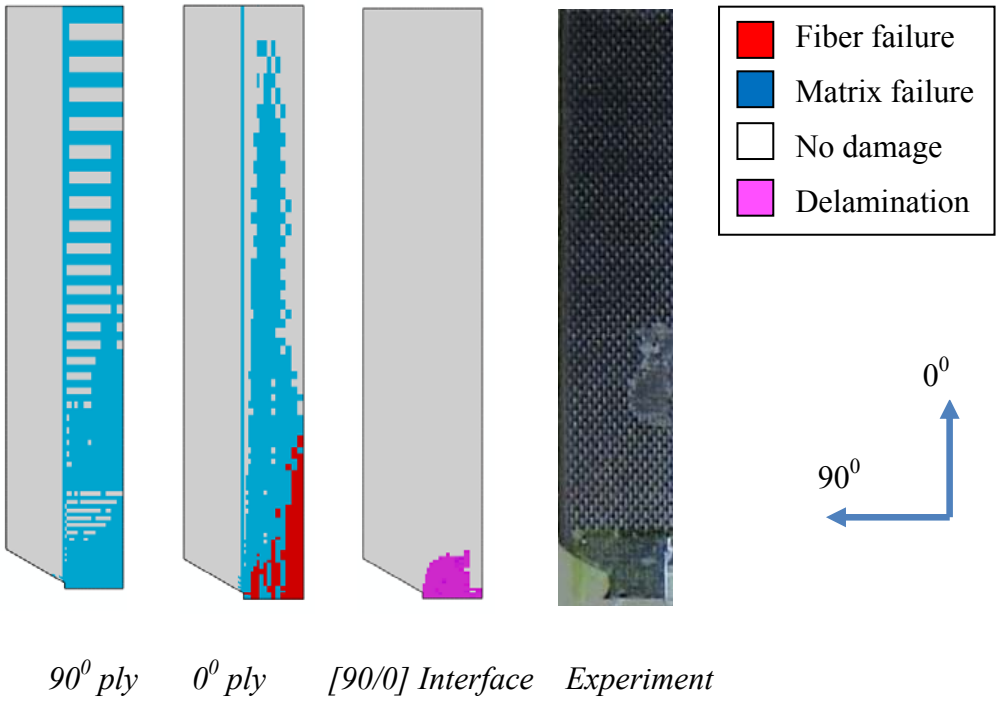

Figure 3-16 Tsai-Wu: extensive matrix failure in the 90^0 ply, splitting and fiber failure in the 0^0 ply, and delamination at the [90/0] interface (ultimate failure).

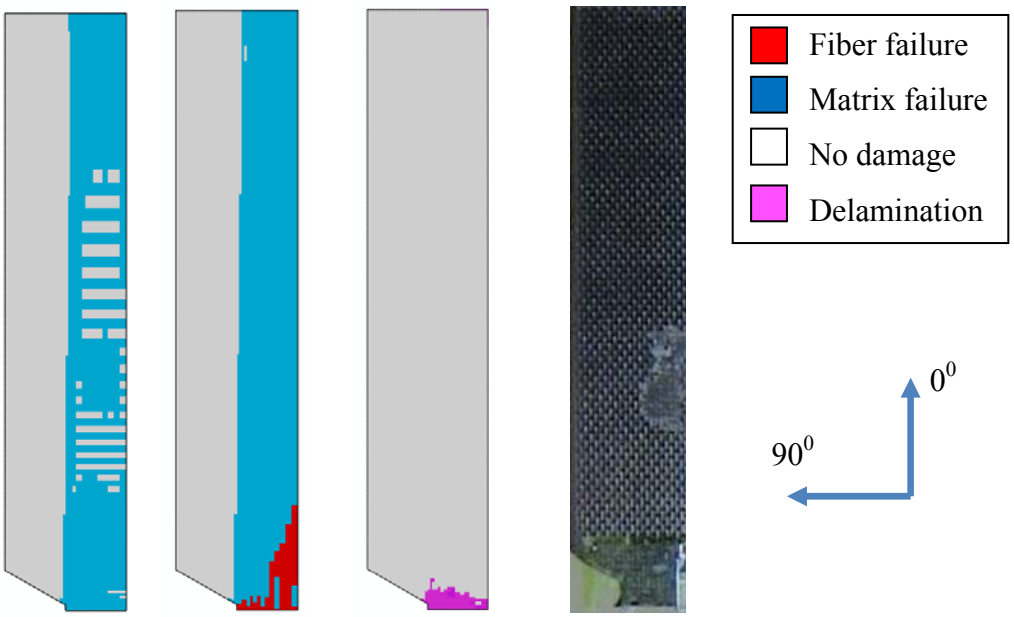

Figure 3-17 MMF: extensive matrix failure in the 90^0 ply, splitting and fiber failure in the 0^0 ply, and delamination at the [90/0] interface (ultimate failure).

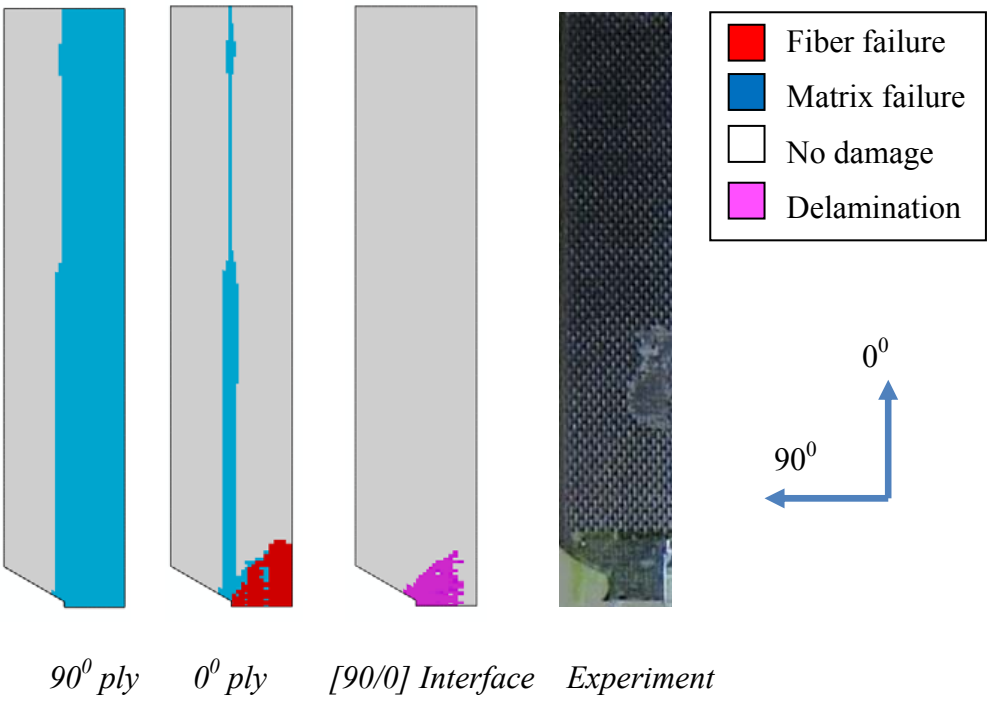

Figure 3-18 CDM: extensive matrix failure in the 90^0 ply, splitting and fiber failure in the 0^0 ply, and delamination at the [90/0] interface (ultimate failure).

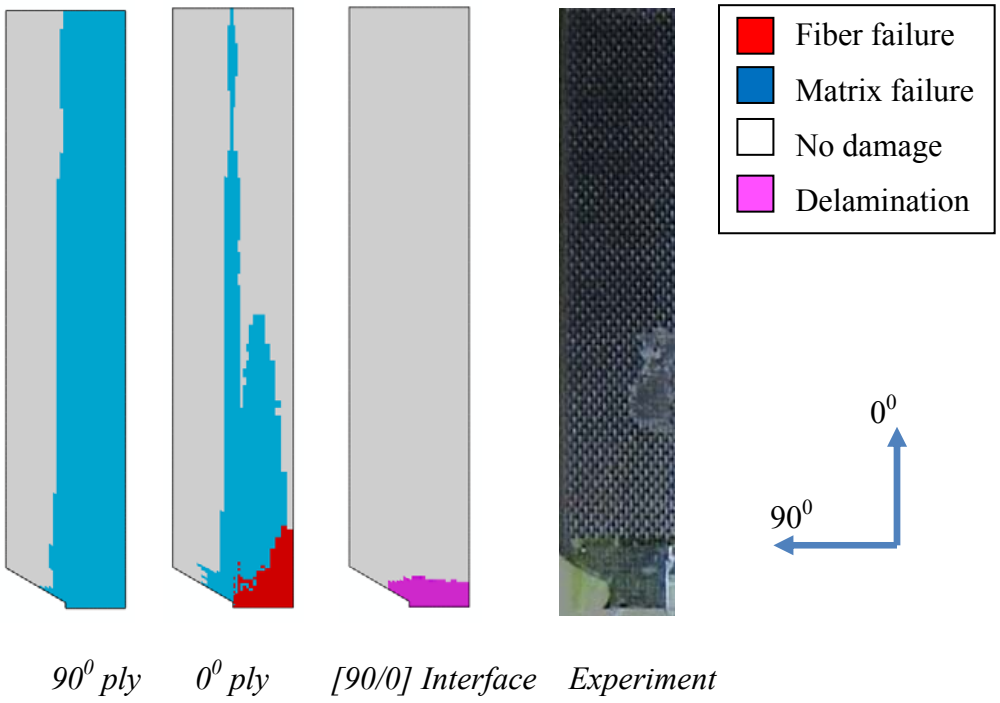

Figure 3-19 MCDM: extensive matrix failure in the 90^0 ply, splitting and fiber failure in the 0^0 ply, and delamination at the [90/0] interface (ultimate failure).

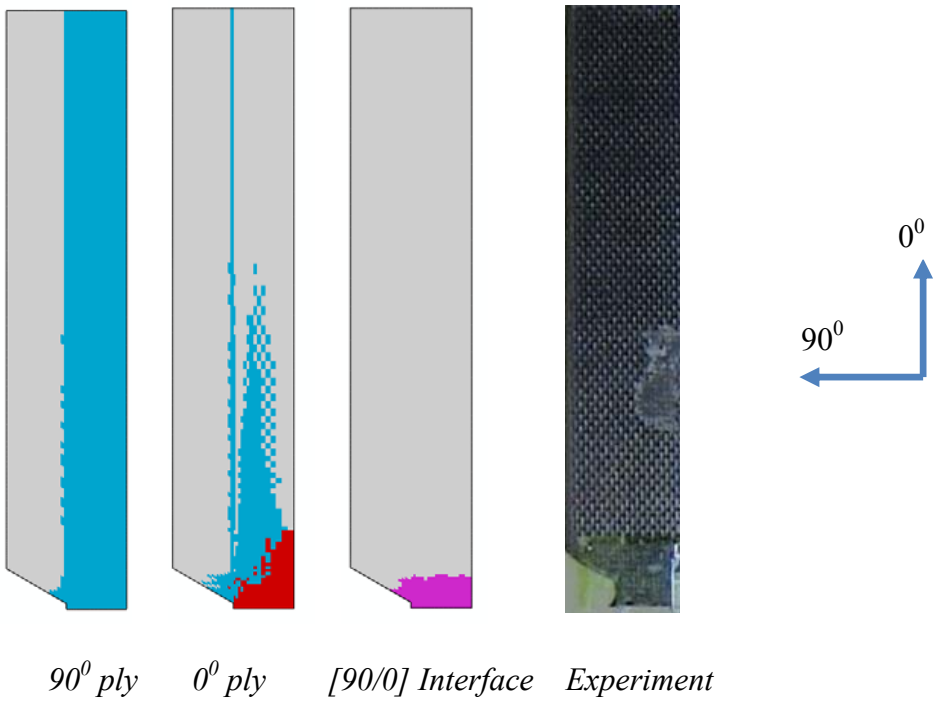

Figure 3-20 MChristensen: extensive matrix failure in the 90^0 ply, splitting and fiber failure in the 0^0 ply, and delamination at the [90/0] interface (ultimate failure).

3.2 Experimental and computational investigation of double-notched $[45/90/-45/0]_s$ carbon/epoxy laminate

3.2.1 Experiment of notched $[45/90/-45/0]_s$ carbon/epoxy laminate

Five specimens of notched $[45/90/-45/0]_s$ composite laminate were tested in tension by Shimadzu machine AG-25TB at a constant rate of displacement of 1 mm/min (Figure 3-21). The notched specimens of the $[45/90/-45/0]_s$ laminate have the same in-plane dimensions and material as those of the $[90/0]_s$ laminate. The experiment setup and procedure are similar to those of $[90/0]_s$ laminate. Strain gauges were also attached on notched $[45/90/-45/0]_s$ specimens to obtain the strain and displacement at the top of specimens corresponding to the gauge length of 100 mm.

Table 3-2 summaries the critical displacements (u_{crit}) and failure load (F_{crit}) of specimens obtained after the experiment. Failures of these specimens after the test are shown in Figure 3-22 and load-displacement curves of these specimens are shown in Figure 3-23. As observed in the experiment, cracks initiate at the notch root of notched $[45/90/-45/0]_s$ specimens and propagate along fiber direction in $\pm 45^0$ and 0^0 plies. The final failure of the $[45/90/-45/0]_s$ specimens are due to fiber breakages in the $\pm 45^0$ plies and 0^0 ply along fiber directions and delamination occurring in the middle of the specimens.

Table 3-2 Critical displacements (u_{crit}) and failure load (F_{crit}) of $[45/90/-45/0]_s$ specimens

Specimen	u_{crit} **(mm)**	Δu_{crit} **(mm)**	F_{crit} **(N)**	ΔF_{crit} **(N)**
1	0.64	0.016	7146	231.8
2	0.70	0.044	7416	38.2
3	0.64	0.016	7542	164.2
4	0.62	0.036	6696	681.8
5	0.68	0.024	8089	711.2
Average	**0.656** ± 0.027		**7377** ± 365.4	

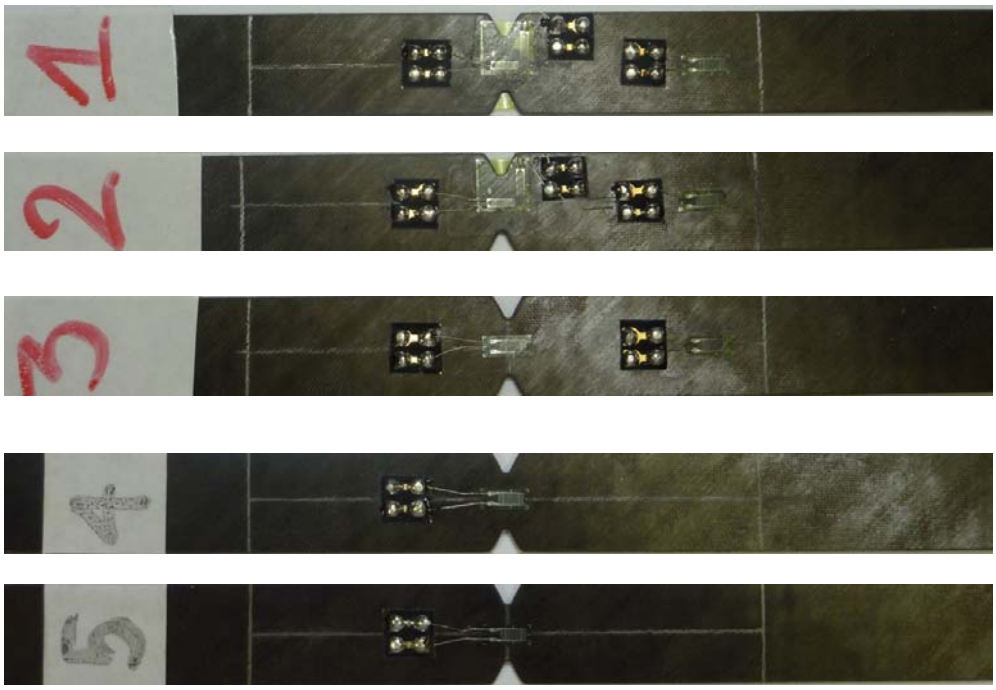

Figure 3-21 $[45/90/-45/0]_s$ carbon/epoxy specimens before testing.

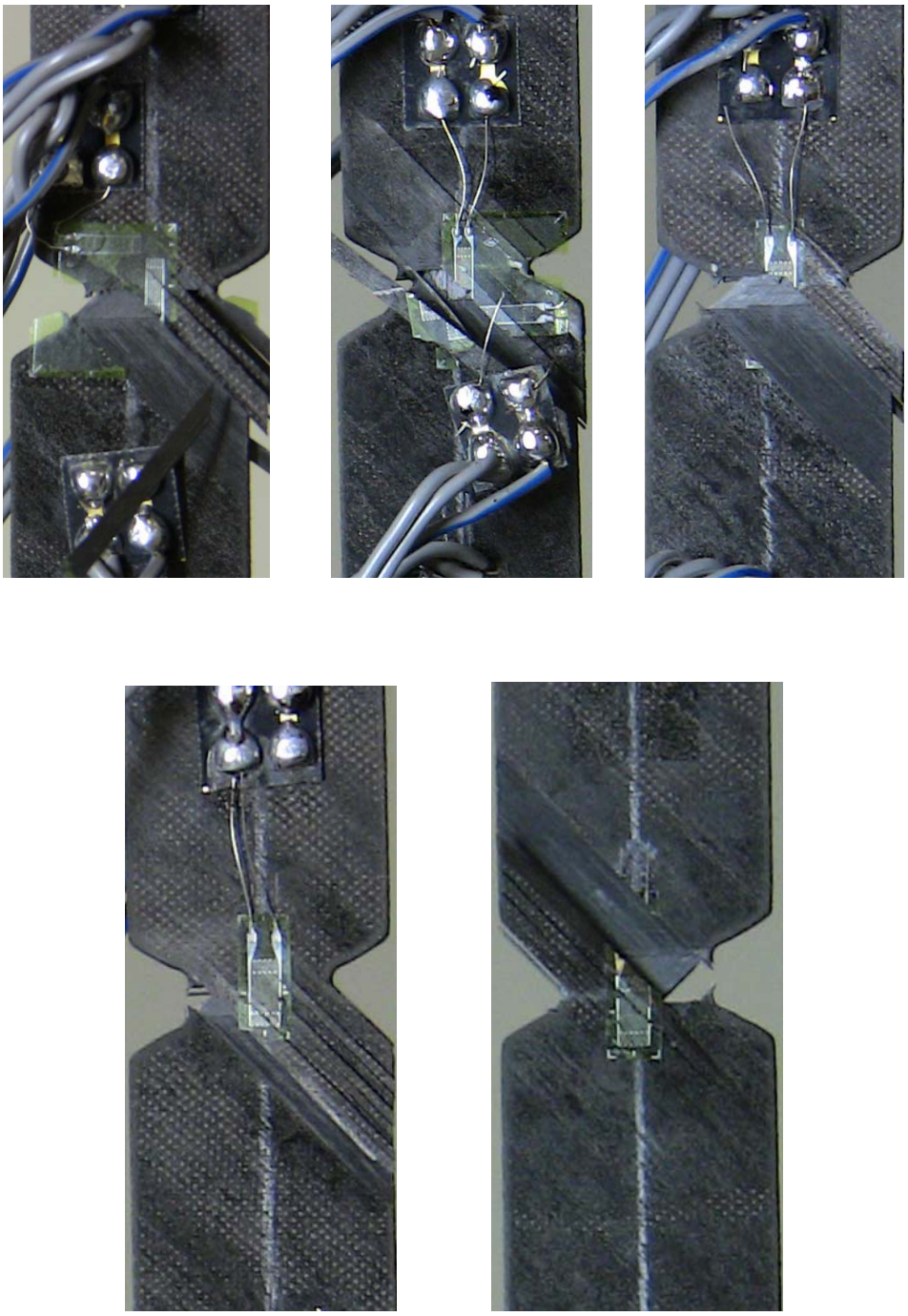

Figure 3-22 Failure of $[45/90/-45/0]_s$ specimens after testing.

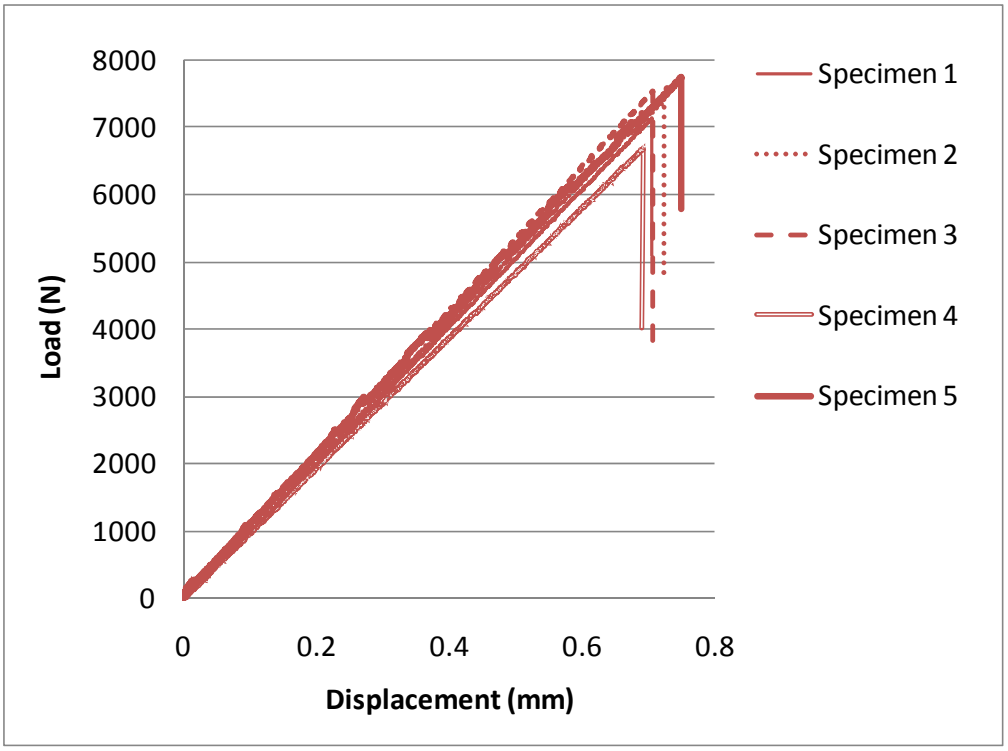

Figure 3-23 Load-displacement curves of notched $[45/90/-45/0]_s$ specimens.

3.2.2 Progressive failure analysis of notched $[45/90/-45/0]_s$ carbon/epoxy laminate

The FE models for the $[45/90/-45/0]_s$ laminate are constructed with 8-node three dimensional continuum shell elements and 8-node hexahedral cohesive elements COH3D8 with one element in the thickness per ply. The boundary conditions and mesh of the FE models are shown in Figure 3-24. Six failure models are employed to predict the progressive failure of the quasi-isotropic laminate including the Tsai-Wu, Christensen, MMF, CDM, MCDM and MChristensen models. Besides, cohesive elements are used to model the delamination at the interfaces. The values of cohesive parameters used for the

analysis of quasi-isotropic laminate are the same as those of the cross-ply laminate since the same carbon/epoxy material is applied for both laminates.

The predicted applied load *vs.* displacement curves for the Tsai-Wu, Christensen, MMF, CDM, MCDM and MChristensen models are shown in Figure 3-25 and compared with the experimental data. The damage patterns predicted by all failure models are presented in Figures 3-26 to 3-36. Only the damage in the 45^0 ply (top ply) of the quasi-isotropic laminate can be observed and compared to the predicted results since the carbon/epoxy material is very dark that damages in inner plies of the laminate such as the -45^0, 90^0 or 0^0 plies are not visible. All the damage patterns predicted for the 45^0 ply show the initiation and development of longitudinal splitting and fiber failure which correlate well with cracks running at 45^0 from the notch tip as observed in the experiment (Figures 3-26 to 3-36). Furthermore, the simulation results also capture delamination which occurs in the middle of the specimens as seen in the experiment. For the ultimate load prediction, the CDM model predicts the fiber failure earlier than the other models and become conservative. In contrast, the MCDM and MChristensen models by describing a fracture process in fiber failure modeling can predict the experimental ultimate loads pretty well. The highest ultimate load predicted by the MCDM and MChristensen models are up to 84% and 90% of the experimental failure load, respectively.

The progressive damage patterns predicted by the Christensen model are demonstrated in Figures 3-26 to 3-31. As can be seen in Figure 3-26, at 30% of the maximum load, short longitudinal splits initiate from the notch roots in

the 45^0 ply and 0° ply while matrix cracks are found in the 90° ply. The intermediate -45^0 ply which is affected by the damage from the 90^0 and 0^0 plies is also found with few matrix cracks and splits. On increasing application of load to 50% of the maximum load, longitudinal splits in the $\pm45^0$ plies and 0° ply begin to lengthen and diffused matrix cracks begin to saturate in $\pm45^0$ plies and 90^0 ply (Figure 3-27). Further evolution of damage shows that matrix cracking is tending to develop in the transverse directions of the $\pm45^0$ and 90^0 plies (Figure 3-28). At the maximum load, additional splitting occurs in the 0^0 ply and fiber failure initiates at the notch roots of the 0^0 and $\pm45^0$ plies (Figure 3-29). It is found that delamination also initiates at the interfaces by this stage. Thereafter, additional splitting in 0^0 ply occurs and fiber failures in the $\pm45^0$ and 0^0 plies start to propagate across the width of the specimen (Figure 3-30). Shortly after, fiber failures quickly spread across the entire width of the 0^0 and $\pm45^0$ plies and extensive delamination is predicted at all the interfaces, leading to the ultimate failure (Figure 3-31). The predicted ultimate load by the Christensen model under-predicts the experiment by about 23.4%.

The progressive failure patterns using Tsai-Wu and MMF models follow those of Christensen models closely. Therefore, only the damage patterns just after the major load drop are shown. Figures 3-32 and 3-33 show the final damage patterns of the Tsai-Wu and MMF models. The final failure of these models is caused fiber failures in the 0^0 and $\pm45^0$ plies and delamination at all the interfaces. However, the MMF model predicts less delamination than the Tsai-Wu model. The ultimate loads by Tsai-Wu and MMF models are under predicted the experiment by 24.6% and 25%, respectively.

Since the progressive failure patterns for CDM model follows those of Christensen, Tsai-Wu and MMF models, only the damage pattern by CDM after the major load drop is presented. The result for CDM is shown in Figure 3-34. In the CDM case, more damage in the $\pm 45^0$ plies are found while little delamination is predicted. The ultimate load by CDM model is low and under-predicted the experiment by 32%.

The final failure patterns predicted by the MCDM and MChristensen are indicated in Figures 3-35 and 3-36. The progressive damage patterns predicted by these failure models are similar to those of Christensen, Tsai-Wu, MMF and CDM. The failure loads predicted by MCDM and MChristensen models under-predict the experiment by about 16% and 10%, respectively.

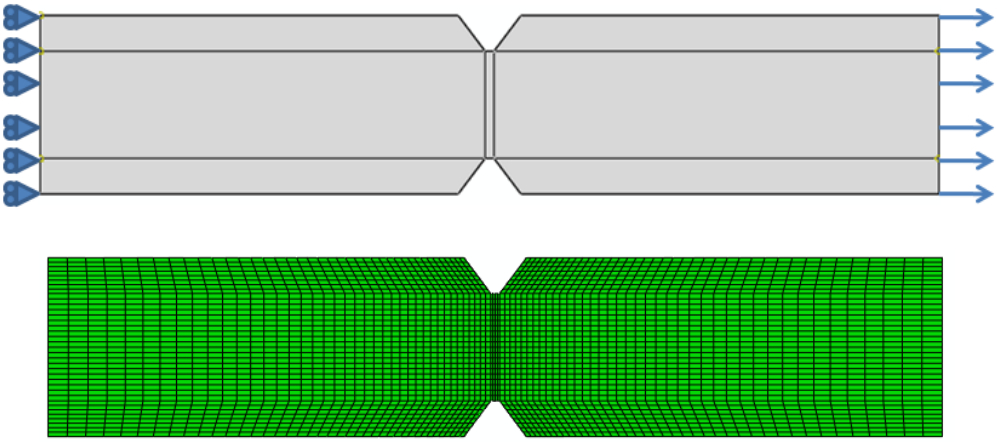

Figure 3-24 Boundary conditions and mesh of the FE model for quasi-isotropic carbon/epoxy laminate.

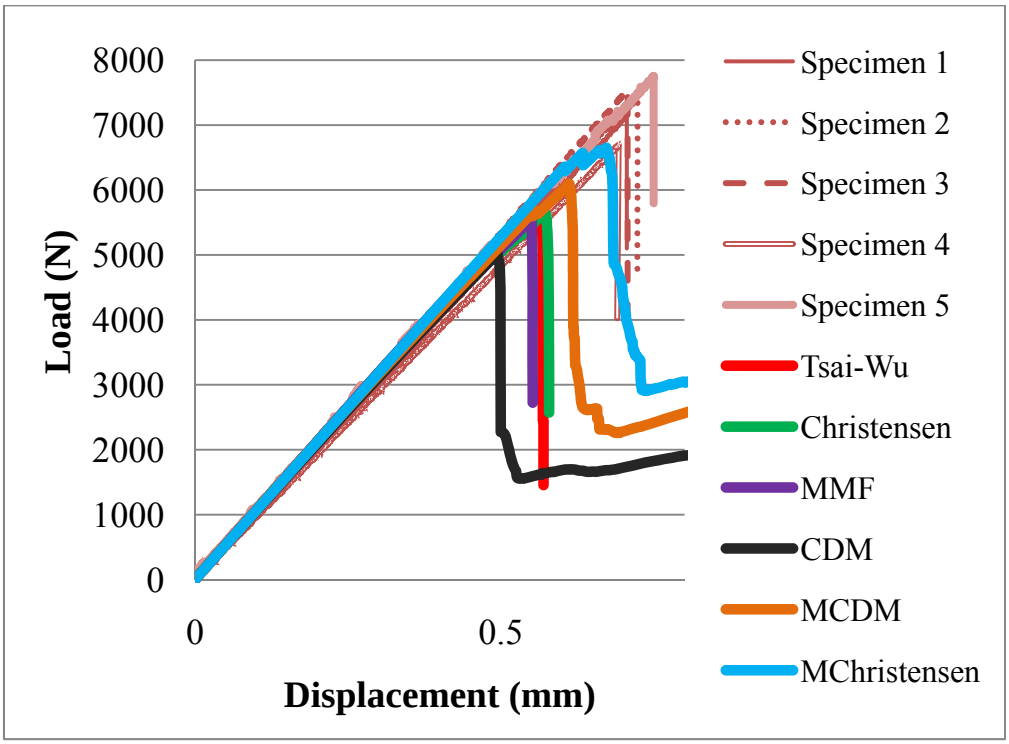

Figure 3-25 Predicted load-displacement curves and comparison with the experiment for the $[45/90/-45/0]_s$ carbon/epoxy laminate.

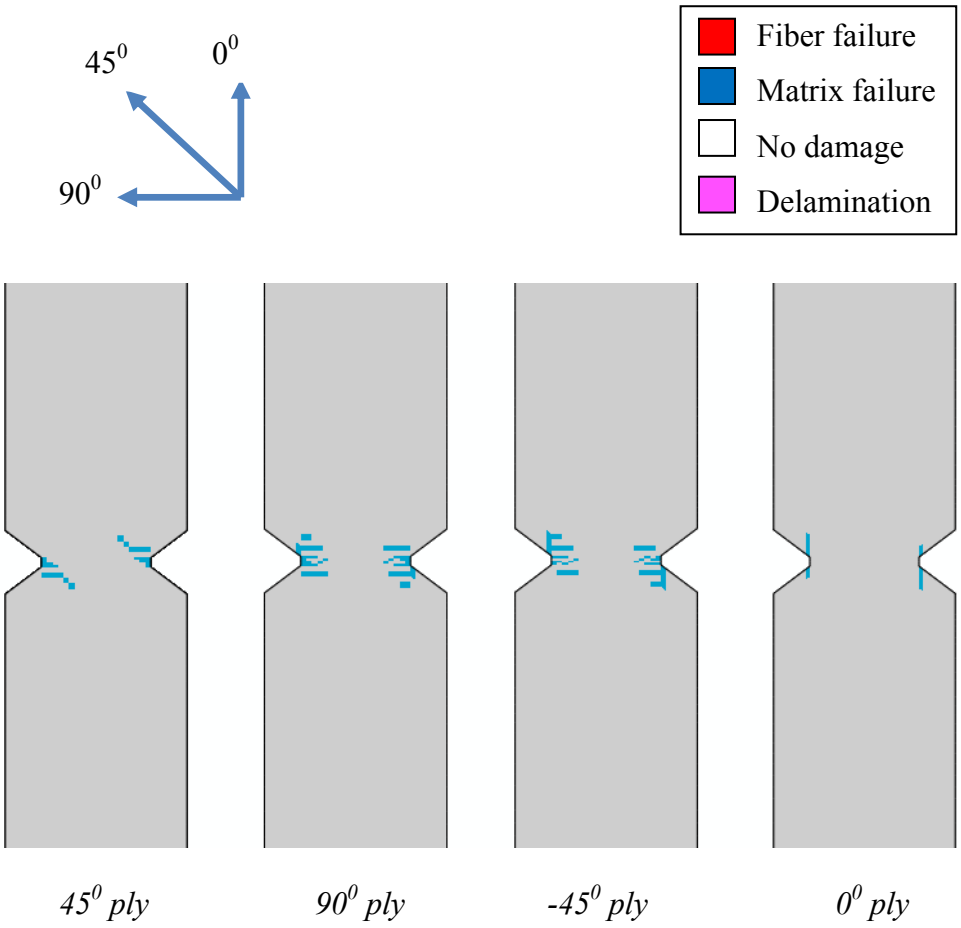

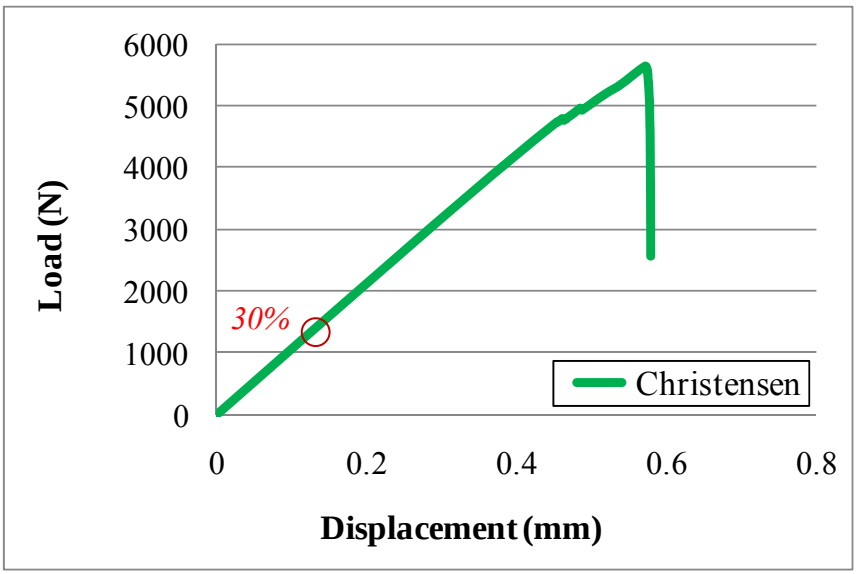

Figure 3-26 Christensen: initiation of splitting in the 45^0 and 0^0 plies, matrix cracking in the 90^0 ply, splitting and matrix cracking in -45^0 ply (30% maximum load).

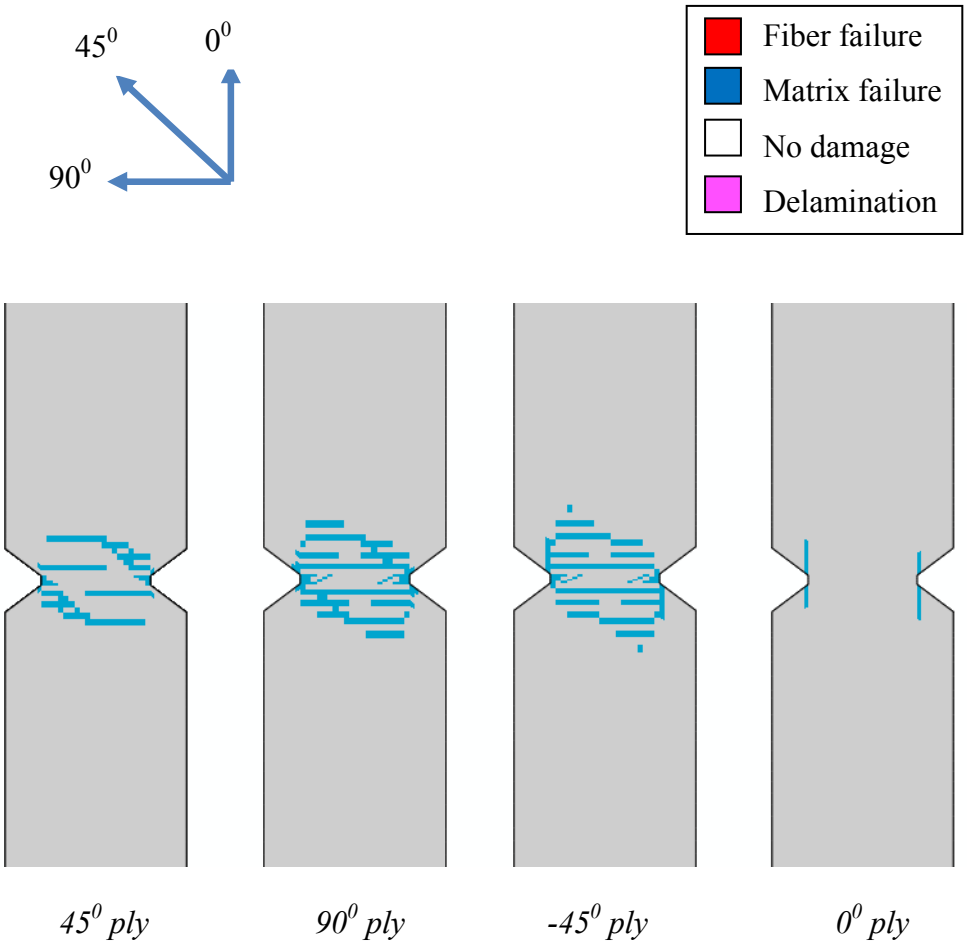

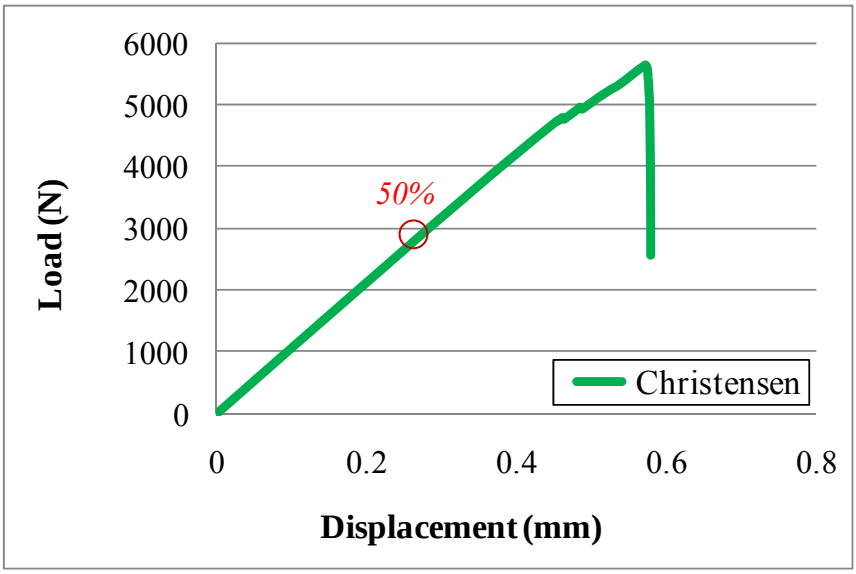

Figure 3-27 Christensen: initiation and propagation of matrix cracking in the 45^0 ply, further development of matrix cracking in the 90^0 and -45^0 plies and splitting in the 0^0 ply (50% maximum load).

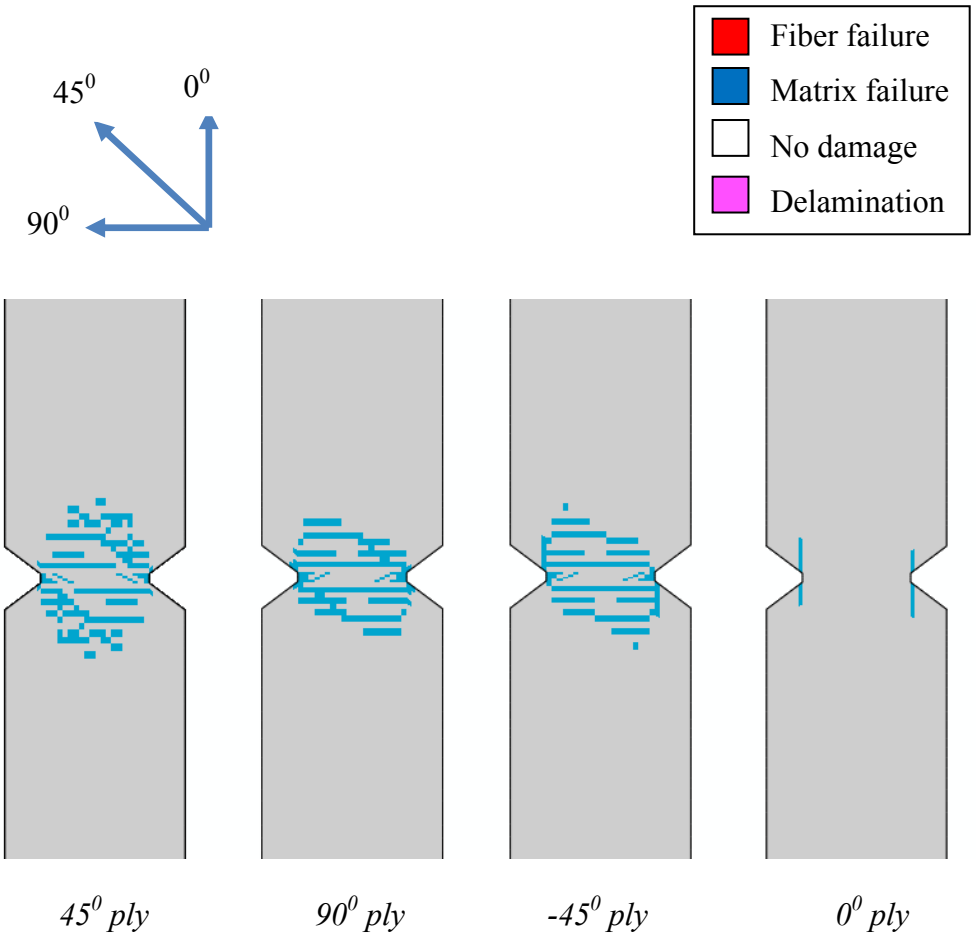

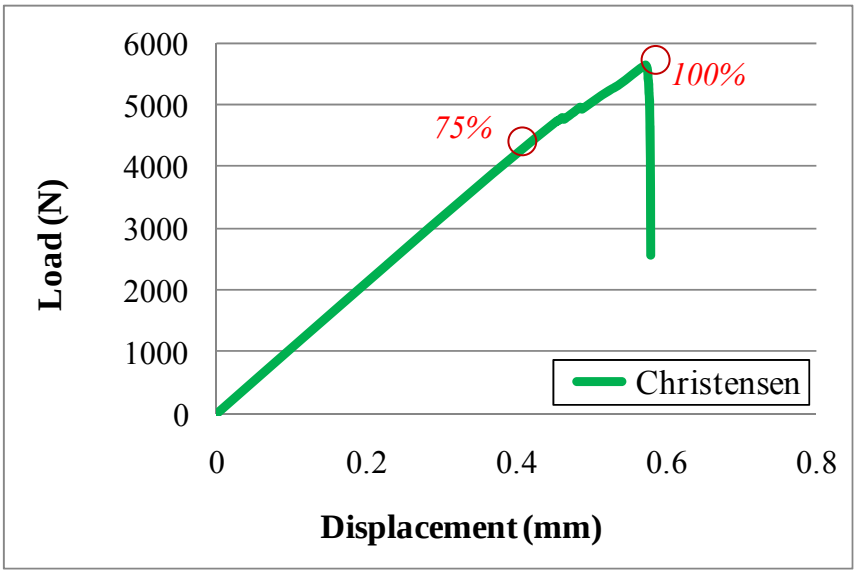

Figure 3-28 Christensen: Further evolution of damage shows clear matrix cracking in transverse direction of the 45^0, 90^0 and -45^0 plies (75% maximum load).

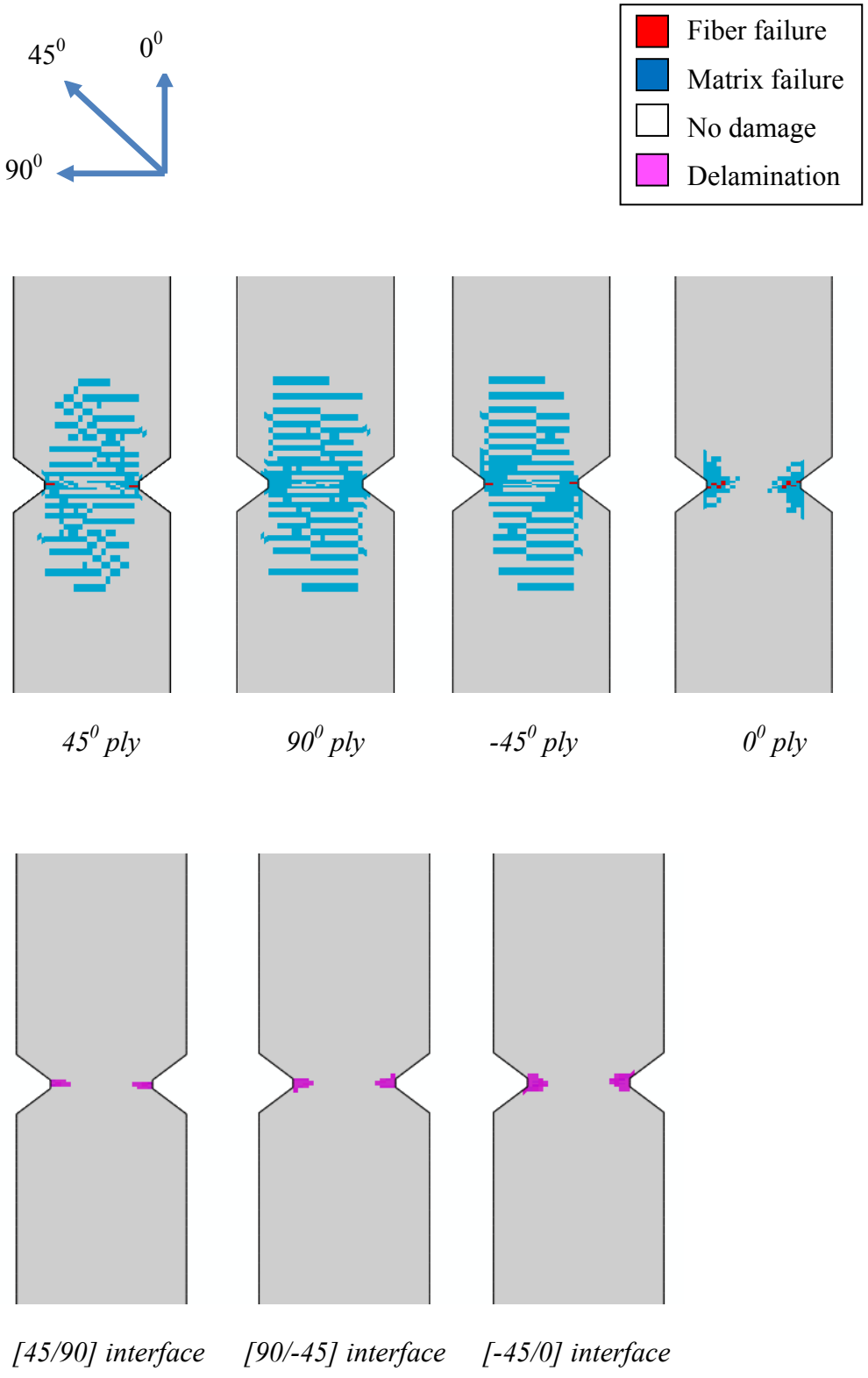

Figure 3-29 Christensen: Additional splitting and fiber failure initiation in the 0^0, $\pm 45^0$ plies and initiation of delamination at the interfaces (100% maximum load).

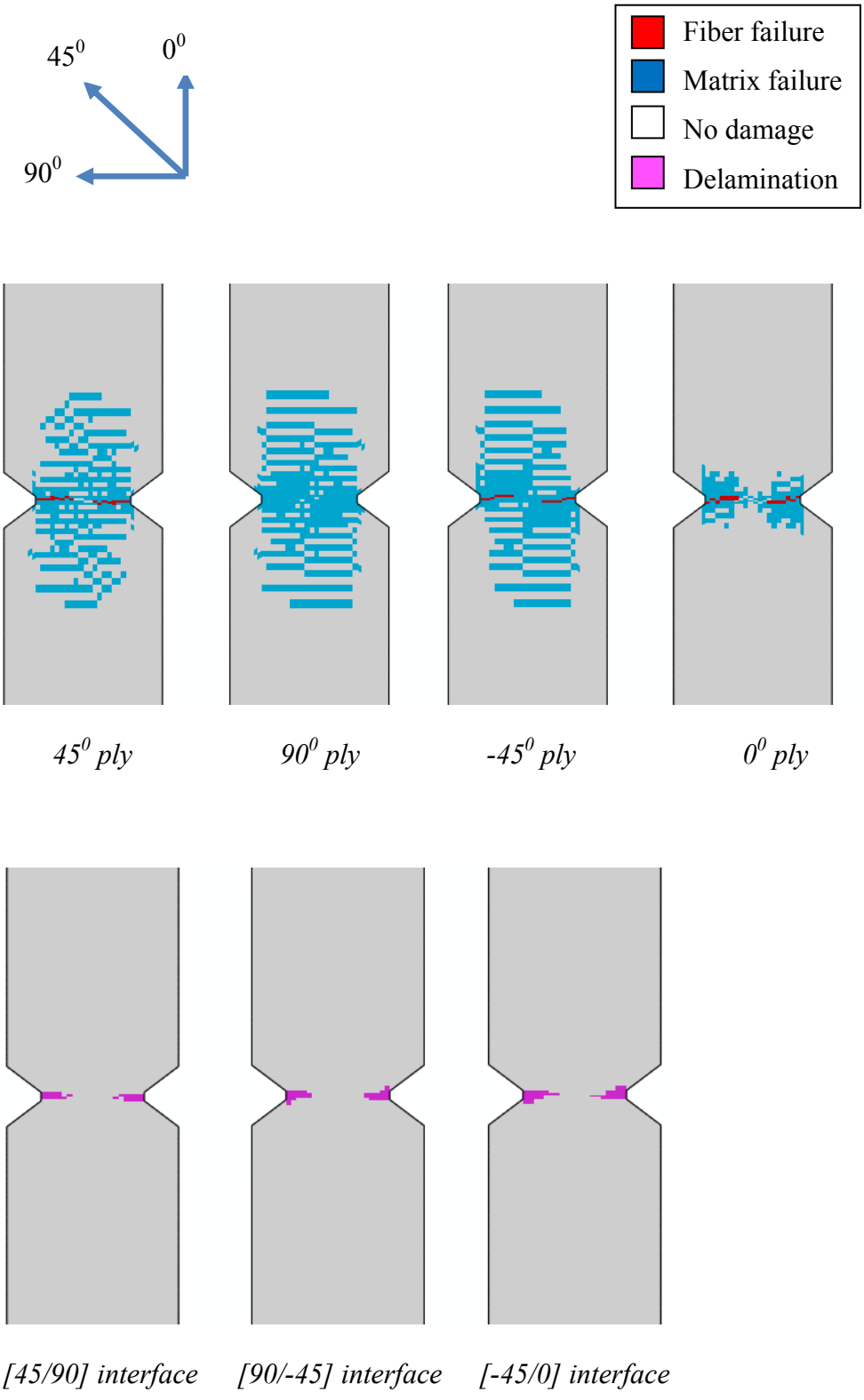

Figure 3-30 Christensen: Additional splitting and propagation of fiber failure in the 0^0 and $\pm 45^0$ plies.

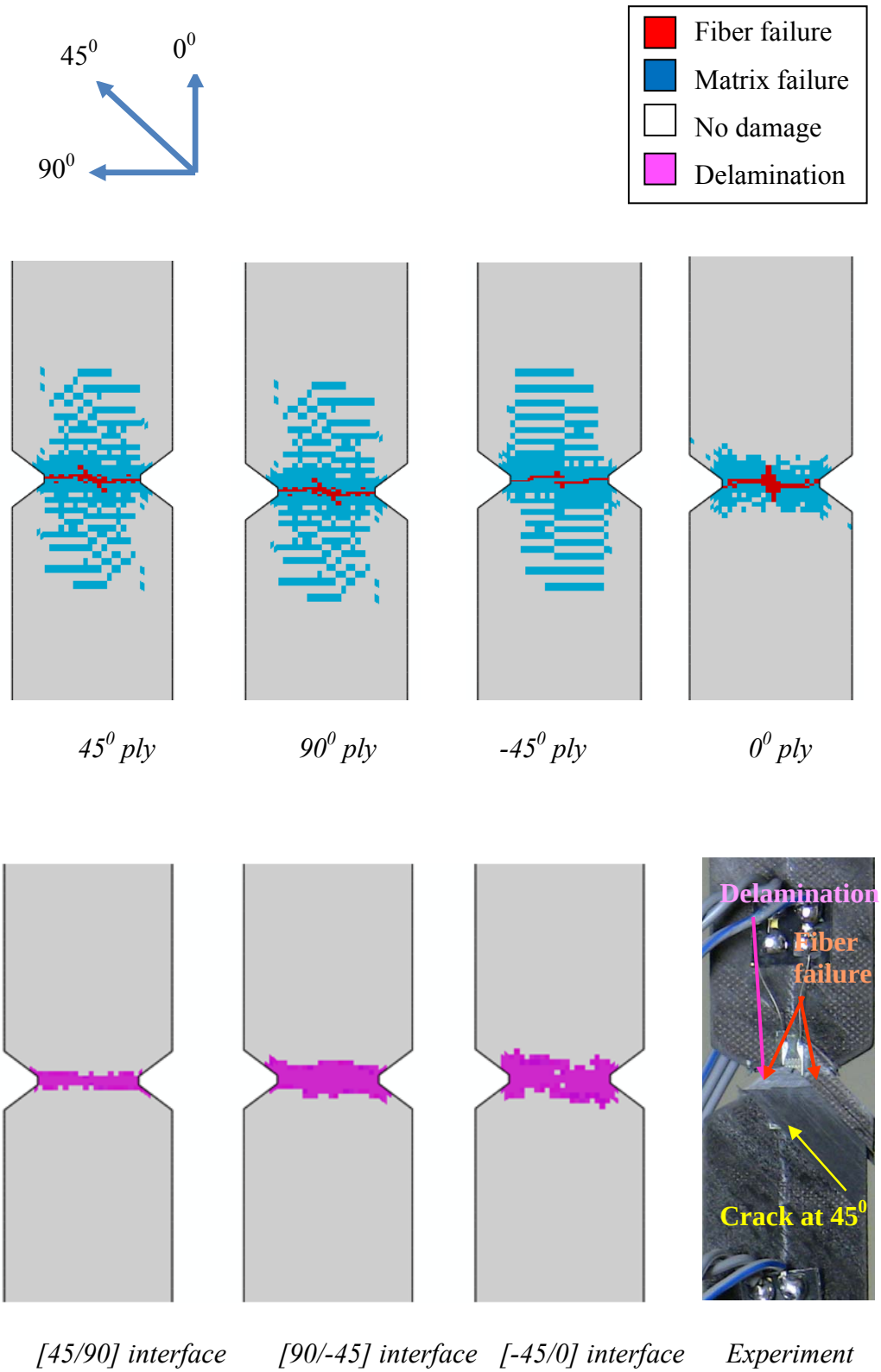

Figure 3-31 Christensen: Final failure in the 45^0 ply, 90^0 ply, -45^0 ply and 0^0 ply and delamination at all the interfaces.

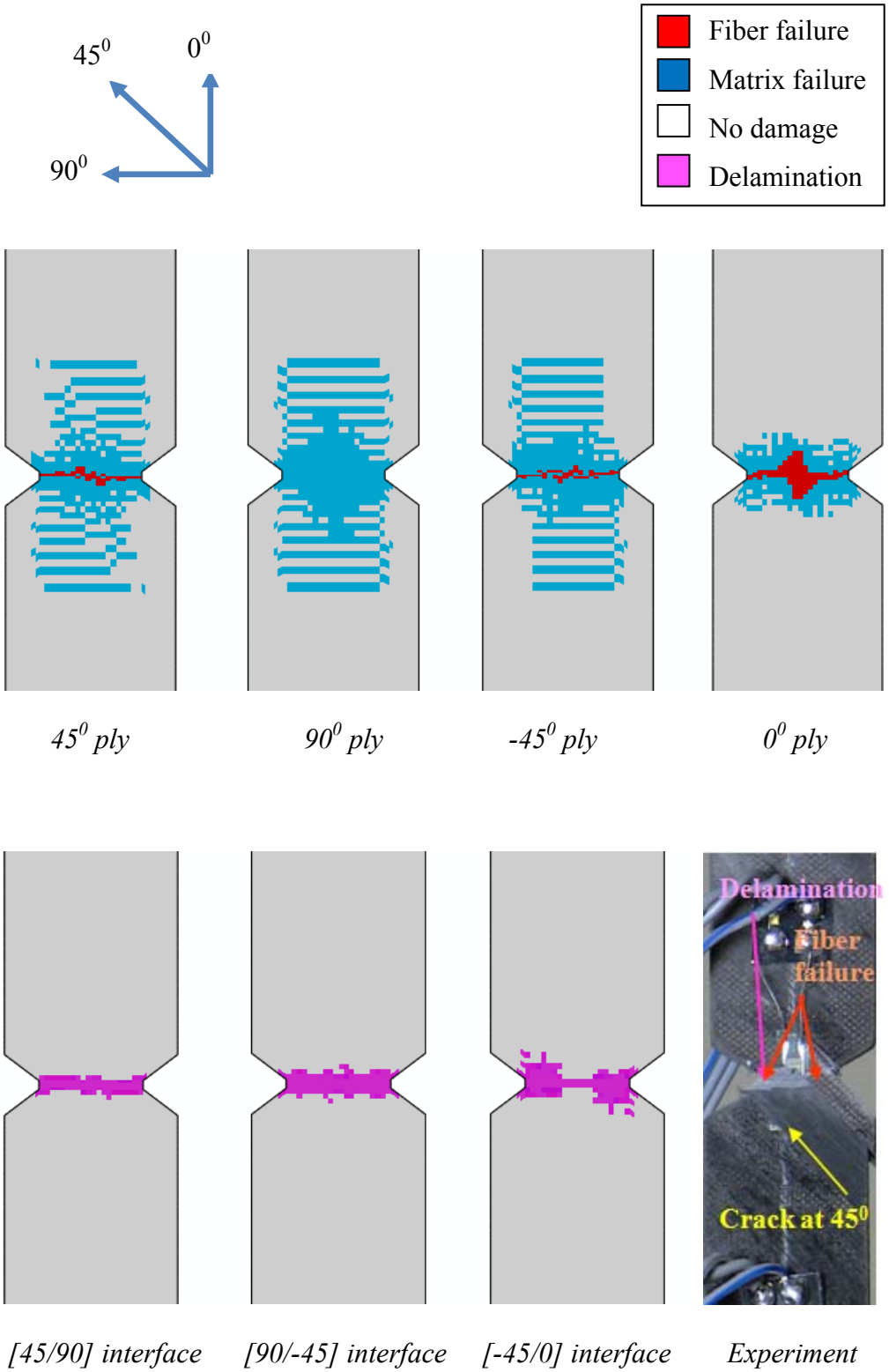

Figure 3-32 Tsai-Wu: Final failure in the 45^0 ply, 90^0 ply, -45^0 ply and 0^0 ply and delamination at all the interfaces.

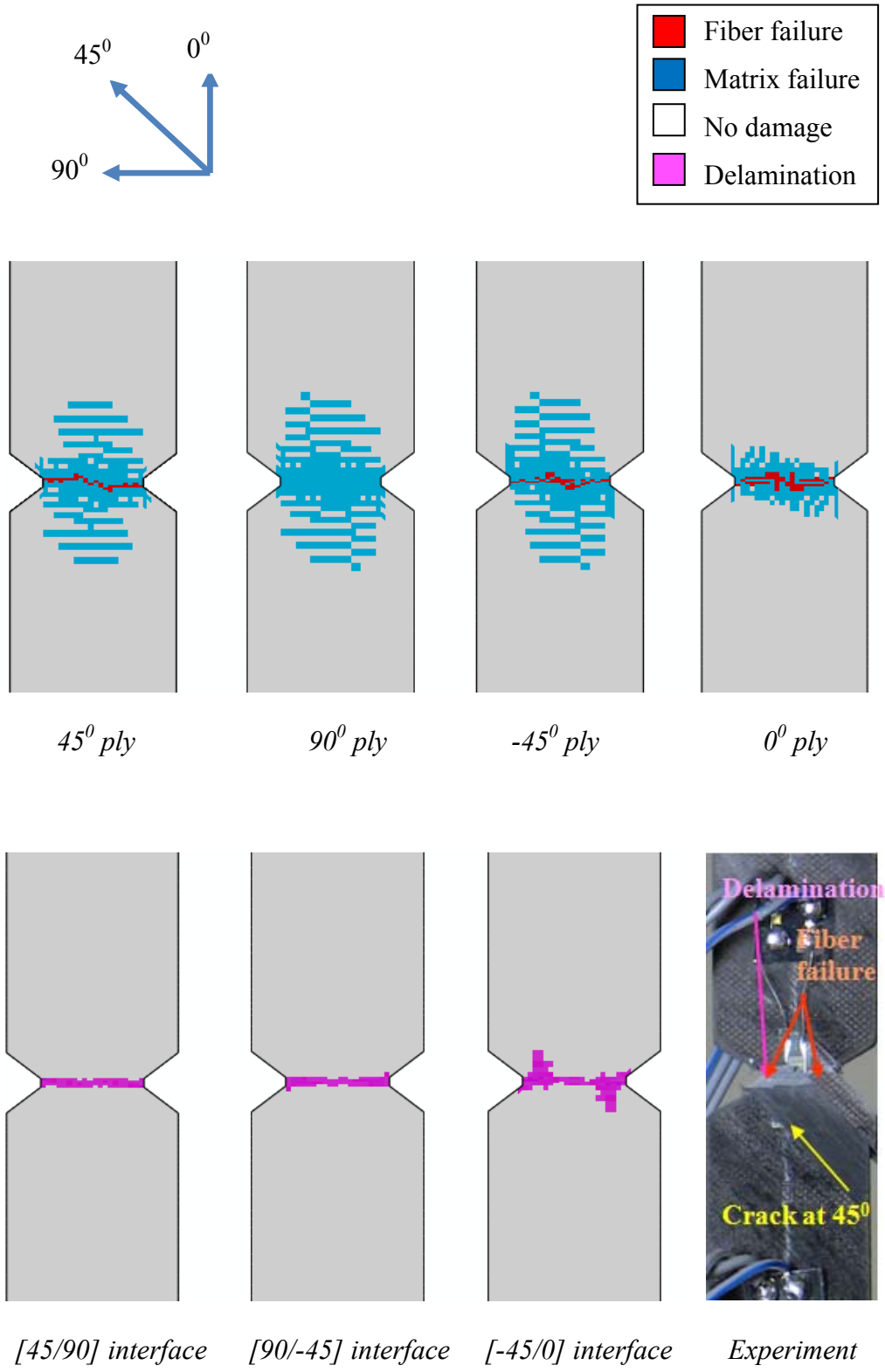

Figure 3-33 MMF: Final failure in the 45^0 ply, 90^0 ply, -45^0 ply and 0^0 ply and delamination at all the interfaces.

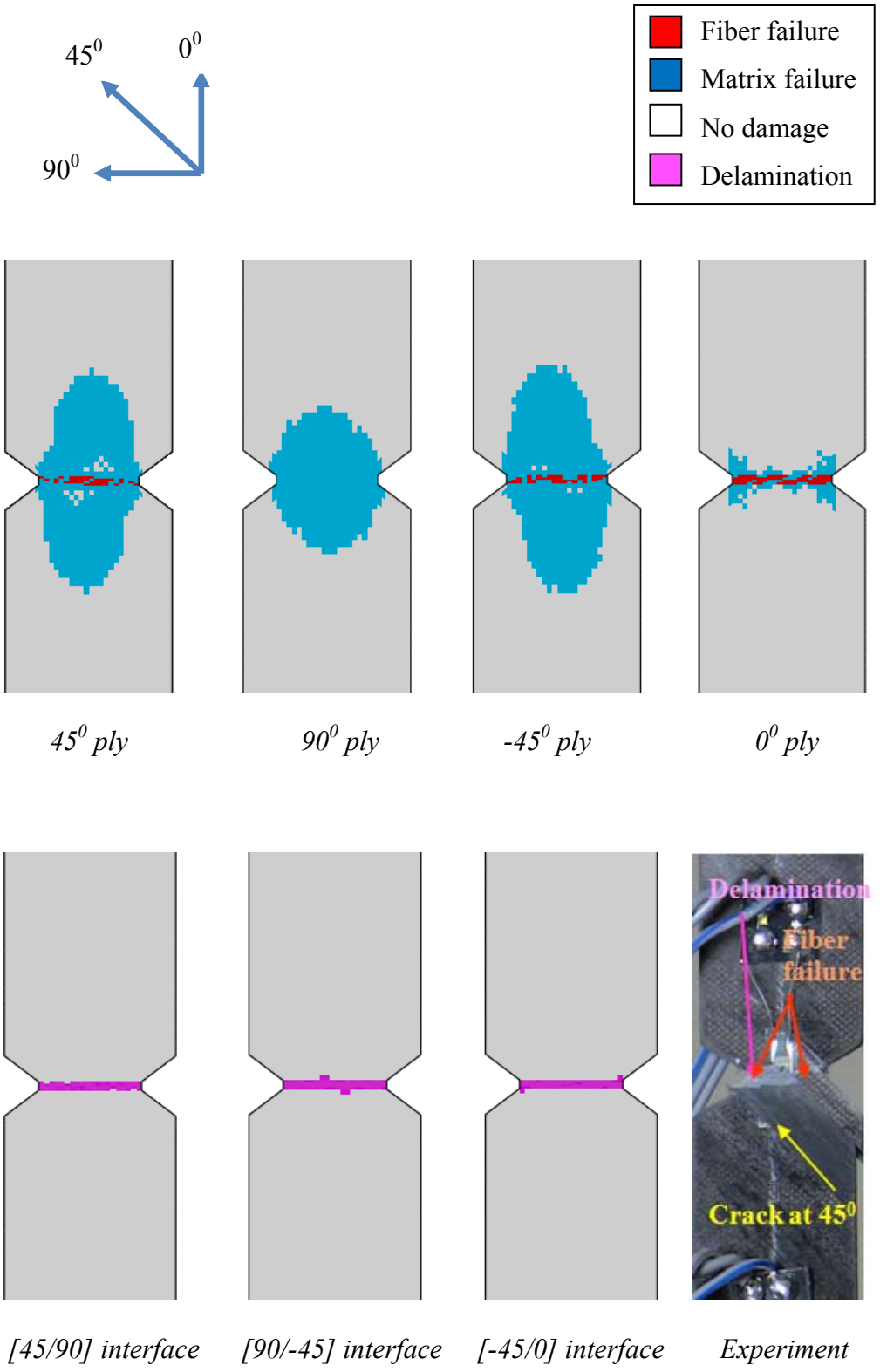

Figure 3-34 CDM: Final failure in the 45^0 ply, 90^0 ply, -45^0 ply and 0^0 ply and delamination at all the interfaces.

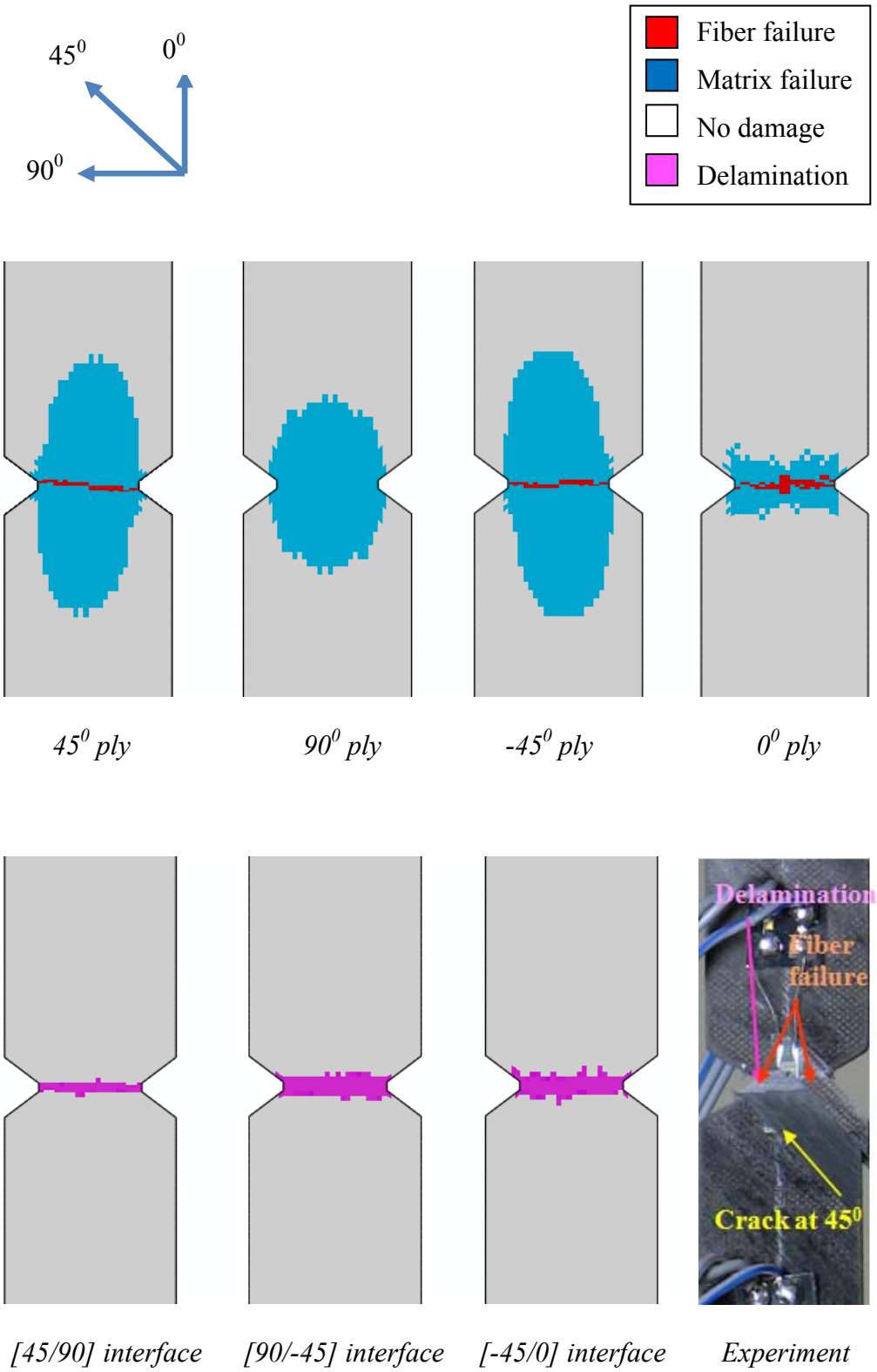

Figure 3-35 MCDM: Final failure in the 45^0 ply, 90^0 ply, -45^0 ply and 0^0 ply and delamination at all the interfaces.

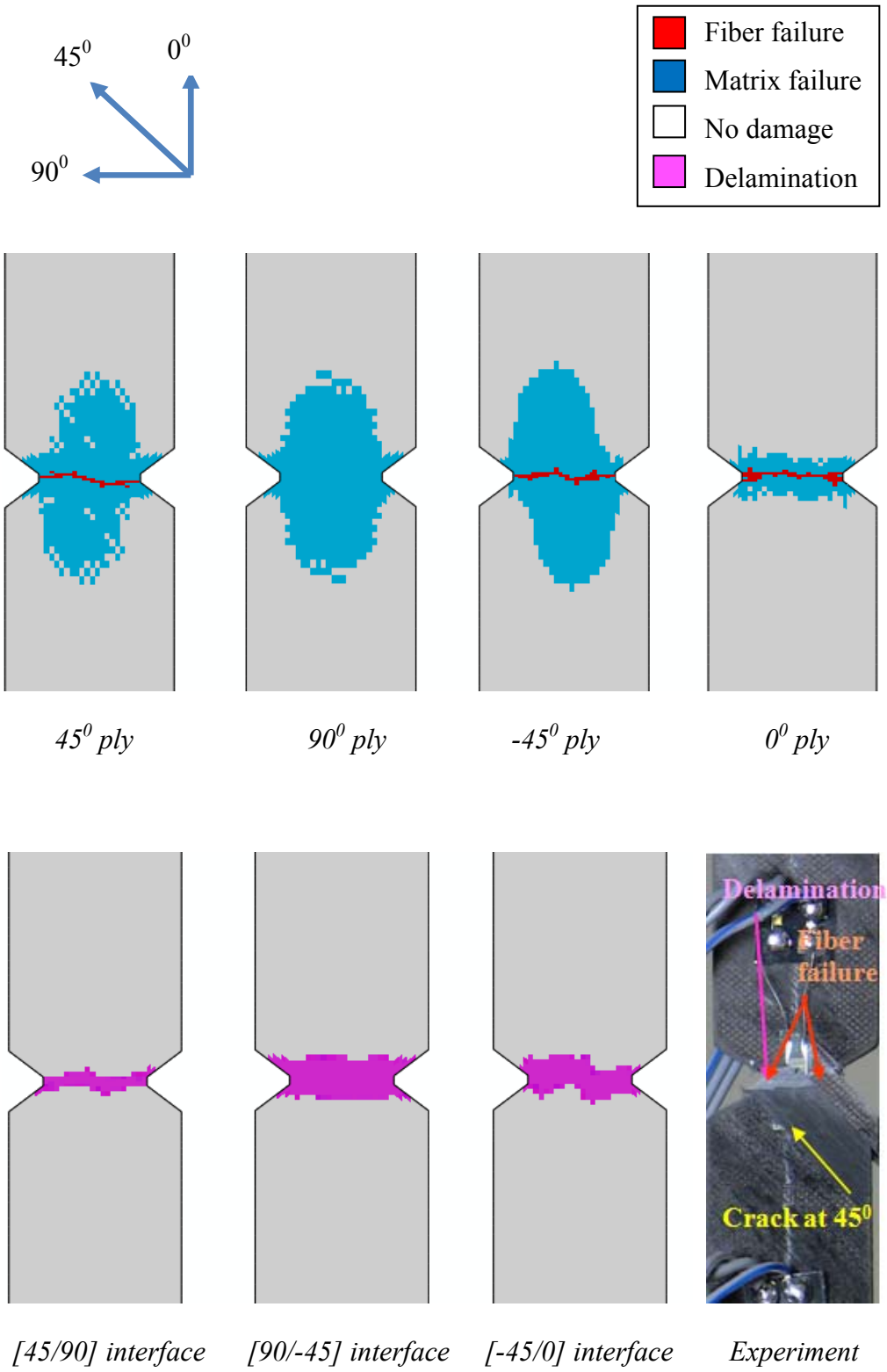

Figure 3-36 MChristensen: Final failure in the 45^0 ply, 90^0 ply, -45^0 ply and 0^0 ply and delamination at all the interfaces.

3.3 Conclusion

Various failure models including models of Tsai-Wu, Christensen, CDM, MCDM and MChristensen are used to predict the damage propagation in notched $[90/0]_s$ and $[45/90/-45/0]_s$ carbon/epoxy laminates subjected to tension. The results for the two laminates are summarized in Figure 3-37 and Table 3-3. Simulation results for the cross-ply laminate show good agreements with the experimental data for the damage patterns and ultimate loads but not for displacements at failure. Six failure models can predict well the matrix cracking in the 90^0 ply, the splitting in the 0^0 ply and delamination at the interface. However, early load drops in the predicted load *vs.* displacement curves have been found due to the substantial stiffness loss of the 90^0 ply at early stage. Modeling of the 90^0 ply is therefore conservative because it predicts a lot of matrix damage in 90^0 ply and cause the critical displacement very big. However, the prediction of ultimate load of composite is still determined by the stiffness of the 0^0 ply since the applied load is in fiber direction of the 0^0 ply. Therefore, after the early load drops, the predicted load-displacement curves still grow up due to the remaining stiffness of the 0^0 ply. Only once the fiber failure in 0^0 ply occurs, the whole stiffness of laminate is lost, resulting a major load drop.

Simulation results for the quasi-isotropic carbon/epoxy laminate show transverse cracking in $\pm 45^0$ and 90^0 plies, longitudinal splitting and fiber failure in $\pm 45^0$ and 90^0 plies and delamination at all the interfaces. It can be

seen that no discontinuity in the load *vs*. displacement curves for this quasi-isotropic laminate is predicted since the matrix cracks and splits seem to occur simultaneously. The CDM model predicts the fiber failure earlier than the other models and becomes conservative. Tsai-Wu, Christensen and MMF models predict the fiber failure later than CDM model, but the consideration of complete damage for fiber failure still make them under-predict the experimental failure load. On the other hand, the MCDM and MChristensen models which consider the damage fibers still can carry additional load until ultimate failure predict closer to the experiment than the others. The MCDM and MChristensen predict up to 84% and 90% of the experimental failure loads, respectively. There are still discrepancies of predicted results compared to experiment which may be due to some experimental errors such that the accuracy of ply orientation when laying up the composite laminate or errors due to conducting the tensile test.

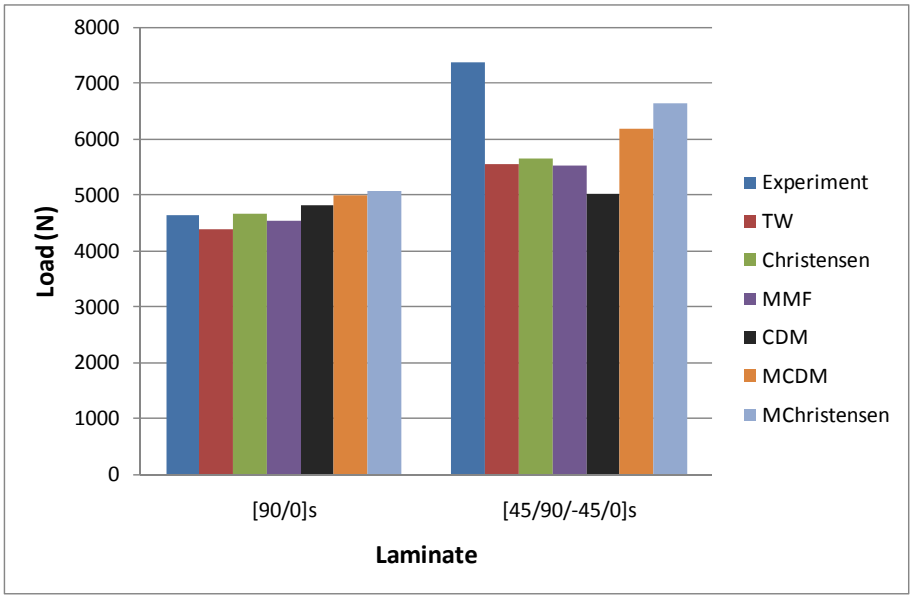

Figure 3-37 Comparison between predicted failure loads by all failure models and the experimental failure load for carbon/epoxy laminates.

Table 3-3 Summary of the ultimate loads predicted by all models for the carbon/epoxy cross-ply and quasi-isotropic laminates.

	Ultimate load (% prediction)	
	$[90/0]_s$ laminate	**$[45/90/-45/0]_s$ laminate**
Experiment	4704 ± 96 N	7377 ± 365.4 N
Christensen model	4677.7 N *(99.4%)*	5650.3 N *(76.6%)*
Tsai-Wu model	4385.5 N *(93.2%)*	5565.7 N *(75.4%)*
MMF model	4531.8 N *(96.3%)*	5535.4 N *(75%)*
CDM model	4807.7 N *(102%)*	5020.7 N *(68%)*
MCDM model	4963.3 N *(105%)*	6195 N *(84%)*
MChristensen model	5001 N *(106%)*	6650.2 N *(90%)*

Chapter 4

Progressive failure analysis in double-notched glass/epoxy laminates

In this chapter, the author's objective is to compare the failure analysis by the MPDM and various failure theories with experimental results of Hallett and Wisnom for notched $[90/0]_s$ and $[45/90/-45/0]_s$ glass/epoxy laminates. Since the glass/epoxy material is transparent, the damage patterns can be observed clearer than carbon/epoxy material. Therefore, the comparison for notched cross-ply and quasi-isotropic glass/epoxy laminates between the experiment and simulation can be done more carefully. A brief summary of the experimental work of Hallett and Wisnom on each cross-ply and quasi-isotropic laminate is first given. The progressive failure analyses of these laminates are then performed and their predicted results are compared to the experimental results of Hallet and Wisnom.

4.1 Failure analysis of double-notched $[90/0]_s$ glass/epoxy laminate

4.1.1 Hallett and Wisnom's experiment

Hallett and Wisnom [74] have done the experiment on the notched $[90/0]_s$ glass-epoxy laminate and recorded the progressive damage carefully. The

specimens are 100mm long, 20mm wide with two notches of 60^0 on either side. The total notch length to specimen width ratio (*2a/w*) is 0.5. The dimension of the specimens is shown in Figure 4.1. Damage initiates at each of the notch root in the form of transverse cracks in the 90° ply and short longitudinal splits may be detected in the 0° ply. On increasing application of load, diffused transverse cracks begin to saturate the 90° ply and the longitudinal splits in the 0° ply begin to lengthen. At very close to the ultimate load, triangular-shaped delamination is detected at the interface between the 90° and 0° plies close to the notch roots. Thereafter, very rapid propagation of damage takes place and the specimen quickly reaches final failure. The progressive damage patterns of Hallett and Wisnom for notched $[90/0]_s$ glass/epoxy laminate is shown in Figure 4.2.

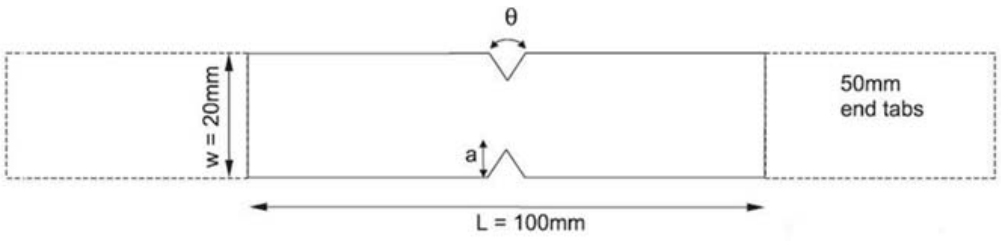

Figure 4-1 Specimen geometry in Hallett and Wisnom's experiment [74].

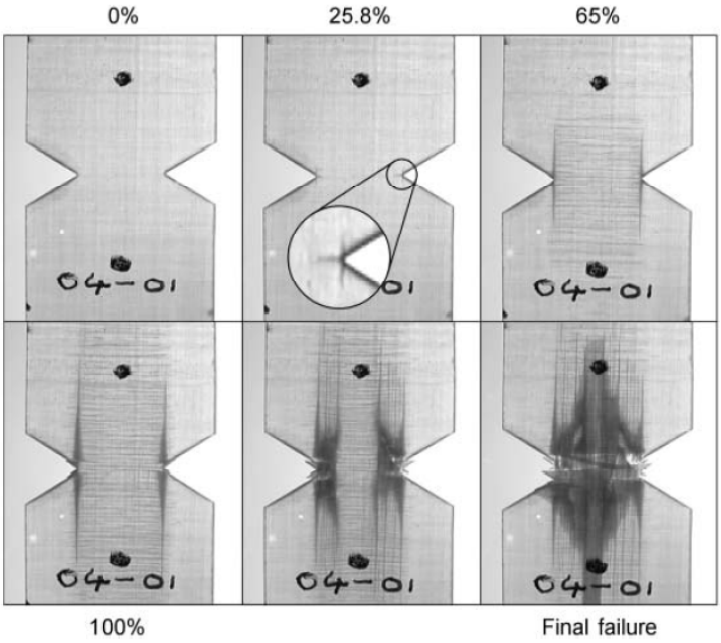

Figure 4-2 Damage progression in cross-ply specimens from Hallett and Wisnom [74]

4.1.2 Progressive failure analysis of notched $[90/0]_s$ glass/epoxy laminate

The candidate's strategy is to attempt to predict the in-plane failure modes such as transverse cracking in the 90° plies and longitudinal splits in the 0° plies by MPDM and CDM approaches, while modeling the delamination initiation and growth with cohesive elements. Similar to the analysis of $[90/0]_s$ carbon/epoxy laminate, only one quarter of the specimen is modeled for the cross-ply layup due to the symmetry of the specimen. To avoid the stress singularity occurring at the notch tips, the author approximates the sharp notch by a blunt notch with a straight edge of 1mm at the notch tip. Figure 4-3 shows the boundary conditions and mesh of the finite element model. Each ply of the finite element model is constructed with 8-node three-dimensional continuum shell elements and with only one 3D element in the thickness

direction (total of two elements in the thickness direction, since the laminate has a symmetric layup), and cohesive elements are placed at the interface between the 90° and 0° plies. Six failure models are used including the Tsai-Wu, Christensen, MMF, CDM, MCDM and MChristensen models to predict the in-plane failure. In addition, cohesive elements adopt a stress-based quadratic criterion proposed by Hou .*et. al* [53] and one energy-based criterion to model the onset and evolution of delamination. The values of parameters of cohesive elements for glass/epoxy material are discussed in Chapter 2, in which the values N = 39 MPa and $S = T$ = 89 MPa are assumed for delamination onset modeling while strain energy release rates (SERRs) $G_n = G_{IC}$ = 0.25 N/mm and $G_s = G_t = G_{IIC}$ = 1.08 N/mm are also assumed. The material properties of the glass-epoxy were reported in Table 2-2 and follow that of Hallett and Wisnom [74] .

The predicted applied stress *vs.* displacement curves are shown in Figure 4-4 and compared to the experimental results of Hallet and Wisnom [74]. The percentage of the maximum load for Wisnom's experiment and MChristensen, MCDM models are marked in Figure 4-4. All the failure models predict the damage patterns and sequences rather well, whereby matrix cracking in 90^0 ply and splitting in 0^0 ply is predicted, followed by the fiber failure in 0^0 ply. However, the ultimate loads, defined as the final load drop, predicted by the Christensen, Tsai-Wu, MMF and CDM models are low and conservative because once fiber failure occurs, it quickly causes the ultimate failure. In contrast, the MCDM and MChristensen models predict very close to the experimental failure load since they introduce a fracture process for fiber

failure modeling where the element's stiffness due to fiber failure is gradually degraded.

The progressive failure patterns predicted by the MCDM model are shown in Figures 4-5 to 4-8. Figure 4-5 shows the initiation of transverse cracks in the 90^0 ply and longitudinal splits in 0^0 ply at 25% of the maximum load. Unlike the evolution of the matrix cracks found in the cross-ply carbon/epoxy laminate where matrix cracks grow in the longitudinal direction before developing in the transverse direction, the matrix cracks for the cross-ply glass/epoxy laminate appear as original transverse cracks and then distribute evenly in the longitudinal direction. As the applied tensile load is increased, transverse cracks in the 90^0 ply start to increase in density and longitudinal splits in the 0^0 ply also increase in length (Figure 4-6). At the maximum load, fiber failure occurs at the notch roots of the 0^0 ply and delamination also initiates at the interface (Figure 4-7). In Figure 4-8, the 90^0 ply has effectively exhausted its load-carrying capability and fiber failure quickly occurs across the specimen width, leading to the ultimate failure. By this stage, a delamination area is found, near the notch roots. All of the above damage patterns and sequence agree reasonably well with the recorded observations of Hallett and Wisnom. The ultimate load by the MCDM model is under-predicted the experiment by 5%.

The progressive failure patterns predicted by the MChristensen model are shown in Figures 4-9 to 4-12 and follow those of MCDM models quite closely. However, the MChristensen model predicts less splitting and fiber failure at

the final failure than the MCDM model. The results by MChristensen model seem to agree better with the experiment of Hallett and Wisnom which did not show very long splits. The ultimate load by the MChristensen model is under-predicted the experiment by about 2%.

The progressive damage patterns using Christensen's theory follows those of MCDM and MChristensen cases. Hence, only the final damage pattern of the Christensen model is shown in Figure 4-13. Extensive matrix cracks and splitting are predicted in the 90^0 and 0^0 plies. Similar to the MCDM model, the Christensen model predicts more splitting and fiber failure in the 0^0 ply than the MChristensen model. Besides, a small triangular delamination area has been found by the Christensen model. This delamination area agrees with the experimental observation of Hallett and Wisnom. However, the ultimate load by the Christensen model is low and under-predicted the experiment by 23%.

The progressive failure patterns predicted by the Tsai-Wu model also follow those of MCDM, MChristensen and Christensen models. The final damage pattern of the Tsai-Wu model is shown in Figure 4-14. The ultimate load by the Tsai-Wu model is under-predicted the experiment by 26%.

The results for MMF are shown in Figure 4-15. Only the damage patterns just after the major load drop are shown because the initiation and propagation of matrix-dominated failure in the 90^0 ply and initiation of longitudinal splits in the 0^0 ply are similar to the Christensen and Tsai-Wu cases. However, in the MMF case, much more damage are found in the 90^0 and 0^0 plies while little

delamination is predicted. The ultimate load by MMF model is under-predicted the experiment by 23.4%.

The final failure patterns predicted by the CDM model are shown in Figures 4-16. The CDM model predicts less transverse cracks and longitudinal splits but more fiber failure and delamination than the MMF model. The ultimate load by CDM is low and under-predicted the experiment by about 26%.

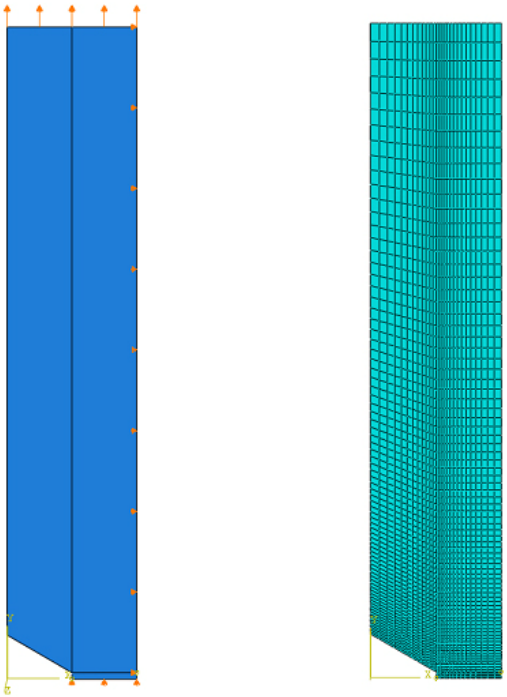

Figure 4-3 Boundary conditions and mesh of finite element model for $[90/0]_s$ glass/epoxy specimens.

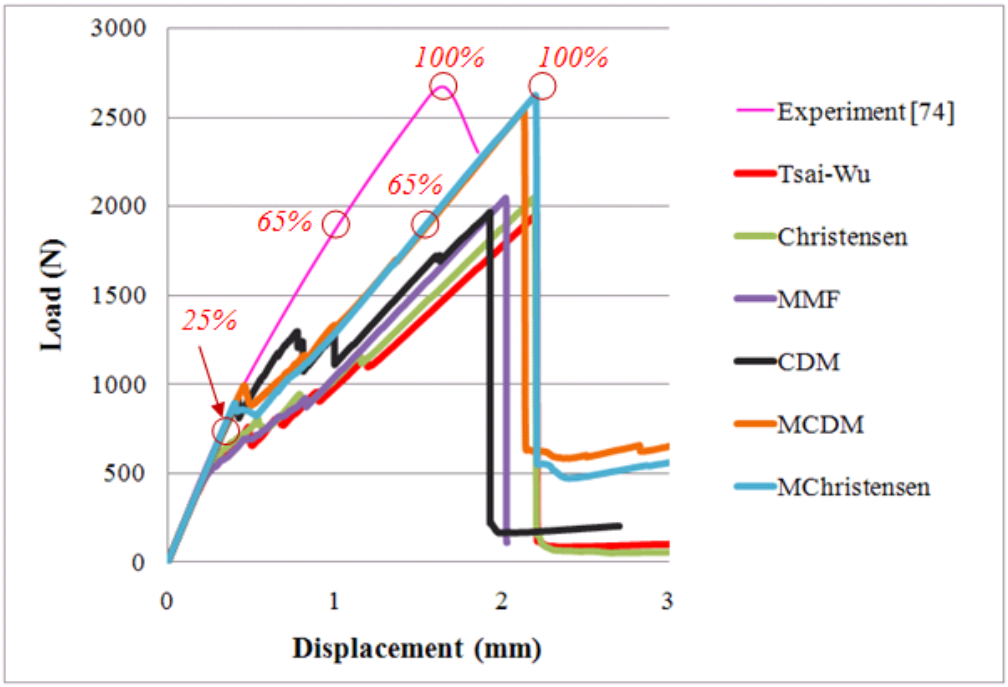

Figure 4-4 Predicted load-displacement curves and comparison with the experiment for the $[90/0]_s$ glass/epoxy laminate.

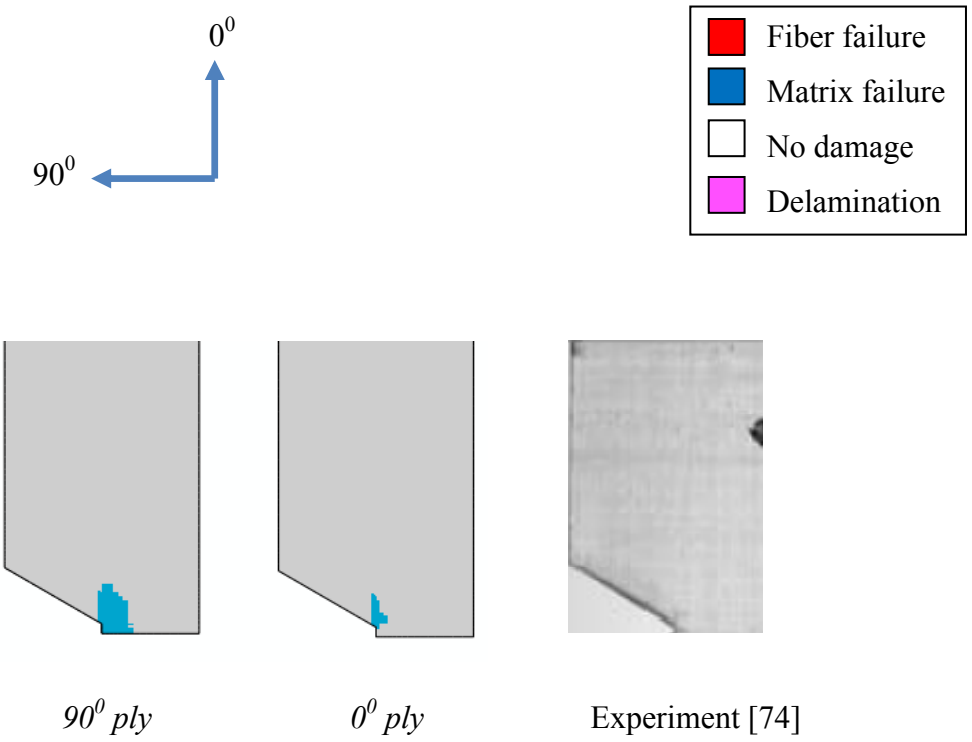

Figure 4-5 MCDM: Predicted damage patterns in comparison with Hallett and Wisnom's experiment (25% maximum load).

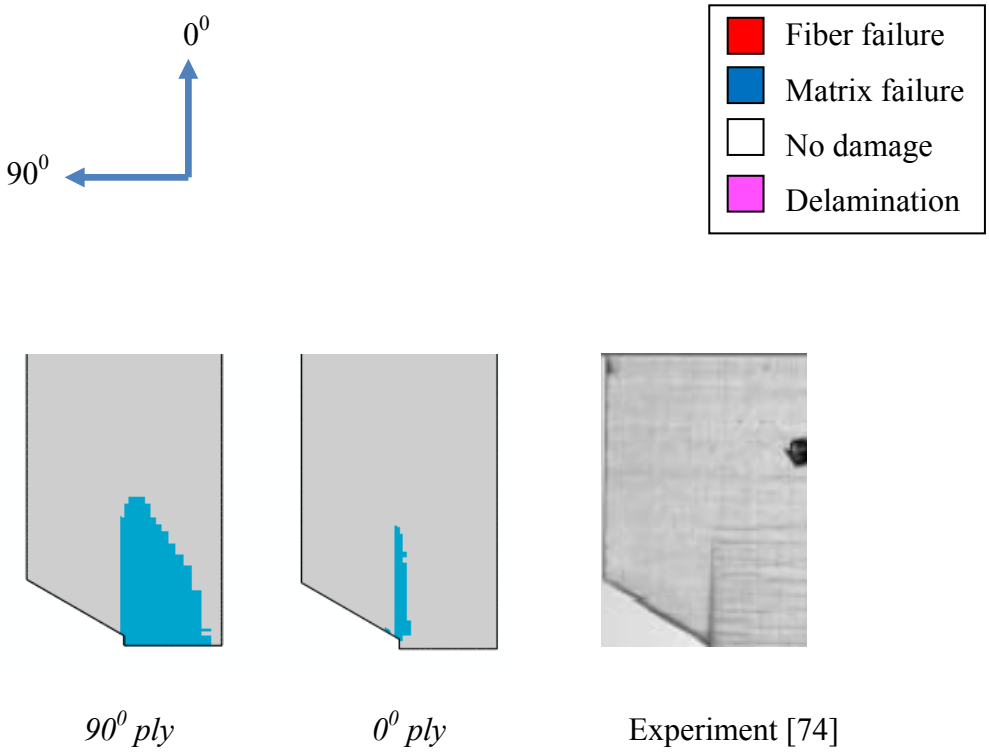

Figure 4-6 MCDM: Predicted damage patterns in comparison with Hallett and Wisnom's experiment (65% maximum load).

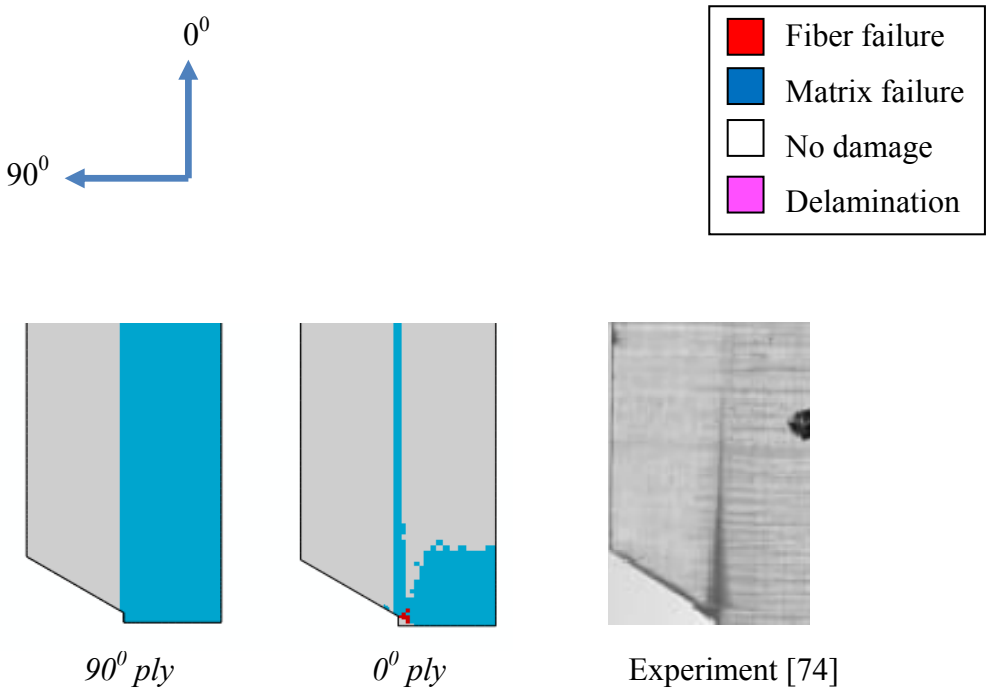

Figure 4-7 MCDM: Predicted damage patterns in comparison with Hallett and Wisnom's experiment (100% maximum load).

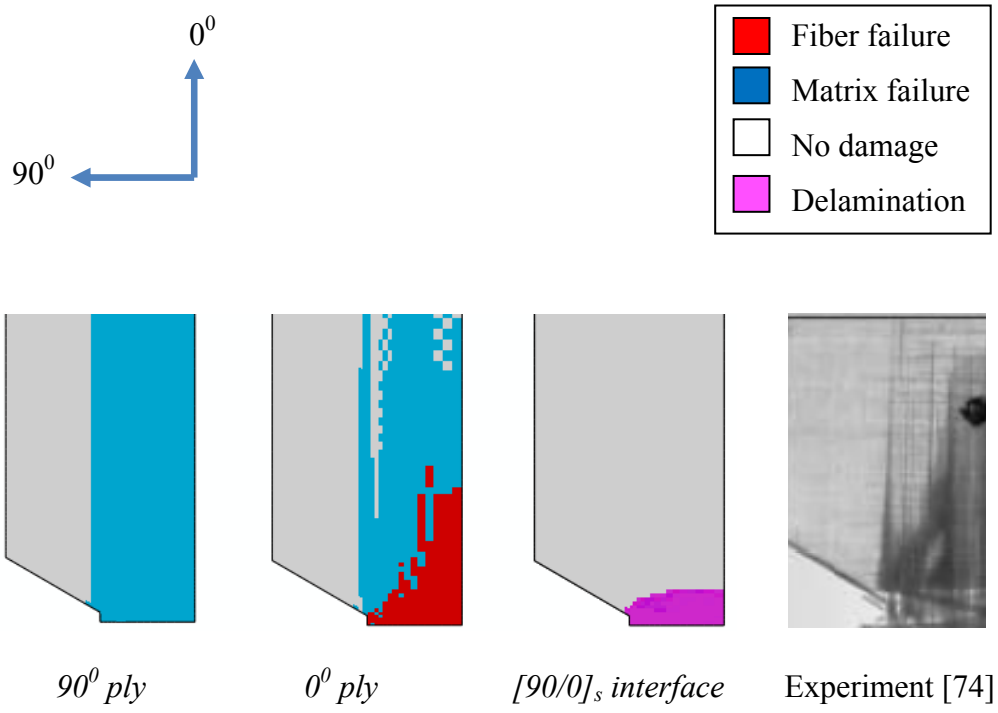

Figure 4-8 MCDM: Matrix crack in the 90^0 ply, splitting and fiber failure in the 0^0 ply and delamination at the [90/0] interface after the final load drop.

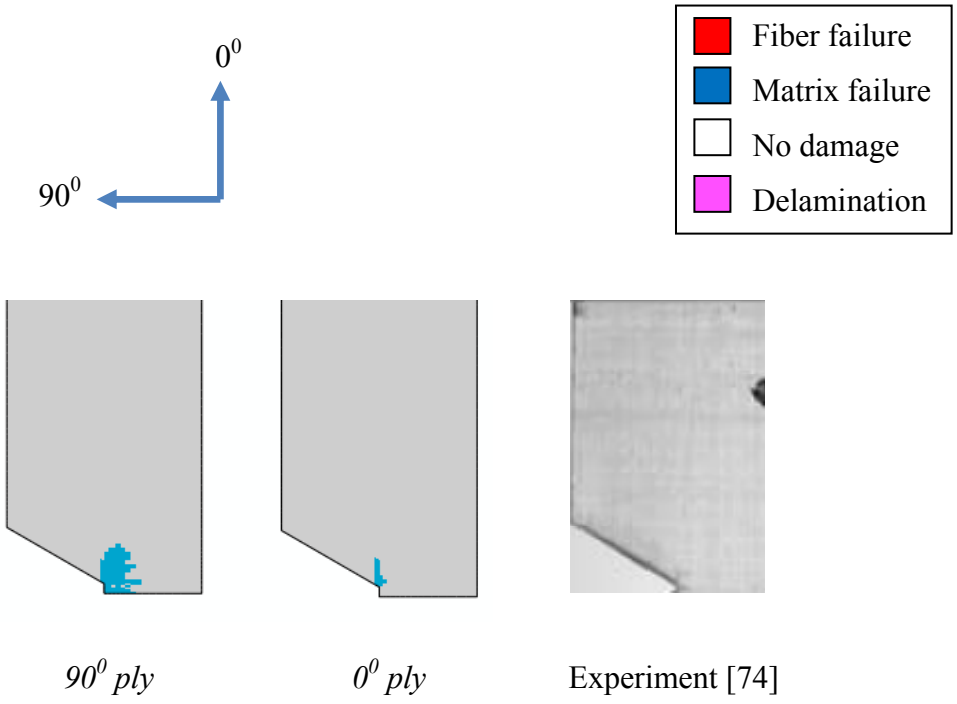

Figure 4-9 MChristensen: Predicted damage patterns in comparison with Hallett and Wisnom's experiment (25% maximum load).

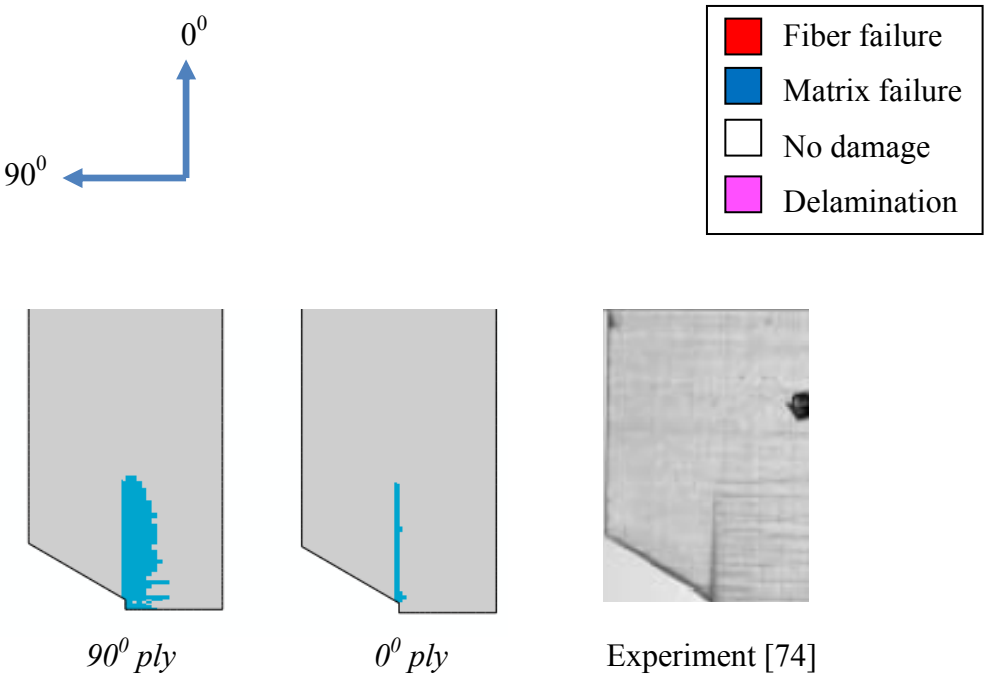

Figure 4-10 MChristensen: Predicted damage patterns in comparison with Hallett and Wisnom's experiment (65% maximum load).

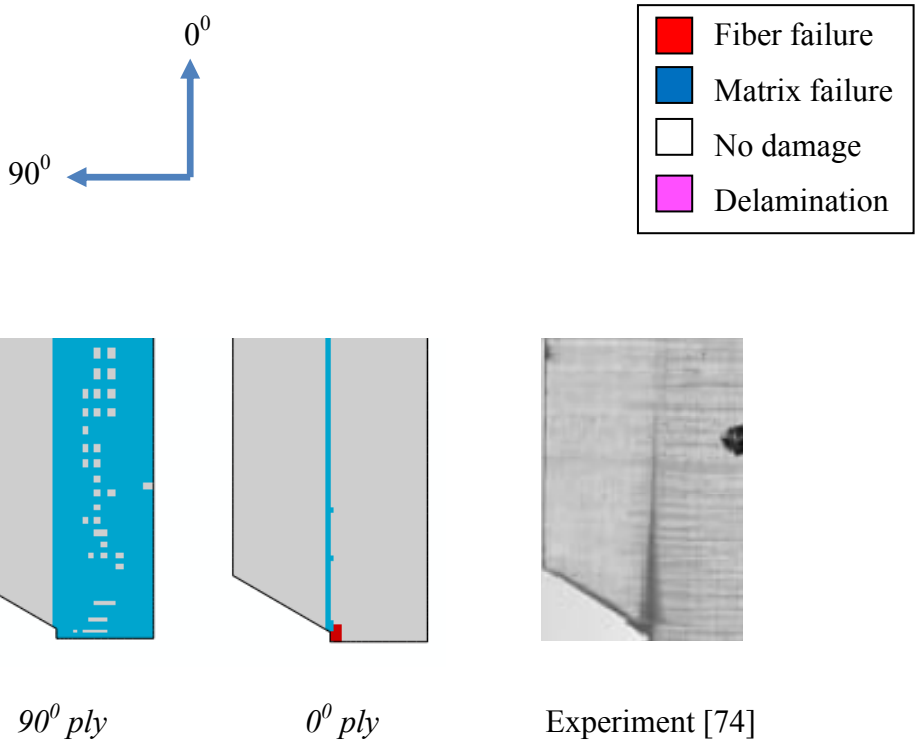

Figure 4-11 MChristensen: Predicted damage patterns in comparison with Hallett and Wisnom's experiment (100% maximum load).

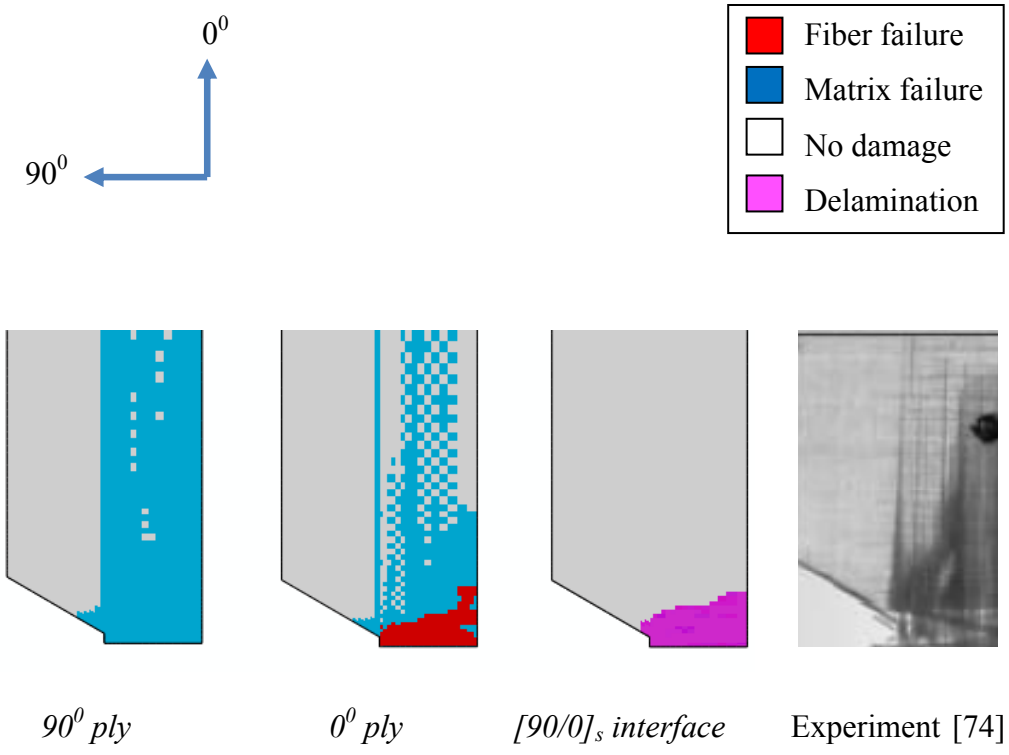

Figure 4-12 MChristensen: Matrix crack in the 90^0 ply, splitting and fiber failure in the 0^0 ply and delamination at the [90/0] interface after the final load drop.

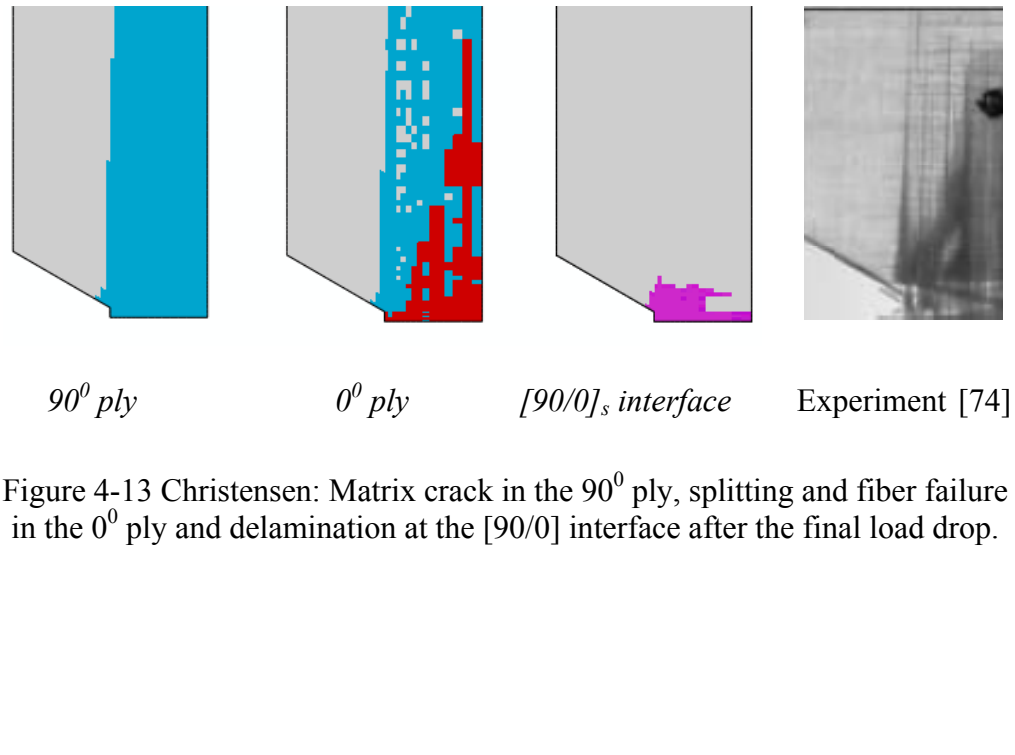

Figure 4-13 Christensen: Matrix crack in the 90^0 ply, splitting and fiber failure in the 0^0 ply and delamination at the [90/0] interface after the final load drop.

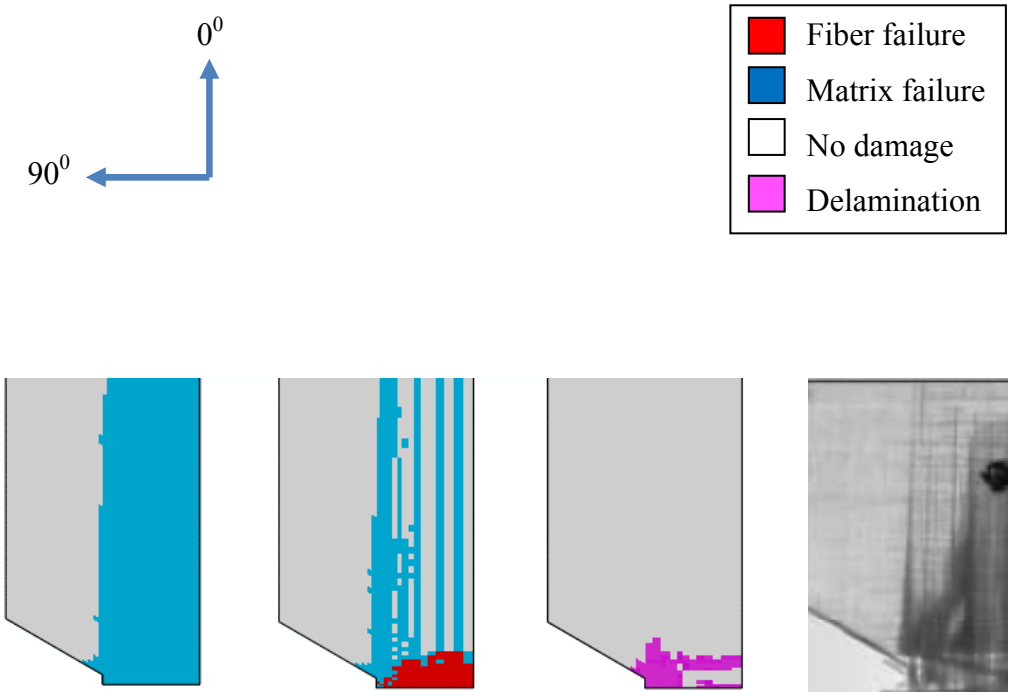

Figure 4-14 Tsai-Wu: Matrix crack in the 90^0 ply, splitting and fiber failure in the 0^0 ply and delamination at the [90/0] interface after the final load drop.

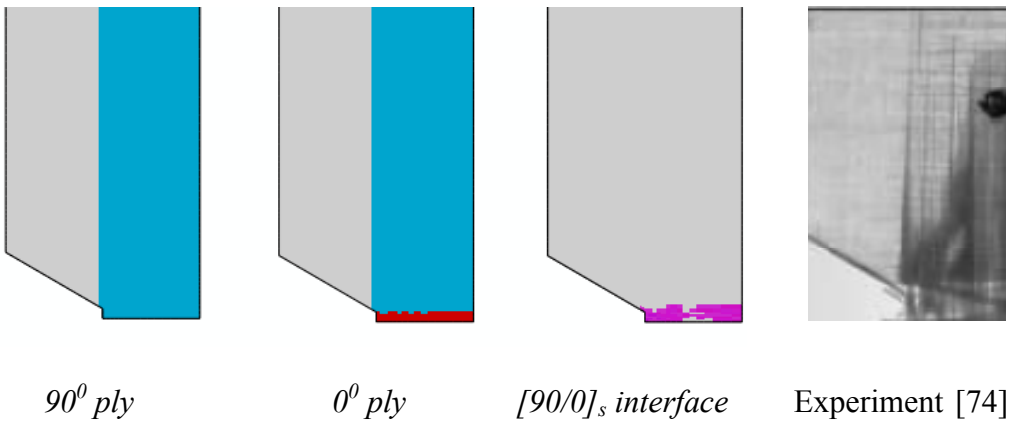

Figure 4-15 MMF: Matrix crack in the 90^0 ply, splitting and fiber failure in the 0^0 ply and delamination at the [90/0] interface after the final load drop.

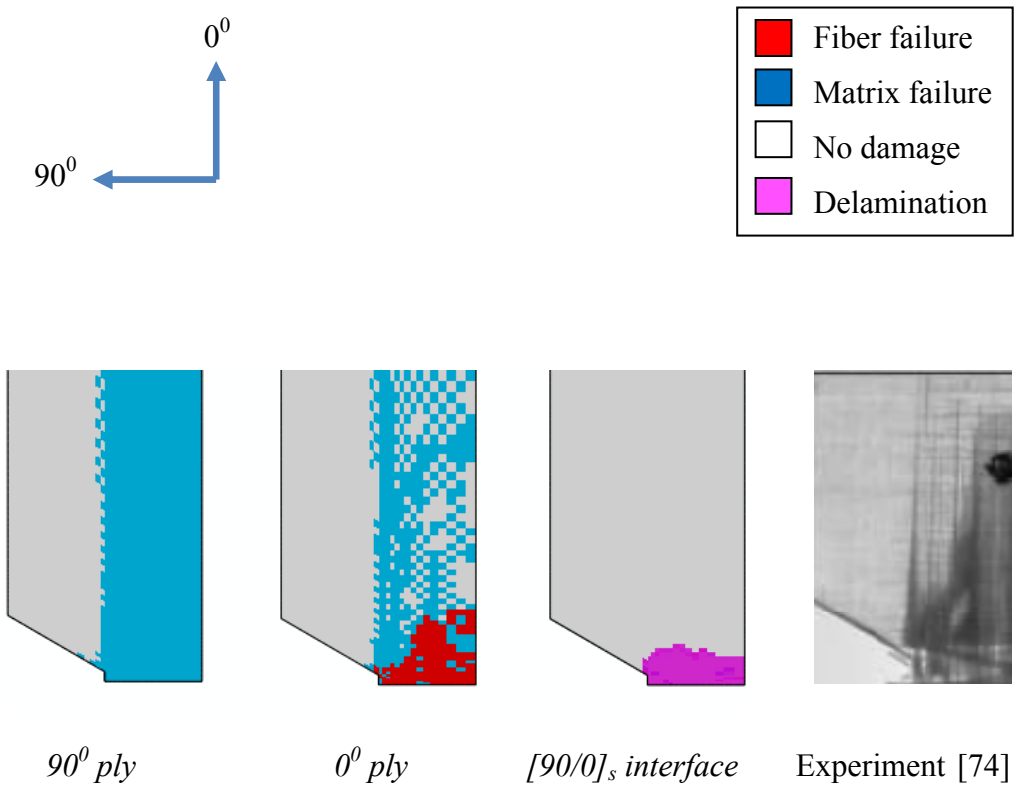

Figure 4-16 CDM: Matrix crack in the 90^0 ply, splitting and fiber failure in the 0^0 ply and delamination at the [90/0] interface after the final load drop.

4.2 Failure analysis of notched $[45/90/-45/0]_s$ glass/epoxy laminate

4.2.1 Hallett and Wisnom's experiment

Hallett and Wisnom [74] also performed experiments on double-notched $[45/90/-45/0]_s$ glass/epoxy laminate and obtained the damage progression in quasi-isotropic specimens. The progressive damage patterns of Hallett and Wisnom for notched quasi-isotropic glass/epoxy laminate is shown in Figure 4-17. The failure of specimens can be seen by the progression of cracks running at 45^0 from the notch tips. When the applied load is increased, additional splitting in the 0^0 ply and $\pm 45^0$ plies and matrix cracking in each ply quickly occur. Further increase in load results in fiber failures and delamination in each ply, causing the specimens to ultimate failure.

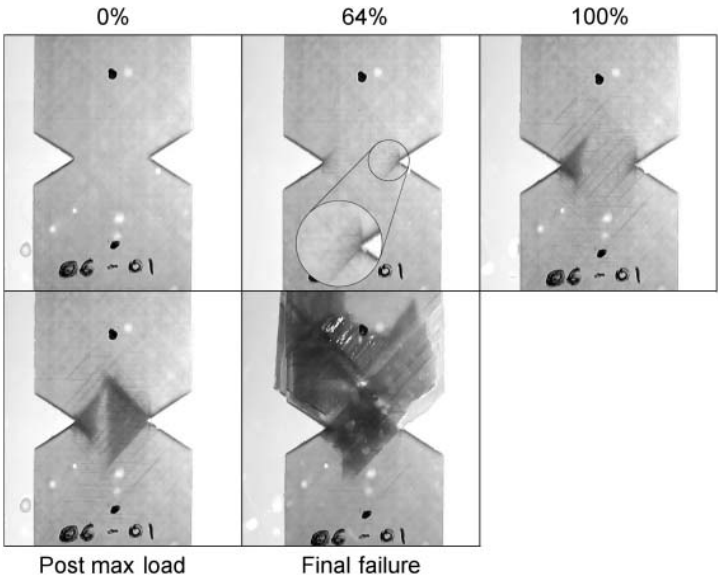

Figure 4-17 Damage progression in quasi-isotropic specimens from Hallett and Wisnom [74].

4.2.2 Progressive failure analysis of notched $[45/90/-45/0]_s$ Glass/Epoxy laminate

The FE models of the $[45/90/-45/0]_s$ laminate are constructed with 8-node three-dimensional continuum shell elements (SC8R) and 8-node hexahedral cohesive elements COH3D8 with one element in the thickness per ply. The ply thickness is 0.125mm and the cohesive element thickness is assumed 0.005 mm. Figure 4-18 shows the boundary conditions and mesh of the finite element (FE) models. Six failure models employing the Tsai-Wu, Christensen, MMF, CDM, MCDM and MChristensen criteria are used to predict the progressive failure of the quasi-isotropic glass/epoxy laminate whereas cohesive elements are inserted as interfaces to model the delamination. The values of cohesive parameters used for the analysis of quasi-isotropic laminate are the same as those used for the analysis of cross-ply laminate since the same glass/epoxy material is applied for both laminates.

The predicted applied load *vs.* displacement curves for the Tsai-Wu, Christensen, MMF, CDM, MCDM and MChristensen models are shown in Figure 4-19 and their peak values are compared to the ultimate load value of $[45/90/-45/0]_s$ glass/epoxy laminate reported in Hallett and Wisnom work [74]. The damage patterns predicted by all failure models are presented from Figures 4-20 to 4-27. As can be seen, the splitting and fiber failure predicted in $\pm 45^0$, 90^0 and 0^0 plies agree reasonably well with cracks running at $\pm 45^0$ from the notch root observed in the experiment of Hallett and Wisnom [74] (Figures 4-22 to 4-27). It is noted that the damage in experimental photo in Figures 4-

22 to 4-27 has been super-imposed by damages in of all plies of the quasi-isotropic glass/epoxy laminate. The simulation results also show that the MCDM and MChristensen models predict the experimental failure load better than conventional models because they implement a fracture process for fiber failure modeling. Conversely, the prediction by the CDM model is very conservative since it predicts the fiber failure quite early which rapidly causes the final failure.

The progressive damage patterns predicted by the MChristensen model are presented in Figures 4-20 to 4-22. The percentage of the maximum load for the MChristensen model is marked in Figure 4-19. As can be seen in Figure 4-20, short longitudinal splits initiate from the notch roots in the 45^0 and 0° plies and transverse matrix cracks can be found in the 90° ply. The -45^0 ply is also found with both matrix cracks and splits. On increasing application of load, longitudinal splits and matrix crack in the $\pm 45^0$ plies and 0° ply quickly grow whereas the 90^0 ply has been saturated by numerous transverse cracks. At very close to the failure load, extensive splitting and matrix cracking are predicted in the 0^0 ply and $\pm 45^0$ plies and fiber failure has been initiated at the notch roots of these plies (Figure 4-21). It is found that delamination also initiates at the interfaces by this stage. Shortly thereafter, fiber failures occur across the width of the $\pm 45^0$ and 0^0 plies and delamination extensively propagate at the all interfaces, leading to the ultimate failure (Figure 4-22). All of the damage patterns and sequence correlate well to the experiment of Hallet and Wisnom. The ultimate load by the MChristensen model is under-predicted the experiment by about 9.5%.

The progressive damage patterns predicted by the MCDM model follow those of the MChristensen model very closely. Only the final damage patterns by the MCDM model is shown in Figure 4-23. The delamination area predicted by MCDM is similar to the MChristensen case but more in-plane damage is found in the MCDM case. The ultimate load predicted by the MCDM is under-predicted the experiment by about 13%.

The progressive failure patterns using Christensen, Tsai-Wu and MMF models also follow those of the MChristensen model. Figures 4-24 to 4-26 present the final damage patterns of the Christensen, Tsai-Wu and MMF models, respectively. The final failure in these models is caused by fiber failures in the 0^0 and $\pm 45^0$ plies and extensive delamination at all the interfaces. The ultimate loads predicted by the Christensen, Tsai-Wu and MMF models are under-predicted the experiment by about 18.8%, 22.4% and 25.8%, respectively.

The results the CDM model is shown in Figure 4-26. The CDM model predicts less delamination than all the other models. The ultimate load by CDM model is low and is under-predicted the experiment by 30%.

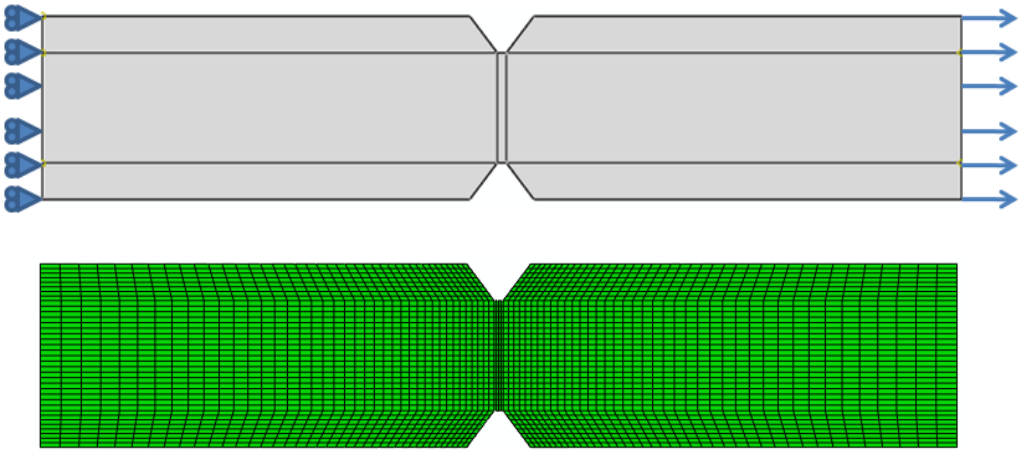

Figure 4-18 Boundary conditions and mesh of the FE model for quasi-isotropic glass/epoxy specimens.

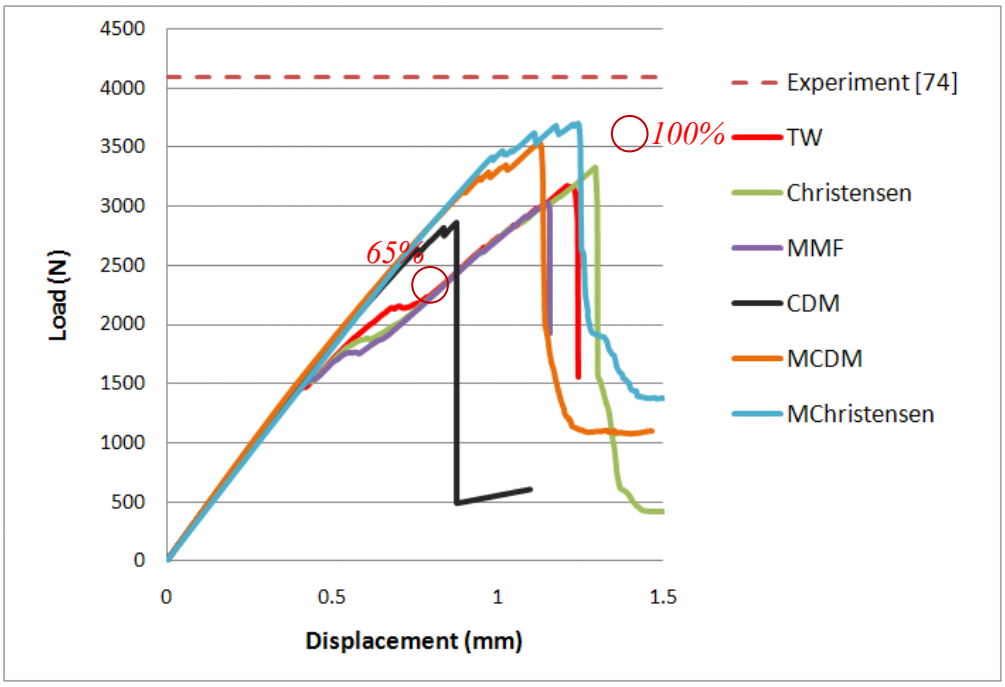

Figure 4-19 Predicted load-displacement curves and comparison with the experiment for the quasi-isotropic glass/epoxy laminate.

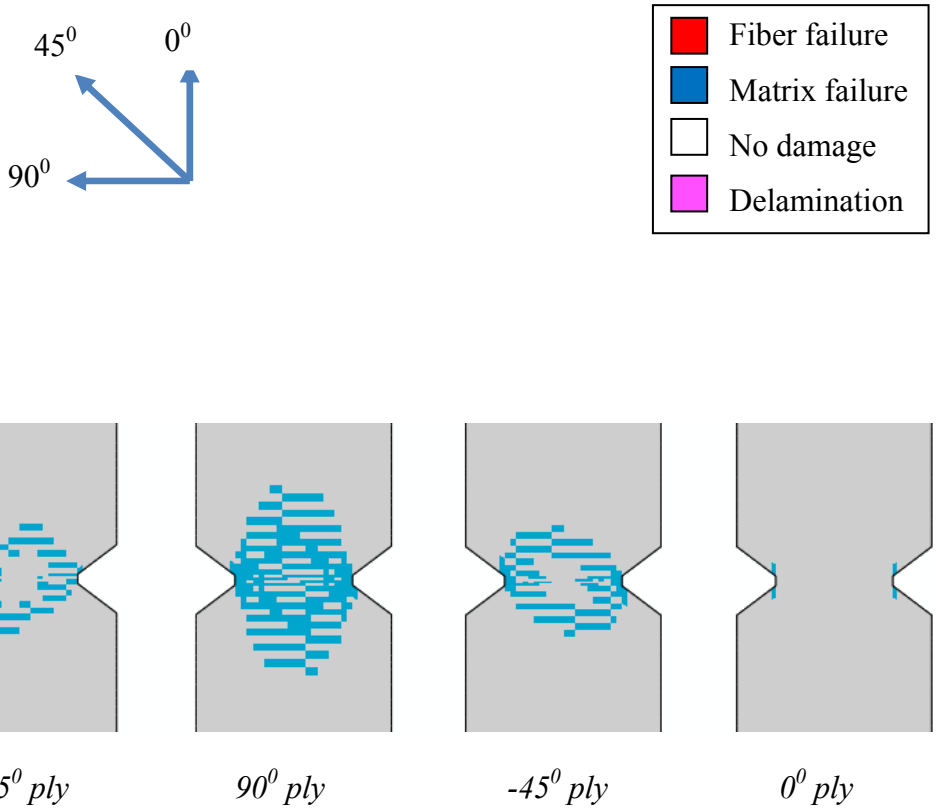

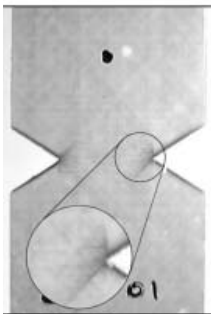

Experiment [74]

Figure 4-20 MChristensen: Predicted damage patterns in comparison with the experiment (6% maximum load).

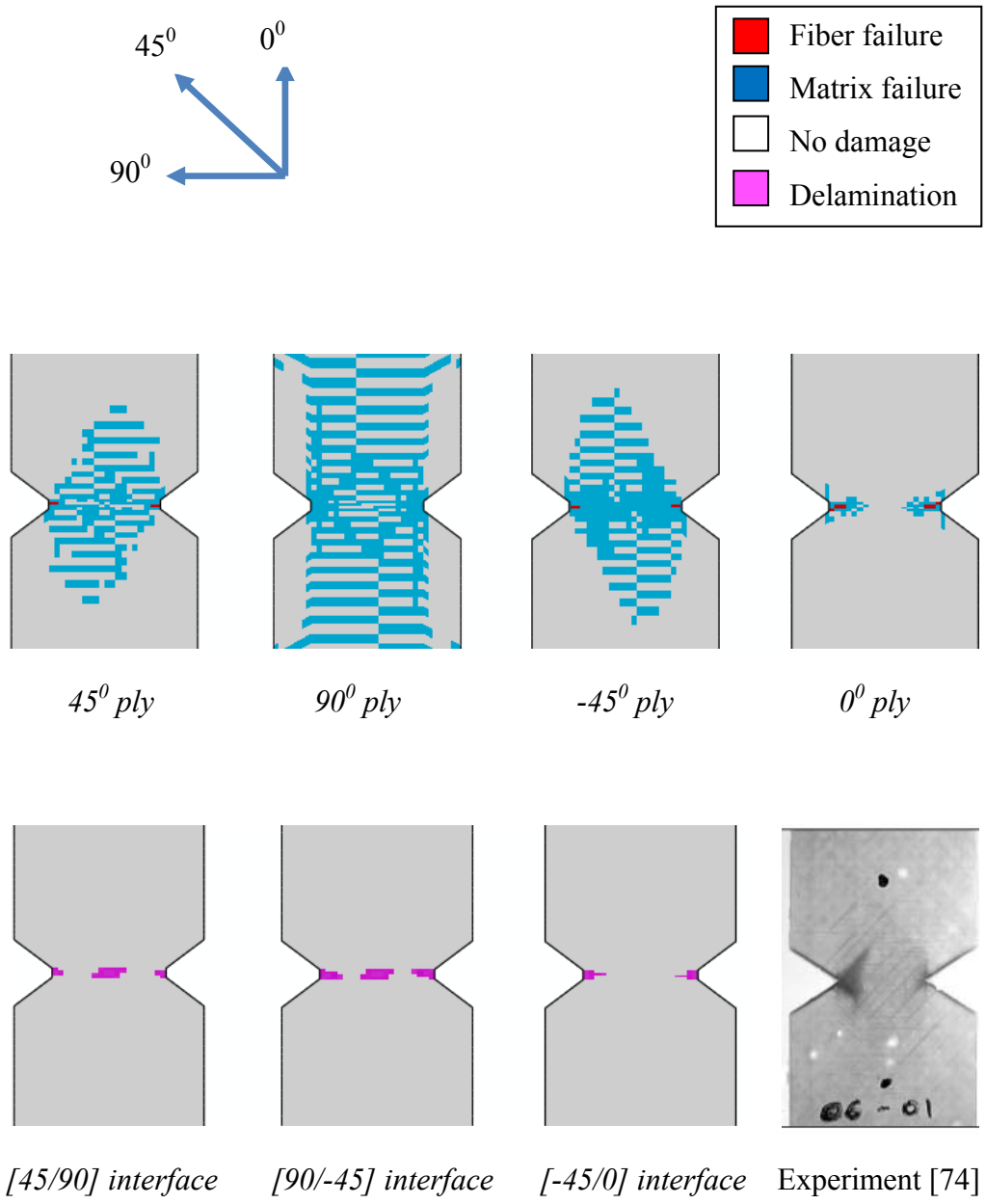

Figure 4-21 MChristensen: Predicted damage patterns in comparison with the experiment (100% maximum load).

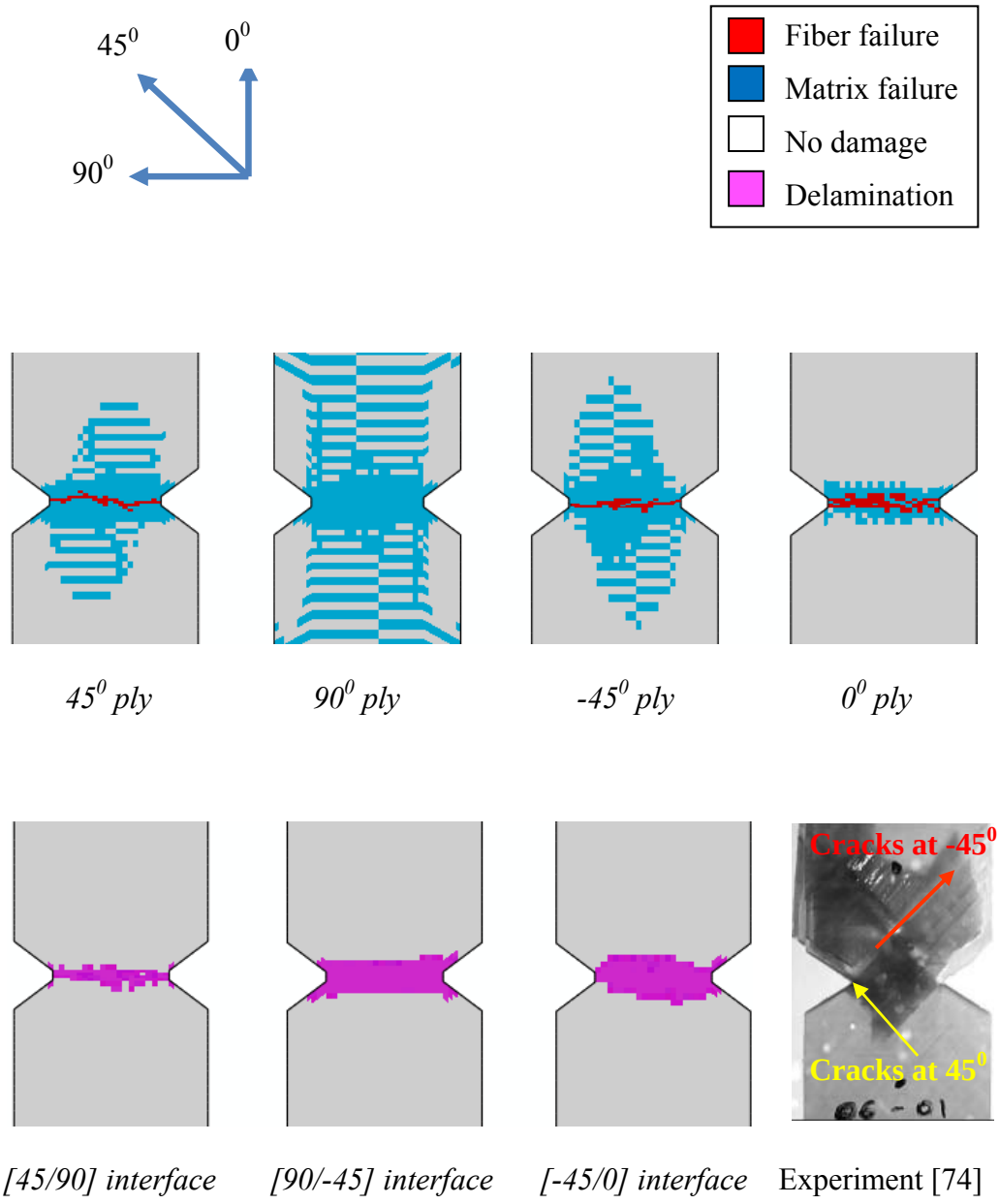

Figure 4-22 MChristensen: Final failure in the 45^0 ply, 90^0 ply, -45^0 ply and 0^0 ply and delamination at all the interfaces.

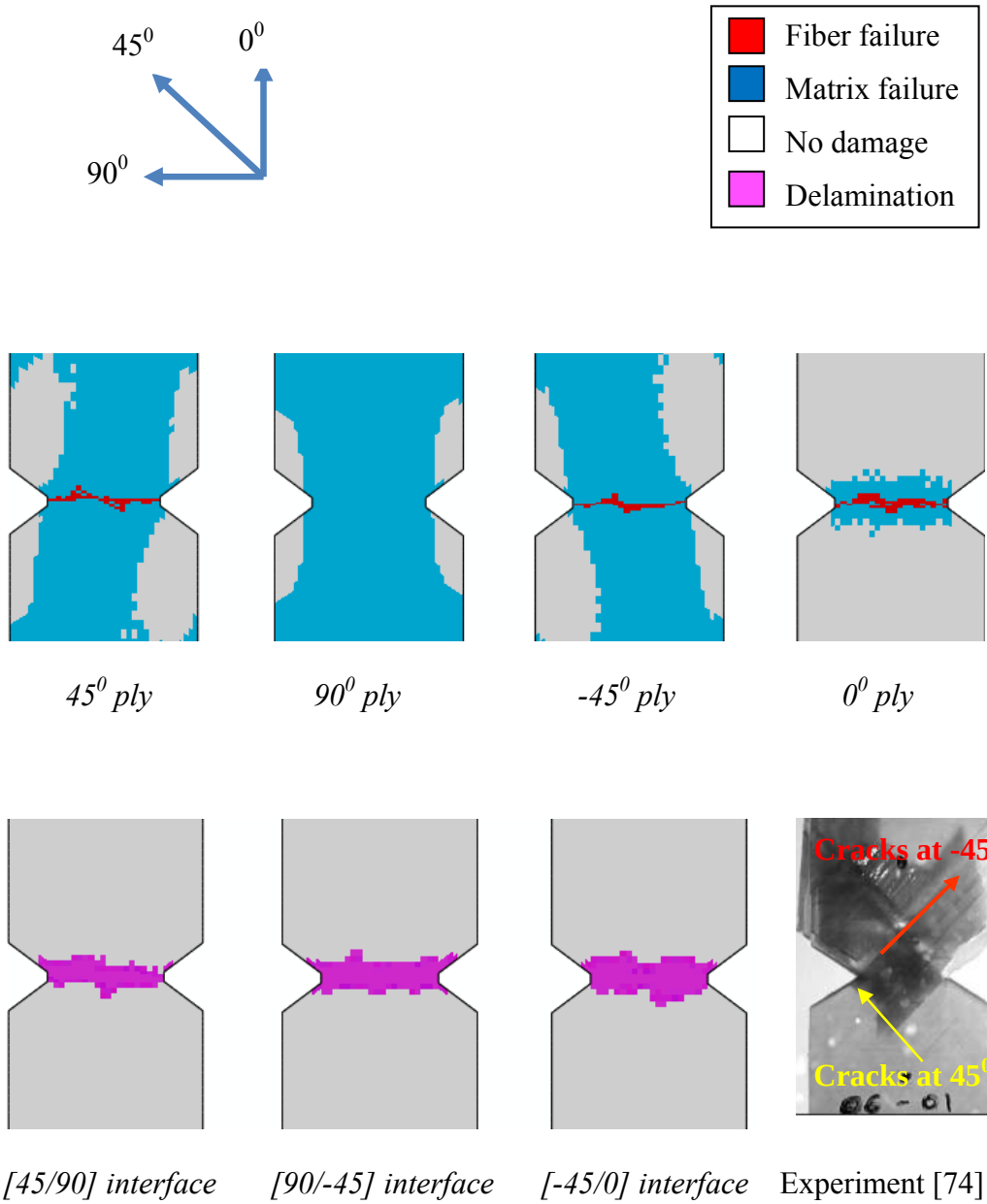

Figure 4-23 MCDM: Final failure in the 45^0 ply, 90^0 ply, -45^0 ply and 0^0 ply and delamination at all the interfaces.

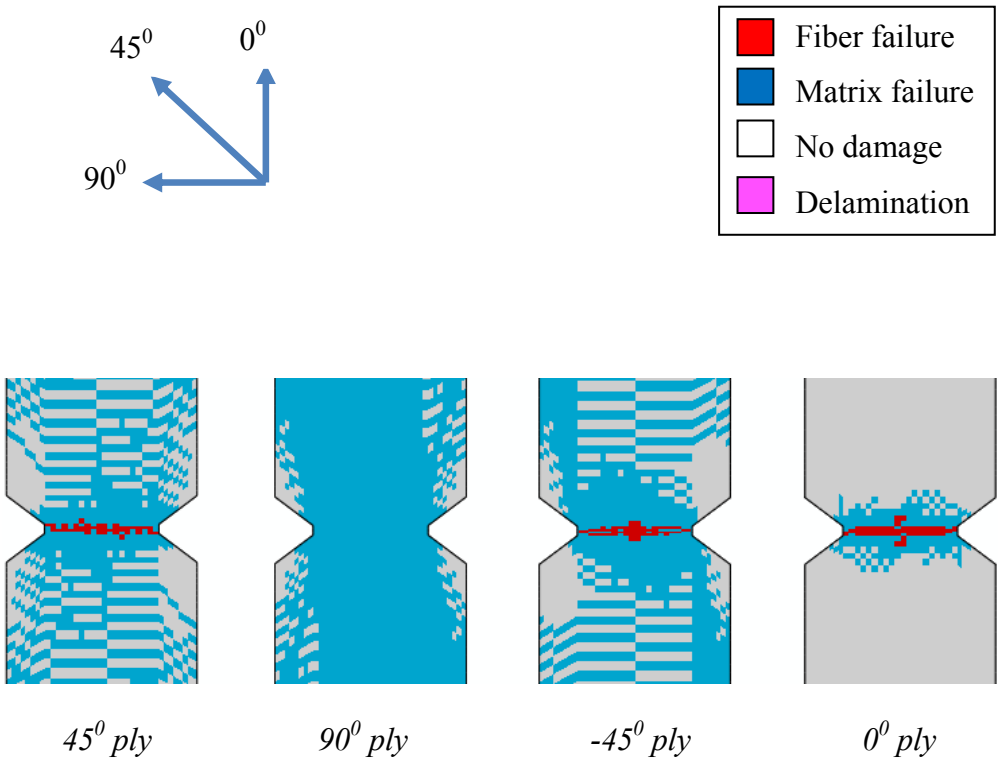

Figure 4-24 Christensen: Final failure in the 45^0 ply, 90^0 ply, -45^0 ply and 0^0 ply and delamination at all the interfaces.

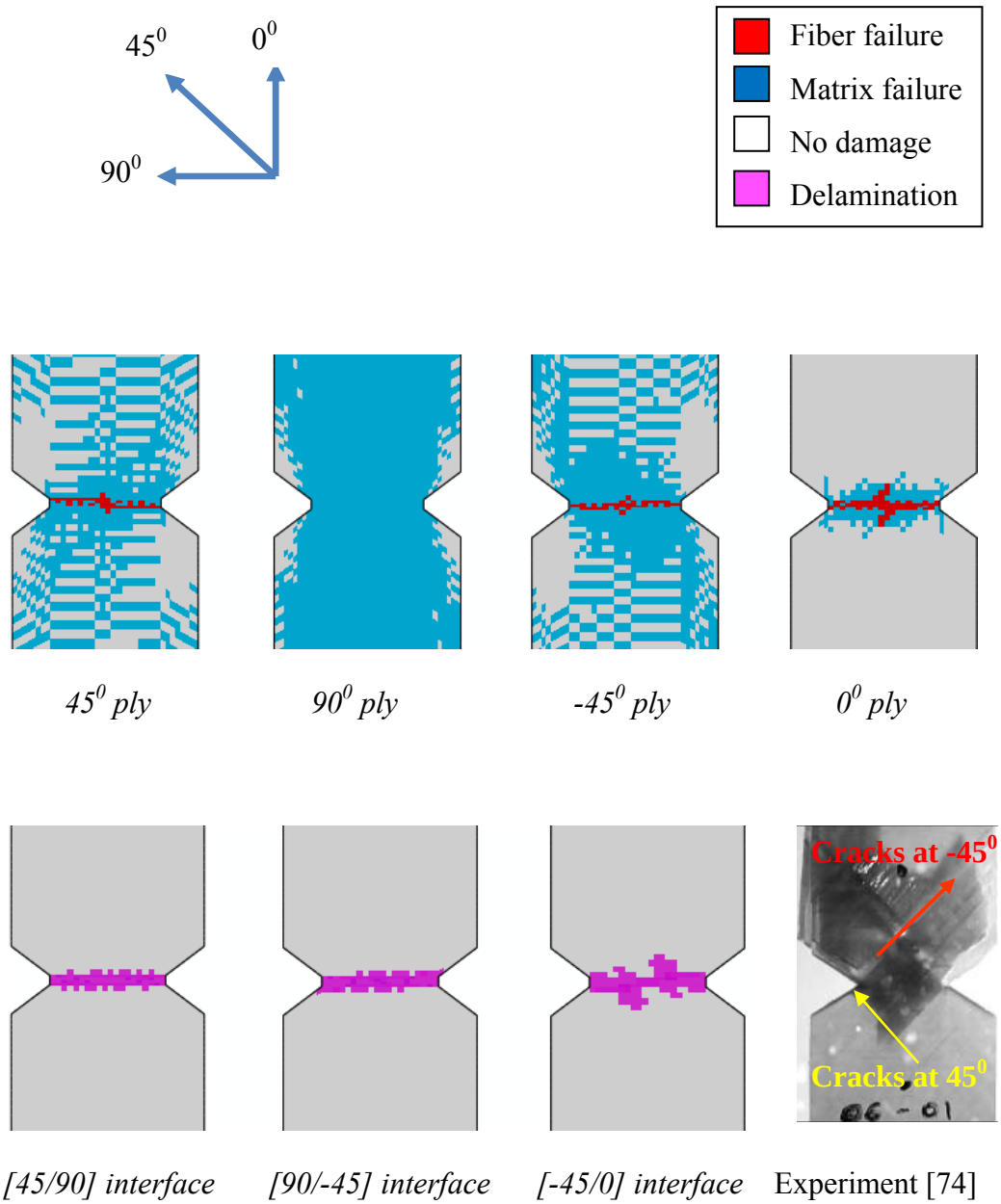

Figure 4-25 Tsai-Wu: Final failure in the 45^0 ply, 90^0 ply, -45^0 ply and 0^0 ply and delamination at all the interfaces.

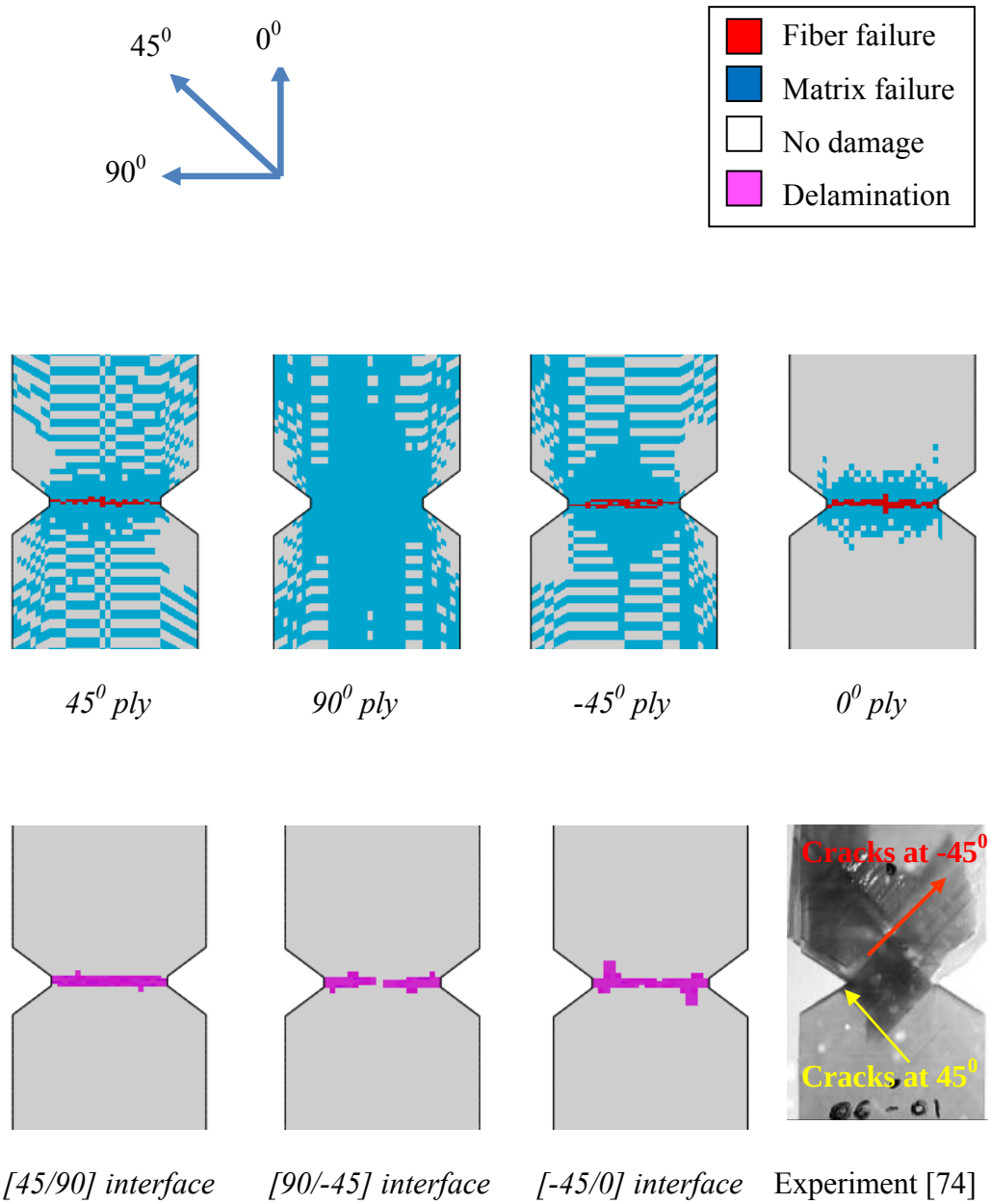

Figure 4-26 MMF: Final failure in the 45^0 ply, 90^0 ply, -45^0 ply and 0^0 ply and delamination at all the interfaces.

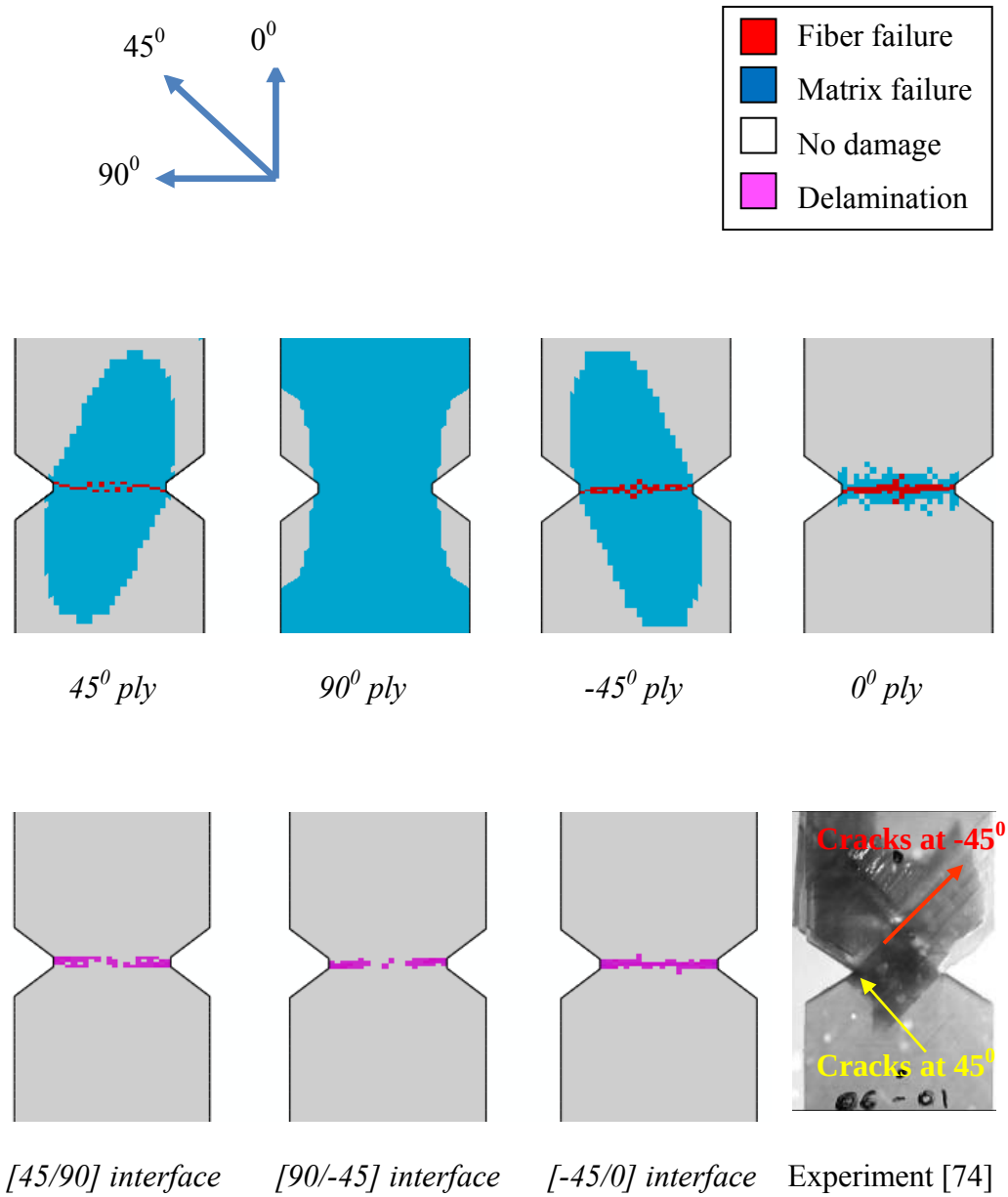

Figure 4-27 CDM: Final failure in the 45^0 ply, 90^0 ply, -45^0 ply and 0^0 ply and delamination at all the interfaces.

4.3 Conclusion

Various failure models are used to predict the damage progression in notched cross-ply and quasi-isotropic glass/epoxy laminates and compared to the experimental results of Hallett and Wisnom [74]. All of the predicted failure loads for the two laminates are summarized in Figure 4-28 and Table 4-1. Simulation results for the cross-ply laminate show good correlation between the analysis and the experiment. The progressive damage patterns observed in the experiment including the initiation and extension of longitudinal splitting, matrix cracking and delamination have been reasonably captured by the simulation. However, the failure loads predicted by Christensen, Tsai-Wu, MMF and CDM models are lower than the experiment because these models consider a complete loss of element's stiffness due to fiber failure, causing the ultimate load prediction very conservative. On the other hand, the MCDM and MChristensen predict the experimental failure load better because they consider that the damaged fibers still have residue stiffness and can carry additional load until ultimate failure. It is noted that a discontinuity in the predicted curves has been observed in the cross-ply glass/epoxy laminate which is similar to the case of cross-ply carbon/epoxy laminate. This can be explained for a substantial stiffness loss of the 90^0 ply before the fiber failure in the 0^0 ply occurs.

Simulation results for the quasi-isotropic glass/epoxy laminate show a good agreement with the experimental ones when transverse cracking in $\pm 45^0$ and

90^0 plies, longitudinal splitting and fiber failure in $\pm 45^0$ and 90^0 plies and delamination at the interfaces are all predicted. A discontinuity in the load *vs.* displacement curves by the Tsai-Wu, Christensen and MMF models is found while the predicted curves by the CDM, MCDM and MChristensen models are continuous. This is because the CDM, MCDM and MChristensen models degrade the stiffness of the failed elements gradually while the other models quickly and completely degrade the stiffness of failed elements. Therefore, when a large number of elements fail in Tsai-Wu, Christensen and MMF models, a sudden loss in their stiffness will cause a discontinuity in the load *vs.* displacement curve. Overall, the MCDM and MChristensen models provide better predictions than the other models. The failure loads predicted by the MCDM and MChristensen models are under-predicted the experiment by 13% and 9.5%, respectively.

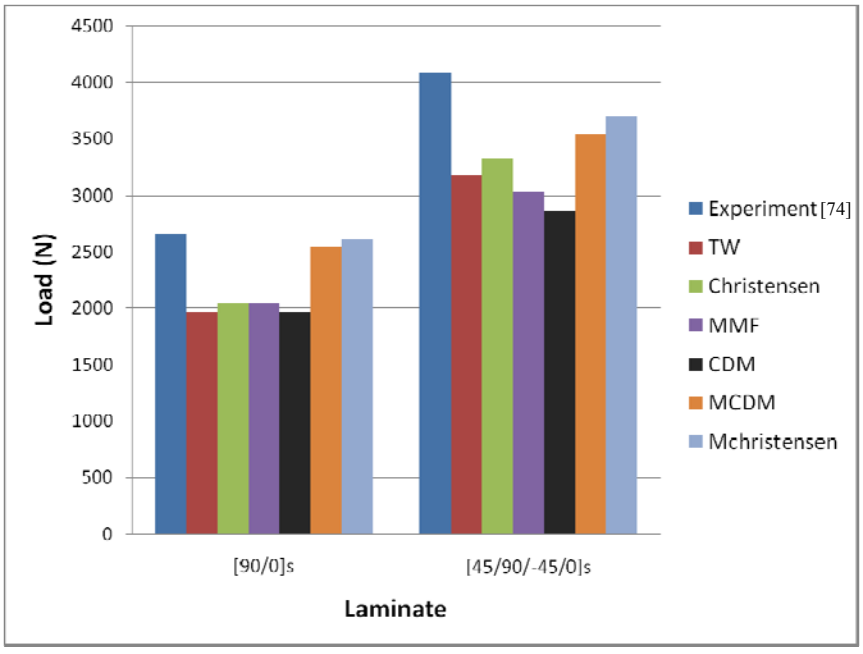

Figure 4-28 Comparison between predicted failure loads by all failure models and the experimental failure loads [74] for glass/epoxy laminates.

Table 4-1 Summary of the ultimate loads predicted by all models for the glass/epoxy cross-ply and quasi-isotropic laminates.

	Ultimate loads (% prediction)	
	$[90/0]_s$ laminate	**$[45/90/-45/0]_s$ laminate**
Experiment [74]	2660 N	4086 N
Christensen model	2049 N *(77%)*	3328 N *(81.2%)*
Tsai-Wu model	1963 N *(74%)*	3171 N *(77.6%)*
MMF model	2032 N *(76.4%)*	3033 N *(74.2%)*
CDM model	1968 N *(74%)*	2862 N *(70%)*
MCDM model	2527 N *(95%)*	3537 N *(87%)*
MChristensen model	2610 N *(98%)*	3699 N *(90.5%)*

Chapter 5

Mesh-dependency study and parametric studies of cohesive elements and MPDM scheme for notched $[45/90/-45/0]_s$ carbon/epoxy laminate

This chapter presents the mesh-dependency and parametric studies of cohesive elements and MPDM scheme for the notched $[45/90/-45/0]_s$ carbon/epoxy laminate. This particular quasi-isotropic carbon/epoxy laminate is chosen since it has been experimentally tested in this thesis and provided with clear delamination at the interfaces. Furthermore, since the quasi-isotropic laminates have been widely used in reality, it is one of the author's aims to provide analytical studies on the quasi-isotropic laminate which is more general and complicated than the cross-ply laminate so that the studies on the cross-ply composite laminate can be performed similarly.

5.1 Mesh dependency study

5.1.1 Description of the mesh dependency study

Several FE meshes are used in this study corresponding to the element types (two dimensional elements or three dimensional elements), notch's geometries

(sharp notch and blunt notch) and mesh density. These meshes can be divided into 4 groups: meshes of two-dimensional elements and sharp notch (2D Sharp), meshes of two-dimensional elements and blunt notch (2D Blunt), meshes of three-dimensional elements and sharp notch (3D Sharp) and meshes of three-dimensional elements and blunt notch (3D Blunt). Each mesh group includes four FE meshes with different mesh density. Details of mesh density and element size at the notch tip are given in Table 5-1 and Table 5-2, respectively. The meshes for the sharp notch and blunt notch are shown in Figures 5-1 and 5-2 and their close-up meshes at the notch tip are presented in Figure 5-3 and 5-4. It is noted that the case of mesh B with 3D Blunt has been used for the progressive failure analysis of the $[45/90/-45/0]_s$ carbon/epoxy laminate in Chapter 3.

Table 5-1 Details of finite element meshes for the mesh-dependency study.

Cases	**Mesh A**	**Mesh B**	**Mesh C**	**Mesh D**
2D Sharp	720 elements	2880 elements	5520 elements	10800 elements
2D Blunt	750 elements	2960 elements	5670 elements	11004 elements
3D Sharp	5040 elements	20160 elements	39640 elements	75600 elements
3D Blunt	5250 elements	20720 elements	40960 elements	77028 elements

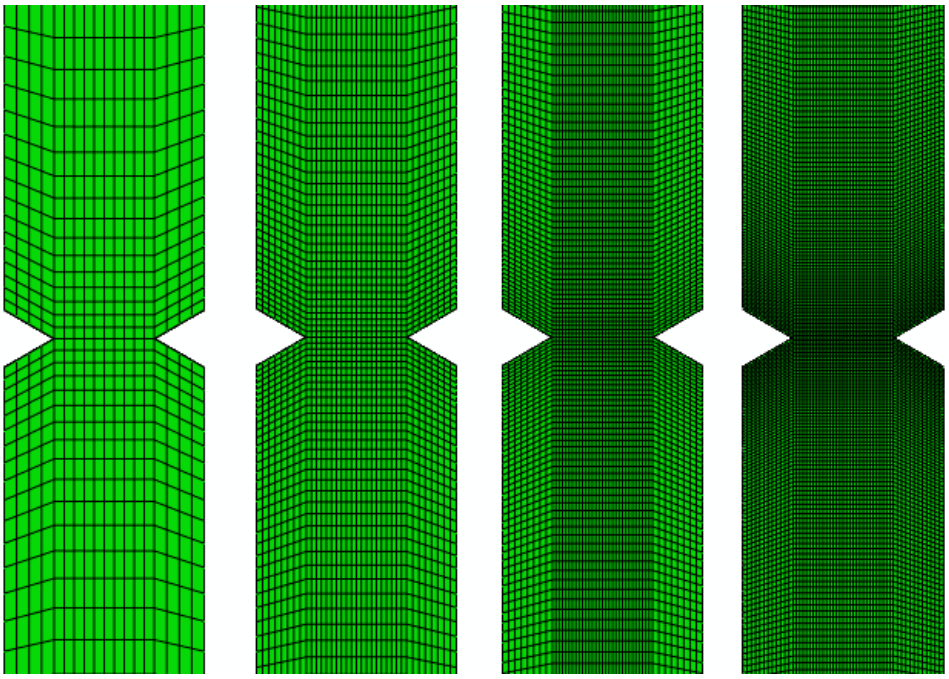

Mesh A Mesh B Mesh C Mesh D

Figure 5-1 Finite element meshes for the sharp notch (either 2D or 3D elements).

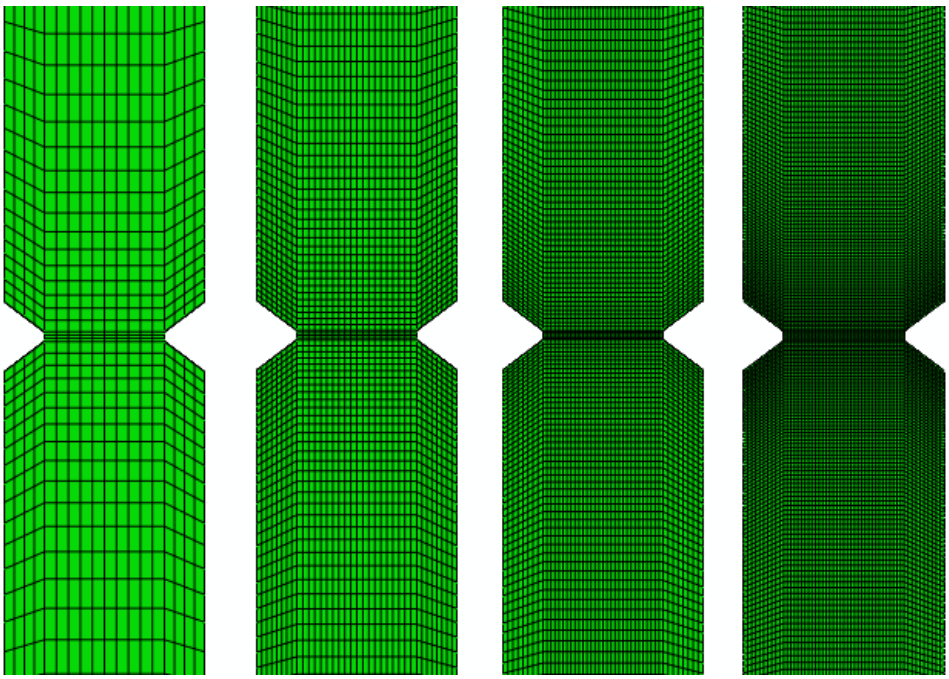

Mesh A Mesh B Mesh C Mesh D

Figure 5.2 Finite element meshes for the blunt notch (either 2D or 3D elements).

Table 5-2 Element size at the notch tip for sharp and blunt notches

Cases	**Mesh A**	**Mesh B**	**Mesh C**	**Mesh D**
Sharp notch	1.14 x 1 mm^2	0.57 x 0.5 mm^2	0.35 x 0.33 mm^2	0.23 x 0.3 mm^2
Blunt notch	0.33 x 1.2 mm^2	0.25 x 0.6 mm^2	0.2 x 0.4 mm^2	0.1 x 0.3 mm^2

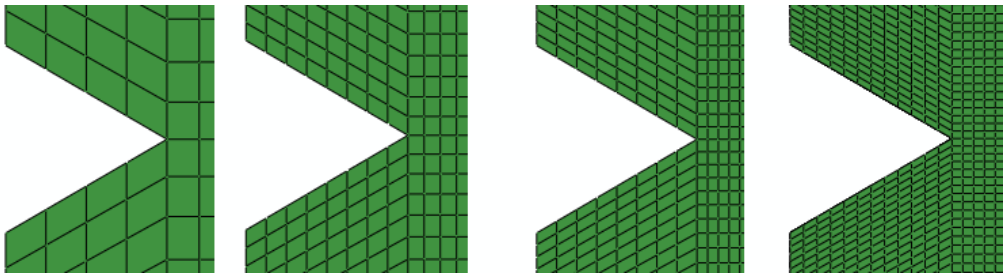

Mesh A Mesh B Mesh C Mesh D

Figure 5-3 Close-up meshes at the notch tip for sharp notch (either 2D or 3D elements).

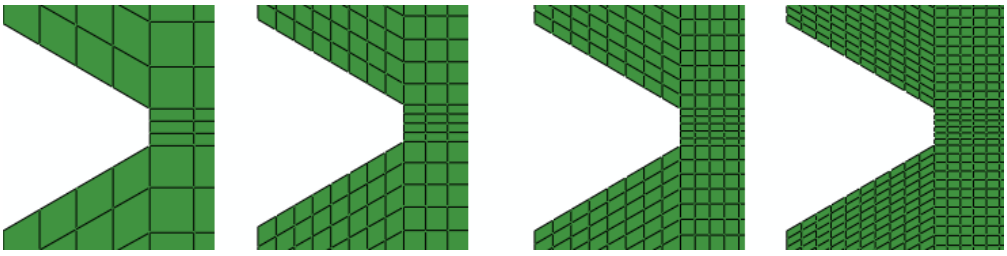

Mesh A Mesh B Mesh C Mesh D

Figure 5-4 Close-up meshes at the notch tip for blunt notch (either 2D or 3D elements).

5.1.2 Result of the mesh dependency study

Four failure models employed in this study are the Christensen, the CDM, the MChristensen and the MCDM models. Each failure model needs to be analyzed for 16 cases of FE meshes corresponding to the element type (2D or 3D element), notch's geometry (sharp or blunt notch) and mesh density (meshes A, B, C, D). Therefore, a total of 64 failure models are constructed for this mesh dependency study.

The computational results predicted by all failure models are reported in Figures 5-5 to 5-8 and compared to the experimental failure load of $[45/90/-45/0]_s$ carbon/epoxy laminate which was reported in chapter 3. In terms of notch's geometry, the effect of sharp notch and blunt notch is analyzed. Models of the 3D Sharp group show mesh-dependence whereas models of the 3D Blunt group show mesh-independence. This is because the blunt notch can help eliminate the stress singularity at the notch tip of the sharp notch, thus providing the results better than the sharp notch. For models of the 2D Sharp group, those using MCDM and MChristensen criteria are less mesh dependent than those using CDM and Christensen criteria. For models of the 2D Blunt group, those employing MCDM and MChristensen are mesh-independent while those using CDM and Christensen criteria are mesh-dependent. Hence, the MCDM and MChristensen models are found to provide better results than the CDM and Christensen models in both cases of sharp and blunt notches.

In terms of element types, the effect of using 2D elements or 3D elements is investigated. Most of models of the 2D Sharp group show less mesh-dependence than those of the 3D Sharp group. This is because the effect of stress singularity due to the sharp notch in 3D problems may be greater than in 2D problems. In contrast, models of the 3D Blunt group can obtain mesh-independent results better than those of the 2D Blunt group. All the failure models of the 3D Blunt group are mesh-independent while only those of the 2D Blunt group using MCDM and MChristensen criteria are mesh-independent.

In terms of mesh density, it can be observed that mesh A predicts the failure loads closer to experimental ones than meshes B,C and D. This is because mesh A has not fully accounted for the effect of high stress concentration at the notch tip. Since mesh A is very coarse and has only a few elements at the notch region, it cannot predict the failure load accurately and achieve mesh-independent results. The mesh-independency for models of 3D Blunt group is only obtained with meshes B, C and D. Therefore, mesh B can be used for FE models to produce mesh-independent results. This mesh has been used for the analyses of $[45/90/-45/0]_s$ carbon/epoxy and glass/epoxy laminates. The use of much finer meshes such as mesh C and mesh D in the analysis may be very expensive and require tremendous computational time.

Overall, it is noted that models of the 3D Blunt group are mesh-independent regardless of any of the four criteria chosen. For the other mesh groups, the MCDM and MChristensen models in general provide less mesh-sensitive

results and achieve faster convergence rates of mesh-independence than the CDM and Christensen models.

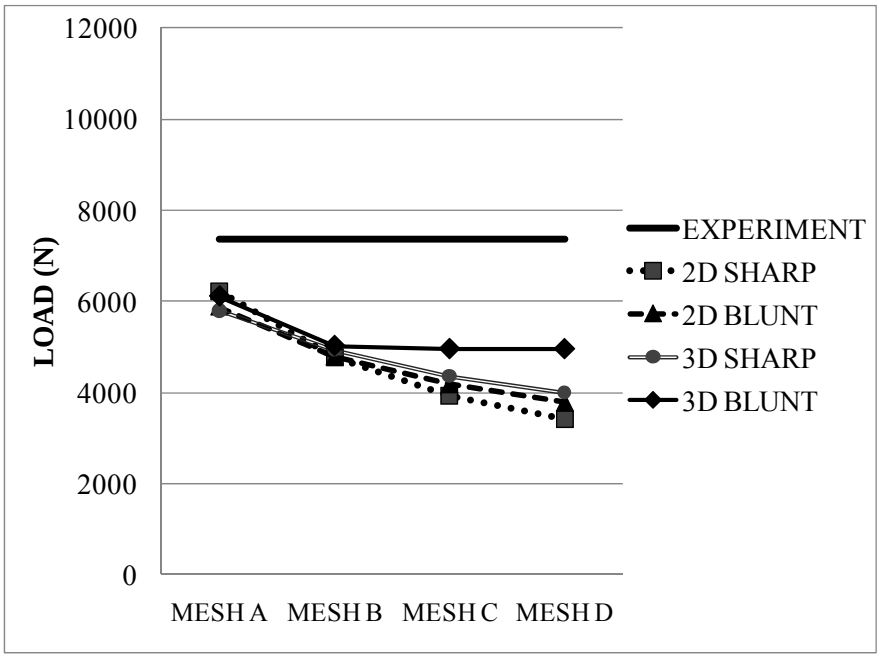

Figure 5-5 Results of mesh-dependency study by the CDM model.

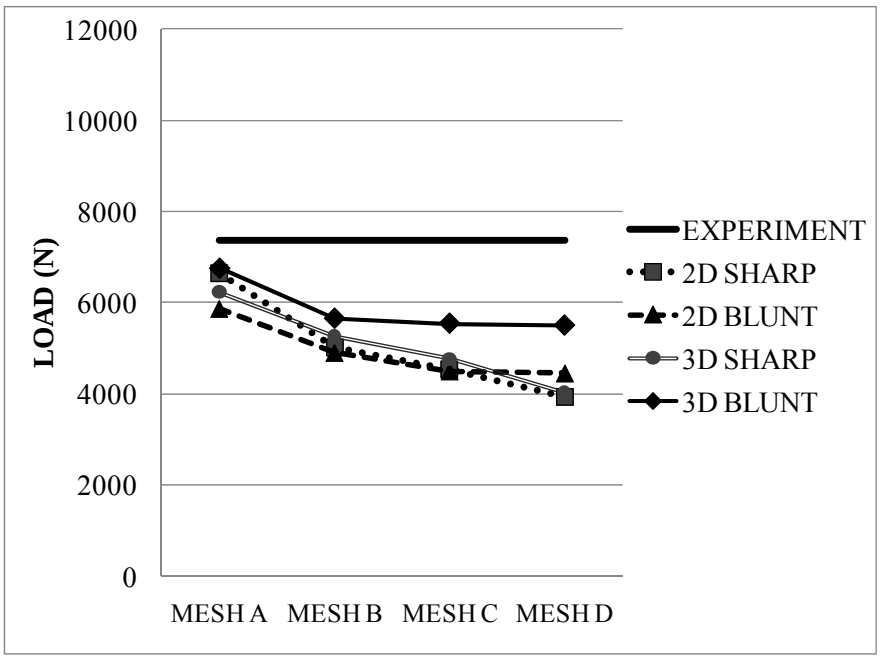

Figure 5-6 Results of mesh-dependency study by the Christensen model.

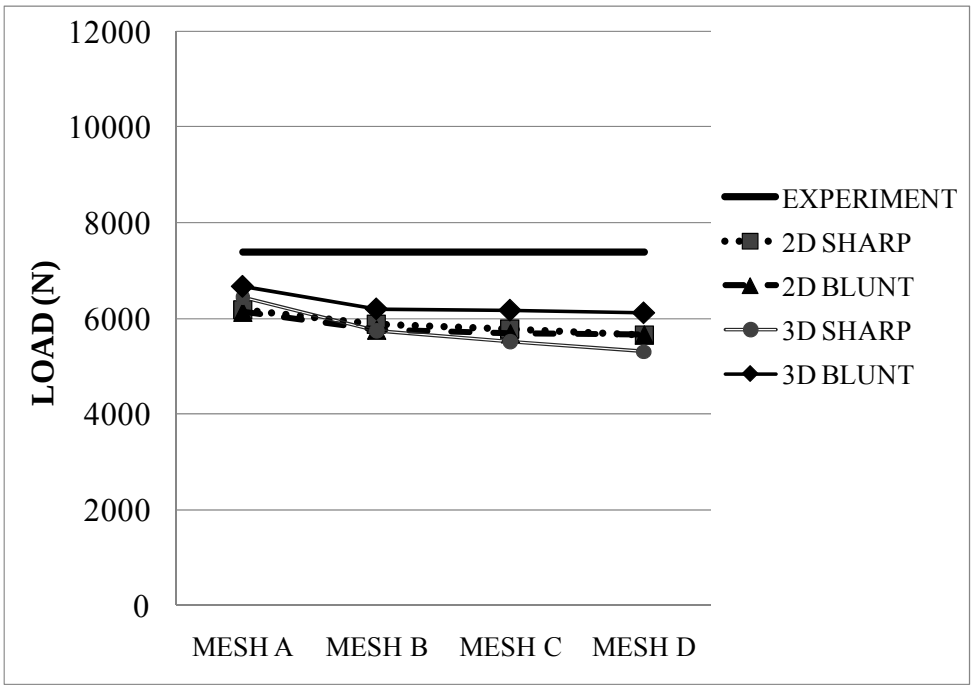

Figure 5-7 Results of mesh-dependency study by the MCDM model.

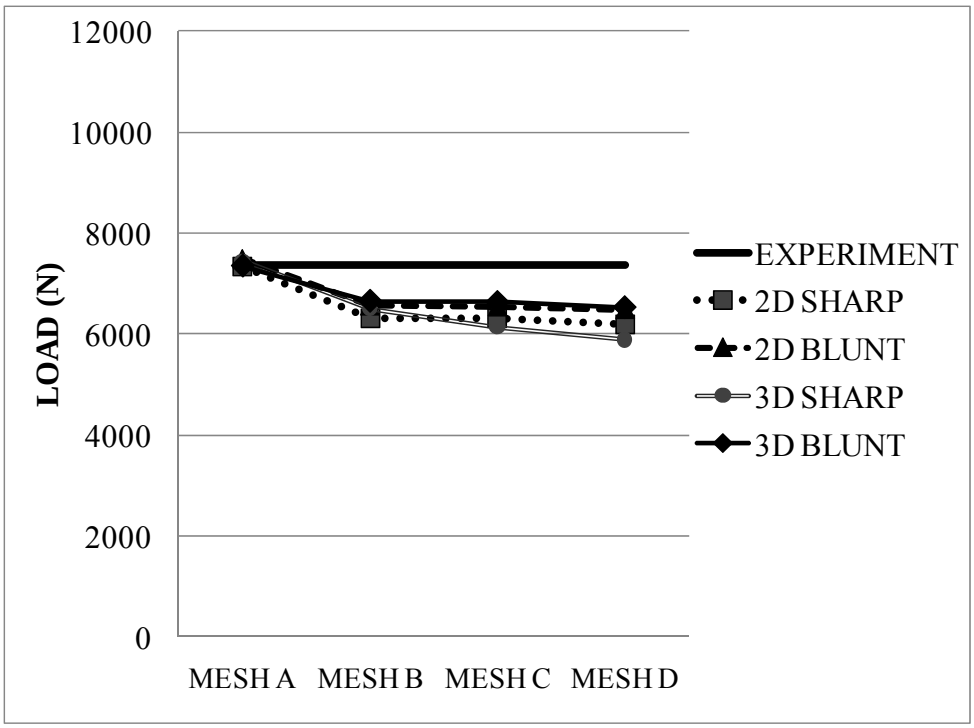

Figure 5-8 Results of mesh-dependency study by the MChristensen model.

5.2 Cohesive parametric study

5.2.1 Description of the cohesive parametric study

In addition to the mesh dependency study, it is also essential to conduct a cohesive parametric study to analyze the effects of cohesive parameters to the failure analysis of notched quasi-isotropic laminate. Among various models of the previous mesh study, only the models of 3D Blunt group which have shown mesh-independence are investigated in this study. To make computational efforts less expensive, only models with mesh B are analyzed. Four failure criteria are employed for these models including Christensen, CDM, MCDM and MChristensen.

A parametric study of cohesive parameters for the models with 3D elements and blunt notch of the $[45/90/-45/0]_s$ carbon/epoxy laminate is performed, varying the values of cohesive strengths and strain energy release rates (SERRs) in Equations 2-67 and 2-68. The original values of cohesive parameters are referred to Camanho [80] for carbon/epoxy material in which the value of 60 MPa for interlaminar normal strength N and the value of 68 MPa for interlaminar shear strengths S, T are assumed. Likewise, the values of SERRs such as G_{Ic} = 0.075 N/mm and G_{IIc} = G_{IIIc} =0.54 N/mm are also assumed. In this analysis, the values of cohesive parameters are first increased by 100% and decreased by 50% from their original values. The ultimate loads predicted by CDM, Christensen, MCDM and MChristensen models are then analyzed to investigate the sensitivity of cohesive element's parameters to the

failure analysis of the notched $[45/90/-45/0]_s$ carbon/epoxy laminate. The simulation results are also compared with the experimental failure load of $[45/90/-45/0]_s$ carbon/epoxy laminate which was reported in Chapter 3.

5.2.2 Result of the cohesive parametric study

Figure 5-9 shows the failure loads predicted by Christensen model when varying the interlaminar normal strength N and the SERR G_{Ic} in Equations 2-67 and 2-68. No change in the failure loads is obtained by the Christensen model. As can be seen in Figure 5-9, the cohesive parameters due to mode I such as N and G_{Ic} cause little effect on the change of failure loads since the quasi-isotropic laminate is mainly in pure shear mode (mode II). Hence, only the results by the Christensen model when varying N or the SERR G_{Ic} are presented. The results by the other failure models can be found similarly.

The predicted results by all models when varying interlaminar shear strengths S, T and SERRS G_{IIc}, G_{IIIc} in Equations 2-67 and 2-68 are shown in Figures 5-10 to 5-12. Figure 5-10 shows the load *vs.* displacement curves predicted by the CDM model when S, T and SERRs G_{IIc}, G_{IIIc} are decreased and increased by 50% from their initial values. A change less than 5% is obtained in the failure load prediction by the CDM model. It is shown in Figure 5-8 that an increase in cohesive shear strengths S, T may result in an increase in the failure load but an increase in fracture energy G_{IIc}, G_{IIIc} results in a decrease in the failure load. However, these changes are small and they do not significantly influence the failure prediction of quasi-isotropic composite.

The results predicted by Christensen, MCDM and MChristensen models are presented in Figure 5-11 to 5-13. As can be observed from results by the Christensen model, an increase in cohesive shear strength *S, T* and G_{IIc}, G_{IIIc} will result in a decrease in the failure load. On the other hand, the MCDM and MChristensen models do not clearly show changes on the failure loads when increasing cohesive shear strengths or G_{IIc}, G_{IIIc}. Similar to the CDM model, the Christensen, MCDM and MChristensen models predict a change less than 5% in failure loads when varying the interlaminar shear strengths *S*, *T* or SERRs G_{IIc}, G_{IIIc}.

Overall, although the analysis of this quasi-isotropic laminate is under shear dominant loading (mode II), the effect by shear tractions or SERRs in mode II are not considerable. As a consequence, the predicted failure loads are not so sensitive to the values of the shear strength *S*, *T* or SERRs G_{IIc}, G_{IIIc} chosen.

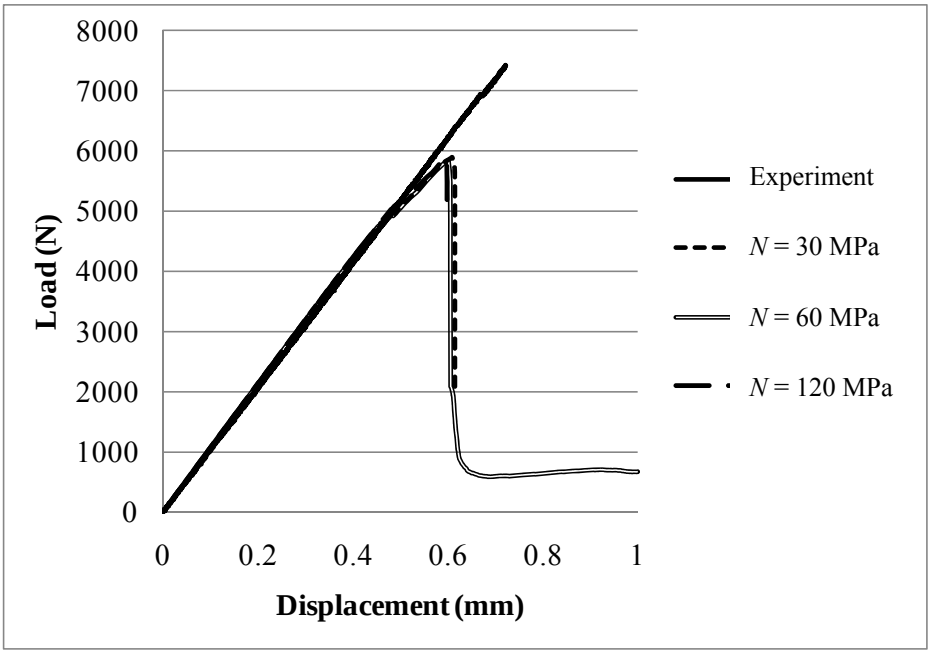

a. Varying N

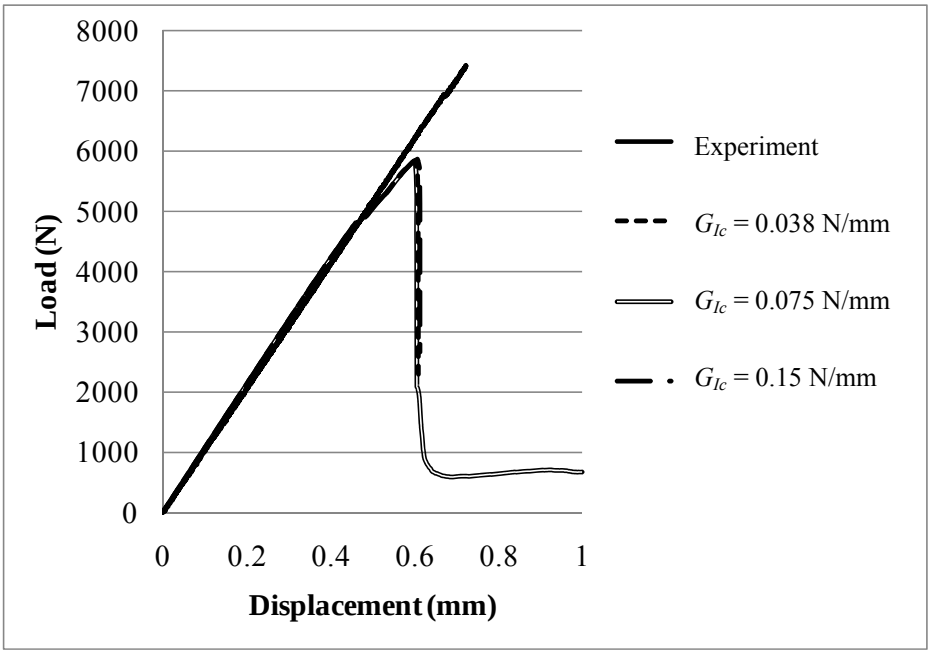

b. Varying SERR G_{Ic}

Figure 5-9 Results predicted by the Christensen model when varying interlaminar normal N and SERR G_{Ic}.

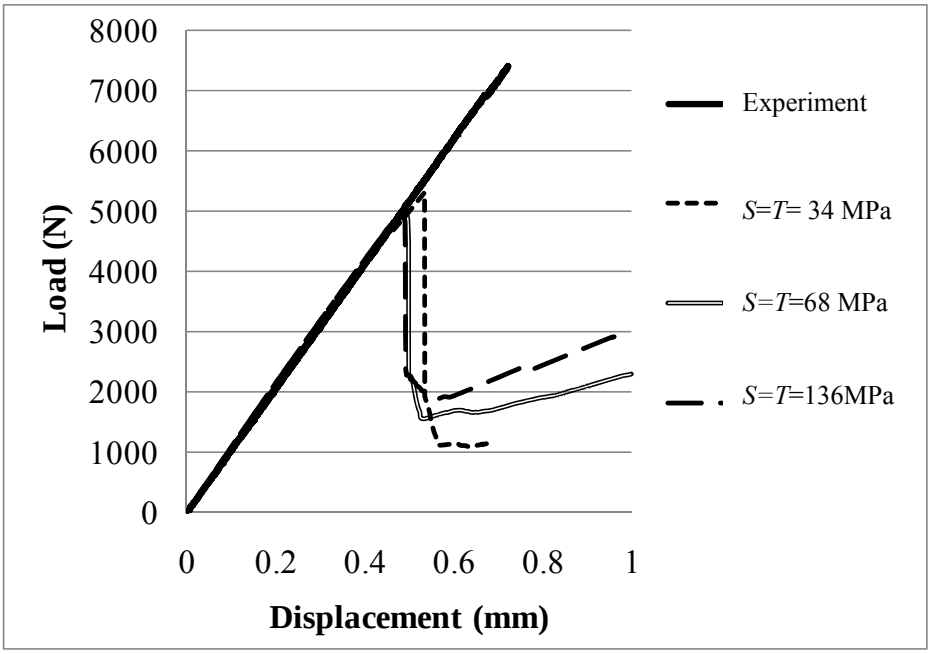

a. Varying *S* and *T*.

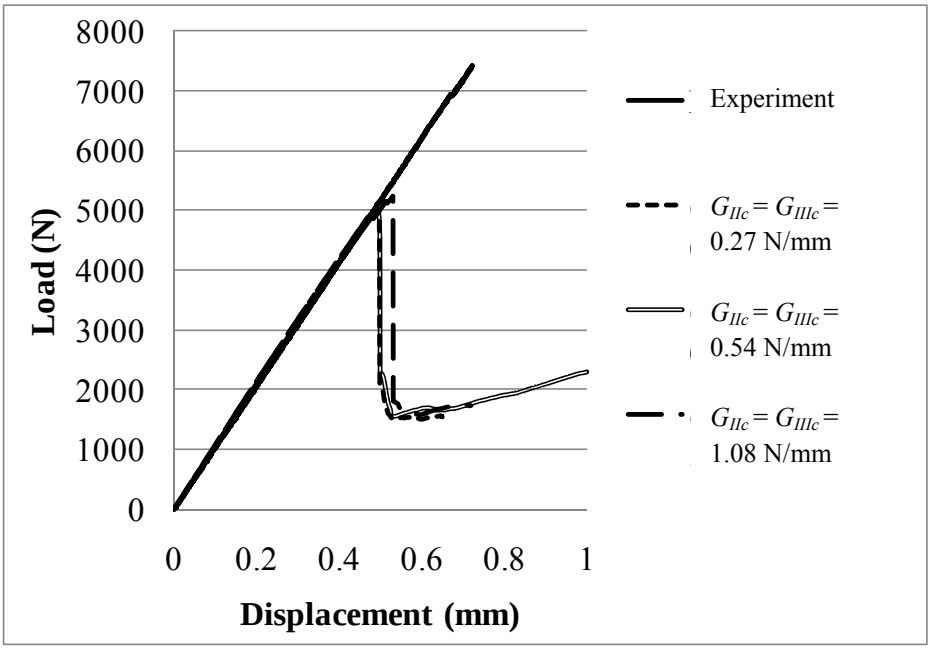

b. Varying G_{IIc} and G_{IIIc}.

Figure 5-10 Results predicted by the CDM model when varying interlaminar shear strengths *S, T* and G_{IIc}, G_{IIIc}

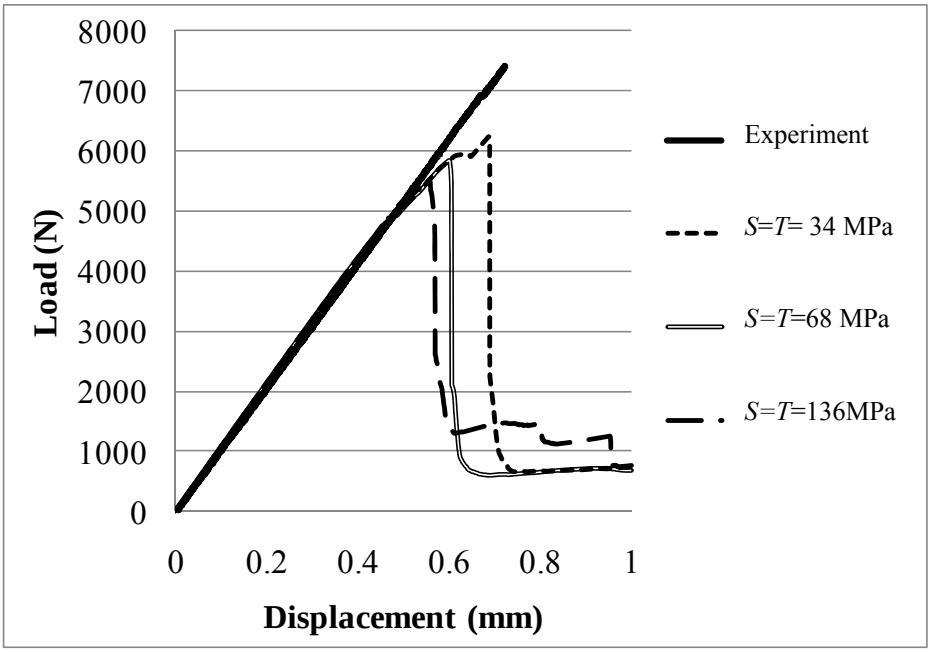

a. Varying *S* and *T*.

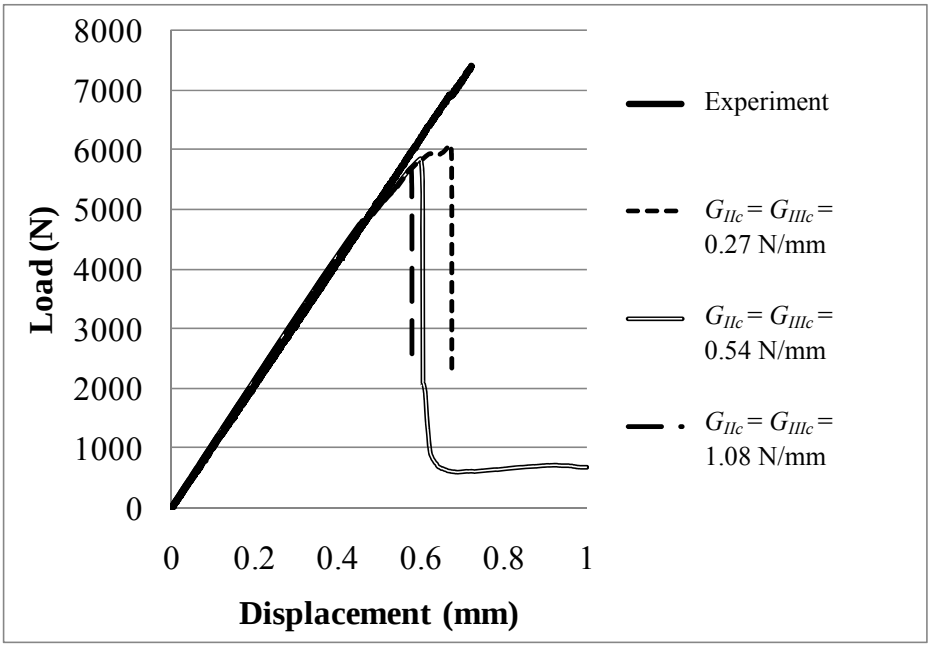

b. Varying G_{IIc} and G_{IIIc}.

Figure 5-11 Results predicted by the Christensen model when varying interlaminar shear strengths *S, T* and G_{IIc}, G_{IIIc}.

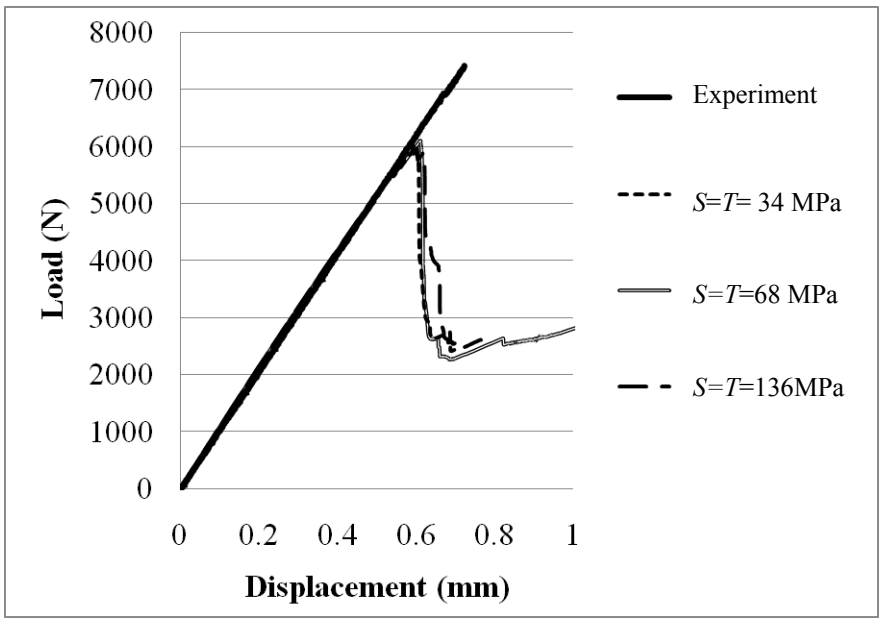

a. Varying *S* and *T*.

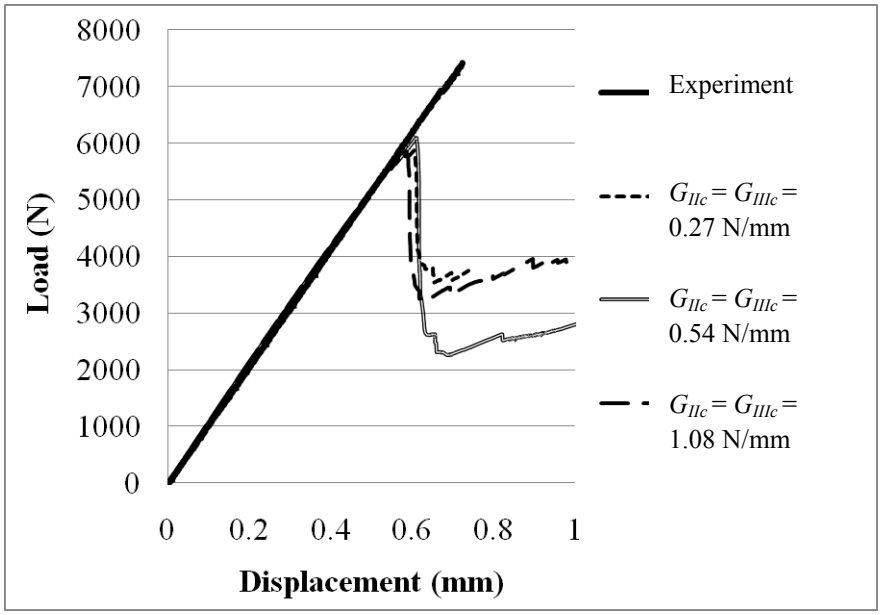

b. Varying G_{IIc} and G_{IIIc}.

Figure 5-12 Results predicted by the MCDM model when varying interlaminar shear strengths *S, T* and G_{IIc}, G_{IIIc}.

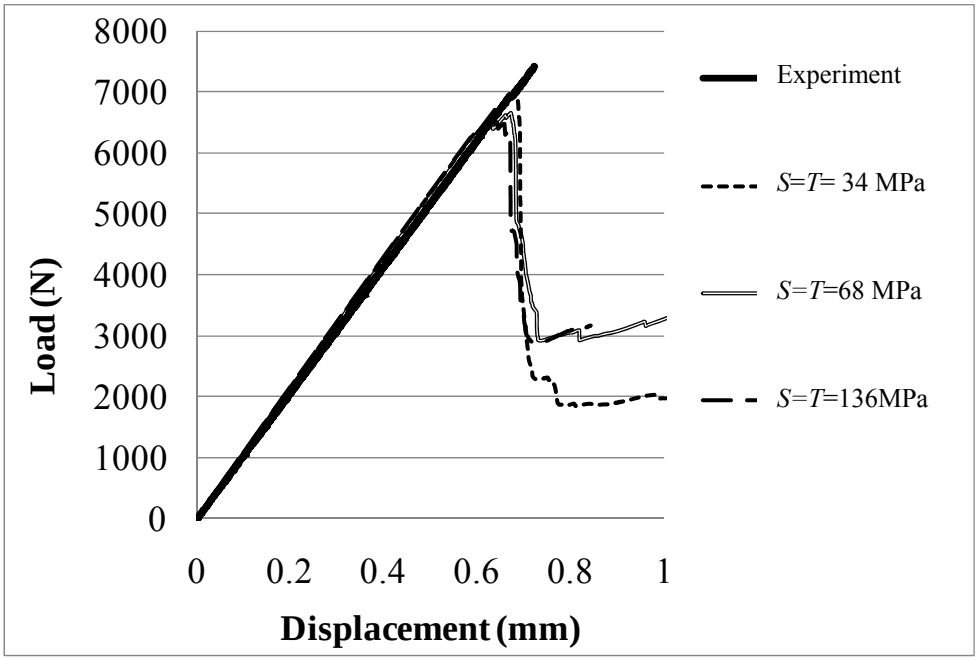

a. Varying *S* and *T*.

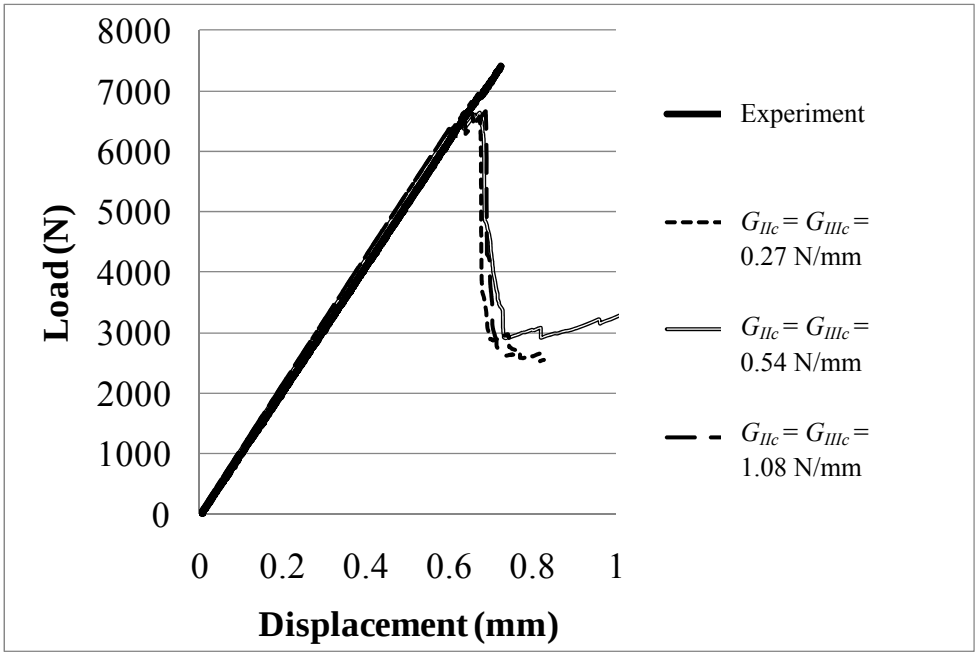

b. Varying G_{IIc} and G_{IIIc}.

Figure 5-13 Results predicted by the MChristensen model when varying interlaminar shear strengths *S, T* and G_{IIc}, G_{IIIc}.

5.3 Parametric study of MPDM scheme

5.3.1 Description of the parametric study of MPDM scheme

This study analyzes the effect of varying the values of degradation factors used in MPDM scheme. The value of 10^{-6} has been originally selected for all the degradation factors in MPDM scheme in the previous analyses of the cross-ply and quasi-isotropic laminates. In this section, a progressive failure analysis of notched $[45/90/-45/0]_s$ carbon/epoxy laminate is investigated with a variation of the degradation factors used in the MPDM scheme. The model of mesh B with 3D element and blunt notch (3D Blunt) using Christensen criterion is analyzed in this section. Mesh B is chosen since it is able to provide mesh-independent results and does not take much computation efforts compared to meshes C and D of the 3D Blunt group.

Five cases of degradation factors D_i are investigated corresponding to $D_i = 10^{-6}$, 0.01, 0.05, 0.1, 0.5. These values reflect the remaining percentage of the stiffness of an element after this element is predicted to be failed by Christensen criterion. For example, $D_i = 0.1$ means that once an element is failed, its remaining stiffness is 10% of its original stiffness. In other words, the MPDM will consider it to have a loss of 90% of its original stiffness. The bigger value of D_i is, the higher the remaining stiffness of the element or the higher the load-carrying capability of the element is.

5.3.2 Result of the parametric study of MPDM scheme

The load *vs.* displacement curves predicted using Christensen criterion with different degradation factors is shown in Figure 5-14 and the close-up view of these curves at the first load drop is shown in Figure 5-15. As can be seen in Figure 5-14, the predicted peak load is increased with increasing values of degradation factors. The peak load predicted for $D_i = 0.5$ is highest while that for $D_i = 10^{-6}$ is lowest. Table 5-4 summarizes the peak loads predicted by five models using different degradation factors.

The first model is built with $D_i = 10^{-6}$. In this case, the MPDM will completely degrade the stiffness of the failed elements. The failure load, defined as the major load drop, is obtained and under-predicted the experiment by about 23.4%. The damage patterns predicted just after the major load drop are shown in Figure 5-16. This was the result presented in the failure analysis of quasi-isotropic carbon/epoxy laminate. It is noted that the major load drop is clearly observed.

The second model adopting $D_i = 0.01$ is constructed. The first load drop predicted by this model is very close to the major load drop predicted by the first model (Figure 5-15). Since the failed elements of the second model still have their remaining stiffness after the first load drop, they can carry additional load. The major load drop is observed as the second load drop of the predicted curve by this model (Figure 5-14). The failure load predicted by the second model is over-predicted the experiment by about 6%. The damage

pattern just after the major load drop is shown in Figure 5-17. More damage in individual plies is obtained by the second model than the first model. However, since the experiment did not show such much damage, the first model seems to agree better with the experimental data.

The third model is built with D_i = 0.05. The first load drop predicted by the third model is higher than the one predicted by the second model (Figure 5-15). Results by the third model show various load drops in the predicted curve, but the major load drop is not very clearly identified. The failed elements of this model still have 5% of their original stiffness and can sustain more loads than those of the second model. The maximum load obtained by the third model can be considered as the failure load. This failure load is found to over-predict the experiment by about 34.6%. The damage patterns at the maximum load are presented in Figure 5-18. Lots of matrix cracks are found in all the plies and fiber failure occurs at the top edge of the 0^0 ply. These results do not correctly match with the experimental observation.

The fourth model with D_i = 0.1 is also built. The first load drop by this model is similar to the third model (Figure 5-15). However, the peak load predicted by the fourth model is higher than the third model. This peak load is considered as the failure load predicted by the fourth model since no clear major load drop is observed. This failure load by the fourth model is over-predicted the experiment by about 54.3%. The failure patterns just after the peak load are shown in Figure 5-19. Lots of fiber failures in the 0^0 ply are obtained and this model fails to correctly simulate the experiment.

The fifth model is constructed with $D_i = 0.5$. The maximum load predicted by this model is very high compared to the experiment (Figure 5-13). The final damage pattern is shown in Figure 5-20. It can be seen that all the plies are almost failed and have exhaustedly lost all their load-carrying capability. However, this will not be reflected in the predicted curve since the predicted maximum load may continue to increase if more load is applied on this model. Hence, the fifth model with $D_i = 0.5$ cannot be used in simulation because the physics of the failed elements are not correctly simulated.

Overall, only the first model with $D_i = 10^{-6}$ and the second model with $D_i = 0.01$ are able to provide reasonable results, among which the first model has been found to agree better with the experiment of the quasi-isotropic laminate. In the first model, a damaged element is modeled by degrading its stiffness to very small value (10^{-6} of the original stiffness). The values of 10^{-6} are used here instead of zero to avoid the divergence of the analysis. The MPDM scheme with $D_i = 10^{-6}$ have been used for all of the previous analyses of cross-ply and quasi-isotropic laminates.

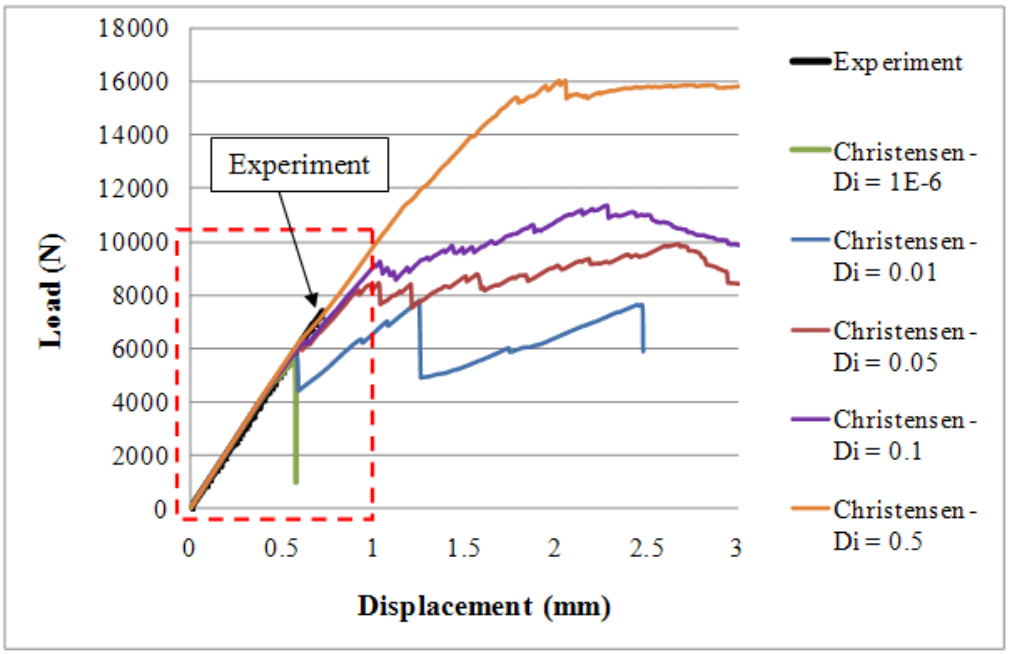

Figure 5-14 Results predicted by the Christensen model when varying the degradation factors D_i.

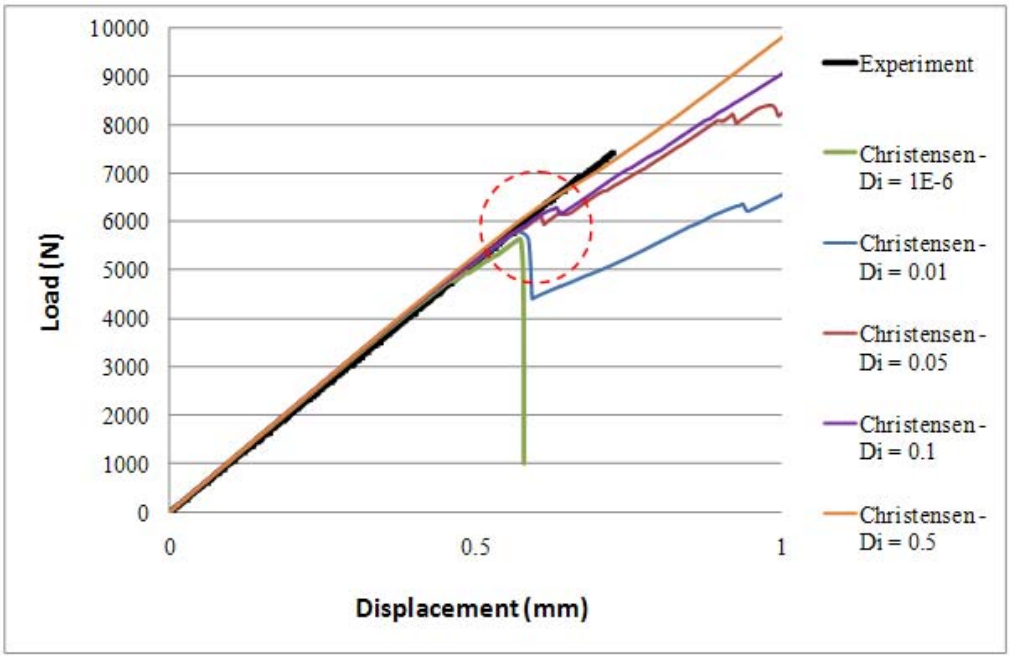

Figure 5-15 A close-up view of the predicted curves by the Christensen model when varying the degradation factors D_i.

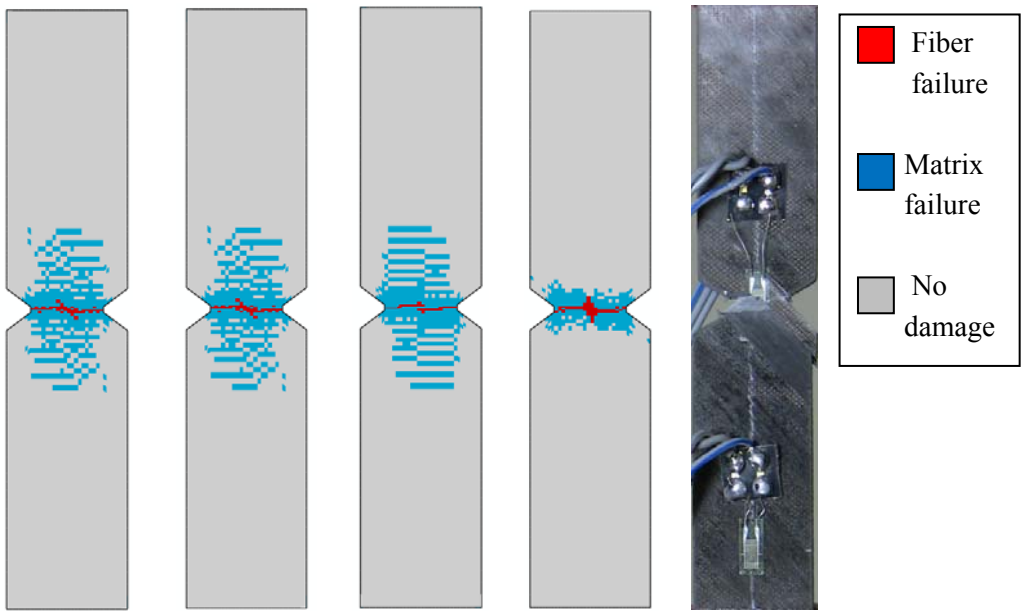

Figure 5-16 Damage patterns obtained just after the major load drop when $D_i = 10^{-6}$

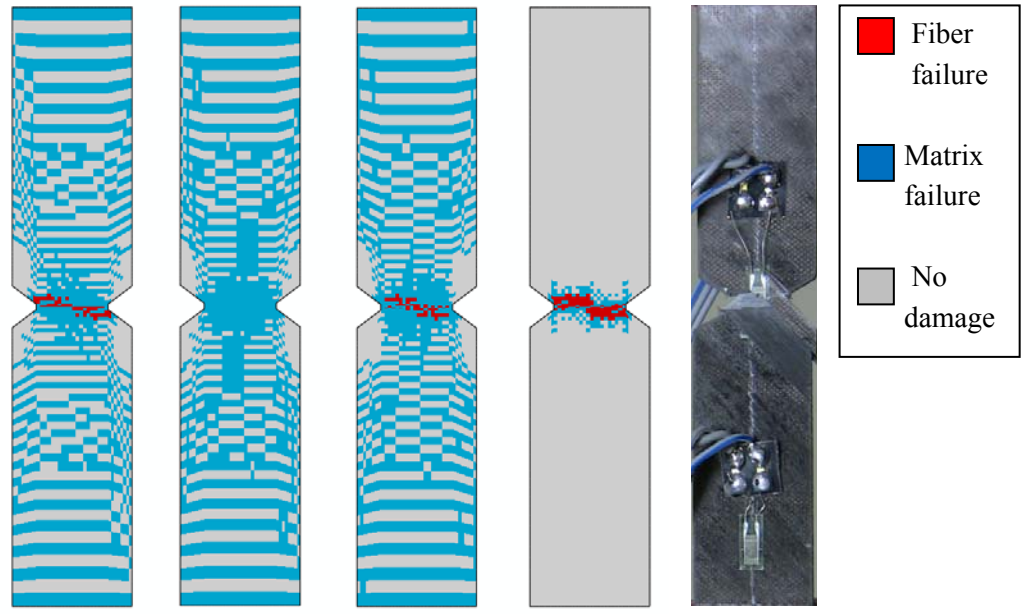

Figure 5-17 Damage patterns obtained just after the major load drop when $D_i = 0.01$

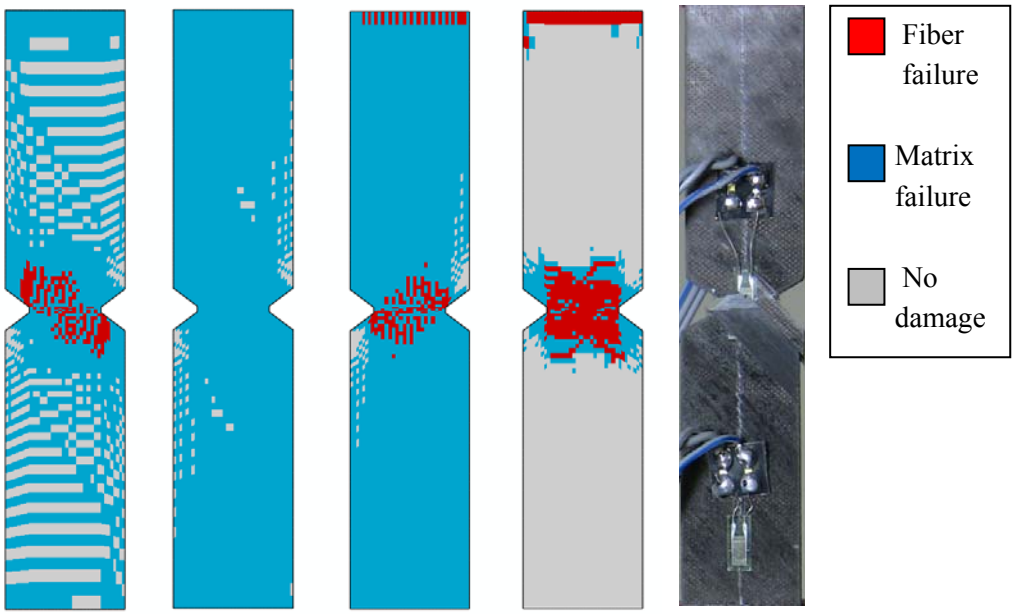

Figure 5-18 Damage patterns obtained just after the major load drop when $D_i = 0.05$

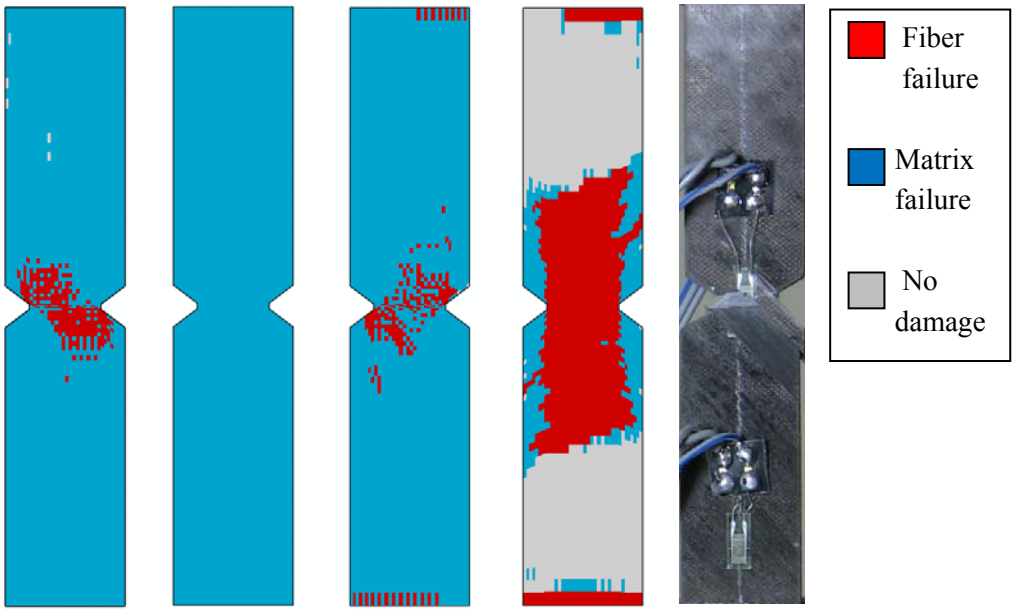

Figure 5-19 Damage patterns obtained just after the major load drop when $D_i = 0.1$

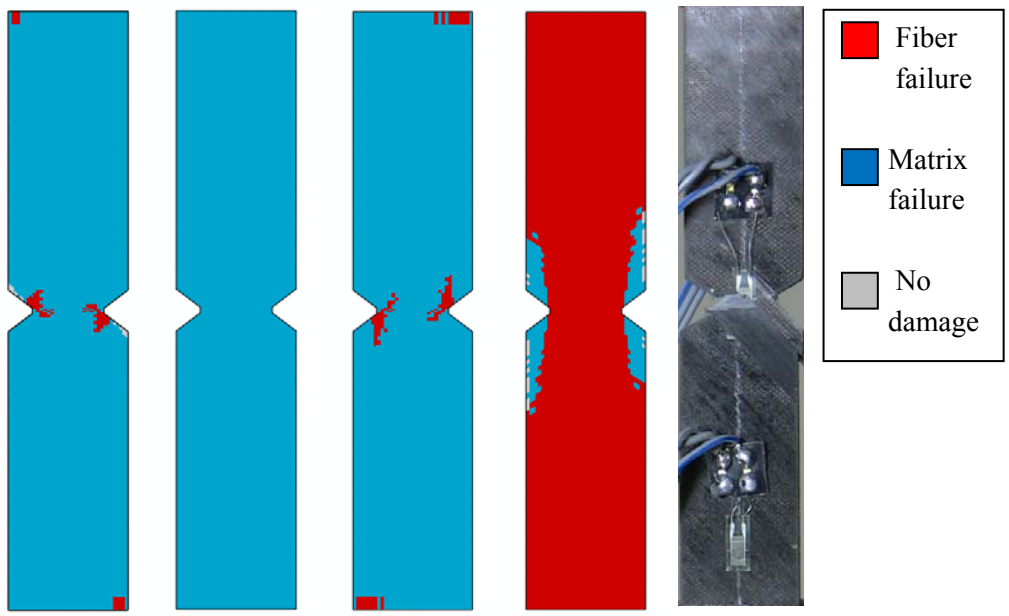

Figure 5-20 Damage patterns obtained at the last step increment when $D_i = 0.5$

Table 5-3 Summary of the highest loads predicted by MPDM models with different degradation factors D_i for the carbon/epoxy quasi-isotropic laminate.

	The highest load predicted *(N)*	**The percentage of the failure load prediction**
Experiment	7377.8 ± 365.4	
MPDM with $D_i = 10^{-6}$	5650.3	76.6%
MPDM with $D_i = 0.01$	7817.7	106%
MPDM with $D_i = 0.05$	9927.6	134.6%
MPDM with $D_i = 0.1$	11385.5	154.3%
MPDM with $D_i = 0.5$	22519.3	305.2%

5.4 Conclusion

The mesh-dependency study for the notched quasi-isotropic carbon/epoxy has been studied in this chapter. The CDM, Christensen, MCDM and MChristensen models are used in this study. Results for the mesh-dependency study highlight that all the models with 3D elements and blunt notch (3D Blunt) are mesh-independent. Besides the 3D Blunt case, it is found that only models of MChristensen and MCDM with 2D elements and blunt notch (2D Blunt) are mesh-independent whereas those of CDM and Christensen are mesh-dependent. Therefore, the MCDM and MChristensen models in general can use either 2D elements or 3D elements with blunt notch to produce mesh-independent results.

In addition, the cohesive parametric study has been presented, analyzing the sensitivity of the failure prediction to the values of cohesive parameters chosen. The results show that a change less than 5% is obtained when increased the interlaminar strengths *N, S, T* and strain energy release rates (SERRs) G_{IC}, G_{IIC} and G_{IIIc} by 100% and decreased by 50% from their original values. Therefore, the failure load prediction is not so sensitive to the choice of cohesive strengths and SERRs.

A parametric study of the MPDM scheme has been investigated, varying the value of degradation factors in MPDM for the analysis of quasi-isotropic laminate. The results show that a value of 10^{-6} needs to be assigned for all the

degradation factors in tension mode to reasonably account for the damage in composites.

Chapter 6

Notch-size and ply-level scaling effects of the double-notched [45/90/-45/0]$_s$ carbon/epoxy laminate

Notched composites also show significant strength reduction with an increase in size of specimens. In this chapter, the candidate performs a size scaling study of notched [45/90/-45/0]$_s$ carbon/epoxy specimens under tension. The experiment and failure analysis of the original [45/90/-45/0]s carbon/epoxy specimens have been reported in chapter 3. These specimens will be scaled with particular geometries referred to the work of Hallett and Wisnom [74] in which a size scaling effect of glass/epoxy specimens has been studied experimentally.

In this chapter, the notch size and ply-level scaling effects of double-notched quasi-isotropic carbon/epoxy laminate are investigated both experimentally and computationally. The experiment and simulation of the notch-size scaled laminate of the [45/90/-45/0]$_s$ laminate are first performed. The experiment and simulation of the ply-level scaled laminate of the [45/90/-45/0]$_s$ laminate are then illustrated. Finally, the notch-size and ply-level scaling effects of the original quasi-isotropic laminate are discussed.

6.1 Experimental and computational investigation of the notch-size scaled laminate of the $[45/90/-45/0]_s$ carbon/epoxy laminate

6.1.1 Experiment of the notch-size scaled laminate

The dimensions of the notch-size scaled laminate are shown in Figure 6-1. The notch-size scaled laminate has the same layup $[45/90/-45/0]_s$ as the original composite laminate. This scaled laminate has been tested in tension. Four specimens are made for the tensile test (Figure 6-2). The strain gauge setup, experiment setup and procedure are similar to those of the $[90/0]_s$ carbon/epoxy laminate reported in Chapter 3. The failures of specimens for this scaled laminate after the test are shown in Figure 6-3. Table 6-1 summaries the failure load (F_{crit}) and critical displacement (u_{crit}) at the top of the specimen corresponding to the gauge length of 100 mm obtained after the test. The load-displacement curves of notch-size scaled specimens are presented in Figure 6-4. The experimental results show that the failures of these specimens are due to the fiber breakage and delamination in a very similar manner to the original $[45/90/-45/0]_s$ carbon/epoxy laminate. It is also noted that no change in failure mode is observed from the original quasi-isotropic laminate to the notch-size scaled laminate. However, more delamination is detected in the notch-sized scaled laminates than the original laminate.

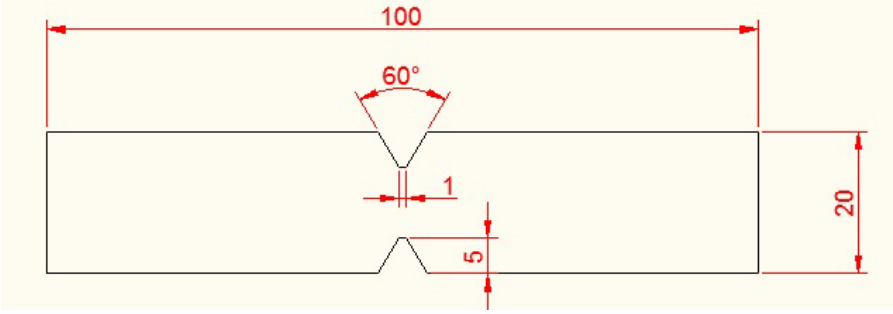

a. Dimensions of the original quasi-isotropic specimen

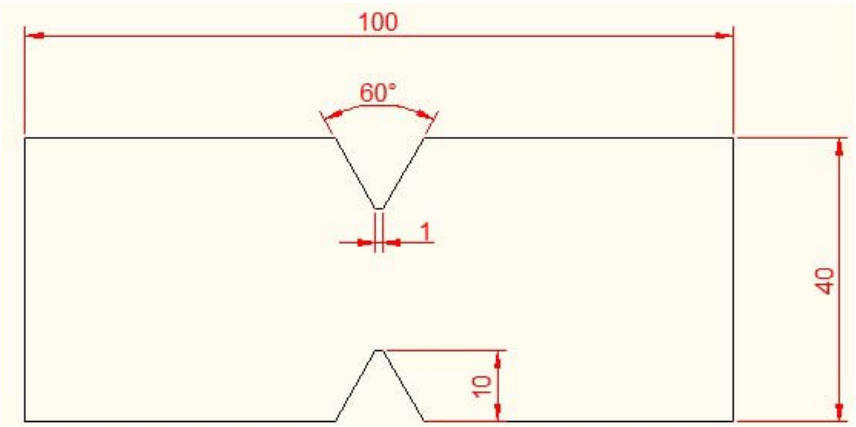

b. Dimensions of the notch-size scaled specimens

Figure 6-1 Dimensions of the notch-size scaled specimen compared to the original quasi-isotropic specimen.

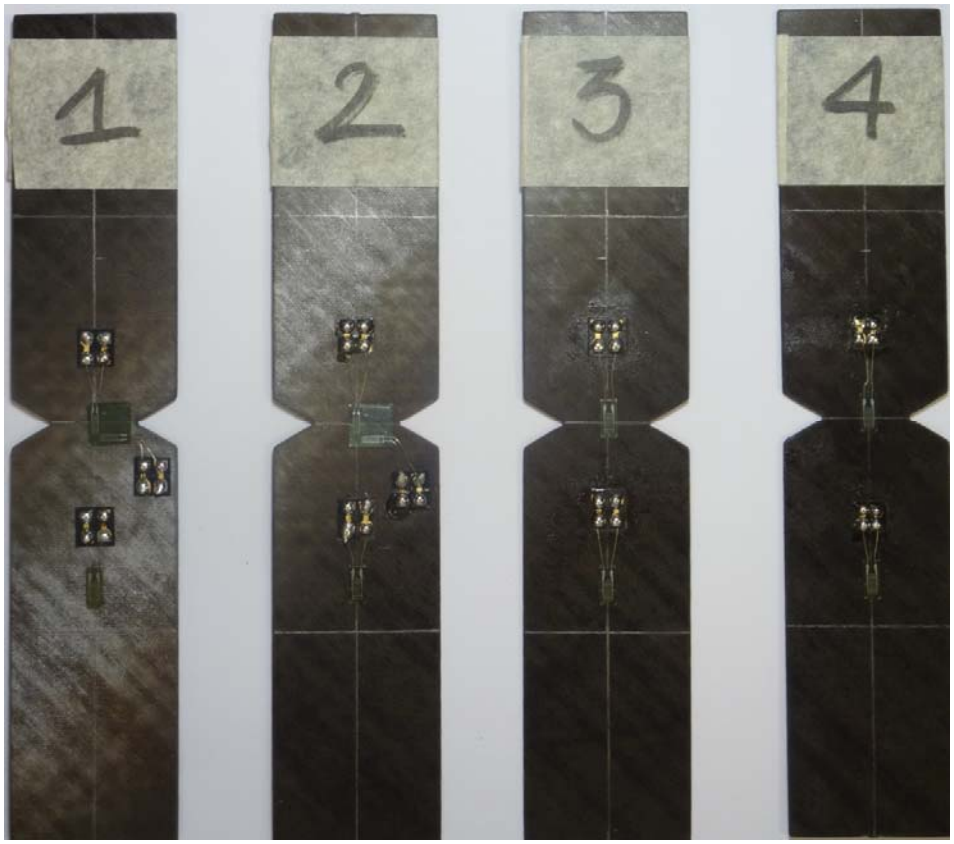

Figure 6-2 The notch-size scaled specimens before testing.

Figure 6-3 Failure of the notch-size scaled specimens after testing.

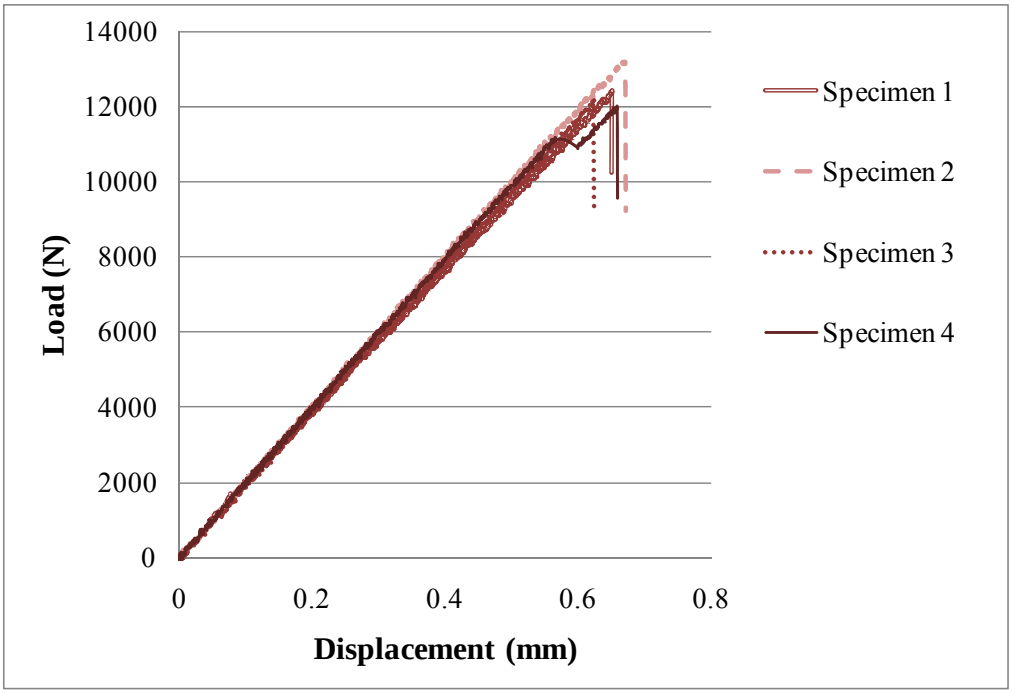

Figure 6-4 Load-displacement curves of notch-size scaled specimens

Table 6-1 Critical displacements (u_{crit}) and failure load (F_{crit}) of notch-size scaled specimens

	Notch-size scaled laminate			
Specimen	u_{crit} **(mm)**	Δu_{crit} **(mm)**	F_{crit} **(N)**	ΔF_{crit} **(N)**
1	0.664	0.009	12419	27
2	0.67	0.015	13186	740
3	0.625	0.029	12184	262
4	0.66	0.005	11995	451
Average	**0.654** ± 0.015		**12446** ± 370	

6.1.2 Progressive failure analysis of the notch-size scaled laminate

Progressive failure analysis of the notch-size scaled laminate by the Tsai-Wu, Christensen, MMF, CDM, MCDM and MChristensen models is performed and compared to the experimental data. The analysis is carried out by Abaqus with the finite element mesh and boundary condition shown in Figure 6-5. The predicted load *vs.* displacement curves for the notch-size scaled laminate is presented in Figure 6-6. The damage patterns predicted by all failure models are shown in Figures 6-7 to 6-12. Since the initiation and propagation of matrix-dominated failure in the $\pm 45^0$ and 90^0 plies and initiation and propagation of longitudinal splits in the $\pm 45^0$ and 0^0 plies are very similar to those of the original quasi-isotropic carbon/epoxy laminate (referred to section 3.2 of chapter 3), only the damage patterns just after the major load drop are shown for all the models.

Simulation results show transverse matrix cracking and longitudinal splitting in the $\pm 45^0$ and 90^0 plies, splitting in 0^0 ply and fiber failure in $\pm 45^0$ and 0^0 plies together with delamination at three interfaces (Figures 6-7 to 6-12). Since the carbon/epoxy specimens are very dark that the damage patterns of inner plies of the quasi-isotropic laminate such as the 90^0, 0^0 or -45^0 plies cannot be observed, only the 45^0 ply (the top ply) of the laminate is compared to the predicted results. The predicted results for the 45^0 ply show that the initiation

and propagation of splitting and fiber failure in the 45^0 ply agrees well with the crack running at 45^0 from the notch tip in the experiment.

Besides, conventional models such as Christensen, Tsai-Wu, MMF models predict the matrix damage quite similarly while the CDM model predicts more matrix damage in $\pm 45^0$ and 90^0 plies. However, there is not much difference on the ultimate loads by conventional models because the fiber failure initiation and development are similar between these models. The Christensen, Tsai-Wu, MMF and CDM models under predict the experiment about 22%, 23.5%, 23.5% and 27%, respectively.

The MCDM and MChristensen models, on the other hand, can sustain more matrix damage before the ultimate failure than conventional models. This is because the damage fibers in the notch region predicted by MCDM and MChristensen models still have their remaining load-capability and can allow more matrix damage to be developed before the ultimate failure. The ultimate failure is predicted only once the damaged fibers are completely failed. As a result, the MCDM and MChristesnsen models predict the experimental ultimate loads higher than conventional models. The MCDM and MChristensen models predict about 83% and 88% of the experimental failure loads, respectively. It is noted that more delamination has been predicted in the notch-size scaled laminate than the original quasi-isotropic laminate and no change in the failure mode is predicted between these two laminates.

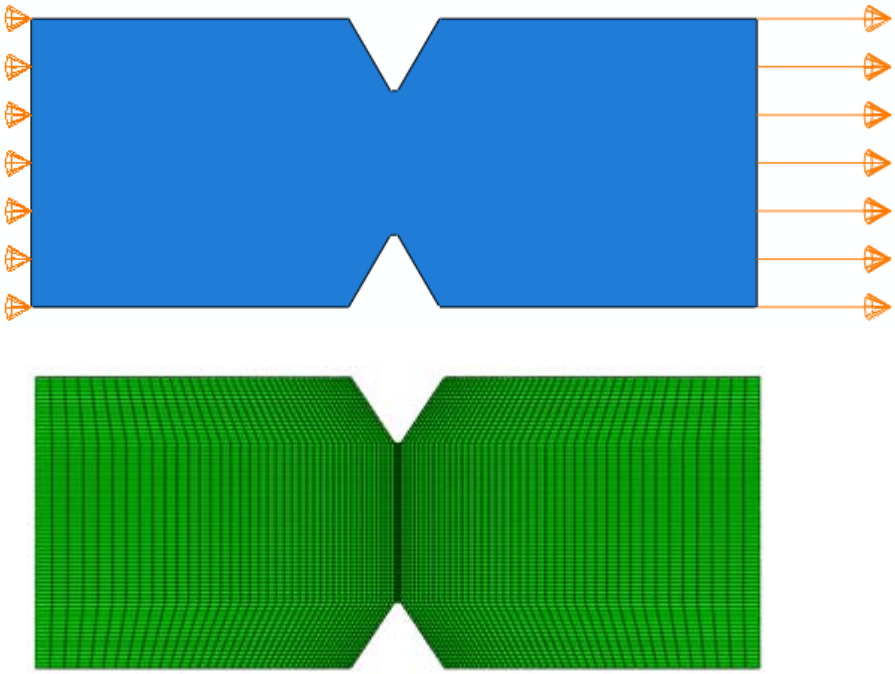

Figure 6-5 Boundary conditions and mesh of the FE model for notch-size scaled laminate.

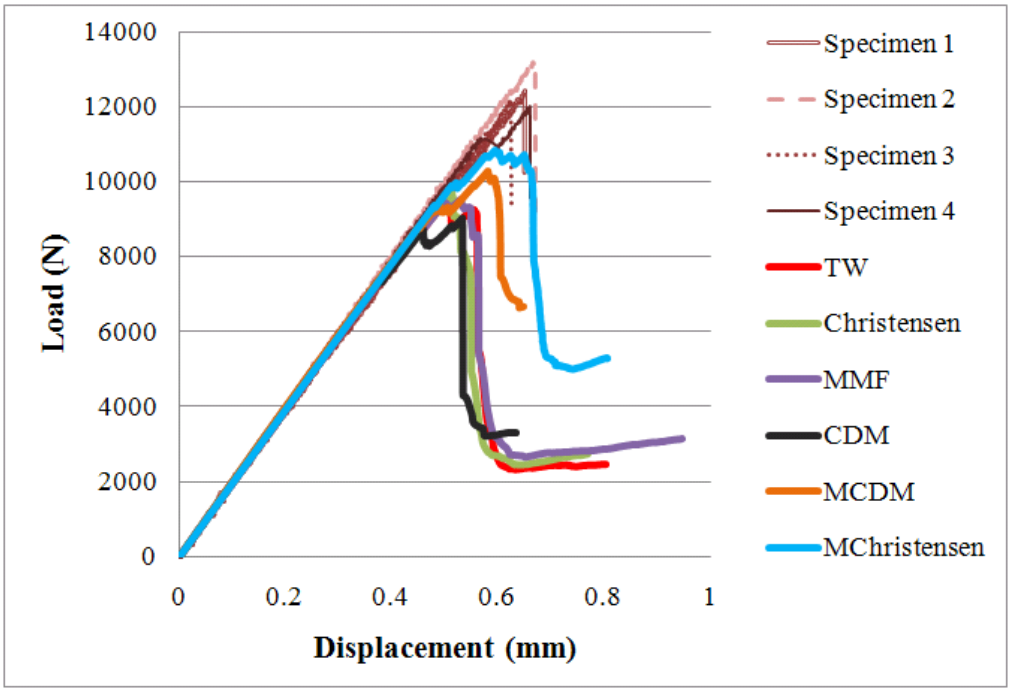

Figure 6-6 Predicted load-displacement curves and comparison with the experiment for the notch-size scaled laminate.

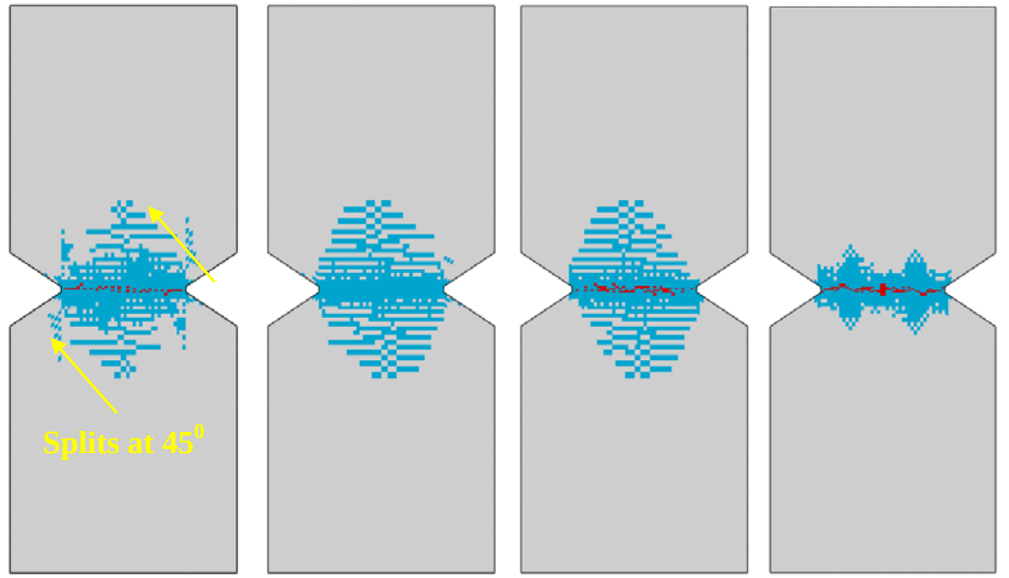

45^0 ply *90^0 ply* *-45^0 ply* *0^0 ply*

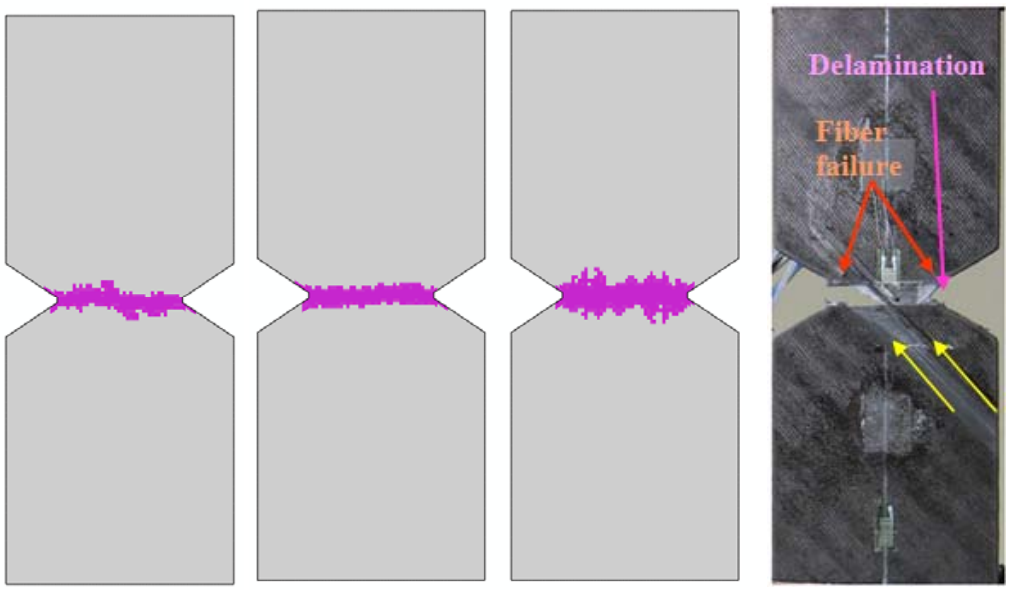

$[45^0/90^0]$ interface *$[90^0/-45^0]$ interface* *$[-45^0/0^0]$ interface* *Experiment*

Fiber failure Matrix failure Delamination No damage

Figure 6-7 Christensen: Final failure in the 45^0 ply, 90^0 ply, -45^0 ply and 0^0 ply and delamination at all the interfaces.

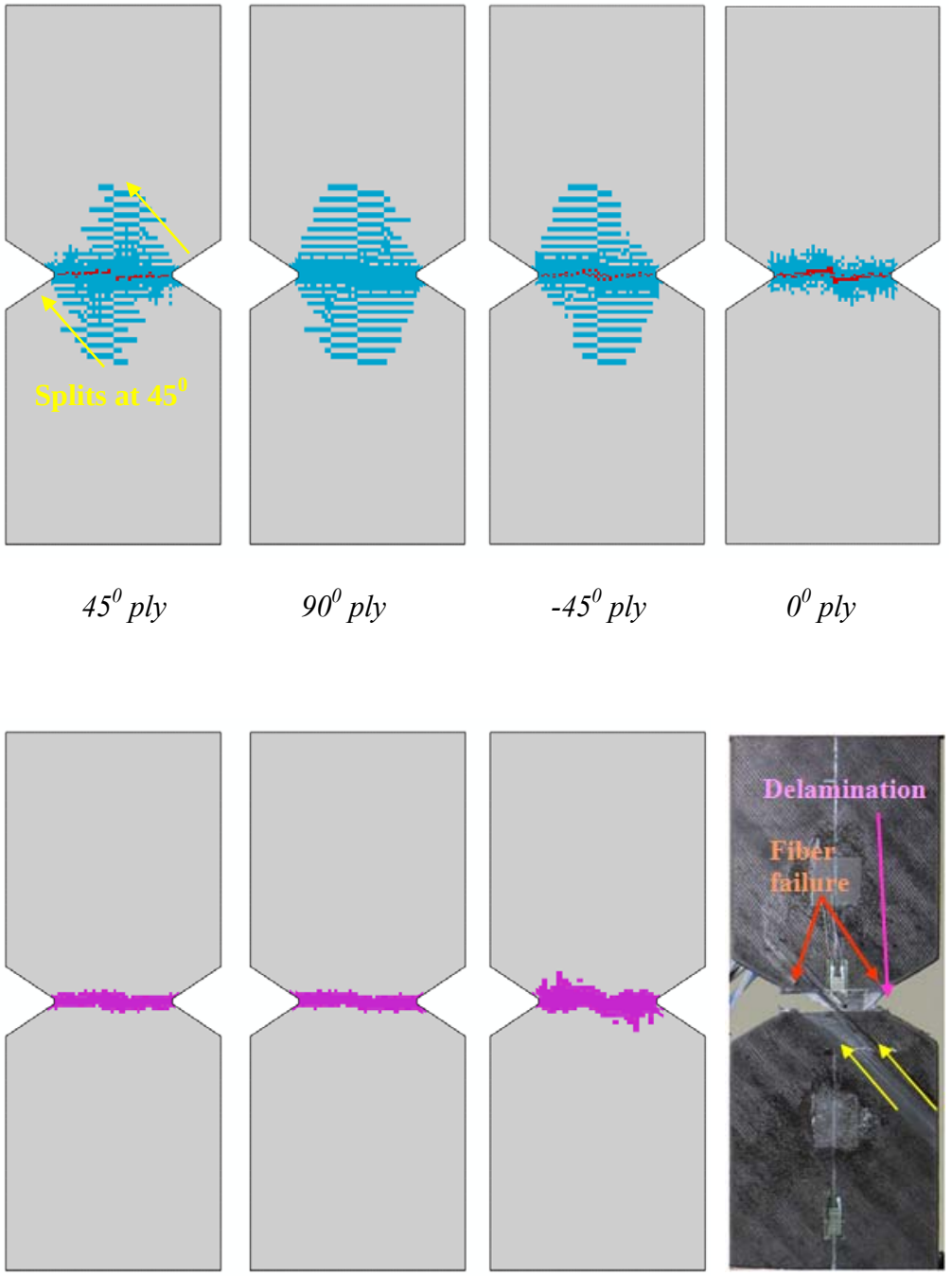

Figure 6-8 Tsai-Wu: Final failure in the 45^0 ply, 90^0 ply, -45^0 ply and 0^0 ply and delamination at all the interfaces.

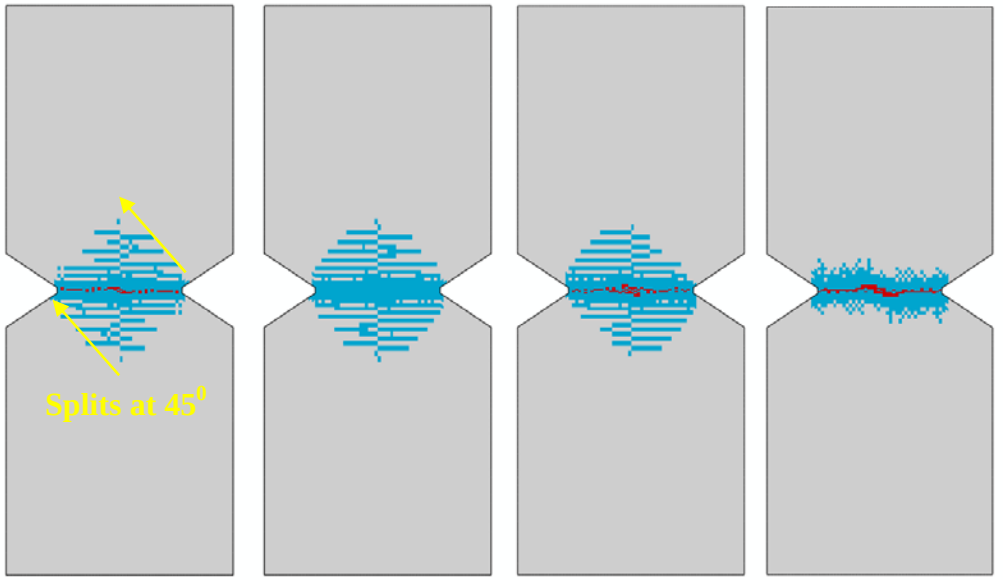

45^0 ply *90^0 ply* *-45^0 ply* *0^0 ply*

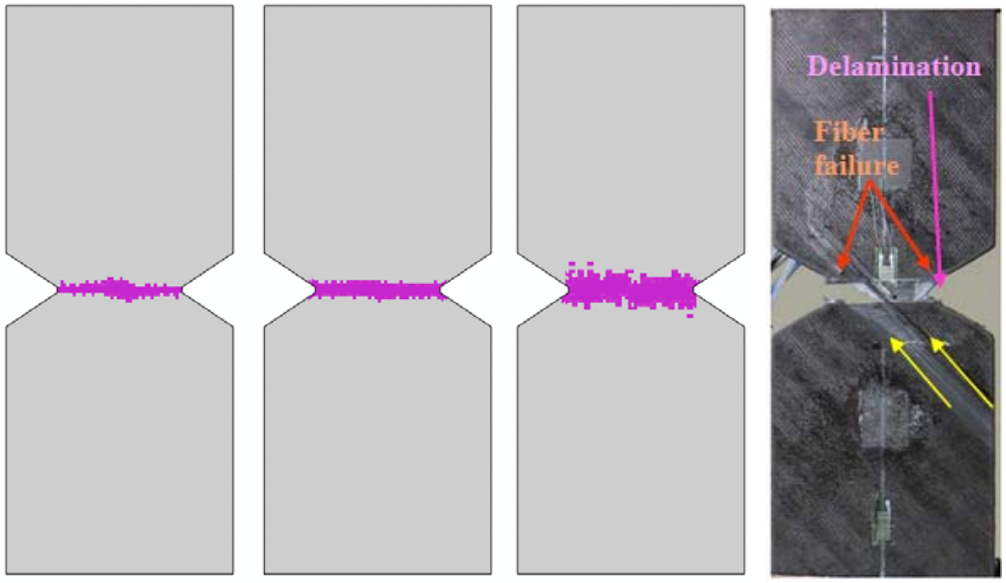

$[45^0/90^0]$ interface *$[90^0/-45^0]$ interface* *$[-45^0/0^0]$ interface* *Experiment*

Fiber failure Matrix failure Delamination No damage

Figure 6-9 MMF: Final failure in the 45^0 ply, 90^0 ply, -45^0 ply and 0^0 ply and delamination at all the interfaces.

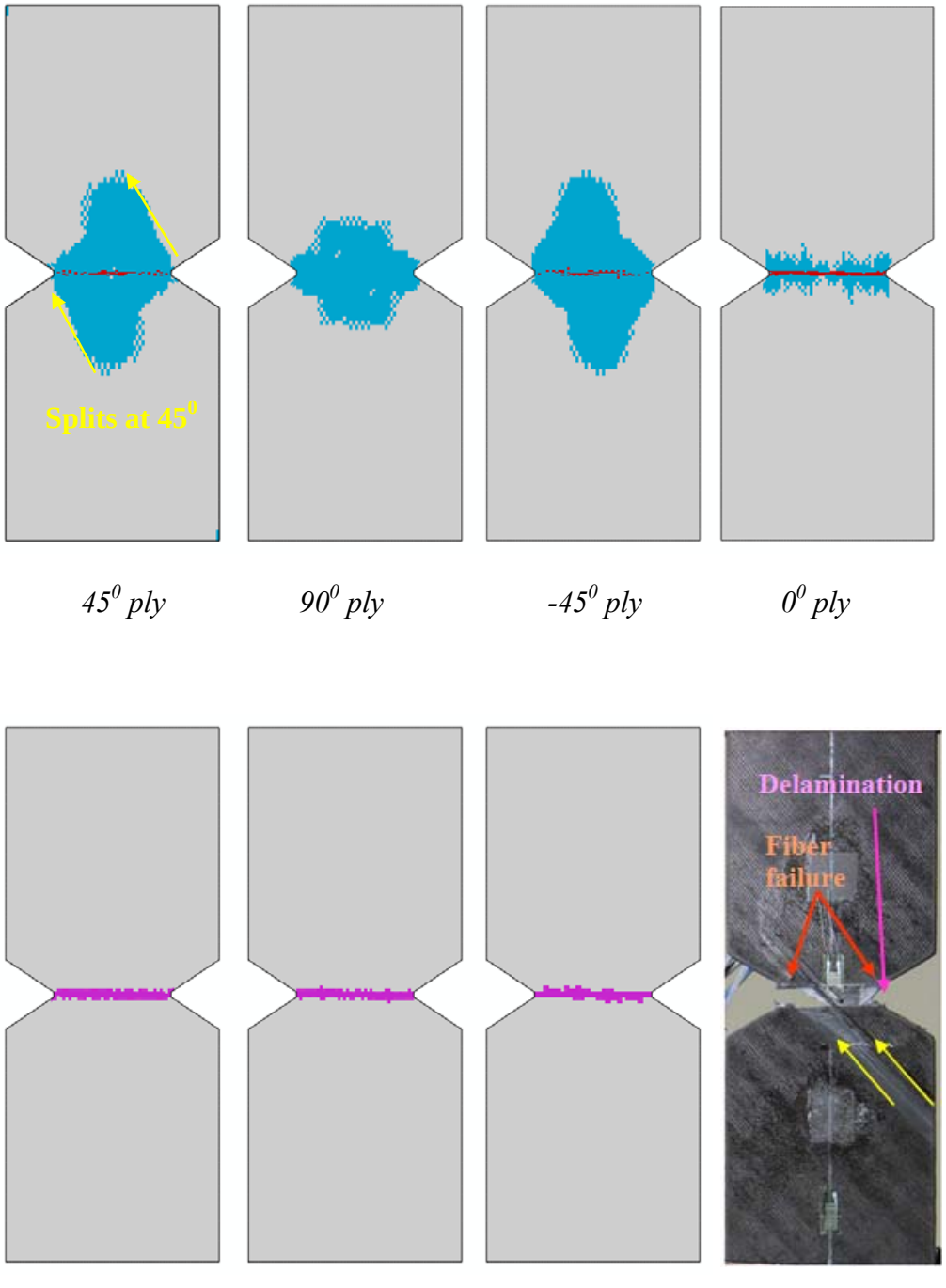

Figure 6-10 CDM: Final failure in the 45^0 ply, 90^0 ply, -45^0 ply and 0^0 ply and delamination at all the interfaces.

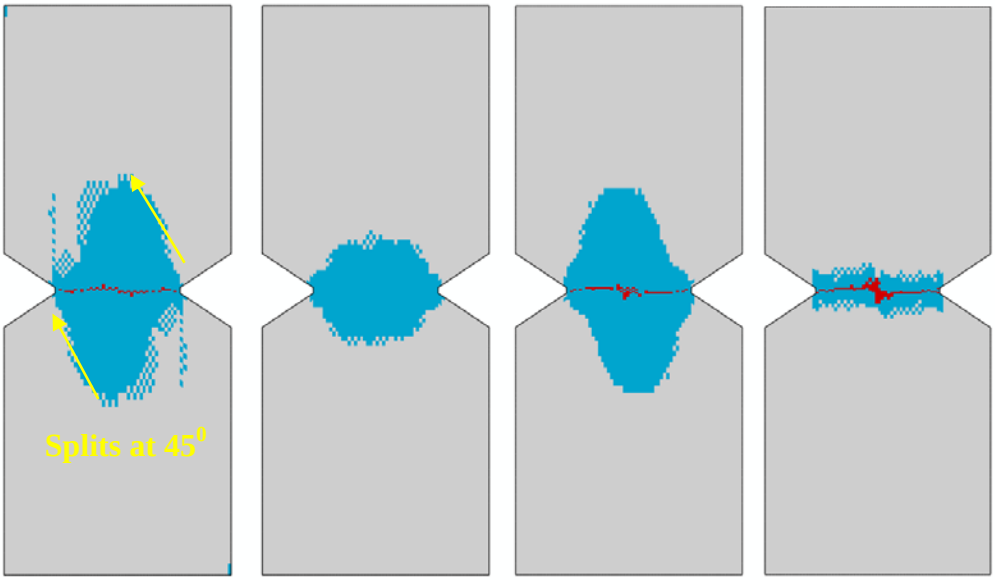

45^0 ply *90^0 ply* *-45^0 ply* *0^0 ply*

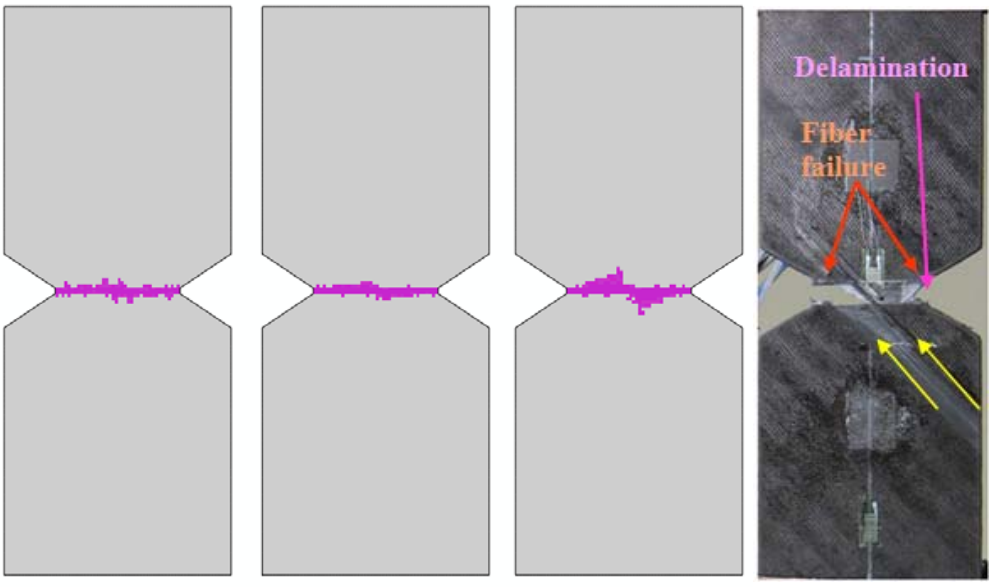

$[45^0/90^0]$ interface *$[90^0/-45^0]$ interface* *$[-45^0/0^0]$ interface* *Experiment*

Fiber failure Matrix failure Delamination No damage

Figure 6-11 MCDM: Final failure in the 45^0 ply, 90^0 ply, -45^0 ply and 0^0 ply and delamination at all the interfaces.

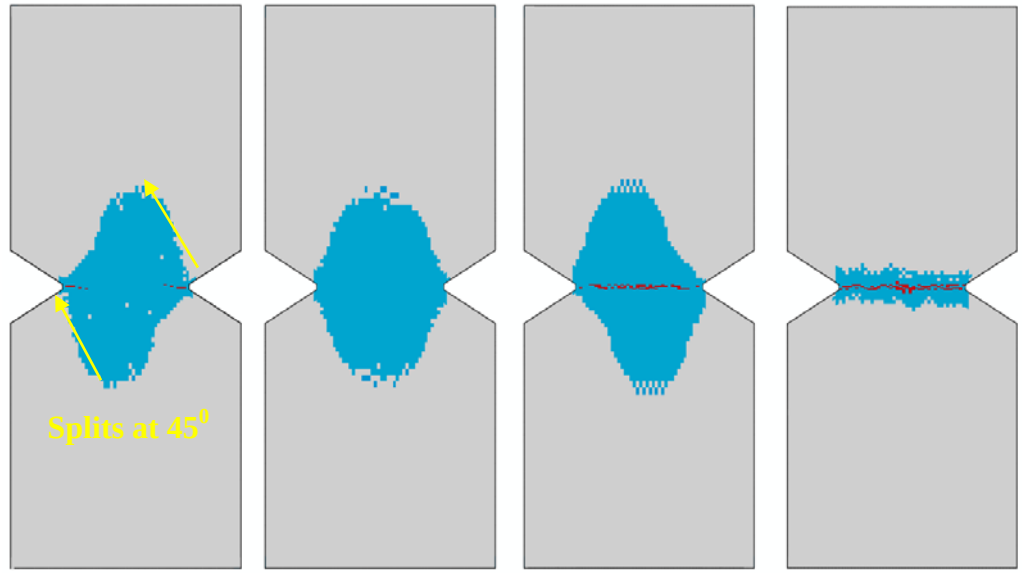

45^0 ply *90^0 ply* *-45^0 ply* *0^0 ply*

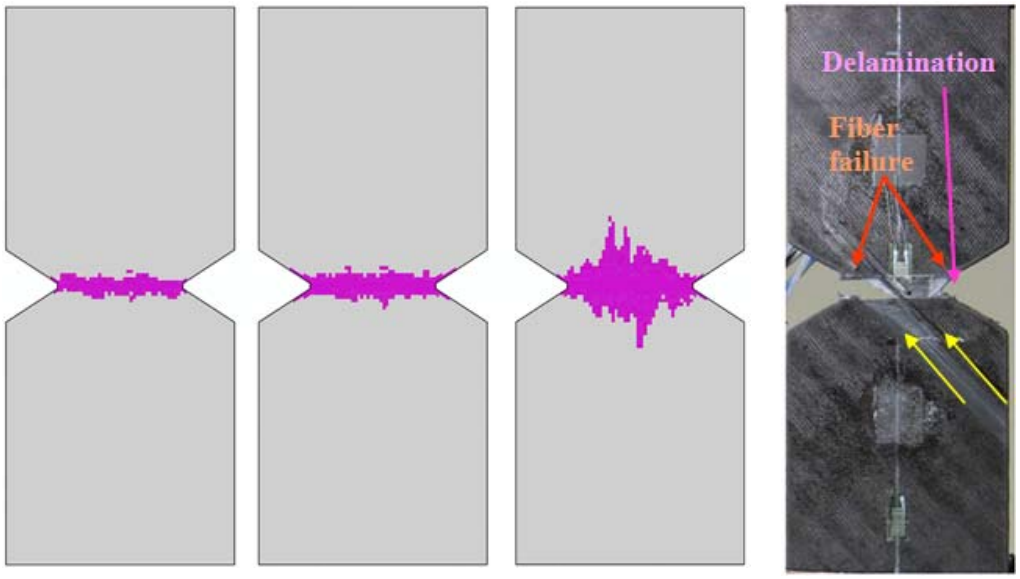

$[45^0/90^0]$ interface *$[90^0/-45^0]$ interface* *$[-45^0/0^0]$ interface* *Experiment*

Fiber failure Matrix failure Delamination No damage

Figure 6-12 MChristensen: Final failure in the 45^0 ply, 90^0 ply, -45^0 ply and 0^0 ply and delamination at all the interfaces.

6.2 Experimental and computational investigation of the ply-level scaled laminate of the $[45/90/-45/0]_s$ carbon/epoxy laminate

6.2.1 Experiment of the ply-level scale laminate

Unlike the notch-size scaled laminate which keep the thickness of the original quasi-isotropic laminate, the ply-level scaled laminate has the layup of $[45_2/90_2/-45_2/0_2]_s$ with all the in-plane dimensions and thickness except the length of the specimen double-scaled. The ply-level scaled laminate has been tested in tension. The strain gauge setup, experiment setup and procedure are similar to those of $[90/0]_s$ carbon/epoxy laminate reported in Chapter 3. Four specimens of this scaled laminate are made for tensile testing (Figure 6-13). Failures of specimens for the ply-level scaled laminate after the test are shown in Figure 6-14. Table 6-2 summaries the failure load (F_{crit}) and critical displacement (u_{crit}) at the top of the specimen corresponding to the gauge length of 100 mm. The load-displacement curves of ply-level scaled specimens are shown in Figure 6-15. The experiment results show that the failures of these specimens are due to the extensive fiber breakage and delamination in the middle of the specimen like the original $[45/90/-45/0]_s$ laminate. However, much more delamination and fiber failure are detected in ply-level scaled laminate than the original laminate.

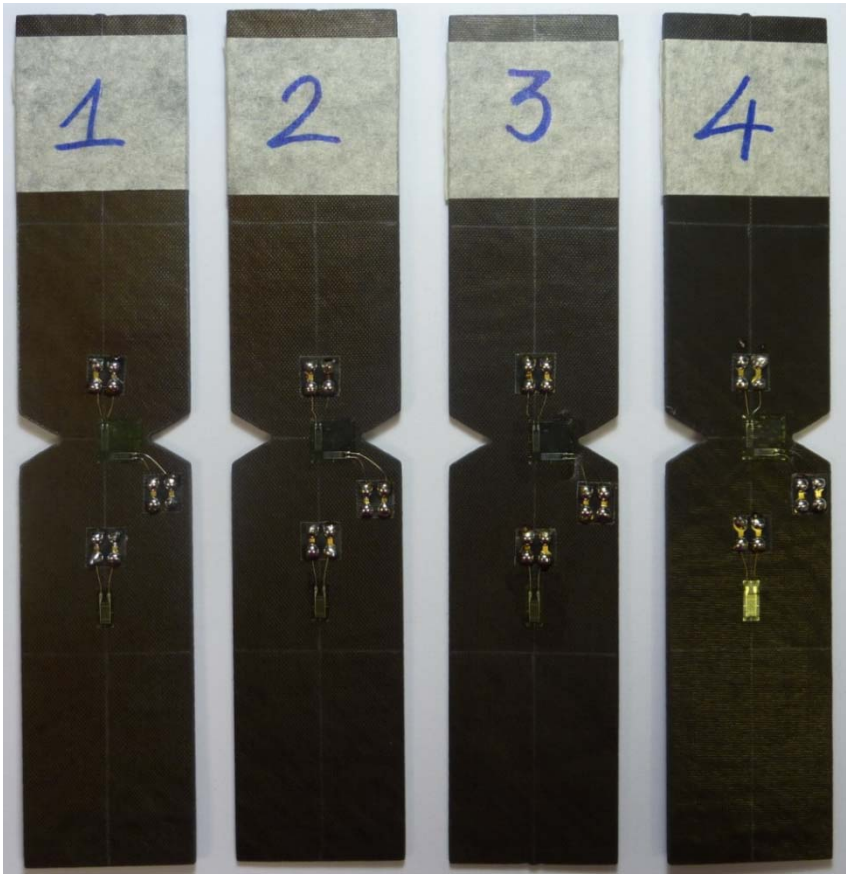

Figure 6-13 The ply-level scaled specimens before testing.

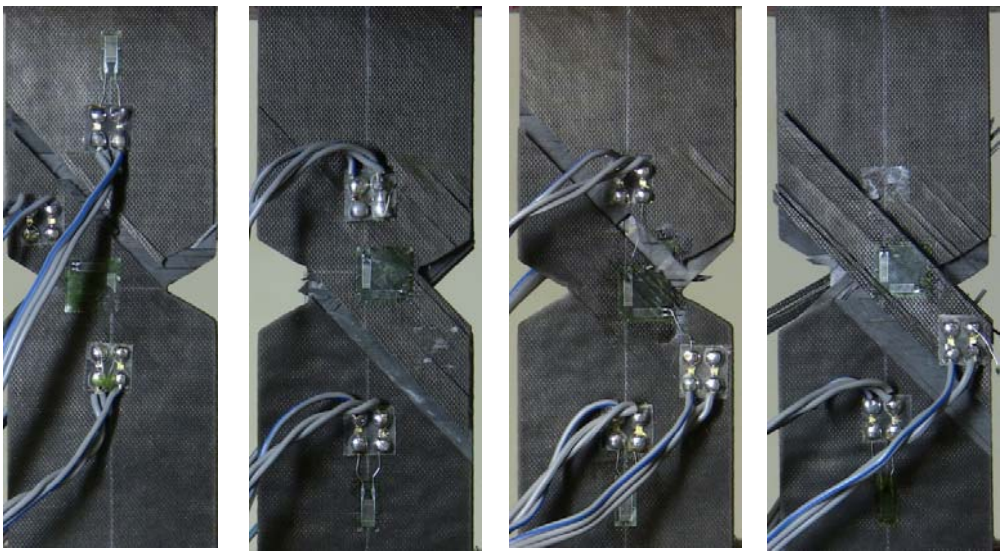

Figure 6-14 Failure of ply-level scaled specimens after testing.

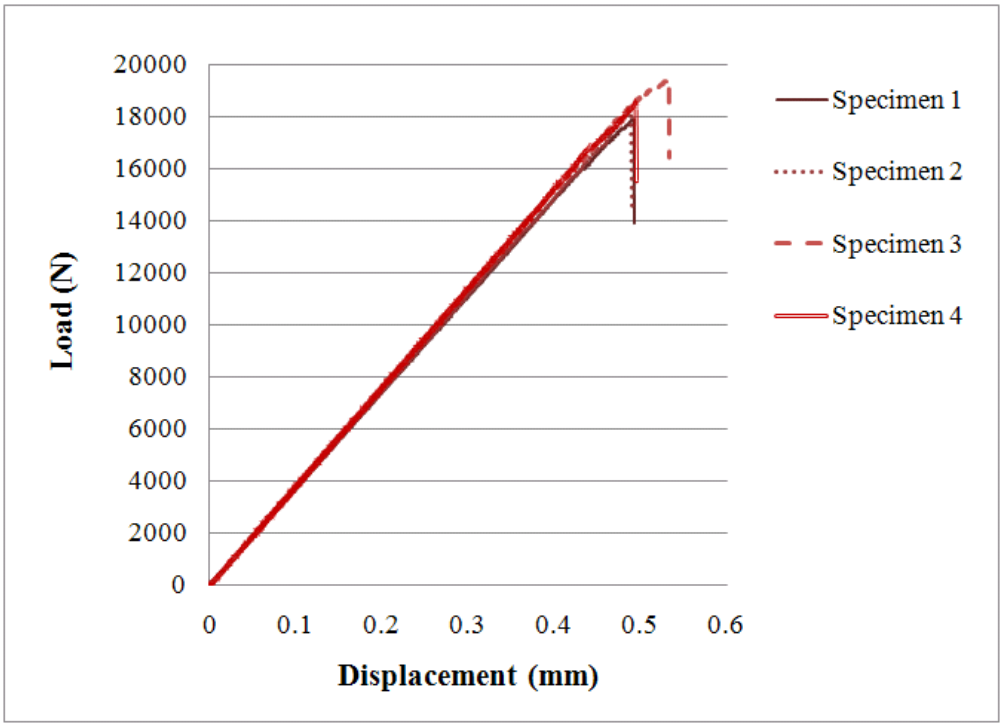

Figure 6-15 Load-displacement curves of ply-level scaled specimens.

Table 6-2 Critical displacements (u_{crit}) and failure load (F_{crit}) of ply-level scaled specimens

	Ply-level scaled laminate			
Specimen	u_{crit} **(mm)**	Δu_{crit} **(mm)**	F_{crit} **(N)**	ΔF_{crit} **(N)**
1	0.493	0.009	17899	640.9
2	0.489	0.013	18275	264.6
3	0.533	0.03	19451	911.4
4	0.494	0.008	18534	5.88
Average	**0.5** ± 0.015		**18539** ± 455.7	

6.2.2 Progressive failure analysis of the ply-level scaled laminate

Six failure models including the Tsai-Wu, Christensen, MMF, CDM, MCDM and MChristensen models are used for the failure analysis of ply-level scaled laminate and validated against the experimental data. The analysis is done by Abaqus with the finite element mesh and boundary conditions reported in Figure 6-16. The predicted load *vs.* displacement curves by all models are presented in Figure 6-17 and the predicted damage patterns are shown in Figures 6-18 to 6-23. Only the damage patterns just after the major load drop are shown since the initiation and propagation of matrix cracks, longitudinal splits, delamination and fiber failures are quite similar to the case of the original $[45/90/-45/0]_s$ carbon/epoxy laminate.

All the transverse matrix cracking in $\pm 45^0$ and 90^0 plies, longitudinal splitting and fiber failure in $\pm 45^0$ and 0^0 plies as well as delamination at three interfaces are predicted by six models. Since the carbon/epoxy specimens are usually dark that the damage patterns of the inner plies of quasi-isotropic laminate such as the 90^0, 0^0 and -45^0 plies are not visible, only the 45^0 ply (top ply) of the laminate is compared to the predicted results. As can be seen, the longitudinal splitting as well as fiber failure predicted for the 45^0 ply correlate well with longitudinal cracks running at 45^0 from the notch tip in the experiment. Moreover, predicted results for the delamination at the $[45/90]_s$ interface (the first interface) reveal that the 45^0 ply tends to slide over the 90^0

ply at 45 degree (Figures 6-18 to 6-23). This agrees well with the experimental observation.

Besides, the failure loads, defined as the major load drop, predicted by the Christensen, Tsai-Wu, MMF and CDM models are similar since there is not much difference on the fiber failure initiation and propagation between these conventional models. The failure load predicted by Christensen, Tsai-Wu, MMF and CDM are under-predicted the experiment by about 18%, 20%, 21% and 23%, respectively. On the other hand, the MCDM and MChristensen models which introduce a fracture process for fiber failure modeling predict the ultimate loads higher than conventional models. The MCDM and MChristensen can predict up to the 87% and 90% of the experimental failure loads, respectively. It is found that more delamination is predicted for the ply-level scaled laminate than the original quasi-isotropic laminate and no change in the failure mode is predicted between these two laminates.

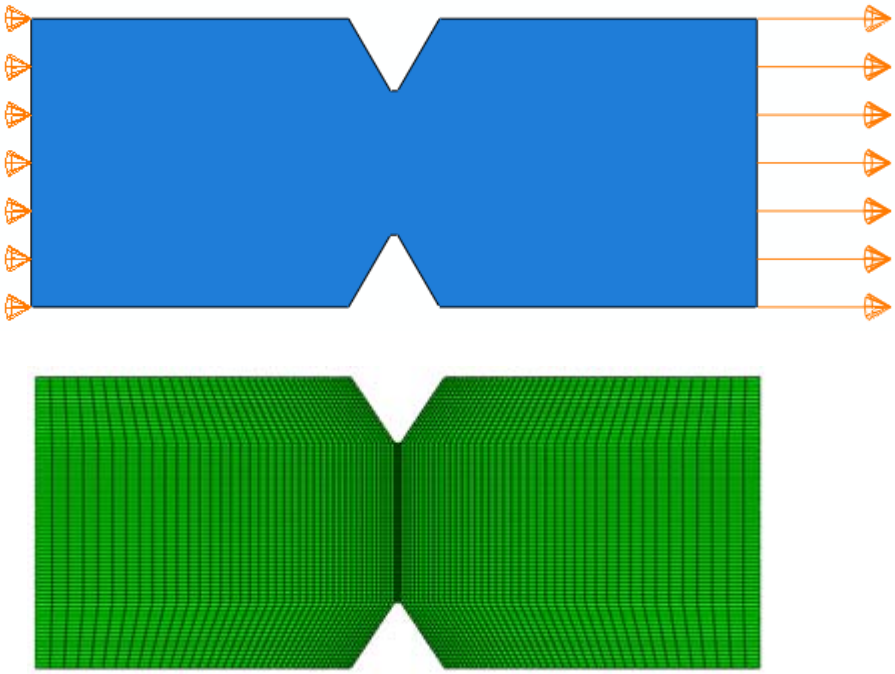

Figure 6-16 Boundary conditions and mesh of the FE model for ply-level scaled laminate.

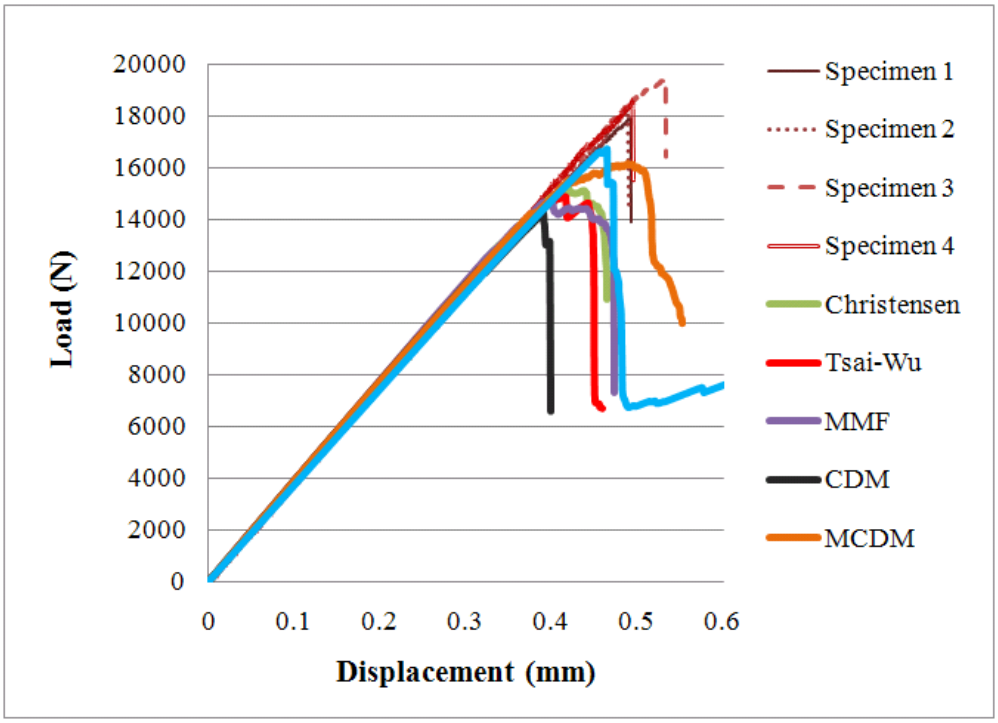

Figure 6-17 Predicted load-displacement curves and comparison with the experiment for the ply-level scaled laminate.

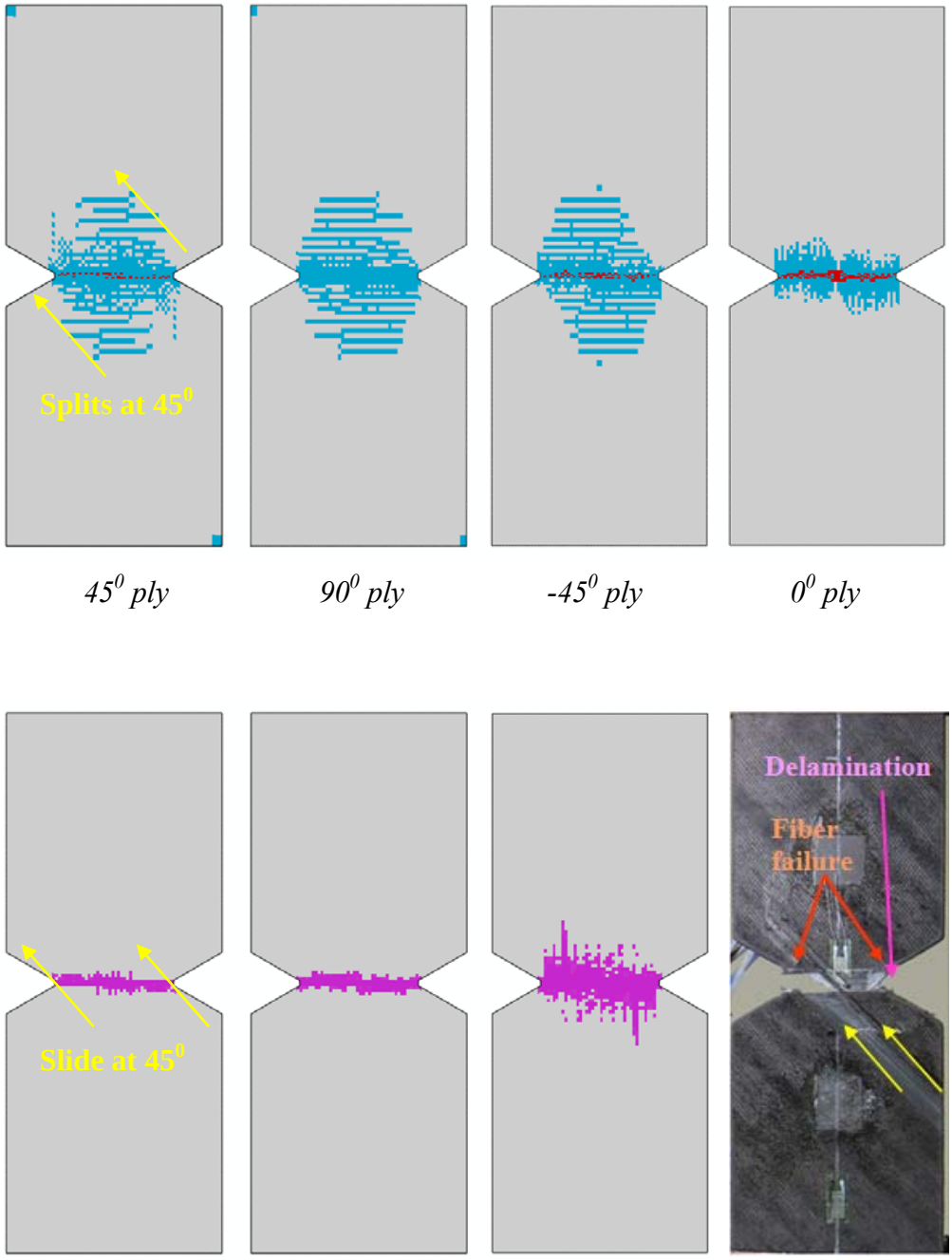

Figure 6-18 Christensen: Final failure in the 45^0 ply, 90^0 ply, -45^0 ply and 0^0 ply and delamination at all the interfaces.

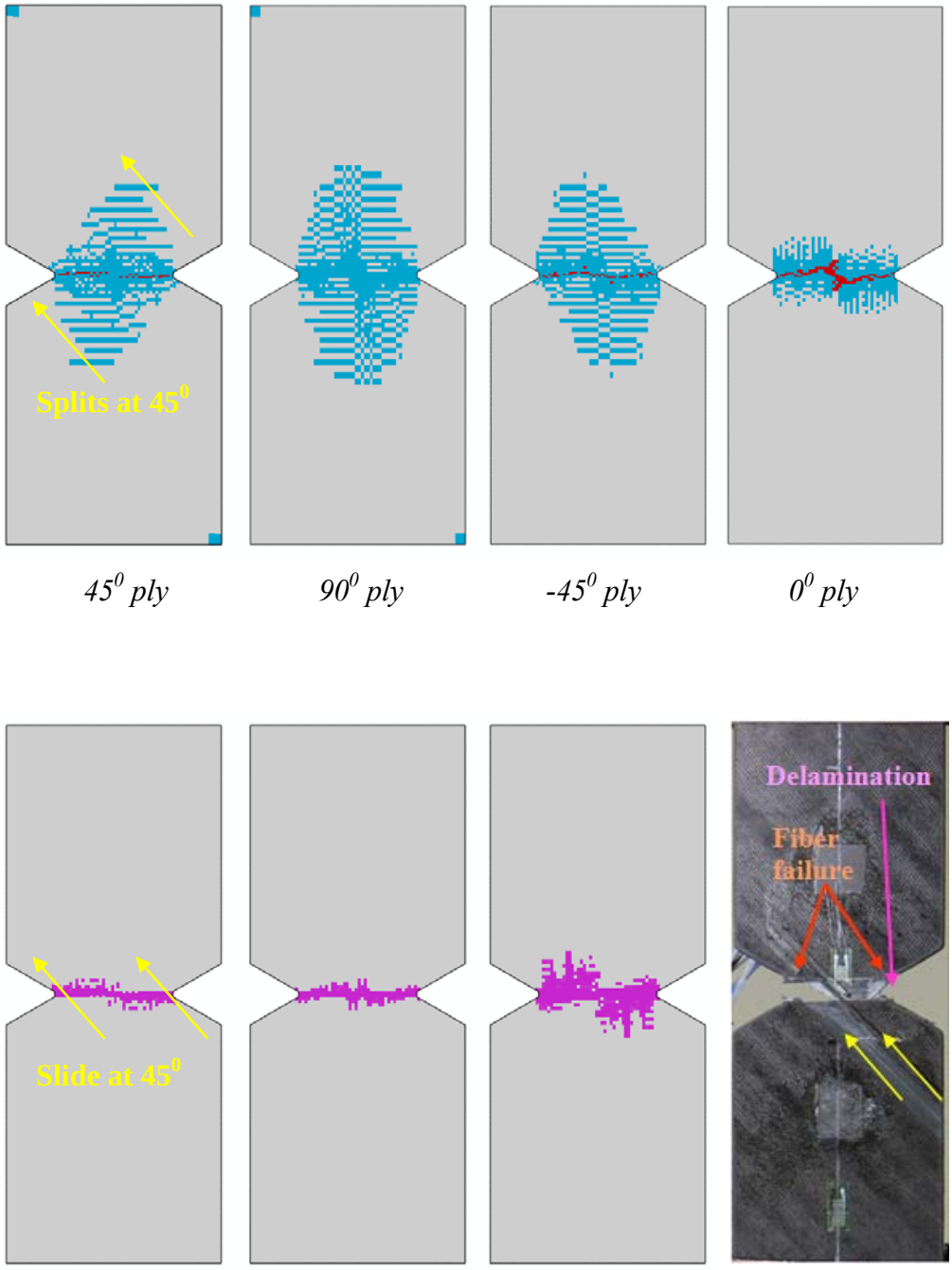

Figure 6-19 Tsai-Wu: Final failure in the 45^0 ply, 90^0 ply, -45^0 ply and 0^0 ply and delamination at all the interfaces.

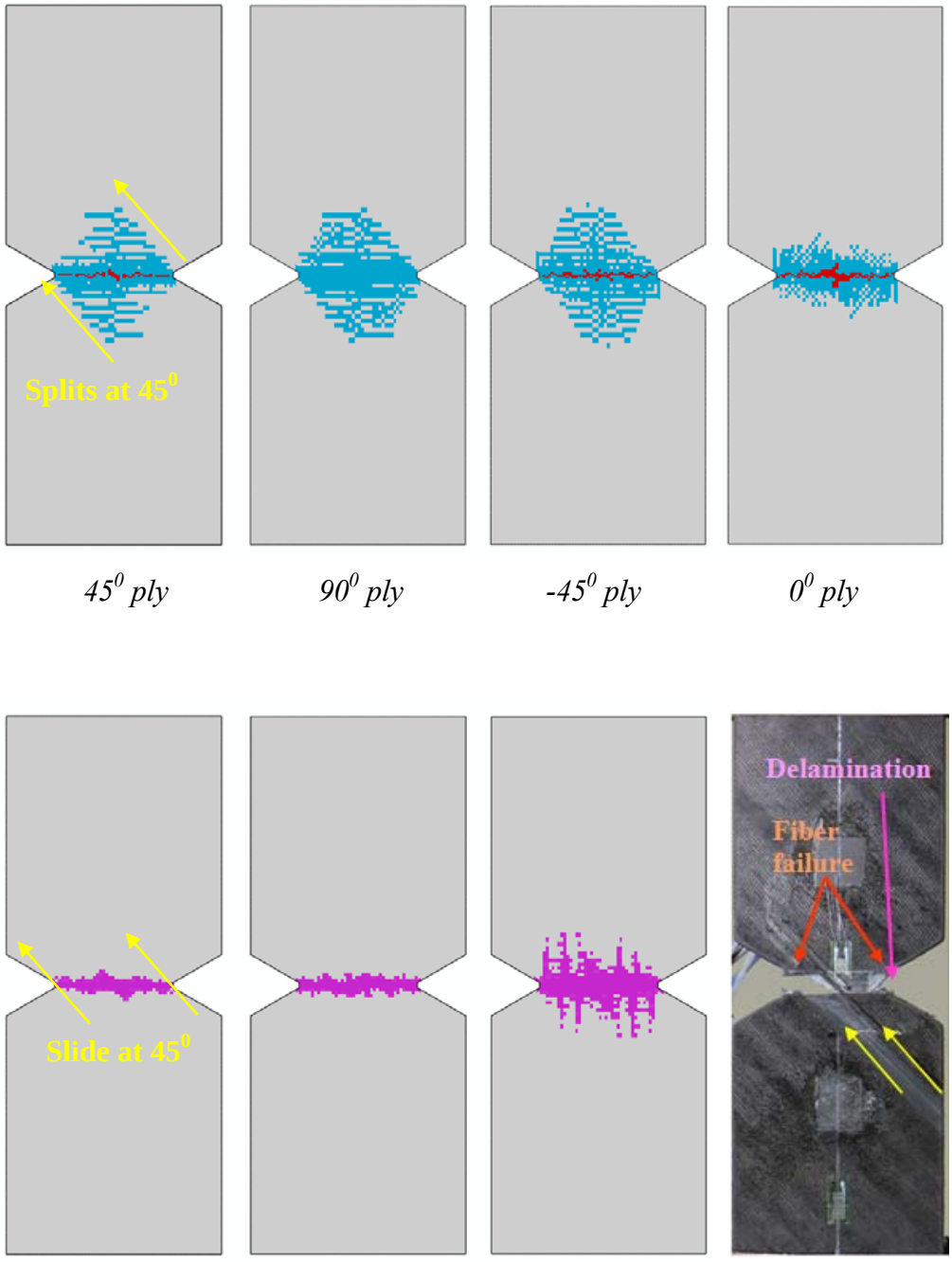

Figure 6-20 MMF: Final failure in the 45^0 ply, 90^0 ply, -45^0 ply and 0^0 ply and delamination at all the interfaces.

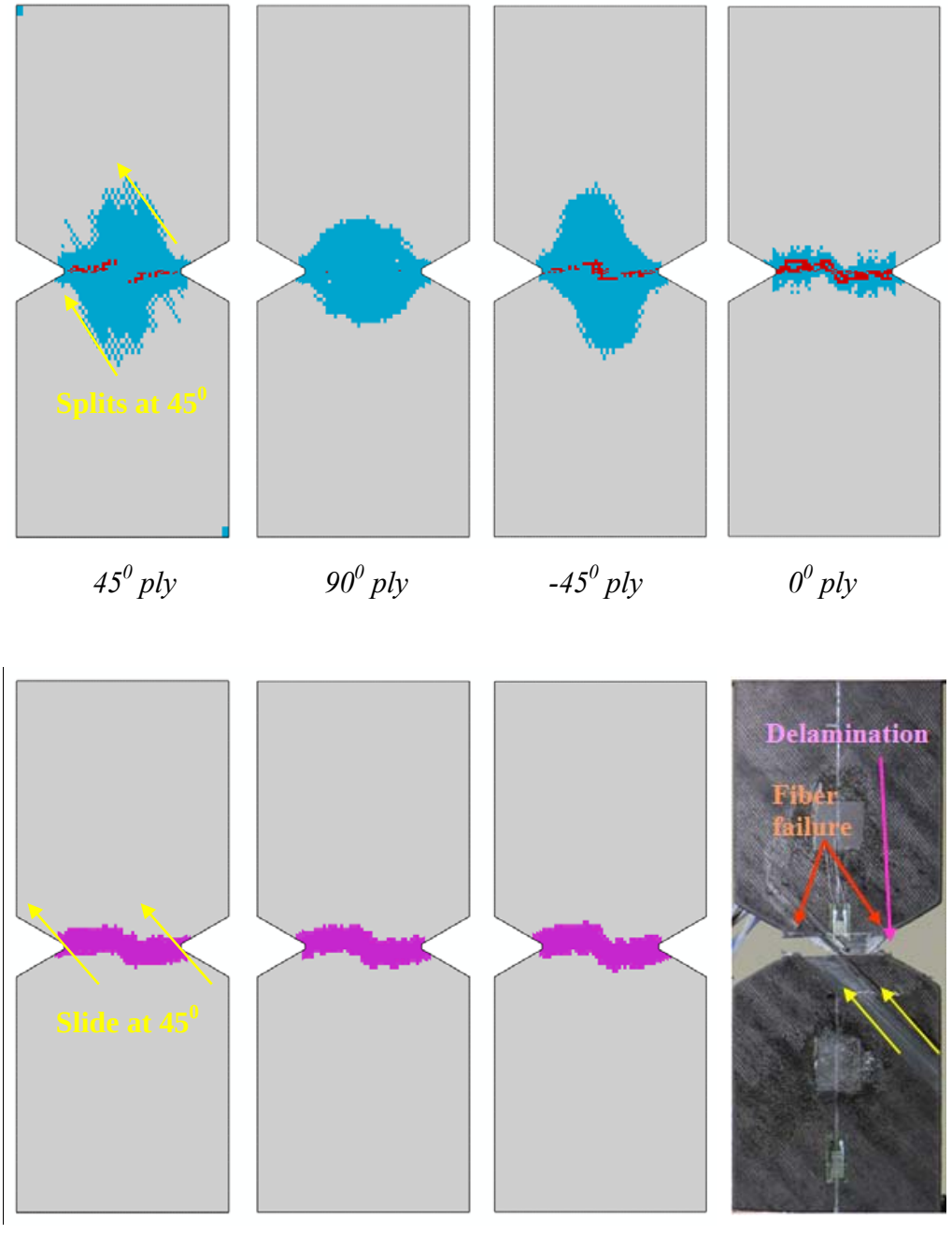

Figure 6-21 CDM: Final failure in the 45^0 ply, 90^0 ply, -45^0 ply and 0^0 ply and delamination at all the interfaces.

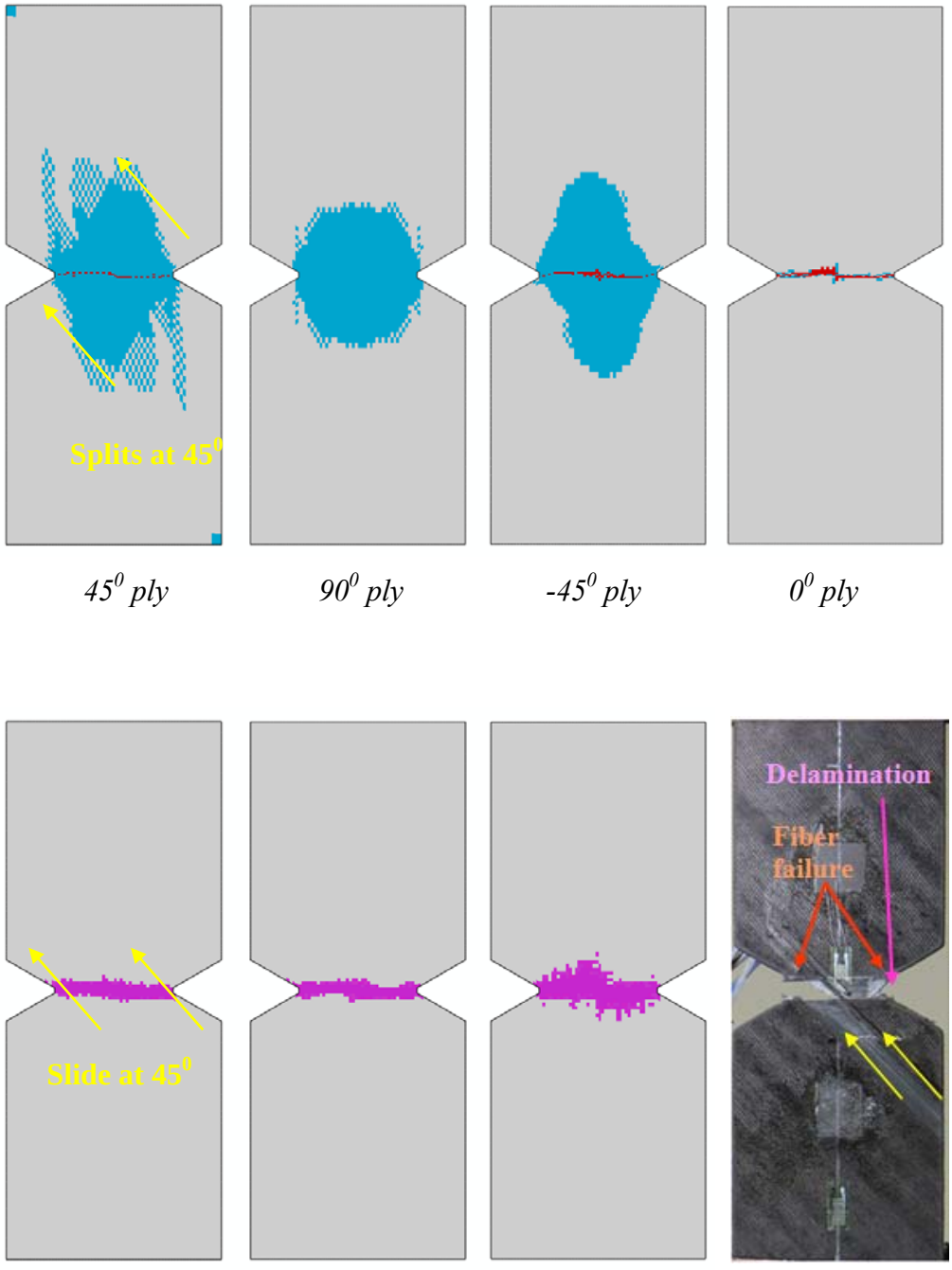

Figure 6-22 MCDM: Final failure in the 45^0 ply, 90^0 ply, -45^0 ply and 0^0 ply and delamination at all the interfaces.

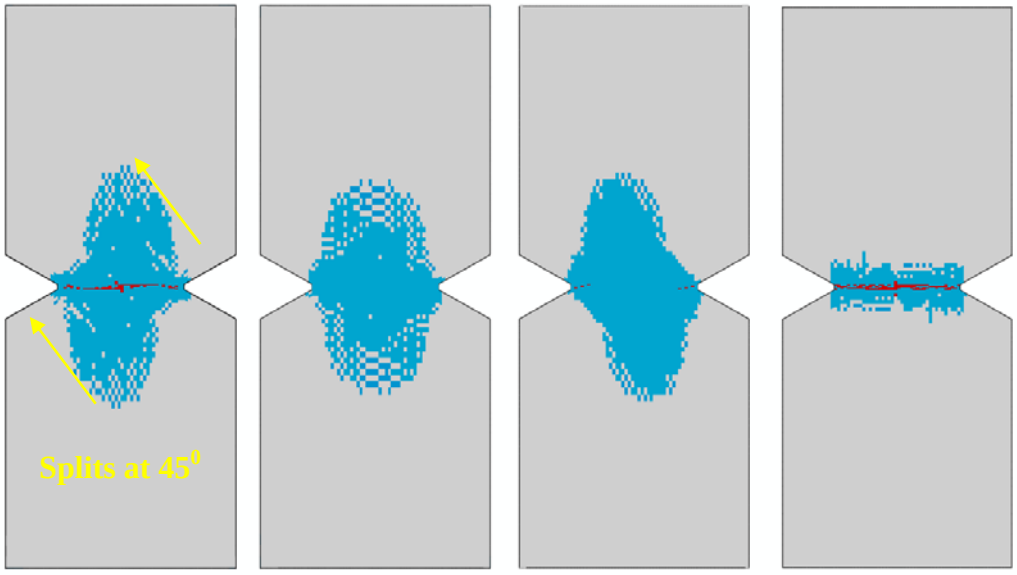

45^0 ply *90^0 ply* *-45^0 ply* *0^0 ply*

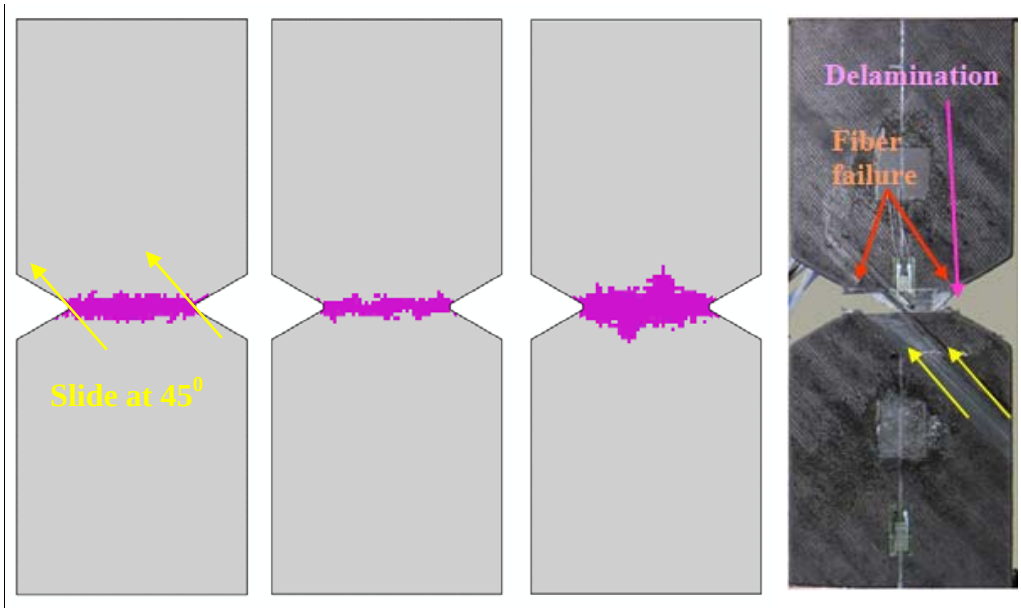

$[45^0/90^0]$ interface *$[90^0/-45^0]$ interface* *$[-45^0/0^0]$ interface* *Experiment*

Fiber failure Matrix failure Delamination No damage

Figure 6-23 MChristensen: Final failure in the 45^0 ply, 90^0 ply, -45^0 ply and 0^0 ply and delamination at all the interfaces.

6.3 Analysis of the scaling effects

Table 6-3 summaries the failure loads and strengths predicted by all failure models in the original quasi-isotropic laminate, notch-size scaled and ply-level scaled laminates. Additionally, Table 6-4 shows the reduction in strength from the original quasi-isotropic laminate to the scaled laminates. As can be seen in Table 6-4, a reduction in strength with increasing size has been obtained in experiment, whereby the original strength of the $[45/90/-45/0]_s$ composite laminate is decreased by 15.6% for the notch-size scaling effect and by 37.2% for the ply-level scaling effect. This trend has been captured computationally. The strengths predicted for the original quasi-isotropic laminate by the MCDM and MChristensen models are decreased by 17.1% and 18.5%, respectively for the notch-size scaling effect and by 34.8% and 37%, respectively for the ply-level scaling effect. On the other hand, the reduction in strength for scaling effects predicted by Christensen, Tsai-Wu and MMF models are quite similar. A strength reduction of 14% for the notch-size scaling effect and about 33% for the ply-level scaling effect are obtained for these models. Besides, the CDM model predicts a strength reduction of 10.2% for notch-size scaling effect and 28.9% for ply-level scaling effect.

Table 6-3 Predicted failure loads and strengths in the original quasi-isotropic laminate and scaled laminates.

	$[45/90/-45/0]_s$		**Notch-size scaled $[45/90/-45/0]_s$**		**Ply-level scaled $[45_2/90_2/-45_2/0_2]_s$**	
	Load (N)	Strength (MPa)	Load (N)	Strength (MPa)	Load (N)	Strength (MPa)
Experiment	7377.8	368.89	12445.8	311.14	18539.6	231.75
Christensen	5650.3	282.52	9708.78	242.72	15205.9	190.07
Tsai-Wu	5565.7	278.29	9523.4	238.09	14890.7	186.13
MMF	5535.4	276.77	9523.71	238.09	14653.2	183.16
CDM	5020.7	251.03	9013.77	225.34	14285	178.56
MCDM	6195	309.75	10261.3	256.53	16146.2	201.83
MChristensen	6650.2	332.51	10834.7	270.87	16754.9	209.44

Table 6-4 Percentage of the reduction in strength obtained from the original quasi-isotropic laminate to notch-size scaled laminate (Notch-size scaling effect) and to ply-level scaled laminate (Ply-level scaling effect).

% Decrease in Strength		
	Notch-size scaling effect	**Ply-level scaling effect**
Experiment	15.65	37.18
Christensen	14.09	32.72
Tsai-Wu	14.45	33.11
MMF	13.97	33.82
CDM	10.23	28.87
MCDM	17.18	34.84
MChristensen	18.54	37.01

6.4 Conclusion

The notch-size and ply-level scaling effects of the [45/90/-45/0]$_s$ carbon/epoxy laminate have been investigated experimentally and numerically in this chapter. Simulation results for the scaled laminates show more matrix cracking, delamination and fiber failure than the original laminate; especially for the ply-level scaled laminate which has shown the most extensive

delamination and fiber failure. It is also found that the MCDM and MChristensen models still provide better predictions for scaled laminates than CDM, Christensen, Tsai-Wu and MMF models.

Furthermore, a reduction in strength with increasing size has been observed in the experiment. This trend has been captured computationally. Simulation results show that a similar amount of the strength reduction in the experiment has been predicted by all of the models except for the CDM model. It is also found that no change in the failure mechanism is obtained from the original quasi-isotropic laminate to the scaled laminates both experimentally and computationally.

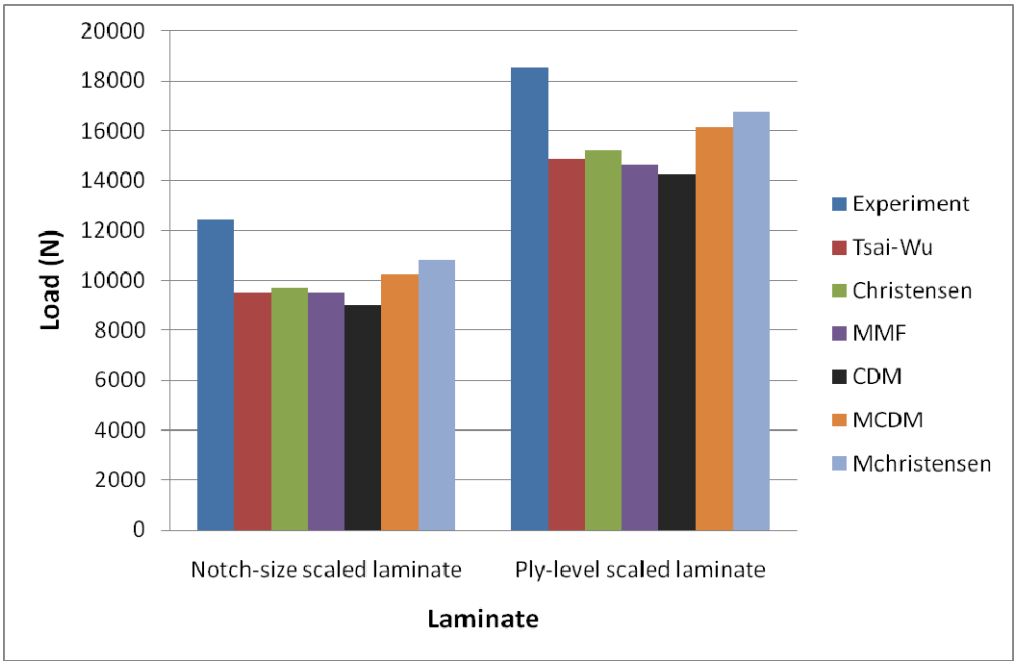

Figure 6-24 Comparison between predicted failure loads and the experimental failure load for notch-size scaled and ply-level scaled laminates.

Chapter 7

Conclusions and Recommendations

7.1 Conclusions

A computational study of progressive failure analysis in composite laminates has been presented in this thesis based on the implementation of the material degradation method (MPDM), continuum damage mechanics (CDM) and cohesive element (CE) method. The combined MPDM-CE and CDM-CE approaches successfully helped predict both the in-plane progressive damage and delamination in cross-ply and quasi-isotropic composite laminates with carbon/epoxy and glass/epoxy composite materials.

Various failure models of double-notched composite laminates have been illustrated in this thesis. The conventional failure models such as the Tsai-Wu, Christensen, MMF and CDM models assume that the failure in composite is determined by the constituent fiber's strengths and that the fiber is perfectly brittle which is either completely broken or intact in the failure analysis. This can lead to the underestimation of composite strengths at high stress concentration areas such as in the vicinity of sharp notches where the prediction of fiber failure is often conservative. Hence, modified versions of the CDM and Christensen models have been introduced, assuming that the

fiber is not very brittle and can undertake a damage evolution. This means that the fiber failure in composite can be described by a fracture process from the initial failure to the ultimate failure like the concept of crack propagation in fracture mechanics. These modified versions of CDM and Christensen models, called MCDM and MChristensen, generally provide better predictions than conventional failure models in most of the analyses of composite laminates.

There are major conclusions:

- A progressive failure analysis of double-notched $[90/0]_s$ and $[45/90/-45/0]_s$ carbon/epoxy laminates has first been performed and validated against the experiment. Simulation results for the cross-ply showed good agreements with the experimental data for the damage patterns and ultimate loads. The predicted loads for the cross-ply laminate by conventional models such as the Christensen, Tsai-Wu, MMF and CDM models were close to the experiment whereas the MCDM and MChristensen models slightly over-predicted the experiment. Besides, simulation results for the quasi-isotropic laminate showed that the conventional failure models were conservative and under-predicted the experiment while the MCDM and MChristensen models predicted closer to the experiment. It has been found that a discontinuity in all the predicted curves for the cross-ply carbon/epoxy laminate was obtained while no discontinuity in the predicted curves was found for the quasi-isotropic laminate. This discontinuity can be explained by a

great stiffness loss of the 90^0 ply at the early stage before the fiber failure in the 0^0 ply occurs.

- A progressive failure analysis of double-notched $[90/0]_s$ and $[45/90/-45/0]_s$ glass/epoxy has also been presented. The predicted results for both the cross-ply and quasi-isotropic glass/epoxy laminates were compared to experiment data of Hallett and Wisnom. Simulation results for the cross-ply laminate showed good correlation between the failure analysis and the experiment, whereby splitting in 0^0 ply, matrix cracking in 90^0 ply and delamination were successfully captured. While the conventional failure models were found to under-predict the experimental failure load, the MCDM and MChristensen models provided pretty well predictions. This is because the MCDM and MChristensen models consider that the fiber failures near the notch roots still can sustain additional loads to a certain extent while conventional models assume fiber failures to have a complete loss in their load-carrying capabilities. Similarly, simulation results for the quasi-isotropic glass/epoxy laminate showed that the MCDM and MChristensen models predict better than conventional failure models. It should be noted that a discontinuity in the predicted curves were found for both the cross-ply and quasi-isotropic glass/epoxy laminates. This is different from the cases of carbon/epoxy laminates in which only the cross-ply carbon/epoxy laminate has been detected with that discontinuity. The glass/epoxy laminates are found with more discontinuity in the predicted curves because the matrix failure in

glass/epoxy laminates is easier to occur than in carbon/epoxy laminates. This can be explained by the ratio of longitudinal modulus to transverse elastic modulus for glass/epoxy material (E_1/E_2 = 3.9) which is much smaller than carbon/epoxy material (E_1/E_2 = 14.3).

- The mesh dependency study has been done on the $[45/90/-45/0]_s$ carbon/epoxy laminate employing the CDM, Christensen, MCDM and MChristensen models. This study analyzed the mesh sensitivity of the quasi-isotropic carbon/epoxy laminate due to the effect of the notch's geometries (sharp notch or blunt notch) and the element types (2D elements or 3D elements). The computational results showed that the models with 3D elements and the blunt notch (3D Blunt) were mesh-independent regardless of any of the four failure model chosen. Besides models of the 3D Blunt group, it would be an advantage to use 2D elements and blunt notch (2D Blunt) for the MChristensen and MCDM models to produce mesh-independent results while it would not for the CDM and Christensen models.

- In addition, the parametric study on cohesive parameters has been performed on the $[45/90/-45/0]_s$ carbon/epoxy laminate to investigate the effect of cohesive parameters on the failure prediction. The results predicted by various failure models revealed that the failure loads were not so sensitive to the values of cohesive strengths and SERRs assigned. A change less than 5% of the failure loads was obtained when increasing the interlaminar shear strengths S, T or SERRs G_{IIc}

and G_{IIIc} by 100% and decreased them by 50% from their original values while the interlaminar normal strength N and G_{Ic} caused no effect to the failure prediction.

- A parametric study of the MPDM scheme has been presented, varying the value of degradation factors in MPDM for the analysis of quasi-isotropic carbon/epoxy laminate. The results show that a value of 10^{-6} needs to be assigned for all the degradation factors in tension mode to reasonably account for the damage in composites.

- Finally, the notch-size and ply-level scaling effects of the $[45/90/-45/0]_s$ carbon/epoxy laminate have been investigated experimentally and numerically. A reduction in strength from the quasi-isotropic laminate to the notch-size and ply-level scaled laminates was observed in the experiment. This trend was captured computationally. As a consequence, a similar amount of the strength reduction with increasing in size was obtained between experiment and simulation. It was also found that no change in the failure mechanism was obtained from the original quasi-isotropic laminate to the scaled laminates or between these scaled laminates.

7.2 Recommendations

- The damage progression of notched composite laminates subjected to tension was studied in this thesis. Since the failure of notched

composites under compression is also of great importance and may be complicated due to the effect of notches, it is therefore recommended to investigate the progressive failure analysis of notched composites due to compressive loading. It should be noted that besides the failure mechanisms for tensile cases such as splitting, matrix cracking or delamination, fiber kinking and local bucking also need to be taken into account for composite laminates under compressive loading. The MPDM-CE approach therefore should be modified accordingly in the compression mode, in which the determination of the degradation factors and cohesive parameters needs to be carefully analyzed.

- The author's research has shown that by describing a fracture process for fiber failure modeling, the MCDM and MChristensen models have improved the strength prediction of composites. Since there is no restriction made for the implementation of the fracture process to conventional models, the Tsai-Wu and MMF models therefore can be also modified to improve their predictions and compare with those of MChristensen and MCDM models. However, while it may be necessary to introduce a fracture process for the fiber failure modeling, little evidence is found in literature to validate this strategy. Theoretically, once fiber is failed, the conventional damage modeling will consider a complete loss in its load-bearing capability. However, a fiber in physics can be damaged like an isotropic material (e.g. glass fibers) and it is still able to carry more loads. Therefore, a progressive

failure analysis for both matrix and fiber may be considered and investigated in the future work.

- In this thesis, only static loading problem is studied. The composite strength could be significantly affected by the dynamic and fatigue loading, especially for notched composites in which the effect of notches becomes more complex and may be unpredictable. Therefore, extension to dynamic and fatigue problems should be topics of future research.

REFERENCE

1. Kwon, Y.W. and L.E. Craugh, *Progressive Failure Modeling in Notched Cross-Ply Fibrous Composites.* Applied Composite Materials, 2001. **8**(1): p. 63-74.

2. Kortschot, M.T. and P.W.R. Beaumont, *Damage mechanics of composite materials: II-- a damaged-based notched strength model.* Composites Science and Technology, 1990. **39**(4): p. 303-326.

3. Tan, S.C. and J. Perez, *Progressive Failure of Laminated Composites with a Hole under Compressive Loading.* Journal of Reinforced Plastics and Composites, 1993. **12**(10): p. 1043-1057.

4. Hallett, S.R. and M.R. Wisnom, *Numerical Investigation of Progressive Damage and the Effect of Layup in Notched Tensile Tests.* Journal of Composite Materials, 2006. **40**(14): p. 1229-1245.

5. Daniel, I.M., *Failure of Composite Materials.* Strain, 2007. **43**(1): p. 4-12.

6. Icardi, U., et al., *Assessment of Recent Theories for Predicting Failure of Composite Laminates.* Applied Mechanics Reviews, 2007. **60**(2): p. 76-86.

7. Hinton, M.J., P.D. Soden, and A.S. Kaddour, *Failure Criteria in Fiber-Reinforced-Polymer Composites*. 2004: Elsevier, Oxford.

8. Hinton, M.J., A.S. Kaddour, and P.D. Soden, *A Comparison of the Predictive Capabilities of Current Failure Theories for Composite Laminates, Judged against Experimental Evidence.* Composites Science and Technology, 2002. **62**(12-13): p. 1725-1797.

9. Jenkins, C.F., *Report on materials of construction used in aircraft and aircraft engines.* Great Britain Aeronautical Research Committee, 1920.

10. Waddoups, M.E., *Advanced composite material mechanics for design and stress analysis.* General Dynamics, Fort Worth Division Report FZM-4763, Fort Worth, TX, 1967.

11. Tsai, S.W. and V.D. Azzi, *Strength of Laminated Composite Materials.* AIAA Journal, 1966. **4**(2): p. 58-80.

12. Tsai, S.W. and E.M. Wu, *A General Theory of Strength for Anisotropic Materials.* Journal of Composite Materials, 1971. **5**(1): p. 58-80.

13. Hashin, Z., *Failure Criteria for Unidirectional Fiber Composites.* Journal of Applied Mechanics, 1980. **47**(1): p. 58-80.

14. Christensen, R.M. *Failure Criteria for Anisotropic Fiber Composite Materials*. 2008.

15. Ha, S.K., K.K. Jin, and Y. Huang, *Micro-Mechanics of Failure (MMF) for Continuous Fiber Reinforced Composites.* Journal of Composite Materials, 2008. **42**(18): p. 1873-1895.

16. Tay, T.E., et al., *Progressive Failure Analysis of Composites.* Journal of Composite Materials, 2008. **42**(18): p. 1921-1966.

17. Chu, G.D. and C.T. Sun, *Failure Initiation and Ultimate Strength of Composite Laminates Containing a Center Hole.* Composite Materials: Fatigue and Fracture, Fourth Volume, ASTM STP 1156, Stinchcomb, W.W. and Ashbaugh, N.E., Eds., American Society for Testing and Materials, Philadelphia, 1993: p. 35-54.

18. Pal, P. and C. Ray, *Progressive Failure Analysis of Laminated Composite Plates by Finite Element Method.* Journal of Reinforced Plastics and Composites, 2002. **21**(16): p. 1505-1513.

19. Prusty, B.G., *Progressive Failure Analysis of Laminated Unstiffened and Stiffened Composite Panels.* Journal of Reinforced Plastics and Composites, 2005. **24**(6): p. 633-642.

20. Chang, F.K., L. Lessard, and J.M. Tang, *Compression Response of Laminated Composites Containing an Open Hole.* SAMPE Quartely,, 1988. **19**(4): p. 46-51.

21. Greif, R. and E. Chapon, *Investigation of Successive Failure Modes in Graphite/Epoxy Laminated Composite Beams.* Journal of Reinforced Plastics and Composites, 1993. **12**(5): p. 602-620.

22. Kim, Y., J.F. Davalos, and E.J. Barbero, *Progressive Failure Analysis of Laminated Composite Beams.* Journal of Composite Materials, 1996. **30**(5): p. 536-560.

23. Kress, G., M. Siau, and P. Ermanni, *Iterative Solution Methods for Damage Progression Analysis.* Composite Structures, 2005. **69**(1): p. 21-33.

24. Liu, K.S. and S.W. Tsai, *A Progressive Quadratic Failure Criterion for a Laminate.* Composites Science and Technology, 1998. **58**(7): p. 1023-1032.

25. Petit, P.H. and M.E. Waddoups, *A Method of Predicting the Nonlinear Behavior of Laminated Composites.* Journal of Composite Materials, 1969. **3**(1): p. 2-19.

26. Sandhu, R.S., G.P. Sendeckyj, and R.L. Gallo, *Modeling of the Failure Process in Notched Laminates.* In: Hashin, Z. and Herakovich, C.T. (eds), Mechanics of Composite Materials: Recent Advances, Pergamon Press, Oxford., 1983: p. 179-189.

27. Zhao, G. and C. Cho, *On Impact Damage of Composite Shells by a Low-Velocity Projectile.* Journal of Composite Materials, 2004. **38**(14): p. 1231-1254.

28. Tan, S.C., *A Progressive Failure Model for Composite Laminates Containing Openings.* Journal of Composite Materials, 1991. **25**(5): p. 556-577.

29. Tan, S.C. and R.J. Nuismer, *A Theory for Progressive Matrix Cracking in Composite Laminates.* Journal of Composite Materials, 1989. **23**(10): p. 1029-1047.

30. Camanho, P.P., S. Bowron, and F.L. Matthews, *Failure Mechanisms in Bolted CFRP.* Journal of Reinforced Plastics and Composites, 1998. **17**(3): p. 205-233.

31. Reddy, Y.S.N., C.M.D. Moorthy, and J.N. Reddy, *Non-Linear Progressive Failure Analysis of Laminated Composite Plates.* International Journal of Non-Linear Mechanics, 1995. **30**(5): p. 629-649.

32. Kortschot, M.T. and P.W.R. Beaumont, *Damage mechanics of composite materials: I-- Measurements of damage and strength.* Composites Science and Technology, 1990. **39**(4): p. 289-301.

33. Barbero, E.J. and P. Lonetti, *An Inelastic Damage Model for Fiber Reinforced Laminates.* Journal of Composite Materials, 2002. **36**(8): p. 941-962.

34. Feih, S. and H.R. Shercliff, *Adhesive and composite failure prediction of single-L joint structures under tensile loading.* International Journal of Adhesion and Adhesives, 2005. **25**(1): p. 47-59.

35. Ahn, J. and A.M. Waas, *The Failure Of Notched Composite Laminates Under Compression Using Integrated Macro-Micromechanics Model.* 46 th AIAA/ASME/ASCE/AHS/ASC Structures, Structural Dynamics, and Materials Conference, 18-21 April 2005, Austin, Texas, AIAA 2005-1954, 2005: p. 1-14.

36. Ahn, J.H. and A.M. Waas, *Micromechanics-Based Predictive Model for Compressively Loaded Angle-Ply Composite Laminates.* AIAA Journal, 2000. **38**(12): p. 2299-2304.

37. Waas, A.M., A. Junghyun, and A.R. Khamseh, *Compressive failure of notched uniply composite laminates.* Composites Part B: Engineering, 1998. **29**(1): p. 75-80.

38. Ahn, J.H. and A.M. Waas, *A Micromechanics-Based Finite Element Model for Compressive Failure of Notched Uniply Composite Laminates Under Remote Biaxial Loads.* Journal of Engineering Materials and Technology, 1999. **121**(3): p. 360-366.

39. Chamis, C.C., P.L.N. Murthy, and L. Minnetyan, *Progressive Fracture in Composite Structures, In: Armanios, E.A. (eds).* Composite Materials: Fatigue and Fracture 6th Volume, ASTM STP 1285, American Society for Testing and Materials, 1997: p. 70-84.

40. Riccio, A., *Effects of Geometrical and Material Features on Damage Onset and Propagation in Single-lap Bolted Composite Joints under Tensile Load: Part II - Numerical Studies.* Journal of Composite Materials, 2005. **39**(23): p. 2091-2112.

41. Talreja, R., *Transverse Cracking and Stiffness Reduction in Composite Laminates.* Journal of Composite Materials, 1985. **19**(4): p. 355-375.

42. Allen, D.H., C.E. Harris, and S.E. Groves, *A Thermomechanical Constitutive Theory for Elastic Composites with Distributed Damage - Part II: Application to Matrix Cracking in Laminated Composites.* International Journal of Solids and Structures, 1987. **23**(9): p. 319-1338.

43. Allen, D.H., C.E. Harris, and S.E. Groves, *A Thermomechanical Constitutive Theory for Elastic Composites with Distributed Damage - Part I: Theoretical Development.* International Journal of Solids and Structures, 1987. **23**(9): p. 1301-1318.

44. Lee, S., et al., *Mechanical Testing of Toughened Resin Composite Materials.* Composites, 1988. **19**(4): p. 300-310.

45. Allix, O. and P. Ladevèze, *Interlaminar interface modelling for the prediction of delamination.* Composite Structures, 1992. **22**(4): p. 235-242.

46. Allix, O., P. Ladeveze, and A. Corigliano, *Damage Analysis of Interlaminar Fracture Specimens.* Composite Structures, 1995. **31**(1): p. 61-74.

47. Ladeveze, P. and E. Le Dantec, *Damage Modeling of the Elementary Ply for Laminated Composites.* Composites Science and Technology, 1992. **43**(3): p. 257-267.

48. Ladevèze, P., et al., *A Mesomodel for Localisation and Damage Computation in Laminates.* Computer Methods in Applied Mechanics and Engineering 2000. **183**(105-122).

49. Bakuckas, J.G., et al., *Computational Methodology to Predict Damage Growth in Unidirectional Composites—I. Theoretical Formulation and Numerical Implementation.* Engineering Fracture Mechanics, 1995. **52**(5): p. 937-951.

50. Tay, T.E., et al., *Mesh Design in Finite Element Analysis of Post-Buckled Delamination in Composite Laminates.* Composite Structures, 1999. **47**(1): p. 603-611.

51. Shen, F., K.H. Lee, and T.E. Tay, *Modeling Delamination Growth in Laminated Composites.* Composites Science and Technology, 2001. **61**(9): p. 1239-1251.

52. Brewer, J.C. and P.L. Lagace, *Quadratic Stress Criterion for Initiation of Delamination.* Journal of Composite Materials, 1988. **22**(12): p. 1141-1155.

53. Hou, J.P., et al., *Prediction of Impact Damage in Composite Plates.* Composites Science and Technology, 2000. **60**(2): p. 273-281.

54. Camanho, P.P., et al., *Prediction of In Situ Strengths and Matrix Cracking in Composites under Transverse Tension and In-Plane Shear.* Composites Part A, 2006. **37**(2): p. 165-176.

55. Dugdale, D.S., *Yielding of Steel Sheets Containing Slits.* Journal of Mechanics and Physics of Solids, 1960. **8**(2): p. 100-104.

56. Barenblatt, G.I., *Mathematical Theory of Equilibrium Cracks in Brittle Failure.* Advances in Applied Mechanics, 1962. **7**: p. 55-129.

57. Camanho, P.P., C.G. Davila, and D.R. Ambur, *Numerical Simulation of Delamination Growth in Composite Materials.* NASA-TP-211041, 2001.

58. Cui, W. and M.R. Wisnom, *A Combined Stress-Based and Fracture-Mechanics-Based Model for Predicting Delamination in Composites.* Composites, 1993. **24**(6): p. 467-474.

59. Borg, R., L. Nilsson, and K. Simonsson, *Simulation of Delamination in Fiber Composites with a Discrete Cohesive Failure Model.* Composites Science and Technology, 2001. **61**(5): p. 667-677.

60. Meo, M. and E. Thieulot, *Delamination Modeling in a Double Cantilever Beam.* Composite Structures, 2005. **71**(3-4): p. 429-434.

61. Xie, D. and A.M. Waas, *Discrete Cohesive Zone Model for Mixed-Mode Fracture Using Finite Element Analysis.* Engineering Fracture Mechanics, 2006. **73**(13): p. 1783-1796.

62. Wisnom, M.R. and F.K. Chang, *Modelling of Splitting and Delamination in Notched Cross-Ply Laminates.* Composites Science and Technology, 2000. **60**(15): p. 2849-2856.

63. Chen, H.R., R.X. Bai, and M. Wang, *Study on Failure Process of Delaminated Stiffened Composite Plates under Compression.* Acta Mechanica Sinica, 2003. **19**(4): p. 289-299.

64. Chen, J., *Predicting Progressive Delamination of Stiffened Fibre-Composite Panel and Repaired Sandwich Panel by Decohesion Models.* Journal of Thermoplastic Composite Materials, 2002. **15**(5): p. 429-441.

65. Chen, J., et al., *Predicting Progressive Delamination of Composite Material Specimens via Interface Elements.* Mechanics of Advanced Materials and Structures, 1999. **6**(4): p. 301-317.

66. Alfano, G. and M.A. Crisfield, *Finite Element Interface Models for the Delamination Analysis of Laminated Composites: Mechanical and Computational Issues.* International Journal for Numerical Methods in Engineering, 2001. **50**(7): p. 1701-1736.

67. Schellekens, J.C.J. and R. Borst, *Free Edge Delamination in Carbon-Epoxy Laminates: a Novel Numerical/Experimental Approach.* Composite Structures, 1994. **28**(4): p. 357-373.

68. Goncalves, J.P., et al., *Interface Element Including Point-to-Surface Constraints for Three-Dimensional Problems with Damage Propagation.* Engineering Computations, 2000. **17**(1): p. 28-47.

69. Camanho, P.P., C.G. Davila, and M.F. de Moura, *Numerical Simulation of Mixed-Mode Progressive Delamination in Composite Materials.* Journal of Composite Materials, 2003. **37**(16): p. 1415-1438.

70. Camanho, P.P., C.G. Davila, and S.T. Pinho, *Fracture Analysis of Composite Co-Cured Structural Joints Using Decohesion Elements.* Fatigue and Fracture of Engineering Materials and Structures, 2004. **27**(9): p. 745-757.

71. Allix, O. and L. Blanchard, *Mesomodeling of Delamination: Towards Industrial Applications.* Composites Science and Technology, 2006. **66**(6): p. 731-744.

72. Herakovich, C.T., *Mechanics of Fibrous Composite*. 1998, New York: John Wiley & Sons, Inc.

73. Sun, C.T. *Strength Analysis of Unidirectional Composites and Laminates*. in *Comprehensive Composite Materials*. 2000: Elsevier Science, Ltd., Oxford.

74. Hallett, S.R. and M.R. Wisnom, *Experimental Investigation of Progressive Damage and the Effect of Layup in Notched Tensile Tests.* Journal of Composite Materials, 2006. **40**(2): p. 119-141.

75. Smith, I.M. and D.V. Griffiths, eds. *Programming the finite element method*. 4th ed. 2004: Wiley, Hoboken, New York.

76. Daniel, I.M., *Engineering mechanics of composite materials*. 2nd ed. ed. 2006, New York :: Oxford University Press. 411 p. : ill. ; 25 cm.

77. Boyang, PhD student (Work in progress), Department of Mechanical Engineering, National University of Singapore.

78. Tvergaard, V. and J.W. Hutchinson, *The relation between crack growth resistance and fracture process parameters in elastic-plastic solids.* Journal of the Mechanics and Physics of Solids, 1992. **40**(6): p. 1377-1397.

79. *Abaqus Analysis User's Manual, Version 6.7*. 2007.

80. Camanho, P.P. and C.G. Davila, *Analysis of the Effects of Residual Strains and Defects on Skin/Stiffener Debonding using Decohesion Elements.* SDM Conference, Norfolk, VA, 2003.

81. Petrossian, Z. and M.R. Wisnom, *Prediction of Delamination Initiation and Growth from Discontinuous Plies Using Interface Elements.* Composites Part A, 1998. **29**(5-6): p. 503-515.

82. Hansen, A. L. and Lund, E., 2009, *A Mixed mode cohesive law for modeling interfacial fracture and fiber bridging*, Int. Journal of Solids and Structures.

83. Blackman, B., H. Hadavinia, et al. (2003), *The use of a cohesive zone model to study the fracture of fibre composites and adhesively-bonded joints*, International Journal of Fracture, **119**(1): 25-46.

84. ASTM standards: http://www.astm.org/Standards/D5379.htm